TRANSACTIONS
OF THE ASME
Series C

Journal of HEAT TRANSFER

November 1959

RADIATION • CONDUCTION • CONVECTION • COMPLEX SYSTEMS • PHASE CHANGES AND MIXTURES • TRANSIENT PHENOMENA • THERMOPHYSICAL PROPERTIES • EXPERIMENTAL TECHNIQUES • THERMOMETRY • ANALOG METHODS • ANALYTICAL AND NUMERICAL METHODS • APPLICATIONS • DESIGN TECHNIQUES • HEAT EXCHANGERS • INSULATION • ECONOMIC FACTORS BIOTECHNOLOGY • ASTRONAUTICS

Published Quarterly by
THE AMERICAN SOCIETY OF MECHANICAL ENGINEERS

TRANSACTIONS
OF THE ASME
Series C

EDITORIAL DEPARTMENT

Editor, J. J. JAKLITSCH, JR.
Consulting Editor, LEO BLOCKETT
Production, JEAN NORTH
Art Editor, HENRY BALFOUR

HEAT TRANSFER DIVISION

Chairman, W. E. HAMMOND
Secretary, J. F. WACHUNAS
Consulting Editor, S. P. KEZIOS

OFFICERS OF THE ASME

President, G. B. WARREN
Secretary, O. B. SCHIER, II
Treasurer, E. J. KATES
Assistant Treasurer, H. J. BAUER

PUBLICATIONS COMMITTEE

Chairman, JOHN de S. COUTINHO
B. G. A. SKROTZKI
HENDLEY H. BLACKMON
R. D. MINDLIN
MARTIN GOLAND
Junior Representatives
A. T. WUSKA
A. S. GOLDSTEIN

REGIONAL ADVISORY BOARD

Region I, ROY L. PARSELL
Region II, GLENN R. FRYLING
Region III, F. J. HEINZE
Region IV, FRANCIS C. SMITH
Region V, H. M. CATHER
Region VI, C. R. EARLE
Region VII, M. POPOVICH
Region VIII, LINN HELANDER

Published quarterly by The American Society of Mechanical Engineers. Publication office at 20th and Northampton Streets, Easton, Pa. The editorial department is located at the headquarters of the Society, 29 West Thirty-Ninth Street, New York 18, N. Y. Cable address, "Mechanaer," New York. Price $3.00 a copy, $10.00 annually; to members, $1.50 a copy, $5.00 annually. Add 50 cents for postage to all countries outside the United States and Canada. Changes of address must be received at Society headquarters seven weeks before they are to be effective on the mailing list. Please send old as well as new address. . . . By-Law: The Society shall not be responsible for statements or opinions advanced in papers or . . . printed in its publications (B13, Par. 4). . . . Second-class mail privileges authorized at Easton, Penna. . . . This publication is authorized to be mailed at the special rates of postage prescribed by Section 132.122 . . . © Copyrighted, 1959, by The American Society of Mechanical Engineers. Reprints from this publication may be made on condition that full credit be given the Transactions of the ASME, Series C—Journal of Heat Transfer, and the author, and that date of publication be stated.

TRANSACTIONS OF THE ASME
is indexed by the Engineering Index, Inc.

Journal of
HEAT TRANSFER

VOL. 81 • SERIES C • NO. 4

November 1959

CONTENTS

253 **Dynamic Response of Heat Exchangers Having Internal Heat Sources—Part III**
V. S. Arpaci and J. A. Clark

267 **Heating and Cooling Air and Carbon Dioxide in the Thermal Entrance Region of a Circular Duct With Large Gas to Wall Temperature Differences**
Helmut Wolf

280 **Turbulent Flow in a Circular Tube With Arbitrary Internal Heat Sources and Wall Heat Transfer**
R. Siegel and E. M. Sparrow

291 **Laminar Condensation Heat Transfer on a Horizontal Cylinder**
E. M. Sparrow and J. L. Gregg

297 **The Use of Thin Films for Increasing Evaporation and Condensation Rates in Process Equipment**
E. L. Lustenader, R. Richter, and F. J. Neugebauer

308 **Some General Considerations of the Heating of Satellites**
A. J. Eggers, Jr., T. J. Wong, and R. E. Slye

315 **The Penetration of Planetary Atmospheres**
Carl Gazley, Jr.

323 **Thermodynamic Properties of Helium at Low Temperatures and High Pressures**
D. B. Mann and R. B. Stewart

327 **Radiation Fin Efficiency for One-Dimensional Heat Flow in a Circular Fin**
R. L. Chambers and E. V. Somers

TRANSACTIONS OF THE ASME Series B

Journal of
ENGINEERING FOR INDUSTRY
Volume 81 • Series B • Number 4

CONTENTS FOR NOVEMBER, 1959

281 Dynamic Problems Associated With Satellite Orbit Control, by B. W. Augenstein. (59—Av-4)
289 Study of Machinability of Metals, by H. Takeyama and E. Usui. (58—A-161)
293 Four-Bar Linkages—Approximate Synthesis, by W. W. Worthley and R. T. Hinkle. (58—A-130)
301 A Theory for the Effect of Mean Stress on Fatigue of Metals Under Combined Torsion and Axial Load or Bending, by W. N. Findley. (58—A-61)
307 An Analysis of Critical Stresses and Mode of Failure of a Wire Rope, by W. L. Starkey and H. A. Cress. (58—A-63)
317 An Application of Statistics to the Dimensioning of Machine Parts, by M. F. Spotts. (58—A-44)
323 The Dynamic Analysis and Design of Relatively Flexible Cam Mechanisms Having More Than One Degree of Freedom, by R. C. Johnson. (58—A-192)
332 Power Heat Balance Considerations in Design and Operation of Industrial Plants, by J. I. Hudson. (58—A-166)
339 Influence of Hot and Cold Storage-Loads on the Refrigerated-Space Temperature of a Cooling Complex, by C. F. Kayan. (58—A-165)
348 Development and Uses of a New Line of Vibratory Feeders and Unit Vibrators, by A. F. Israelson. (59—SA-33)
353 A Mechanical Time-Delay Device Sensitive to Centrifugal Fields, by J. R. Baumgarten, R. Cohen, and A. S. Hall, Jr. (59—SA-9)

TRANSACTIONS OF THE ASME Series A

Journal of
ENGINEERING FOR POWER
Volume 81 • Series A • Number 4

CONTENTS FOR OCTOBER, 1959

361 The Aerodynamic Approach to Furnace Design, by J. H. Chesters. (58–A-72)
371 Use of Flow Models for Boiler-Furnace Design, by R. W. Curtis and L. E. Johnson. (58–A-120)
380 Use of Models for Studying Pulverized-Coal Burner Performance, by G. C. Whitney. (58–A-95)
383 Basic Principles of Combustion-Model Research, by A. A. Putnam and E. W. Ungar. (58–A-73)
389 A New Performance Criterion for Steam-Turbine Regenerative Cycles, by J. Kenneth Salisbury. (58–A-205)
403 Power Test Code Thermometer Wells, by J. W. Murdock. (58–A-176)
417 Flow-Induced Noise in Heat Exchangers, by A. A. Putnam. (58–A-103)
423 The Effect of Fuel Types and Admission Method Upon Combustion Efficiency, by H. N. McManus, Jr., W. E. Ibele, and T. E. Murphy. (58–A-128)
428 Torsion of a Prismatical Bar Whose Section Is a Crescent, by F. Sisto. (59–GTP-6)
433 The Transient Response of Gas-Turbine-Plant Heat Exchangers—Regenerators, Intercoolers, Precoolers, and Ducting, by A. L. London, F. R. Biancardi, and J. W. Mitchell. (59–GTP-5)
449 Stresses in Hollow Cylinders Due to Asymmetrical Heat Generation, by Harry Kraus and George Sonnemann.

TRANSACTIONS OF THE ASME Series D

Journal of
BASIC ENGINEERING
Vol. 81 • Series D • No. 3

CONTENTS FOR SEPTEMBER, 1959

275 Static and Dynamic Control Characteristics of Flapper-Nozzle Valves, by T.-Y. Feng. (58—A-160)
285 Some Measurements of Boundary-Layer Growth in a Two-Dimensional Diffuser, by J. F. Norbury. (58—A-196)
297 The Skewed Boundary Layer, by E. S. Taylor. (58—A-113)
305 On the Nature of Stall, by S. J. Kline. (58—A-170)
321 Optimum Design of Straight-Walled Diffusers, by S. J. Kline, D. E. Abbott, and R. W. Fox. (58—A-137)
332 Labyrinth-Seal Leakage Analysis, by W. Zabriskie and B. Sternlicht. (58—A-118)
341 Centrifugal Manometer, by J. F. Kemp. (58—A-111)
349 The Aerodynamic Design of Two-Dimensional Turbine Cascades for Incompressible Flow With a High-Speed Computer, by H. N. Cantrell and J. E. Fowler. (58—A-141)
362 An Analysis of Axial Compressor Cascade Aerodynamics, Part I, by G. L. Mellor. (58—A-83)
379 An Analysis of Axial Compressor Cascade Aerodynamics, Part II, by G. L. Mellor. (58—A-84)
387 Loss and Stall Analysis of Compressor Cascades, by Seymour Lieblein. (58—A-91)
401 Stall Prediction in Gas-Turbine Engines, by R. J. Lubick and L. E. Wallner. (58—A-133)
409 A Survey of Stall Propagation—Experiment and Theory, by H. W. Emmons, R. E. Kronauer, and J. A. Rockett. (58—A-150)
417 Modulation Phenomena in Stall Propagation, by J. A. Rockett. (58—A-152)
426 Studies of Jet Compression—I, Apparatus and Methods. Results With Air at Room Temperature, by H. J. Hoge, S. S. Eichacker, and D. L. Fiske. (58—SA-13)

TRANSACTIONS OF THE ASME
Series E

Journal of
APPLIED MECHANICS
Vol. 81 • Series E • No. 3

CONTENTS FOR SEPTEMBER, 1959

TECHNICAL PAPERS

319 On Supersonic Wind Tunnels With Low Free-Stream Disturbances, M. V. Morkovin. (59—APM-10)
325 Velocity and Temperature Fluctuation Measurements in a Turbulent Boundary Layer, D. S. Johnson. (58—A-81)
337 Density Variation Effects in Stepped-Thrust Bearings, C. F. Kettleborough. (59—APM-19)
341 Response of a Nonlinear String to Random Loading, T. K. Caughey. (59—APMW-4)
345 Response to Van Der Pol's Oscillator to Random Excitation, T. K. Caughey. (59—APMW-5)
349 A Perturbation Solution of the Equations of Motion of a Gyroscope, Robert Goodstein. (59—A-5)
353 Vibration of Beam-Mass Systems With Time-Dependent Boundary Conditions, T. C. Yen and S. Kao. (59—APM-22)
357 Dynamic Loading Tests of an Aircraft-Type Beam, E. A. Ripperger and W. R. Barton.
367 Viscous Damping in Flexural Vibrations of Bars, M. K. Newman. (59—APMW-8)
377 Natural Modes and Their Stability in Two-Degree-of-Freedom Systems, R. M. Rosenberg and C. P. Atkinson. (58—A-57)
386 On Finite Bending of Pressurized Tubes, Eric Reissner. (59—APM-5)
393 Instability and Folding Deformation of a Viscoelastic Medium in Compression, M. A. Biot. (59—APMW-21)
401 Stress Distribution in Semi-Infinite Strip Subjected to Concentrated Load, P. S. Theocaris. (59—APM-17)
407 Postbuckling Behavior of Rectangular Plates With Small Initial Curvature, Noboru Yamaki. (58—A-59)
415 New Theory of Elastic Sandwich Plates—One-Dimensional Case, Yi-Yuan Yu. (59—APM-23)
422 On Invariant Perforation in an Infinite Strip, Chih-Bing Ling. (59—APM-20)
432 Thermal Stresses in Moderately Thick Elastic Plates, B. E. Gatewood. (59—APM-7)
437 Analysis of Plane Stress in Polar Co-ordinates, H. D. Conway. (59—APM-1)
440 The Stress Function of a Radial Strain, F. Goded. (59—APM-25)
442 Determination of Safe Loads of Beams Subjected to Twisting and Bending Moments, P. G. Hodge, Jr., and R. Sankaranarayanan. (59—APM-26)

DESIGN DATA AND METHODS

448 Factors of Stress Concentration Due to Elliptical Fillets, M. M. Frocht and D. Landsberg.

BRIEF NOTES

451 Creep of Elastic Belt on a Pulley, G. V. Tordion. 452 Modification of Rayleigh's Principle for Calculating Beam Frequencies, F. M. Lewis. 454 Yield Point Load of an Annular Plate, P. G. Hodge, Jr. 455 Analysis of Indeterminate Structures by Displacement Method, P. H. Denke and C. K. Wang. 456 Internal Damping of Thermal Origin in Thin Wires, P. Srinivasan. 457 Lateral Buckling of Tapered Narrow Beam, L. H. N. Lee. 458 Stresses in Infinite Wedges Tapered in Width and Thickness, H. D. Conway. 460 Minimization of Spring Torque, T. Vreeland, Jr. 461 Steady-State Response of Linear Vibration Systems, M. E. Gurtin. 462 Further Understanding of Shakedown Theorems, Melvin Zaid. 462 Series Solution for Ellipsoidal Shells, Robert Schmidt.

DISCUSSION

465 Discussion of previously published papers by E. L. Reiss; G. N. Hatsopoulos and J. H. Keenan; F. A. McClintock; F. M. White, B. F. Barfield, and M. J. Goglia; M. M. Abbassi; Eli Sternberg and W. T. Koiter; M. J. Schilhansl

BOOK REVIEWS

475

Dynamic Response of Heat Exchangers Having Internal Heat Sources—Part III

VEDAT S. ARPACI[1]

Instructor, Mechanical Engineering Faculty, Istanbul Technical University, Istanbul, Turkey

JOHN A. CLARK

Professor of Mechanical Engineering, University of Michigan, Ann Arbor, Mich. Assoc. Mem. ASME

This paper is an extension of two of the authors' previous papers [1, 2][2] and considers the dynamic response of the temperature of the heat-transfer surface and the fluid-surface temperature difference in a heat exchanger having internal heat sources. A general solution is presented for a transient resulting from an arbitrary time rate of change of heat generation starting from an arbitrary initial condition. The results are obtained by a direct mathematical attack on the governing differential equations. As a special case, the transient resulting from a linear time rate of change of internal heat generation is given, and this is compared with both experimental and theoretical results corresponding to a step change in heat generation. Satisfactory comparison is obtained. The results for this special case are presented such that the surface temperature and fluid-surface temperature difference may be computed as a function of space and time using four dimensionless, mathematical functions which are given in graphical form. It is shown how the case of the linear time rate of change of internal heat generation may be used to compute the dynamic response of this type of heat exchanger for any transient resulting from excursions in heat-generation rate which may be approximated piecewise by a series of linear functions of time. Heat exchangers to which these solutions apply include the heterogeneous nuclear reactor.

Introduction

PROBLEMS ASSOCIATED with the dynamic behavior of systems have application in the field of automatic control which is becoming of increasing technical importance. It was in this connection that, during the summer of 1954, the authors became interested in the dynamic behavior of heat exchangers, particularly those having internal heat sources. At that time it was necessary to determine the time response of a fluid circuit containing a nuclear reactor, piping, valves, and heat exchangers in which the disturbance was caused by power transients in the reactor. The reactor was characterized as a heat exchanger having internal heat sources. One approach included an attempt to obtain a mathematical solution to the response of the temperature of the reactor coolant. As a consequence of this study, the solution for the response of this type of heat exchanger to several different kinds of induced transients was obtained and has resulted in this series of papers. These results apply, of course, to other types of heat exchangers having internal heat sources, including an electrical heater and a chemical reactor in which a chemical reaction occurs within the solid walls. Apart from the use in the control of the systems, knowledge of transient behavior is important in design where thermal stresses are to be considered or when temperature-time information is required from a device such as a heat exchanger.

This is the third in a series of papers which has been planned on the general subject of the dynamic response of heat exchangers having time-variant internal heat sources. The first two papers [1, 2] were presented in June and August, 1957.

It is recognized that often it is convenient and practical to program such problems as these on digital or analog computing machines, particularly if a great many different cases are to be studied. However, the programming is by no means trivial and machine time is not always available or possible to those seeking solutions. Furthermore, for those having access to machines,

[1] Present address: Department of Mechanical Engineering, M.I.T., Cambridge, Mass.

[2] Numbers in brackets designate References at end of paper.

Contributed by the Heat Transfer Division and presented at the Semi-Annual Meeting, Detroit, Mich., June 15–19, 1958, of THE AMERICAN SOCIETY OF MECHANICAL ENGINEERS.

NOTE: Statements and opinions advanced in papers are to be understood as individual expressions of their authors and not those of the Society. Manuscript received at ASME Headquarters, April 7, 1958. Paper No. 58—SA-39.

Nomenclature

A = area of the fluid in contact with wall, sq ft
a = flow area of fluid, sq ft
a' = cross-sectional area of wall, sq ft
a_1 = defined by equation (3*a*), deg F
a_2 = defined by equation (3*b*), hr
a_3 = defined by equation (3*a*), hr
a_4 = defined by equation (3*b*), ft
b_1 = $a_2 + a_3 = (M + 1)/K$, hr
b_2 = $a_2a_3 = M/K^2$, $(\text{hr})^2$
c = circumference (wetted perimeter), ft
c_p = specific heat of the fluid, Btu/lb deg F
c_{pw} = specific heat of the wall, Btu/lb deg F
d_o = outside diameter of the tube, ft
d_i = inside diameter of the tube, ft
e = internal energy, Btu/lb_M, $e = h - pv$
e = base of natural logarithms, dimensionless
f_1, f_2 = functions defined in Appendix 2
$F_{13}, \ldots, F_{16}$ = see Appendix 2
$G_{13}, \ldots, G_{16}$ = see Appendix 2
h = coefficient of heat transfer between the wall and the fluid, $\text{Btu/hr-ft}^2\text{-deg F}$
h = enthalpy, Btu/lb_M
I_0 = Bessel function of first kind, zeroth order
k = the kth term of the series
K = $(h/\rho c_p)A/V$, $(\text{hour})^{-1}$, for fluid
K_w = $h/(\rho c_p)_w (A/V)_w$, $(\text{hour})^{-1}$, for wall
m = mass, lb_M
M = a_2a_3, heat capacity ratio, $(\rho c_p V)_w/\rho c_p V$
p = pressure, psia
p = Laplace variable, $(\text{hour})^{-1}$
P_x = rate of work done by system, Btu/hr

(Continued on next page)

these solutions may serve as helpful check solutions, and for those who do not, the solutions presented here may be a useful tool. In any event, with a small expenditure of time and at little expense, a human computer using a desk calculator may run out a number of cases in order to demonstrate the effect of a chosen variable on the response, thus giving a "feel" for this type of dynamic system. Actually, machine computation was employed in these solutions as most of the functions which are given were obtained on an IBM 650 digital computer. Only the function $\psi_6(s, q^*)$ was reduced by hand computation.

Literature Survey

Since the writing of the first two papers [1, 2], several new papers on this topic have come to the authors' attention. To avoid unnecessary repetition, the literature previously reviewed will not be included in the body of this paper, but for convenience the References are listed at the end. Comment will be made on the new material.

The analysis of the response of counterflow and parallel-flow heat exchangers is partially treated by Rizika [11] and solved by Carslaw and Jaeger [10] for zero wall-heat capacity. Rizika [11] has computed and presented as graphs two infinite series, one of which is employed in this paper (ψ_2^{**}) as part of the solution to the present problem. A numerical method for calculating heat-exchanger dynamics is given by Dusinberre [12] who presents explicit iteration formulas and computation guides. Detailed examples are given. A problem allied with that of the present paper is published by Fritz [13] in which the response of a nuclear-reactor coolant owing to time-varying flow rates is given for a lumped-temperature system. Thermal response of a homogeneous-type nuclear reactor has been treated by Gallagher [14]. Silvers and Dietrich [15] have computed the response of the surface and coolant temperatures in a heterogeneous nuclear reactor resulting from a step increase in power using the method of finite differences. Their results bear exact similarity to those corresponding to the exact mathematical solution given in Figs. 7 and 8 of reference [2].

An extension of the problem studied by Rizika [9] and Carslaw and Jaeger [10] has been made by Dabora [16] in which the effect of heat loss to the surroundings from a regenerative-type (nonperiodic) heat exchanger is considered. The solution is obtained by ignoring the time rate of change of fluid temperature, similar to that of Rizika [11]. The effectiveness of a periodic-flow heat exchanger (rotary regenerator) has been computed by Lambertson [17] using the finite-difference technique. Nine tables of numerical results corresponding to a fairly wide range of operating conditions are given. The effect of heat transfer between a gas and the walls and other solid material in a container tank on the charging and blowdown processes is examined by Reynolds and Kays [18]. The authors have considered the two cases of constant-mass flow and blowdown through a critical-flow nozzle. Analytical solutions assuming a lumped-parameter system are presented which agree favorably with experimental results. Cima and London [19] have studied experimentally the transient response of a particular two-fluid counterflow heat exchanger using an electrical analog computer having four discrete lumped circuits corresponding to equal increments of flow length in the exchanger. The heat exchanger studied is a gas-turbine regenerator of equal hot and cold-side fluid-capacity rates and equal thermal resistances. Dimensionless results are given for the response of the outlet cold-gas temperature to step changes in the inlet hot-gas temperature and for step changes in the flow rate of the cold—and hot—gas. A procedure is discussed for the estimation of the response of the cold-gas outlet temperature to an arbitrary disturbance in the hot-gas inlet temperature and results are given for a particular case.

Other recent work concerning the transient flow of heated fluids is that of Rea and Ablow [20]. Their system consisted of an insulated duct through which heated air was passed for conditions approximating a sudden and oscillating change in both flow and temperature of the inlet air. Measurements are reported of the response of the wall temperature and the inlet and outlet air temperatures and these are compared with a finite-difference calculation. Siegel [21] has reported on the transient process in free convection from a semi-infinite vertical flat plate, initially at

Nomenclature

p_{z_0}'' = initial power input, Btu/ft³ hr
$\Delta p_z''$ = change in power input, Btu/ft³ hr
q/A = heat flux, Btu/hr-ft²
$(q/A)_0$ = initial heat flux, Btu/hr-ft²
q = heat flow rate, Btu/hr
r_o = outside radius of the tube, ft
r_i = inside radius of the tube, ft
r = $(K/M)\,x/u$, dimensionless
s = $K(x/u)$, dimensionless
$t(x, \tau)$ = temperature of the fluid, deg F
$t(x, \tau) = t_1(x, 0) + t_2(x, \tau)$
$t_1(x, 0)$ = steady-state component of fluid temperature, deg F
$t_2(x, \tau)$ = transient component of fluid temperature, deg F
t_0 = temperature of the fluid entering coolant channel, deg F
u = velocity of the fluid, fps
v = specific volume, ft³/lb$_M$
V = volume of the fluid, ft³
V_w = volume of the wall, ft³
w = fluid flow rate, lb$_M$/hr
x = axial distance, ft
ρ = density, lb$_M$/ft³
$\Phi(\tau)$ = transient in volumetric heat-generation rate, Btu/hr-ft³
$\theta(x, \tau)$ = wall temperature, deg F, $\theta(x, \tau) = \theta_1(x, 0) + \theta_2(x, \tau)$
$\theta_1(x, 0)$ = steady-state component of wall temperature, deg F
$\theta_2(x, \tau)$ = transient component of wall temperature, deg F
τ = time, hr
τ^* = $\tau - x/u$, hr
τ_0 = characteristic time for linear transient, hr, see equations (11)
$\Pi(\tau)$ = see equation (10e)
$\Lambda(\tau)$ = see equation (10f)
Δt = $\theta - t$, deg F
$\psi_2^{**}(s, q^*)$ = see Appendix 2, dimensionless (Fig. 4)
$\psi_4(r, \gamma^*)$ = see Appendix 2, dimensionless (Fig. 2)
$\psi_5(s, q^*)$ = see Appendix 2, dimensionless (Fig. 3)
$\psi_6(s, q^*)$ = see Appendix 2, dimensionless (Fig. 5)

$$\alpha \equiv \frac{t(x, \tau) - t(x, 0)}{\Delta(q/A)/h}, \text{ dimensionless}$$

$$\beta \equiv \frac{\theta(x, \tau) - \theta(x, 0)}{\Delta(q/A)/h}, \text{ dimensionless}$$

$$\delta \equiv \frac{\Delta t(x, \tau) - \Delta t(x, 0)}{\Delta(q/A)/h}, \text{ dimensionless}$$

γ = $K\tau$, dimensionless
$\overline{(\ )}$ = transformed function
$\bar{\Phi}(p)$ = see equation (20)

ambient temperature. The transients are introduced by (*a*) suddenly increasing the plate temperature and (*b*) suddenly producing a uniform heat flux at the plate surface. The method of characteristics is employed to obtain the results which are reported as the approximate time required for the plate to reach steady state subsequent to the introduction of the transient. Anantanarayanan and Ramachandran [22] have studied the effects of traverse vibrations (75 to 120 cps) in a wire on the heat transfer to a turbulent air stream flowing parallel with the axis of the unexcited wire. Their results indicate that an increase takes place in the heat-transfer coefficient with an increase in both amplitude and frequency, and is correlated as essentially the ratio of vibrating to stationary Nusselt numbers versus mean vibrational velocity of air-stream velocity.

Summary of the Present Problem

The solution of the time response of the heat-transfer surface temperature and the fluid-surface temperature difference, at any point in a channel of this type of heat exchanger in which the rate of internal heat generation is an arbitrary function of time, results from a direct mathematical attack on the differential equations derived from the appropriate natural laws with the suitable boundary and initial conditions. The mathematical details are given in Appendix 2 and involve the use of the Laplace transform. While the solution is not algebraically simple, numerical results should be reasonably easy to obtain as all the functions necessary for such a computation are presented in graphical form. The authors have not rigorously proved the mathematical convergence of the complete solution to the steady-state values. It appears from their own calculations in comparison with their experimental data, however, that such convergence is obtained. As a special case, the solution also is given for an exchanger in which the heat generation is a linear function of time. These results are computed for a particular exchanger and compared with the experimental and theoretical results of references [1, 2] in which the transient was caused by a step change in internal heat generation. Reasonable comparison is obtained. By way of this comparison, it is shown how the case of linear time rate of change of heat generation may be used to compute the general case in which the heat generation is given by an arbitrary function of time, providing this function may be approximated piecewise by a series of linear variations.

Analysis

The physical system analyzed is shown in Fig. 1. This consists of a circular tube through which a coolant flows steadily, and in the solid walls of which energy is generated. In the steady state, all of this energy appears as a flow of heat at the interface between coolant and solid causing the coolant to increase in enthalpy (and temperature) as it flows through the tube. The outside surface of the tube is adiabatic. During the transient, however, both the tube-wall material and the coolant experience local temperature excursions, the magnitude of the former and their difference being evaluated here as a function of distance and time. A circular tube has been selected for convenience in comparison of theory and experiment. Where a nonsymmetrical geometry is involved in the analysis, such as a triangular flow cross section, the results given may be reduced to an area-to-volume ratio and, to a degree of approximation, can be used for other geometry for which the restraints on the solution apply.[3] The solution will be valid as presented for flow inside circular tubes and between parallel plates.

[3] The authors are indebted to Prof. T. F. Irving, Jr., and J. P. Hartnett of the Heat Transfer Laboratory, University of Minnesota, for pointing out the importance of this distinction (see *Discussion Section* [1, 2]). The nature of the approximation is discussed in the authors' closure of reference [1].

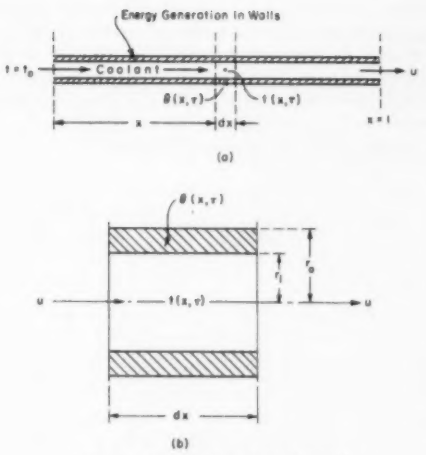

Fig. 1 Simulated coolant channel

The following assumptions are imposed on the solution:

(*a*) The fluid temperature and velocity are constant across the flow cross section.

(*b*) The duct wall temperature does not depend on radius. Valid for thin-walled metal systems.

(*c*) Axial heat conduction is negligible in both fluid and duct walls and heat flows only to the coolant. This is a reasonable assumption when the Peclet number exceeds 100 [23]. The outer surface is adiabatic.

(*d*) The heat-transfer coefficient is constant with length and time.

(*e*) The fluid is incompressible and all fluid properties are constant. The flow channel has constant area.

(*f*) Energy (heat) generation within the walls is constant with length but is time-dependent.

(*g*) The temperature of the fluid entering the duct is constant and equal to t_0.

With these assumptions, the application of the First Law of Thermodynamics and the law of conservation of mass for an incompressible fluid to the system shown in Fig. 1(*b*) produces the following two differential equations, one for the duct wall, the other for the fluid. Details of this derivation are outlined in Appendix 1.

Wall
$$-(\theta - t) + a_1 p_s''(\tau) = a_2 \frac{\partial \theta}{\partial \tau} \tag{1}$$

Fluid
$$(\theta - t) = a_3 \frac{\partial t}{\partial \tau} + a_4 \frac{\partial t}{\partial x} \tag{2}$$

For a circular tube and in generalized terms, the constants are written:

$$a_1 = \frac{r_o^2 - r_i^2}{2r_i h} = \frac{1}{(\rho c_p)_w K_w}, \quad a_2 = \frac{\rho c_p r_i}{2h} = \frac{1}{K} \tag{3a}$$

$$a_3 = \frac{(\rho c_p)_w (r_o^2 - r_i^2)}{2r_i h} = \frac{1}{K_w}, \quad a_4 = \frac{\rho c_p r_i}{2h} u = \frac{u}{K} \tag{3b}$$

and
$$p_s''(\tau) = p_{s_0}'' + \Phi(\tau) \tag{3c}$$

where p_{s_0}'' is the initial uniform volumetric heat-generation rate and $\Phi(\tau)$ is the arbitrary time-variant volumetric heat-generation-rate function, having a zero value at zero time, which introduces the transient into the system. As shown in Appendix 2, both

functions $\theta(x, \tau)$ and $t(x, \tau)$ of equations (1) and (2) are split into two components, one being a steady-state part, $t_1(x, 0)$ and $\theta_1(x, 0)$, the other of the transient contribution, $t_2(x, \tau)$ and $\theta_2(x, \tau)$. For purposes of transient analysis, it is necessary only to carry out detailed mathematical analysis of the latter functions. It will be noted that $t_1(x, 0) = t(x, 0)$ and $\theta_1(x, 0) = \theta(x, 0)$. Hence the governing differential equations become

Wall

$$-(\theta_2 - t_2) + \frac{1}{(\rho c_p)_w K_w} \Phi(\tau) = \frac{1}{K_w}\left(\frac{\partial \theta_2}{\partial \tau}\right) \tag{4}$$

Fluid

$$\theta_2 - t_2 = \frac{1}{K}\left(\frac{\partial t_2}{\partial \tau}\right) + \frac{u}{K}\left(\frac{\partial t_2}{\partial x}\right) \tag{5}$$

Equations (4) and (5) are operated on by the Laplace-transform technique. The transformed equations in transient wall temperature (θ_2) and transient fluid-wall-temperature difference ($\Delta t_2 = \theta_2 - t_2$), are integrated with the appropriate initial and boundary conditions, the inverse transformation performed, and then recombined with the steady-state functions $t_1(x, 0)$ and $\theta_1(x, 0)$ as outlined in detail in Appendix 2. The nature of the mathematical attack on this problem produces solutions for both $\theta(x, \tau)$ and $\Delta t(x, \tau)$ in two domains of physical time: Case 1, a physical time following the introduction of the transient which is greater than zero but equal to or less than x/u; and Case 2, a physical time equal to or greater than x/u. It will be noted that the physical time x/u is that required for fluid particles flowing at a velocity u to traverse the distance x. The results for Cases 1 and 2 for arbitrary timewise-variant internal volumetric heat generation $\Phi(\tau)$ are as follows

Case 1 $0 \leq \dfrac{\tau u}{x} \leq 1$

(*a*) Wall temperature $\theta(x, \tau)$

$$\theta(x, \tau) - \theta(x, 0) = \frac{M/(M+1)}{(\rho c_p)_w} \int_0^\tau \Phi(s)\left[1 + \frac{1}{M}\, e^{\frac{K(M+1)}{M}(S-\tau)}\right] ds \tag{6}$$

(*b*) Fluid-wall temperature difference, $\Delta t\,(x, \tau)$

$$\Delta t(x, \tau) - \Delta t(x, 0) = \frac{1}{(\rho c_p)_w}\, e^{-\frac{K(M+1)}{M}\tau} \int_0^\tau \Phi(s) e^{\frac{K(M+1)S}{M}} ds \tag{7}$$

In equations (6) and (7) the quantities $\theta(x, \tau) - \theta(x, 0)$ and $\Delta t(x, \tau) - \Delta t(x, 0)$ represent the transient increase of wall temperature and fluid-wall-temperature difference at the location $x = x$ and are independent of the magnitude of $\theta(x, 0)$ or $\Delta t(x, 0)$. The constants all are defined later.

Case 2 $\dfrac{\tau u}{x} \geq 1$

(*c*) Wall temperature $\theta(x, \tau)$

$$\theta(x, \tau) - \theta(x, 0) = \frac{M/(M+1)}{(\rho c_p)_w}\left\{\int_0^\tau \Phi(s)\left[1 + \frac{1}{M}\, e^{\frac{K(M+1)}{M}(S-\tau)}\right] ds - \frac{K}{M}\, e^{-K\frac{x}{u}} \int_0^{\tau^*} \Pi(\tau - s) e^{-\frac{K}{M}S} I_0\left[2K\left(\frac{sx}{Mu}\right)^{1/2}\right] ds\right\} \tag{8}$$

(*d*) Fluid-wall-temperature difference $\Delta t(x, \tau)$

$$\Delta t(x, \tau) - \Delta t(x, 0) = \frac{1}{(\rho c_p)_w}\left\{e^{-\frac{K(M+1)}{M}\tau} \int_0^\tau \Phi(s) e^{-\frac{K(M+1)}{M}S} ds + Ke^{-K\frac{x}{u}} \int_0^{\tau^*} \Lambda(\tau - s) e^{-\frac{K}{M}S} I_0\left[2K\left(\frac{sx}{Mu}\right)^{1/2}\right] ds\right\} \tag{9}$$

The quantities and functions given in equations (6) through (9) are defined

$$M = \frac{(\rho c_p V)_w}{\rho c_p V} = \frac{K}{K_w} = \frac{\text{total heat capacity of wall material}}{\text{total heat capacity of fluid}} \tag{10a}$$

$$K = \frac{h(A/V)}{\rho c_p} = \text{fluid time constant} \tag{10b}$$

$$K_w = \frac{h(A/V)_w}{(\rho c_p)_w} = \text{wall time constant} \tag{10c}$$

$$\tau^* = \tau - x/u \tag{10d}$$

$$\Pi(\tau) = \int_0^\tau \Phi(z)dz - \Lambda(\tau) \tag{10e}$$

$$\Lambda(\tau) = e^{-K\frac{M+1}{M}\tau} \int_0^\tau \Phi(z) e^{\frac{K(M+1)}{M}z} dz \tag{10f}$$

$\Phi(\tau)$ = arbitrary time-variant volumetric heat-generation rate

Equations (6), (7), (8), and (9) represent the general solutions for the dynamic response of the wall temperature $\theta(x, \tau)$ and the fluid-wall temperature difference $\Delta t(x, \tau)$ above their initial values for an arbitrary transient in volumetric internal heat generation $\Phi(\tau)$. Owing to their definition it will be noted that the fluid temperature response $t(x, \tau) = \theta(x, \tau) - \Delta t(x, \tau)$, which may be formed from equations (6) and (7) or (8) and (9). Should $\Phi(\tau)$ in equations (6) through (9) be set equal to a step change in volumetric heat source, that is, $\Delta(q/A)(A/V)_w$, it will be observed that the results of reference [2] are obtained.

Special Case of Transient in $\Phi(\tau)$ Being Linear in Time

A simple but important case of the general solutions, equations (6) through (9), is that in which $\Phi(\tau)$ varies linearly with time. This may be represented by the function

$$\Phi(\tau) = \Delta p_x''\left(\frac{\tau}{\tau_0}\right) \tag{11a}$$

$$= \Delta(q/A)(A/V)_w\left(\frac{\tau}{\tau_0}\right), \tag{11b}$$

where $\Delta p_x''$ and $\Delta(q/A)$ are the volumetric heat-generation-rate increment and the heat-flux increment, respectively, corresponding to any time τ_0 subsequent to the introduction of the linear transient.

For this case, as shown in Appendix 2, the equations (6) through (9) may be written in dimensionless form, as follows

Case 1 $0 \leq \tau u/x \leq 1$

(*e*) Wall temperature $\theta(x, \tau)$

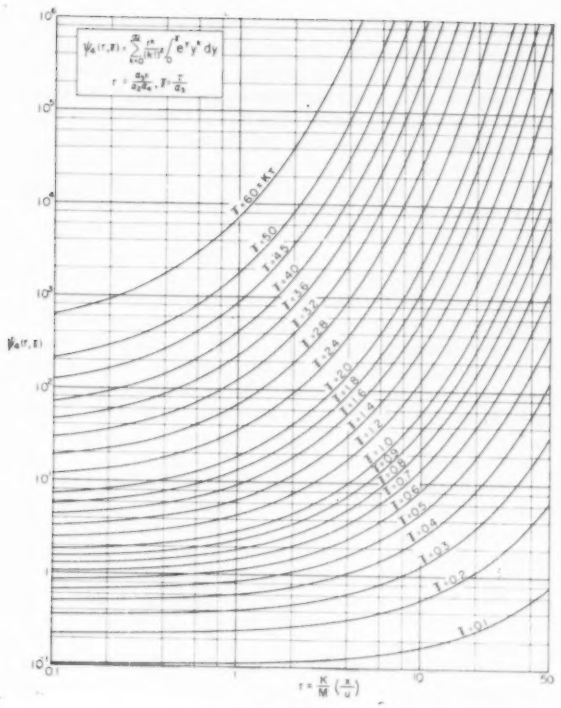

Fig. 2

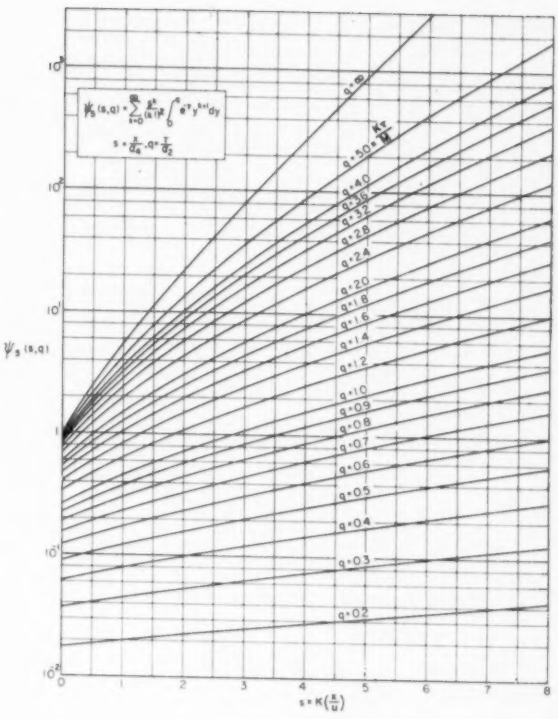

Fig. 3

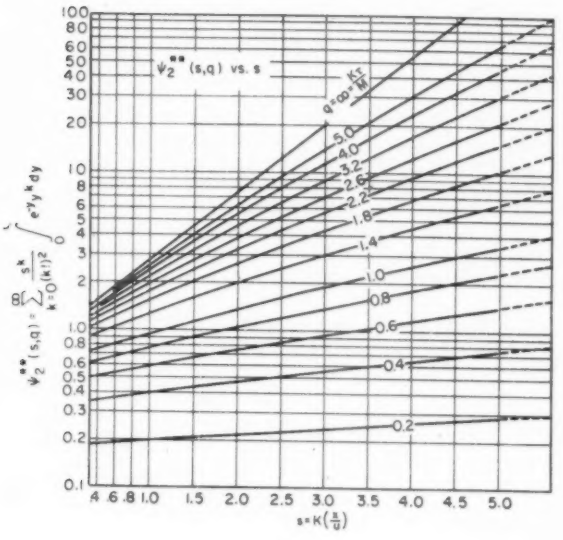

Fig. 4

$$\frac{\theta(x,\tau) - \theta(x,0)}{\Delta(q/A)/h} = \frac{M}{M+1}\left(\frac{\tau}{\tau_0}\right) \left\{ \frac{1}{K\tau(M+1)^2}\left[e^{-\frac{M+1}{M}K\tau} + \frac{M+1}{M}K\tau - 1\right] + \frac{1}{2}\frac{K\tau}{M} \right\} \quad (12)$$

(*f*) Fluid-wall temperature difference $\Delta t(x, \tau)$

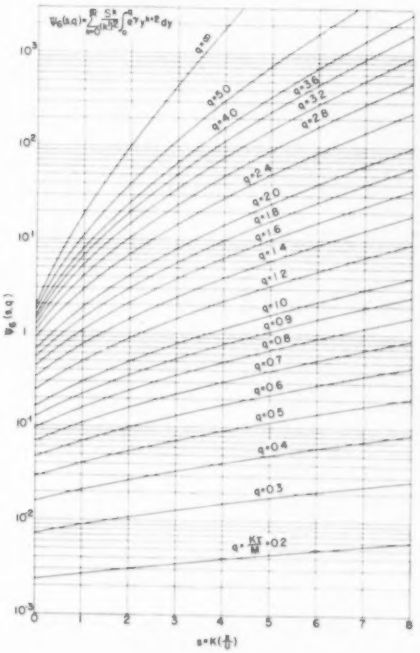

Fig. 5

$$\frac{\Delta t(x,\tau) - \Delta t(x,0)}{\Delta(q/A)/h} = \frac{M}{K\tau(M+1)^2}\left(\frac{\tau}{\tau_0}\right)\left[e^{-\frac{M+1}{M}K\tau} + \frac{M+1}{M}K\tau - 1\right] \quad (13)$$

Case 2 $\tau u/x \geq 1$

(g) Wall temperature $\theta(x, \tau)$

$$\frac{\theta(x,\tau) - \theta(x,0)}{\Delta(q/A)/h} = \frac{M}{M+1}\left(\frac{\tau}{\tau_0}\right)\left\{\frac{1}{K\tau(M+1)^2}\left[e^{-\frac{M+1}{M}K\tau} + \frac{M+1}{M}K\tau - 1\right] + \frac{1}{2}\frac{K\tau}{M} - \frac{M}{(M+1)^2}\frac{1}{K\tau}e^{-K\frac{x}{u}}\left\{\left[\frac{1}{2}\left(\frac{M+1}{M}K\tau^*\right)^2 - \frac{M+1}{M}K\tau^* + 1\right]\psi_2^{**}(s,q^*) - \frac{1}{M}e^{-\frac{M+1}{M}K\tau^*}\psi_4(r,\gamma^*) - (M+1)\left[\frac{M+1}{M}K\tau^* - 1\right]\psi_5(s,q^*) + \frac{(M+1)^2}{2}\psi_6(s,q^*)\right\}\right\} \quad (14)$$

(h) Fluid-wall-temperature difference $\Delta t(x, \tau)$

$$\frac{\Delta t(x,\tau) - \Delta t(x,0)}{\Delta(q/A)/h} = \frac{M}{K\tau(M+1)^2}\left(\frac{\tau}{\tau_0}\right)\left\{\left[e^{-\frac{M+1}{M}K\tau} + \frac{M+1}{M}K\tau - 1\right] + Me^{-K\frac{x}{u}}\left\{\left[\frac{M+1}{M}K\tau^* - 1\right]\psi_2^{**}(s,q^*) + e^{-\frac{M+1}{M}K\tau^*}\psi_4(r,\gamma^*) - (M+1)\psi_5(s,q^*)\right\}\right\} \quad (15)$$

In equations (14) and (15), q^* and γ^* are to be interpreted as that value of q and γ for which τ corresponds to $\tau^* = \tau - x/u$. It will be noted that $q = K\tau/M$; hence $q^* = K\tau^*/M$. The functions necessary to the use of equations (14) and (15), $\psi_4(r, \gamma^*)$, $\psi_5(s, q^*)$, $\psi_2^{**}(s, q^*)$, and $\psi_6(s, q^*)$ are defined in Appendix 2, and have been calculated and are presented in graphical form in Figs. 2, 3, 4, and 5. $\psi_6(s, q^*)$ is a new function; $\psi_2^{**}(s, q^*)$, $\psi_4(r, \gamma^*)$, and $\psi_5(s, q^*)$ have been introduced in references [1] and [2].

Discussion of Theoretical Results

Owing to the relative complexity of equations (14) and (15), it is simpler to examine equations (12) and (13) for the effect of the various physical parameters on the response of the wall temperature, $\theta(x, \tau) - \theta(x, 0)$ and the fluid-wall-temperature difference $\Delta t(x, \tau) - \Delta t(x, 0)$ for the case of a linear transient in p_x[*].

The constant M has been defined as

$$M = \frac{a_2}{a_3} = \frac{(\rho c_p)_w}{(\rho c_p)}\frac{(r_o^2 - r_i^2)}{r_i^2} = \frac{(\rho c_p V)_w}{\rho c_p V} = \frac{\text{total heat capacity of wall material}}{\text{total heat capacity of fluid}}$$

Hence M is a heat-capacity ratio, dependent upon geometry as well as upon materials and is the quantity which introduces these properties into the equations. For the usual materials and geometry it may be expected that M will vary from near zero for water-steel systems with thin metal walls to something in excess of 1000 for similar gas-steel systems.

The effect of the heat-capacity-ratio parameter M on the wall-temperature response (for the first time domain) may be seen by an examination of equation (12) which may be regarded as a dimensionless wall-temperature response. For small values of M, equation (12) approaches $[1 + (1/2)K\tau]\tau/\tau_0$ while at larger values of M, this quantity rapidly approaches zero. This indicates that, at least in the first domain ($0 \leq \tau u/x \leq 1$), the magnitude of the wall-temperature response is greatly diminished for a fixed $K\tau$, for systems having a large value of M as compared with those of smaller value of M. This result is a direct consequence of the nature of the imposed transient. That is, with the transient resulting from changes in the rate of internal generation of energy within the wall, the magnitude of the increase in wall temperature, at a fixed $K\tau$ and $\Delta(q/A)/h$, will be inversely proportional to heat capacity $(\rho c_p V)_w$ of the wall. Hence as M is increased the heat capacity of the wall relative to the fluid is increased and the expected reduction in the response of θ results.

A similar result may be obtained for the response of the fluid-wall-temperature difference, also in the first time domain, by an examination of equation (13). For systems with small magnitudes of M, that is, heat capacity of the wall very much smaller than that of the fluid, equation (13) approaches τ/τ_0. Hence for this case, $\Delta t(x, \tau) - \Delta t(x, 0)$ approaches $[\Delta(q/A)/h]\tau/\tau_0$. On the other hand, for systems having very large M, equation (13) approaches zero and $\Delta t(x, \tau)$ approaches $\Delta t(x, 0)$. This is an approach to a condition of complete lack of transient which, like that already mentioned for $\theta(x, \tau)$, may be expected from physical considerations.

The asymptotic limits of the temperature-response functions for values of M equal to zero and infinity are given for the first time domain in Table 1.

Asymptotic limits for the second time domain have not been evaluated for the case of $M = 0$ owing to an indeterminate form of 0/0 in q^* when $\tau = x/u$ and $\tau^* = 0$. Equations (14) and (15) indicate that each of the functions β, δ, and α has a limit of 0 for infinitely large values of M, as would be expected.

As is shown in Appendix 2, the functions $\psi_4(r, \gamma^*)$, $\psi_2^{**}(s, q^*)$, $\psi_5(s, q^*)$, and $\psi_6(s, q^*)$, which are required in equations (14) and (15) to describe the heat-exchanger response, are presented in Figs. 2, 3, 4, and 5 as various functions of the dimensionless quantities r, γ, s, and q. It will be noted that these quantities may be written in the following form

$$r = \frac{h}{(\rho c_p)_w}\left(\frac{A}{V}\right)_w\left(\frac{x}{u}\right) = K_w\left(\frac{x}{u}\right); \qquad \gamma = \frac{h}{\rho c_p}\left(\frac{A}{V}\right)\tau = K\tau \quad (16)$$

$$s = \frac{h}{\rho c_p}\left(\frac{A}{V}\right)\left(\frac{x}{u}\right) = K\left(\frac{x}{u}\right); \qquad q = \frac{h}{(\rho c_p)_w}\left(\frac{A}{V}\right)\tau = K_w\tau \quad (17)$$

Table 1 Asymptotic limits of temperature-response functions for values of $M = 0$ and $M = \infty$

First time domain $0 \leq \tau u/x \leq 1$

Function	$M = 0$	$M = \infty$
$\frac{\theta(x,\tau) - \theta(x,0)}{\Delta(q/A)/h} \equiv \beta$	$\left(1 + \frac{1}{2}K\tau\right)\frac{\tau}{\tau_0}$	0
$\frac{\Delta t(x,\tau) - \Delta t(x,0)}{\Delta(q/A)/h} \equiv \delta$	τ/τ_0	0
$\frac{t(x,\tau) - t(x,0)}{\Delta(q/A)/h} \equiv \alpha$	$\frac{1}{2}K\tau\left(\frac{\tau}{\tau_0}\right)$	0

Hence in the second time domain, $\tau u/x \geq 1$, the response of the heat exchanger also is governed by the product of a time constant for the fluid K or the wall K_w and either a physical time τ or a "lag time" x/u. Because the heat-transfer coefficient h and the area A are common to both wall and fluid, it may also be shown that $K/K_w = M$ and that $sq = \gamma r$.

Method of Superposition of Linear Transients

The results for the linear transient given in equations (12), (13), (14), and (15) may be used to compute the response of θ, t, and Δt resulting from any other type of transient in heat-generation rate providing this transient can satisfactorily be represented by a series of piecewise linear combinations. This technique follows from the method of superposition and is possible owing to the linearity of equations (47) and (48), which may be written

$$\frac{\bar{\theta}_2}{a_1 b_2/b_1^2} = \begin{bmatrix}\text{function of } F_{13}, F_{14}, F_{16} \\ \text{from equation (47)}\end{bmatrix} \sum_{i=1}^{k} \bar{\varphi}_i(p) \qquad (18)$$

$$\frac{\overline{\Delta t}_2}{a_1 b_2/b_1^2} = \begin{bmatrix}\text{function of } F_{15}, F_{16} \\ \text{from equation (48)}\end{bmatrix} \sum_{i=1}^{k} \bar{\varphi}_i(p) \qquad (19)$$

where

$$\bar{\Phi}(p) = \bar{\varphi}_1(p) + \bar{\varphi}_2(p) + \ldots = \sum_{i=1}^{k} \bar{\varphi}_i(p) \qquad (20)$$

$\bar{\varphi}_i(p)$ = transformed form of an energy-generation transient having a linear form

If one were to solve the equations (18) and (19) separately for each $\bar{\varphi}_i(p)$ and then superpose the resulting solutions, one obtains the solution to equations (47) and (48) in which the transient in energy generation $\bar{\Phi}(p)$ is made up of a linear combination of linear functions $\bar{\varphi}_i(p)$, in accordance with equation (20).

As an example, consider the transient shown in the inset of Fig. 6, labeled curve (c). In this case the energy transient consists of a linear increase until two seconds (τ_0) have elapsed, after which the energy-generation rate remains constant. Such a transient may be represented by an energy-generation rate from 0 to 2 sec by

$$\varphi_1(\tau) = \Delta p_{z_1}{}'' \left(\frac{\tau}{\tau_0}\right) \qquad (21)$$

and

$$\bar{\varphi}_1(p) = \Delta p_{z_1}{}'' \left(\frac{1}{\tau_0} \cdot \frac{1}{p^2}\right) \qquad (22)$$

At τ equal τ_0 (2 seconds) another energy generation rate function is introduced which is written as

$$\varphi_2(\tau) = -\Delta p_{z_1}{}'' \left(\frac{\tau - \tau_0}{\tau_0}\right)$$

and

$$\bar{\varphi}_2(p) = -\Delta p_{z_1}{}'' \left(\frac{1}{\tau_0} \cdot \frac{1}{p^2}\right) e^{-p\tau_0} \qquad (23)$$

Then subsequent to $\tau = \tau_0$ the resultant condition of energy generation, which is constant and equal to $p_{z_0}{}'' + \Delta p_z{}''$, is expressed as

$$\varphi(\tau) = \varphi_1(\tau) + \varphi_2(\tau) = \Delta p_{z_1}{}'' \left(\frac{\tau}{\tau_0}\right) - \Delta p_{z_1}{}'' \left(\frac{\tau - \tau_0}{\tau_0}\right) \qquad (24)$$
$$= \Delta p_{z_1}{}''$$

and

$$\bar{\Phi}(p) = \bar{\varphi}_1(p) + \bar{\varphi}_2(p) = \Delta p_{z_1}{}'' \frac{1}{\tau_0} \cdot \frac{1}{p^2} (1 - e^{-p\tau_0}) \qquad (25)$$

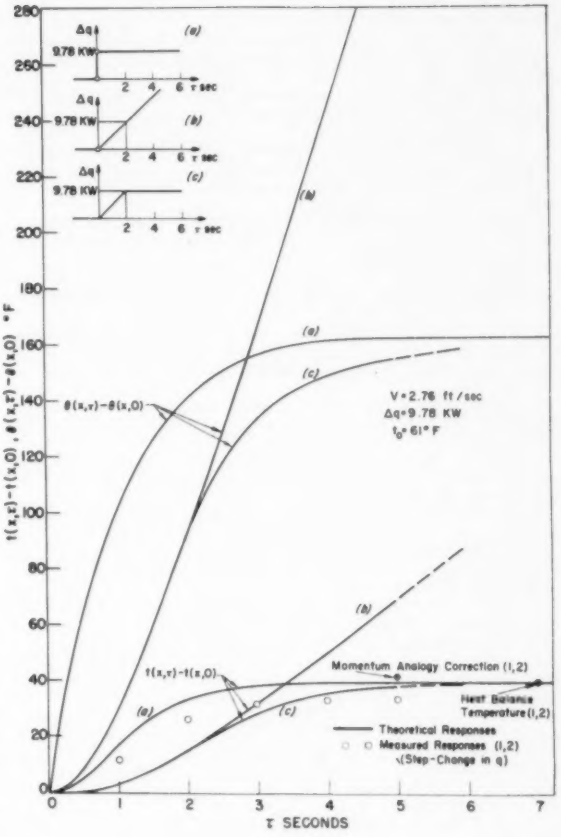

Fig. 6

Since $\epsilon^{-p\tau_0}$ does not change the solution but shifts it by an amount τ_0, it would be sufficient to solve the problem for the case $(1/\tau_0)$ $(1/p^2)$ and plot the resulting temperature curves for θ, t, and Δt. Then after $\tau = \tau_0$ subtract the same curve (starting at $\tau = \tau_0$) from the previous one which begins at the origin ($\tau = 0$). The initial conditions are identical for both cases because the second solution (φ_2) also actually starts from the origin ($\tau = 0$) but in the region $0 \leq \tau \leq \tau_0$ it is exactly equal to zero.

The case of a linear increase in heat-generation rate, shown as curve (c) in the inset of Fig. 6, was computed and compared with both experimental data and theoretical results corresponding to a step increase in heat-generation rate taken from references [1, 2]. The final heat-generation rate and the initial conditions in the computed result were assumed to be the same as those corresponding to the experimental data. The results of the computation are shown in Fig. 6 for both $\theta(x, \tau) - \theta(x, 0)$ and $\Delta t(x, \tau) - \Delta t(x, 0)$, and correspond to the transients shown as curves (a), (b), and (c) in the inset. Reasonable agreement is obtained, the computed response for case (c) lagging the step response, as would be anticipated. Also the asymptotic approach of t to its steady-state value is identically the same for both transients and the experimental data, also as would be expected.

References

1 J. A. Clark, V. S. Arpaci, and K. M. Treadwell, "Dynamic Response of Heat Exchangers Having Internal Heat Sources—Part I," TRANS. ASME, vol. 80, 1958, pp. 612–624.

2 V. S. Arpaci and J. A. Clark, "Dynamic Response of Heat

Exchangers Having Internal Heat Sources—Part II," TRANS. ASME, vol. 80, 1958, pp. 625–634.

3 W. C. Cohen and E. F. Johnson, "Dynamic Characteristics of Double-Pipe Heat Exchangers," *Industrial and Engineering Chemistry*, vol. 48, 1956, p. 1031.

4 J. M. Mosley, "Predicting Dynamics of Concentric Pipe Heat Exchangers," *Industrial and Engineering Chemistry*, vol. 48, 1956, p. 1035.

5 J. M. Gallagher, Jr., "Equivalent Transfer Function of Systems With Space and Time as Independent Variables," DACL Internal Memo M-922-2, M.I.T., Cambridge, Mass., September 15, 1955.

6 H. M. Paynter and Y. Takahashi, "New Method of Evaluating Dynamic Response of Counterflow and Parallel-Flow Heat Exchangers," TRANS. ASME, vol. 78, 1956, pp. 749–758.

7 Y. Takahashi, "You Need No Computers to Graphically Determine the Dynamics of Heat Percolation," *Control Engineering*, vol. 2, May, 1955, pp. 46–50.

8 Y. Takahashi, "Transfer Function Analysis of Heat Exchangers," in "Automatic and Manual Control," edited by A. Tustin, Buttersworth Science Publishing Company, London, England, 1952, p. 235.

9 J. W. Rizika, "Thermal Lags in Flowing Incompressible Fluid Systems Containing Heat Capacitors," TRANS. ASME, vol. 78, 1956, p. 1407.

10 H. S. Carslaw and J. C. Jaeger, "Conduction of Heat in Solids," Oxford University Press, London, England, 1948, pp. 325–329 and pp. 329–330.

11 J. W. Rizika, "Thermal Lags in Flowing Systems Containing Heat Capacitors," TRANS. ASME, vol. 76, 1954, p. 411.

12 G. M. Dusinberre, "Calculation of Transient Temperatures in Pipes and Heat Exchangers by Numerical Methods," TRANS. ASME, vol. 76, 1954, p. 421.

13 R. J. Fritz, "Analysis of Temperature Transients in a Nuclear Power System," Preprint No. 234, Nuclear Engineering and Science Conference, Cleveland, Ohio, December, 1955.

14 J. M. Gallagher, Jr., "Thermal Aspects of Externally Cooled Homogeneous Circulating-Fuel Reactor System," DACL Internal Memo M-922-6, M.I.T., Cambridge, Mass., May 1, 1956.

15 J. P. Silvers and J. R. Dietrich, "The Reactor Handbook," vol. 2, "Engineering," pp. 156–157. US AEC, May, 1955.

16 E. K. Dabora, "Regenerative Heat Exchanger With Heat Loss Consideration," Engineering Research Institute, Aircraft Propulsion Laboratory, Project 2284, University of Michigan, Ann Arbor, August, 1957.

17 T. J. Lambertson, "Performance Factors at a Periodic-Flow Heat Exchanger," TRANS. ASME, vol. 80, 1958, pp. 586–592.

18 W. C. Reynolds and W. M. Kays, "Blowdown and Charging Processes in a Single Gas Receiver With Heat Transfer," TRANS. ASME, vol. 80, 1958, p. 1160.

19 R. M. Cima and A. L. London, "The Transient Response of a Two-Fluid Counterflow Heat Exchanger—the Gas Turbine Regenerator," TRANS. ASME, vol. 80, 1958, p. 1169.

20 S. E. Rea and C. M. Ablow, "Transient Air Temperatures in a Duct," TRANS. ASME, vol. 79, 1957, p. 1536.

21 R. Siegel, "Transient Free Convection From a Vertical Flat Plate," TRANS. ASME, vol. 80, 1958, pp. 347–359.

22 R. Anantanarayanan and A. Ramachandran, "Effect of Vibration on Heat Transfer From a Wire to Air in Parallel Flow," TRANS. ASME, vol. 80, 1958, p. 1426.

23 P. J. Schneider, "Effect of Axial Fluid Conduction on Heat Transfer in the Entrance Regions of Parallel Plates and Tubes," TRANS. ASME, vol. 79, 1957, p. 765.

24 R. V. Churchill, "Modern Operational Mathematics in Engineering," McGraw-Hill Book Company, New York, N. Y., chaps. 1, 2, 3, 1944.

25 C. A. Campbell and R. M. Foster, "Fourier Integrals for Practical Application," D. Van Nostrand Company, New York, N. Y., 1954.

26 A. Erdélyi, W. Magnus, F. Oberhettinger, and F. G. Tricomi, "Tables of Integral Transforms," vol. 1, McGraw-Hill Book Company, New York, N. Y., 1954.

APPENDIX 1

Derivation of the Basic Differential Equations

The system analyzed is shown in Fig. 1 and consists of a constant-diameter circular tube through which a fluid (coolant) is pumped steadily and in the walls of which energy is dissipated.

With the assumptions and conditions as indicated in the analysis section of the paper, two differential equations, one for the wall and one for the fluid, may be derived from the First Law of Thermodynamics and the law of conservation of mass for an incompressible fluid [1].

Fluid

$$\frac{\partial(\rho e)}{\partial \tau} + \frac{\partial(\rho h u)}{\partial x} = \frac{hc}{a}(\theta - t) \tag{26}$$

Wall

$$\frac{\partial(\rho e)_w}{\partial \tau} = -\frac{hc}{a_1}(\theta - t) + p_{x_0}'' + \Phi(\tau) \tag{27}$$

where

a = flow wetted cross-sectional area (πr_i^2 for circular tube)
c = wetted perimeter ($2\pi r_i$ for circular tube)
a' = cross-sectional area of duct wall ($\pi_o r^2 - \pi r_i^2$ for circular tube)
p_{x_0}'' = initial volumetric heat-generation rate
$\Phi(\tau)$ = arbitrary transient in volumetric heat-generation rate
e = internal energy per lb_M in absence of the effects of motion, capillarity, and so forth

Equations (26) and (27) may be reduced to the following

$$(\theta - t) = \frac{\rho c_p a}{hc}\left(\frac{\partial t}{\partial \tau}\right) + \frac{\rho c_p a}{hc} u \left(\frac{\partial t}{\partial x}\right) \tag{28a}$$

$$= \frac{\rho c_p r_i}{2h}\left(\frac{\partial t}{\partial \tau}\right) + \frac{\rho c_p r_i}{2h} u \left(\frac{\partial t}{\partial x}\right) \tag{28b}$$

$$= \frac{1}{K}\left(\frac{\partial t}{\partial \tau}\right) + \frac{u}{K}\left(\frac{\partial t}{\partial x}\right) \tag{28c}$$

Equation (28*b*) is for circular-tube geometry and (28*c*) is for generalized geometry. Both are equivalent to equation (2) in the body of the paper.

For the wall, equation (27) may be rearranged to

$$-(\theta - t) + \frac{a'}{hc}[p_{x_0}'' + \Phi(\tau)] = \frac{a'(\rho c_p)_w}{hc}\left(\frac{\partial \theta}{\partial \tau}\right) \tag{29a}$$

or,

$$-(\theta - t) + \frac{r_o^2 - r_i^2}{2hr_i}[p_{x_0}'' + \Phi(\tau)] = \frac{(\rho c_p)_w (r_o^2 - r_i^2)}{2hr_i}\left(\frac{\partial \theta}{\partial \tau}\right) \tag{29b}$$

or,

$$-(\theta - t) + \frac{1}{(\rho c_p)_w K_w}[p_{x_0}'' + \Phi(\tau)] = \frac{1}{K_w}\left(\frac{\partial \theta}{\partial \tau}\right) \tag{29c}$$

Equation (29*b*) is for circular-tube geometry and (29*c*) is for generalized geometry. Both are equivalent to equation (1) in the body of the paper.

At this point, it is convenient to partition both temperatures $\theta(x, \tau)$ and $t(x, \tau)$ into transient and steady-state components. Thus we define

$$\theta(x, \tau) = \theta_1(x, 0) + \theta_2(x, \tau) \tag{30a}$$

$$t(x, \tau) = t_1(x, 0) + t_2(x, \tau) \tag{30b}$$

where θ_1 and t_1 are the steady-state and θ_2 and t_2, the transient components. For the steady-state condition, θ_1 and t_1 satisfy the following differential equations which are equations (28*c*) and (29*c*) with all time derivatives and $\Phi(\tau)$ set equal to zero,

$$(\theta_1 - t_1) = \frac{u}{K}\left(\frac{\partial t_1}{\partial x}\right) \tag{31}$$

$$-(\theta_1 - t_1) + \frac{1}{(\rho c_p)_w K_w}\, p_{r_0}{}'' = 0 \tag{32}$$

From this set with the introduction of assumption (g) we find,

$$t_1(x, 0) = t_0 + \frac{(q/A)_0}{wc_p}\, cx \tag{33}$$

$$\theta_1(x, 0) = t_0 + \frac{(q/A)_0}{wc_p}\, cx + \frac{(q/A)_0}{h} \tag{34}$$

where $(q/A)_0$ is the initial steady-state heat flux at $\tau = 0$. Since it will be noted that $\theta(x, 0) = \theta_1(x, 0)$, $t(x, 0) = t_1(x, 0)$, and $t(0, \tau) = t_1(0, \tau) = t_0$, we have the following conditions on θ_2 and t_2:

$$\begin{aligned} t_2(0, \tau) &= 0 \\ t_2(x, 0) &= 0 \\ \theta_2(x, 0) &= 0 \end{aligned} \tag{35}$$

Substitution of equations (30) into equations (28c) and (29c), and subtracting equations (31) and (32) from the result gives

$$\theta_2 - t_2 = \frac{1}{K}\left(\frac{\partial t_2}{\partial \tau}\right) + \frac{u}{K}\left(\frac{\partial t_2}{\partial x}\right) \tag{36}$$

$$-(\theta_2 - t_2) + \frac{1}{(\rho c_p)_w K_w}\, \Phi(\tau) = \frac{1}{K_w}\left(\frac{\partial \theta_2}{\partial \tau}\right) \tag{37}$$

These equations are the same as equations (4) and (5) in the main body of the paper and are subject to the initial and boundary conditions given in equations (35).

The final solutions to this problem are expressed as $\theta(x, \tau) - \theta(x, 0)$, and $t(x, \tau) - t(x, 0)$ which are identical with $\theta_2(x, \tau)$ and $t_2(x, \tau)$ since, as was noted, $\theta(x, 0) = \theta_1(x, 0)$ and $t(x, 0) = t_1(x, 0)$. In this way, the solution $\theta(x, \tau) - \theta(x, 0) = \theta_2(x, \tau)$, for example, is the transient increase in θ above an arbitrary initial value $\theta(x, 0)$ and is independent of the value of $\theta(x, 0)$, so long as the system conforms to the requirements of the analysis.

APPENDIX 2

The Integration of Equations (4) and (6)

Equations (4) and (5) may be operated on by the Laplace operator with respect to time (τ) to produce the following transformed equations:

$$-(\bar{\theta}_2 - \bar{t}_2) + a_1\bar{\Phi} = a_2[p\bar{\theta}_2 - \theta_2(x, 0)] \tag{38}$$

and

$$(\bar{\theta}_2 - \bar{t}_2) = a_3[p\bar{t}_2 - t_2(x, 0)] + a_4\frac{d\bar{t}_2}{dx} \tag{39}$$

The boundary and initial conditions to be imposed according to the results of Appendix 1 are:

$$t_2(x, 0) = 0 \tag{40a}$$

$$\theta_2(x, 0) = 0 \tag{40b}$$

Hence equations (38) and (39) become

$$-(\bar{\theta}_2 - \bar{t}_2) + a_1\bar{\Phi} = a_2 p\bar{\theta}_2 \tag{41}$$

$$(\bar{\theta}_2 - \bar{t}_2) = a_3 p\bar{t}_2 + a_4\frac{d\bar{t}_2}{dx} \tag{42}$$

Solving equations (41) and (42) for $\bar{t}_2(x, p)$ gives

$$\frac{d\bar{t}_2}{dx} + f_1\bar{t}_2 = f_2 \tag{43}$$

The solution of this linear first-order differential equation, with the boundary condition $\bar{t}_2(0, p) = 0$, is

$$\bar{t}_2 = \frac{f_2}{f_1}\,(1 - e^{-f_1 x}) \tag{44}$$

where

$$f_1 = \frac{1}{a_4}\left(1 + a_3 p - \frac{1}{1 + a_2 p}\right) \tag{45}$$

$$f_2 = \frac{a_1}{a_4}\,\frac{\bar{\Phi}}{1 + a_2 p} \tag{46}$$

Substituting equation (44) into equations (41) and (42) and solving for $\bar{\theta}_2$, gives

$$\begin{aligned} \frac{\bar{\theta}_2}{\dfrac{a_1 b_2}{b_1{}^2}} &= a_3\left(\frac{b_1}{b_2}\right)^2 \frac{\dfrac{1}{a_3} + p}{p\left(\dfrac{b_1}{b_2} + p\right)}\,\Phi \\ &\quad - \frac{1}{a_2}\left(\frac{b_1}{b_2}\right)^2 e^{-\frac{x}{a_4}} e^{-\frac{x}{u}p}\, \frac{\bar{\Phi}}{p\left(\dfrac{b_1}{b_2} + p\right)}\, \frac{e^{\frac{\frac{1}{a_3 a_4}\left(\frac{1}{a_3} + p\right)}{x}}}{\left(\dfrac{1}{a_2} + p\right)} \\ &= \left(\frac{b_1}{b_2}\right) F_{13}(p)\bar{\Phi}(p) - \frac{1}{a_2}\,\frac{b_1}{b_2}\, e^{-\frac{x}{a_4}} e^{-\frac{x}{u}p} \\ &\qquad F_{14}(p)\bar{\Phi}(p)F_{16}(p) \end{aligned} \tag{47}$$

In like manner, the fluid-wall-temperature difference

$$\Delta\bar{t}_2 = \bar{\theta}_2 - \bar{t}_2$$

is found to be

$$\begin{aligned} \frac{\Delta\bar{t}_2}{\dfrac{a_1 b_2}{b_1{}^2}} &= a_3\left(\frac{b_1}{b_2}\right)^2 \frac{\bar{\Phi}}{\dfrac{b_1}{b_2} + p} + \left(\frac{b_1}{b_2}\right)^2 e^{-\frac{x}{a_4}} e^{-\frac{x}{u}p} \\ &\quad \frac{\bar{\Phi}}{\left(\dfrac{b_1}{b_2} + p\right)}\, \frac{e^{\frac{\frac{1}{a_3 a_4}\left(\frac{1}{a_3} + p\right)}{x}}}{\left(\dfrac{1}{a_2} + p\right)} = a_3\left(\frac{b_1}{b_2}\right)^2 F_{15}(p)\bar{\Phi}(p) \\ &\quad + \left(\frac{b_1}{b_2}\right)^2 e^{-\frac{x}{a_4}} e^{-\frac{x}{u}p} F_{15}(p)\bar{\Phi}(p)F_{16}(p) \end{aligned} \tag{48}$$

where $b_1 = a_2 + a_3$ and $b_2 = a_2 a_3$.

In equations (47) and (48) the functions F_{13}, F_{14}, F_{15}, and F_{16} are Laplace-transformed functions in the variable p which have corresponding original functions G_{13}, G_{14}, G_{15}, and G_{16} in the variable τ obtained by performing an inverse transformation on the functions F. This operation is usually outlined in most textbooks on operational mathematics, such as Churchill [24]. Extensive tables of the functions $F(p)$ and $G(\tau)$ may be found in the works of Campbell and Foster [25] and Erdélyi [26]. The Laplace-transformed functions F and the inverse-transformed functions G appropriate to equations (47) and (48) are listed in the following table:

	$F(p)$		$G(\tau)$	Restriction
F_{13}	$a_2\left(\frac{b_1}{b_2}\right)\frac{\frac{1}{a_2}+p}{p\left(\frac{b_1}{b_2}+p\right)}$	G_{13}	$\left(1+\frac{a_2}{a_2}\,e^{-\frac{b_1}{b_2}\tau}\right)$	$\tau>0$
F_{14}	$\frac{b_1}{b_2}\,\frac{1}{p\left(\frac{b_1}{b_2}+p\right)}$	G_{14}	$1-e^{-\frac{b_1}{b_2}\tau}$	$\tau>0$
F_{15}	$\frac{1}{\frac{b_1}{b_2}+p}$	G_{15}	$e^{-\frac{b_1}{b_2}\tau}$	$\tau>0$
F_{16}	$e^{\frac{1}{\frac{x}{a_2a_4}\left(\frac{1}{a_2}+p\right)}}\Big/\left(\frac{1}{a_2}+p\right)$	G_{16}	$e^{-\frac{\tau}{a_2}}I_0\left[2\left(\frac{x\tau}{a_2a_4}\right)^{1/2}\right]$	$\tau>0$

The product of transformed functions, such as $F_{14}F_{16}$, may be treated by the method of convolution, a technique of the inverse transformation for product of functions. This is discussed by Churchill ([24], chap. 2, p. 36.) Hence the transformed equations in the physical domain of x and τ, which are the solutions to the differential equations (4) and (5), and for boundary and initial conditions of equation (40) are found to be

Case 1 $0 \le \frac{\tau u}{x} \le 1$

$$\frac{\theta_2(\tau)}{\frac{a_1b_2}{b_1^2}} = \frac{b_1}{b_2}\int_0^\tau \Phi(s)\left[1+\frac{a_2}{a_2}\,e^{-\frac{b_1}{b_2}\tau}e^{\frac{b_1}{b_2}s}\right]ds \qquad (49)$$

$$\frac{\Delta t_2(\tau)}{\frac{a_1b_2}{b_1^2}} = a_1\left(\frac{b_1}{b_2}\right)^2 e^{-\frac{b_1}{b_2}\tau}\int_0^\tau \Phi(s)e^{\frac{b_1}{b_2}s}\,ds \qquad (50)$$

Case 2 $\frac{\tau u}{x} \ge 1$

$$\frac{\theta_2(x,\tau)}{\frac{a_1b_2}{b_1^2}} = \frac{\theta_2(\tau)}{\frac{a_1b_2}{b_1^2}} - \frac{1}{a_2}\cdot\frac{b_1}{b_2}\,e^{-\frac{x}{a_4}}\int_0^{\tau^*}\mathrm{II}(\tau-s)e^{-\frac{s}{a_2}}I_0\left[2\left(\frac{xs}{a_2a_4}\right)^{1/2}\right]ds \qquad (51)$$

$$\frac{\Delta t_2(x,\tau)}{\frac{a_1b_2}{b_1^2}} = \frac{\Delta t_2(\tau)}{\frac{a_1b_2}{b_1^2}} + \left(\frac{b_1}{b_2}\right)^2 e^{-\frac{x}{a_4}}\int_0^{\tau^*}\Lambda(\tau-s)e^{-\frac{s}{a_2}}I_0\left[2\left(\frac{xs}{a_2a_4}\right)^{1/2}\right]ds \qquad (52)$$

where

$$\Lambda(\tau) = e^{-\frac{b_1}{b_2}\tau}\int_0^\tau \Phi(z)e^{\frac{b_1}{b_2}z}\,dz \qquad (53)$$

$$\mathrm{II}(\tau) = \int_0^\tau \Phi(z)dz - \Lambda(\tau) \qquad (54)$$

$$\tau^* = \tau - \frac{x}{u} \qquad (55)$$

$\Phi(\tau)$ = arbitrary time-variant volumetric heat-generation rate Equations (49), (50), (51), and (52) are the same as equations (6), (7), (8), and (9) in the main body of the paper.

Special Case of Transient in $\Phi(\tau)$ Being Linear in Time

In the event $\Phi(\tau)$ be represented by a linear function of time, such as $\Delta p_x''(\tau/\tau_0)$, equations (49), (50), (51), and (52) become

Case 1 $0 \le \frac{\tau u}{x} \le 1$

$$\frac{\theta_2(\tau)}{\frac{\Delta p_x''}{\tau_0}\frac{a_1b_2}{b_1^2}} = \frac{a_2}{a_2}\cdot\frac{b_2}{b_1}\left(e^{-\frac{b_1}{b_2}\tau}+\frac{b_1}{b_2}\tau-1\right)+\frac{1}{2}\frac{b_1}{b_2}\tau^2 \qquad (56)$$

$$\frac{\Delta t_2(\tau)}{\frac{\Delta p_x''}{\tau_0}\frac{a_1b_2}{b_1^2}} = a_2\left(e^{-\frac{b_1}{b_2}\tau}+\frac{b_1}{b_2}\tau-1\right) \qquad (57)$$

Case 2 $\frac{\tau u}{x} \ge 1$

$$\frac{\theta_2(x,\tau)}{\frac{\Delta p_x''}{\tau_0}\frac{a_1b_2}{b_1^2}} = \frac{\theta_2(\tau)}{\frac{a_1b_2}{b_1^2}\frac{\Delta p_x''}{\tau_0}} - e^{-\frac{x}{a_4}}\left\{\left(\frac{b_2}{b_1}\right)\left[\frac{1}{2}\left(\frac{b_1}{b_2}\tau^*\right)^2 - \frac{b_1}{b_2}\tau^*+1\right]\psi_2^{**}(s,q^*) - \frac{a_2}{a_2}\frac{b_2}{b_1}e^{-\frac{b_1}{b_2}\tau^*}\psi_4(r,\gamma^*) - a_2\left(\frac{b_1}{b_2}\tau^*-1\right)\psi_5(s,q^*) + \frac{a_2^2}{2}\frac{b_1}{b_2}\psi_6(s,q^*)\right\} \qquad (58)$$

$$\frac{\Delta t_2(x,\tau)}{\frac{\Delta p_x''}{\tau_0}\frac{a_1b_2}{b_1^2}} = \frac{\Delta t_2(\tau)}{\frac{a_1b_2}{b_1^2}\frac{\Delta p_x''}{\tau_0}} + a_2e^{-\frac{x}{a_4}}\left[\left(\frac{b_1}{b_2}\tau^*-1\right)\psi_2^{**}(s,q^*) + \frac{a_2}{a_2}e^{-\frac{b_1}{b_2}\tau^*}\psi_4(r,\gamma^*) - a_2\frac{b_1}{b_2}\psi_5(s,q^*)\right] \qquad (59)$$

The functions in these equations are defined. The function $\psi_2^{**}(x,\tau)$ is identical with two functions which have been computed and presented by Rizika [11]. The functions are reproduced here in equivalent form in Fig. 4. The remaining functions $\psi_4(x,\tau)$ and $\psi_5(x,\tau)$ have been presented in reference [2] given here in equivalent form in Figs. 2 and 3. $\psi_6(x,\tau)$ is a new function with this paper and is given in Fig. 5.

$$\psi_4(x, \tau^*) = \frac{1}{a_2}\int_0^{\tau^*} e^{\frac{s}{a_1}} I_0\left[2\left(\frac{xs}{a_2a_4}\right)^{1/2}\right] ds$$

$$= \frac{1}{a_2}\sum_{k=0}^{\infty}\frac{\left(\frac{x}{a_2a_4}\right)^k}{(k!)^2}\int_0^{\tau^*} e^{\frac{s}{a_1}} s^k ds$$

$$= \frac{a_3}{a_2}\sum_{k=0}^{\infty}\frac{\left(\frac{a_3x}{a_2a_4}\right)^k}{(k!)^2}\int_0^{\frac{\tau^*}{a_3}} e^z z^k dz = \frac{a_3}{a_2}\sum_{k=0}^{\infty}\frac{r^k}{(k!)^2}\int_0^{\gamma^*} e^z z^k dz$$

$$= \frac{a_3}{a_2}\psi_4(r, \gamma^*) \quad (60)$$

$$\psi_2{}^{**}(x, \tau^*) = \frac{1}{a_2}\int_0^{\tau^*} e^{-\frac{s}{a_2}} I_0\left[2\left(\frac{xs}{a_2a_4}\right)^{1/2}\right] ds$$

$$= \frac{1}{a_2}\sum_{k=0}^{\infty}\frac{\left(\frac{x}{a_2a_4}\right)^k}{(k!)^2}\int_0^{\tau^*} e^{-\frac{s}{a_2}} s^k ds = \sum_{k=0}^{\infty}\frac{\left(\frac{x}{a_4}\right)^k}{(k!)^2}\int_0^{\frac{\tau^*}{a_2}} e^{-z} z^k dz$$

$$= \sum_{k=0}^{\infty}\frac{s^k}{(k!)^2}\int_0^{q^*} e^{-z} z^k dz = \psi_2{}^{**}(s, q^*) \quad (61)$$

$$\psi_5(x, \tau^*) = \frac{1}{a_2}\int_0^{\tau^*} s e^{-\frac{s}{a_2}} I_0\left[2\left(\frac{xs}{a_2a_4}\right)^{1/2}\right] ds$$

$$= \frac{1}{a_2}\sum_{k=0}^{\infty}\frac{\left(\frac{x}{a_2a_4}\right)^k}{(k!)^2}\int_0^{\tau^*} e^{-\frac{s}{a_2}} s^{k+1} ds$$

$$= a_2\sum_{k=0}^{\infty}\frac{\left(\frac{x}{a_4}\right)^k}{(k!)^2}\int_0^{\frac{\tau^*}{a_2}} e^{-z} z^{k+1} dz = a_2\sum_{k=0}^{\infty}\frac{s^k}{(k!)^2}\int_0^{q^*} e^{-z} z^{k+1} dz$$

$$= a_2\psi_5(s, q^*) \quad (62)$$

$$\psi_6(x, \tau^*) = \frac{1}{a_2}\int_0^{\tau^*} s^2 e^{-\frac{s}{a_2}} I_0\left[2\left(\frac{xs}{a_2a_4}\right)^{1/2}\right] ds$$

$$= \frac{1}{a_2}\sum_{k=0}^{\infty}\frac{\left(\frac{x}{a_2a_4}\right)^k}{(k!)^2}\int_0^{\tau^*} e^{-\frac{s}{a_2}} s^{k+2} ds$$

$$= a_2{}^2\sum\frac{\left(\frac{x}{a_4}\right)^k}{(k!)^2}\int_0^{\frac{\tau^*}{a_2}} e^{-z} z^{k+2} dz$$

$$= a_2{}^2\sum_{k=0}^{\infty}\frac{s^k}{(k!)^2}\int_0^{q^*} e^{-z} z^{k+2} dz = a_2{}^2\psi_6(s, q^*) \quad (63)$$

DISCUSSION

G. M. Dusinberre[4]

While this paper is admirable from the point of view of applied mathematics, it is open to a number of criticisms from the point of view of practical engineering:

1 It is much too difficult a way to solve a relatively easy problem.

2 The assumptions are quite restrictive. Assumption (*f*), that heat generation is constant with length, practically excludes many applications to nuclear reactors.

This type of problem is readily solved by the methods of the authors' reference [12], with the addition of a heat-generation term. In fact, a simple hand calculation will easily reproduce the result shown in Fig. 6 of the paper.

Table 2 of this discussion shows data from Fig. 6, from the authors' reference [1], and certain data which were not stated by the authors and had to be assumed. (The quantitative agreement of the results depends on a lucky guess as to the specific heat of the material. Qualitative agreement would have been attained in any case.)

Table 2

From Fig. 6

v = 2.76 fps	t_0 = 61 F
q = 9.78 kw	$t_{mean} \cong$ 80 F

From reference [1]

ID = 1/2 in.	Length = 35 in.
OD = 9/16 in.	Material—stainless steel

Assumed

ρ = 500 pcf	c_p = 0.120 Btu/lb deg F

Table 3

Flow area, $A_f = 1.364 \times 10^{-3}$ sq ft
Heat-transfer area, $A_h = 0.382$ sq ft
Surface coefficient, $h = 700$ Btu/hr sq ft deg F
Flow rate, $w = 2.76 \times 3600 \times 62.2 \times 1.364 \times 10^{-3} = 844$ lb per hr
Capacity rate, $V = 844 \times 1.0 = 844$ Btu/hr deg F
Heat generation, $\bar{q} = 9.78 \times 3413 = 33{,}400$ Btu/hr
Steady-state temperature rise = 33,400/844 = 39.6 deg F
Weight of tube = 0.526 lb
Heat capacity of tube, $\bar{W} = 0.526 \times 0.120 = 0.0631$ Btu/deg F
Weight of water in tube = 0.248 lb
Heat capacity of water, $\bar{C} = 0.248$ Btu/deg F
Surface conductance of tube, $\bar{H} = 0.382 \times 700 = 267$ Btu/hr deg F

Table 3 of this discussion shows certain preliminary calculations of a routine nature. Table 4 shows the actual calculation of the first 2 sec of transient (*a*) of Fig. 6. If the results of column 4 and column D are plotted on that figure, it will be seen that the discrepancy is negligible.

The preliminary calculations took about an hour. The time required for the calculations in Table 4, by slide rule, was 24 min. This seems to substantiate the claim that the authors' method is too difficult a way to solve a relatively simple problem.

It must be noted that an extremely crude subdivision has been used, and in spite of this the results are comparable with those of the paper. The numerical analysis may be refined to any degree which is warranted by the precision of the data. At the same time the computer programming is elementary. All the detailed calculations are explicit. No evaluation of series is required.

It was observed that condition (*f*) is quite restrictive in nuclear-reactor applications. But in the numerical analysis there is no difficulty in introducing information as to the actual distribution of the heat generation.

To demonstrate this, Table 5, herewith, shows the result of calculations for the same total generation as the foregoing, but with 45.6 per cent of the generation in the middle third of the tube. The calculation runs for 3 sec, and the steady-state data are also shown. Column D is not computed, as the highest wall temperature is found near the center.

For a crude solution, assume three subdivisions, as in Fig. 1 of reference [12].

$H = 267/3 = 89$ $\quad W = 0.0631/3 = 0.0210$
$C = 0.248/3 = 0.0827$ $\quad q = 33{,}400/3 = 11{,}130$
$H/2V = 89/1688 < 1$
$\Delta\tau < W/H = 0.0201/89 = 0.000275$ hr $= 0.99$ sec

[4] Department of Mechanical Engineering, The Pennsylvania State University, University Park, Pa. Fellow ASME.

Table 4

Point	1	A	2	B	3	C	4	D
Coefficients		0.196	0.895	0.196	0.895	0.196	0.895	
		0.608	0.100	0.608	0.100	0.608	0.100	1.5
		0.196	0.005	0.196	0.005	0.196	0.005	−0.5
Q		49.0		49.0		49.0		
$\tau/\Delta\tau$								
0	0	0	0	0	0	0	0	0
1	0	49.0		49.0		49.0		49.0
		0	0	0	0	0	0	0
		29.8	4.4	29.8	4.4	29.8	4.4	
		0	0	0	0	0	0	
		49.0		49.0		49.0		
2	0	78.8	4.4	78.8	4.4	78.8	4.4	78.8
		0	0	0.9	3.9	0.9	3.9	
		47.9	7.9	47.9	7.9	47.9	7.9	
		0.9	0	0.9	0	0.9	0	
		49.0		49.0		49.0		
3		97.8	7.9	98.7	11.8	98.7	11.8	98.7
		0	0	1.5	7.0	2.3	10.6	
		59.5	9.8	60.0	9.9	60.0	9.9	
		1.5		2.3	0.1	2.3	0.1	170.4
		49.0		49.0		49.0		56.4
4	0	110.0	9.8	112.8	17.0	113.6	20.6	114.0
		0	0	1.9	8.8	3.3	15.2	
		66.9	11.0	68.5	11.3	69.0	11.4	
		1.9		3.3	0.1	4.0	0.1	188.0
		49.0		49.0		49.0		61.4
5	0	117.8	11.0	122.7	20.2	125.3	26.7	126.6
		0	0	2.2	8.9	4.0	18.1	
		71.5	11.8	74.5	12.3	76.2	12.5	
		2.2	0.1	4.0	0.1	5.2	0.1	201.6
		49.0		49.0		49.0		64.8
6		122.7	11.9	129.7	21.3	134.4	30.7	136.8

Table 5

Point	1	A	2	B	3	C	4
$\tau/\Delta\tau$							
0	0	0	0	0	0	0	0
1	0	40.0	0	67.0	0	40.0	0
2	0	64.3	4.0	107.7	6.7	64.3	4.0
3	0	79.9	6.4	134.5	14.4	81.2	12.4
4	0	89.8	8.0	152.7	19.2	94.5	21.1
5	0	96.1	9.0	165.0	22.6	105.4	26.7
6	0	100.3	9.6	173.5	24.7	113.7	30.8
7	0	102.9	10.0	179.1	26.1	119.9	33.7
8	0	104.5	10.4	183.0	27.0	124.6	35.6
9	0	105.5	10.5	185.3	27.7	127.9	36.9
∞	0	107.4	10.8	190.8	28.8	136.2	39.6

$$\Delta\tau < \frac{2C}{2V + H} = \frac{2 \times 0.0827}{1688 + 89} = 0.0000931 \text{ hr} = 0.335 \text{ sec}$$

Choose $\Delta\tau = {}^1/_2$ sec $= 1/10{,}800$ hr
1, 2, 3, 4 designate points in the fluid
A, B, C designate intermediate points in the wall
D designates outlet end of wall, extrapolated

$$F_{A2} = \frac{H\Delta\tau}{C} = \frac{89}{0.0827 \times 10{,}800} = 0.100$$

$$F_{12} = \frac{(2V - H)\Delta\tau}{2C} = \frac{1599}{0.1654 \times 10{,}800} = 0.895$$

$$F_{22} = 1 - 0.100 - 0.895 = 0.005$$

$$F_{1A} = F_{2A} = \frac{H\Delta\tau}{2W} = \frac{89}{0.042 \times 10{,}800} = 0.196$$

$$F_{AA} = 1 - 0.196 - 0.196 = 0.608$$

$t_2' = 0.895t_1 + 0.100t_A + 0.005t_2$, etc.

$t_A' = 0.196t_1 + 0.196t_2 + 0.608t_A + 49.0$, etc.

Use linear extrapolation for t_D

$$t_D' = 1.5t_C' - 0.5t_B'$$

$$Q = \frac{q\Delta\tau}{W} = \frac{11{,}130}{0.0210 \times 10{,}800} = 49.0 \text{ deg}$$

Authors' Closure

We appreciate the contribution Professor Dusinberre has made in his discussion of our work but regret that he has not also taken this opportunity to show in a broader sense the relationship among various computational procedures for engineering problems. Our problem and analytical solution and Professor Dusinberre's method provide an excellent vehicle for doing this. It should be pointed out that Professor Dusinberre has directed his discussion entirely to the results of our two previous papers [1, 2]. The subject of this present paper, which is an extension of our work reported in [1, 2] and significantly broadens it, is not specifically discussed.

It is possible that Professor Dusinberre has overlooked the principal purpose of our work. It was not our intent to determine the dynamic response of a ${}^1/_2$-in. ID stainless-steel tube having a ${}^1/_{32}$-in. wall thickness and a length of about 3 ft, as Professor Dusinberre appears to suggest, nor to solve any other specific heat-exchanger problem. Rather, it was to obtain a rigorously complete and resolutely exact analytical solution to a model

which closely resembles the physical system corresponding to an important engineering problem of current interest—the heat exchanger having internal heat sources. We know of no such previous published solution, although the literature is quite large on problems of a similar nature. Mathematical solutions continuous in space and time have the advantage of exactness and are subject to parameterization, as is well known.

We shall not attempt to defend our solution "from the point of view of practical engineering" as this type of criticism is pretty much a matter of experience, the demands of one's professional work and his personal taste. What is practical to one person may be impractical to another, etc. However, within our own experience we have found the use of applied mathematics to be of great value in the solution of engineering problems. But this does not constitute our defense of applied mathematics as it requires no defense, at least not by us. We wish to be careful, however, to emphasize that we also have found numerical methods to be powerful tools in engineering practice and we have used them in instances where a solution to a problem could be obtained in no other way. We are in full agreement with Professor Dusinberre on the importance of numerical methods and we fully support his emphasis of this. In fact, as we have attempted to make clear in the introduction to this paper and in both the previous papers [1, 2], we recognize that a numerical solution to a problem of this sort is often convenient and practical. Actually, in obtaining our "analytical" solution we had to resort to numerical procedures which required the use of an IBM 650 computer, as was indicated. Furthermore, as we already have stated Silvers and Dietrich [15] have used numerical methods in the solution of the response of a specific heterogeneous nuclear reactor. Hence, it does not seem necessary to redemonstrate this, as Professor Dusinberre has done, although it probably is of some value to reemphasize the use and importance of numerical methods. We thought we had freely recognized that in the paper.

Like analytical methods, numerical procedures require no defense nor apology. Both are well established, recognized techniques used often in concert to bring about a solution to an engineering problem. We would champion the knowledge of both for engineers, not one to the exclusion of the other.

Professor Dusinberre states that our solution is much too difficult. The task of obtaining it was great but now that it has been found and the necessary functions given it is irrelevant to be concerned with the magnitude of our task, since to use our results does not require one to repeat the efforts we put into the problem. Certainly one does not have to evaluate a single series. We already have done that. The use of our results is quite simple, requiring a knowledge only of algebra, while considerably more knowledge and experience is required to solve the same problem by numerical methods.

In a sense Professor Dusinberre's criticisms are not reasonable. He states that by using even a crude subdivision his numerical computations provide a result essentially equivalent to ours and implies, therefore, the futility of all but a numerical solution to this problem. But this is hardly a proper evaluation of this situation. It is important to recognize that in forming this conclusion he relies on our exact solution as a criterion for the completeness of his own numerical solution. That is why he stresses the importance of the essential agreement between his solution and ours. However, the question now arises as to what one would do if an exact solution were not available. Would one be satisfied with a network as crude as dividing a channel length into thirds? We doubt it, if a solution is being sought to a significant engineering problem. Does Professor Dusinberre's result now mean that it is unnecessary to divide a channel into any subdivisions smaller than one third? Probably not. Hence, it is only *because* he has our exact solution that he is able in a single attempt with a crude network to obtain a solution with which he is satisfied. Without the results of an exact solution available considerably more effort would be required to obtain the solution by numerical means than the one hour and 24 minutes it took Professor Dusinberre. It would be our guess that something like two or three more finer networks would be tried to establish the convergence of the solution to its true value. In such a case the time required would be considerably greater even for an experienced worker. In this regard it is important to remember that Professor Dusinberre's solution has been produced by one of the highest authorities on the subject of numerical methods and his one hour and 24 minute computation time cannot be taken as par for the course. While this is somewhat speculative, it would seem to us that an engineer with average experience in these matters could well take something more like two days to work out a satisfactory numerical solution to this type of problem and still give due consideration to the convergence and stability of his result.

We believe that what this discussion really has shown is the interplay between an exact analytical solution and a numerical solution to the same problem. The former often is of great value in computational work as a check solution on a numerical program, acting as an important point of reference.

It is possible to bring about a simplification of our results in another way. Taking equation (48) as an example, we find that the complex form of the final solution arises from the term

$$e^{\frac{1}{\frac{a_2 a_4}{x}\left(\frac{1}{a_3}+p\right)}}$$

However, by the use of reduction techniques given in reference [5] this term may be approximated as follows:

$$e^{\frac{1}{\frac{a_2 a_4}{x}\left(\frac{1}{a_3}+p\right)}} \sim \frac{a_4}{a_2 x} \cdot \frac{e^{\frac{x}{a_4}}}{\frac{a_4}{a_2 x}+p}$$

If this approximate form is substituted into equation (48) one finds:

$$\frac{\overline{\Delta t_2}}{\frac{a_1 b_2}{b_1^2}} = a_3\left(\frac{b_1}{b_2}\right)^2 \frac{\bar{\Phi}}{\frac{b_1}{b_2}+p} + \left(\frac{b_1}{b_2}\right)^2 e^{-\frac{x}{u}p} \cdot \frac{\bar{\Phi}}{\left(\frac{b_1}{b_2}+p\right)} \cdot \frac{\frac{a_4}{a_2 x}}{\left(\frac{1}{a_2}+p\right)\left(\frac{a_4}{a_2 x}+p\right)}$$

If we let $\bar{\Phi} = \frac{\Delta p_x''}{\tau_0} \cdot \frac{1}{p^2}$ then an inverse transformation of the foregoing gives the following two results

(*i*) $0 \leq \frac{\tau u}{x} \leq 1$

$$\frac{\Delta t_2(\tau)}{\frac{\Delta p_x''}{\tau_0} \cdot \frac{a_1 b_2}{b_1^2}} = a_3\left(e^{-\frac{b_1}{b_2}\tau} + \frac{b_1}{b_2}\tau - 1\right) \qquad \text{(EXACT)}$$

(ii) $\dfrac{\tau u}{x} \geq 1$ (EXACT)

$$\frac{\Delta t_2(x,\tau)}{\dfrac{\Delta p_x''}{\tau_0}\cdot\dfrac{a_1 b_2}{b_1^2}} = \frac{\Delta t_2(\tau)}{\dfrac{\Delta p_x''}{\tau_0}\cdot\dfrac{a_1 b_2}{b_1^2}} + \underbrace{\qquad\qquad\qquad\qquad}_{\text{(APPROXIMATE)}}$$

$$+\frac{a_4}{a_2 x}\left(\frac{b_1}{b_2}\right)^2\left[N\tau^* - \frac{a_2^2 a_3}{B}\left(1 - e^{-\frac{\tau^*}{a_2}}\right)\right.$$

$$\left. - \frac{a_2}{A}\left(\frac{b_2}{b_1}\right)^2\left(1 - e^{-\frac{b_1}{b_2}\tau^*}\right) + \frac{\left(\dfrac{a_2 x}{a_4}\right)^2\left(1 - e^{-\frac{a_4\tau^*}{a_2 x}}\right)}{AB}\right]$$

where

$$N = \frac{a_2 a_3}{B}\left(1 + \frac{B}{A}\,\frac{b_2}{a_2 b_1} - \frac{x/a_2 a_4}{A}\right)$$

$$A = \frac{b_1}{b_2} - \frac{a_4}{a_2 x}$$

$$B = \frac{a_4}{a_2 x} - \frac{1}{a_2}$$

This approximation, which also could be applied to equation (47) for $\bar{\theta}_2$ and reduced to $\theta_2(x, \tau)$, requires the calculation of three x-dependent parameters and the use of three exponential functions. However, only the use of algebra is necessary and the time required to obtain a solution would be no longer than that for Professor Dusinberre's method.

Heating and Cooling Air and Carbon Dioxide in the Thermal Entrance Region of a Circular Duct With Large Gas to Wall Temperature Differences[1]

HELMUT WOLF

Senior Research Engineer,
Research Center, Rocketdyne,
A Division of North American Aviation, Inc.,
Canoga Park, Calif. Assoc. Mem. ASME

The local heat-transfer characteristics for air and carbon dioxide in the thermal entrance region have been determined experimentally and are compared with predicted values computed from an extension of the theoretical analysis due to Deissler. The experiments were conducted in smooth round tubes having a fully developed turbulent velocity profile and a uniform temperature distribution at the entrance. The boundary conditions of uniform heat flux for heating the gas, and wall temperature constant and variable with axial distance for cooling the gas, were investigated with large temperature differences between the gas and the tube wall. For heating, the experimental results yielded one per cent thermal entrance lengths ranging from 11 to 27 diameters over the bulk Reynolds number range from 50,000 to 246,000. For cooling, one per cent thermal entrance lengths ranging from 12 to 26 diameters were obtained for bulk Reynolds numbers ranging from 17,000 to 218,000. The agreement between theory and experiment was favorable in most cases.

Introduction

WHEN A FLUID FLOWING ADIABATICALLY in a circular duct enters a region having a wall temperature different from that of the fluid, the temperature difference may be treated mathematically as a discontinuity. At that cross section, *termed the entrance*, the temperature gradient in the fluid layer near the wall is, in theory, infinite. The resulting local heat-transfer coefficient and Nusselt number are in theory likewise infinite and decrease rapidly in the direction of fluid flow. In the design of heat-transfer apparatus, it is of considerable interest that quantitative data be available regarding the rate of heat transfer to or from the fluid as a function of the distance from the entrance.

This paper summarizes the results of an analytical and experimental investigation of the heat-transfer characteristics of air and carbon dioxide in turbulent flow in the entrance region of a smooth round duct with large temperature differences between the gas and the wall. In the analytical investigation the fluid was assumed to have a fully developed velocity profile and a uniform temperature profile at the cross section where energy exchange was initiated. In the experimental investigations, a duct length 30 diameters long was provided upstream to the test sections to insure a fully developed velocity profile (with a uniform temperature profile) at the entrance [24].[2]

Theoretical calculations of heat transfer in the entrance region are presented in references [1, 2, 3, 4, 5, 6] for the flow of fluids in tubes and in references [3, 7, 8] for flow between flat plates with the wall temperature constant with axial distance. References [5, 9, 7, 20] discuss the calculation of heat transfer in the entrance region for the constant heat flux boundary condition, but assumed that the physical properties of the flowing fluid did not vary with temperature. Only the analyses presented in references [5, 9] permit including the temperature dependence of the fluid physical properties. Experimental determinations of heat transfer in the entrance region are reported in references [10, 11, 12, 13] for Prandtl numbers ranging from 0.7 to 350 and for temperature differences between the fluid and the wall ranging from 8 to 390 R. Cooling experiments with large temperature differences are described in reference [14] at a Reynolds number of approximately 10,000; however, the variation of the local heat-transfer coefficient with axial distance was not determined.

The investigation reported herein encompasses the following conditions: $|\bar{t}_w - \bar{t}_b| > 400$ R, Reynolds numbers ranging from 17,000 to 246,000, Prandtl number 0.7, and for heating and cooling the gases.

[1] The research reported in this paper was performed at the Jet Propulsion Center, Purdue University, and was sponsored by Project SQUID.

Contributed by the Heat Transfer Division and presented at the Semi-Annual Meeting, St. Louis, Mo., June 14–18, 1959, of THE AMERICAN SOCIETY OF MECHANICAL ENGINEERS.

NOTE: Statements and opinions advanced in papers are to be understood as individual expressions of their authors and not those of the Society. Manuscript received at ASME Headquarters, March 4, 1959. Paper No. 59—SA-15.

[2] Numbers in brackets designate References at end of paper.

Nomenclature

A_i = inner surface area of the test section, ft²

A_c = cross-sectional area of the duct, ft²

c_p = specific heat at contant pressure, Btu/lb

D = inner tube diameter, ft

e = heat balance, per cent

g = gravitational constant, 32.17 ft/sec²

h_x = local heat-transfer coefficient, Btu/hr ft² R

h_∞ = asymptotic heat-transfer coefficient, Btu/hr ft² R

k = thermal conductivity, Btu/hr ft R

L = heated length of the tube, ft

L_{A1} = one per cent entrance length, diameters

L_{A5} = five per cent entrance length, diameters

Nu = Nusselt number, hD/k

N_{Re} = Reynolds number, $(D/A_c g)w_g/\mu$

N_{Pr} = Prandtl number, $3600gc_p\mu/k$

Q_{Ai} = energy per unit time passing through A_i, Btu/sec

Q_g = energy per unit time absorbed by or extracted from the gas in passing through the test section, Btu/sec

(*Continued on next page*)

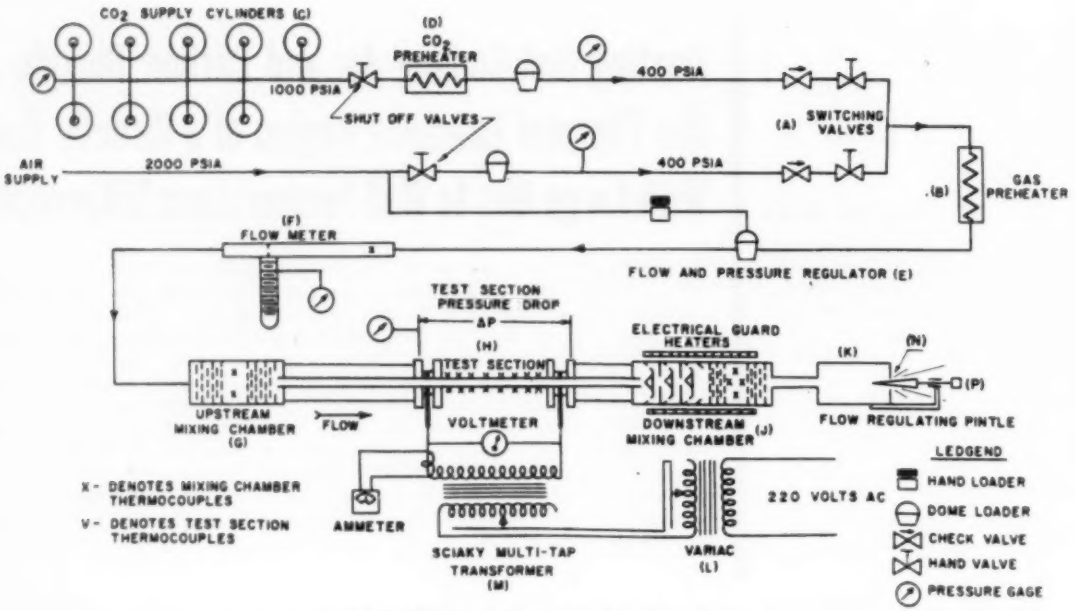

Fig. 1 Schematic flow diagram of heating system

Experimental Apparatus

Two different sets of apparatus were employed for the *heating* and the *cooling* experiments. Each apparatus was designed so that either air or carbon dioxide could be admitted to the test sections without interrupting the gas flow. The gas-flow rate was measured with calibrated sharp-edged orifices in conjunction with appropriate water manometers. Simultaneous control of a dome loaded pressure regulator and a variable area orifice downstream from the test section permitted varying the gas-flow rate in the test section while maintaining the pressure at its entrance at a selected value.

Apparatus for Heating Experiments. Fig. 1 presents the flow diagram for the apparatus employed in the heating experiments. Three different test sections, fabricated from Haynes Alloy 25 (L605) tubing, were employed in the heating experiments. All of the tubes had an ID = 0.569 in. and an OD = 0.629 in.; their L/D ratios were 21.1, 40.3, and 59.75. Each test section for the heating and cooling experiments was preceded by a 30-diameter isothermal starting length and followed by a 10-diameter isothermal length. The surface temperature of each test section was measured at 16 stations along its length by chromel-alumel thermocouples capacitance welded to the surface. The temperature of the gas in the inlet and exit mixing chambers was measured with chromel-alumel thermocouples carefully calibrated against a standard platinum versus platinum-10-per-cent-rhodium thermocouple whose emf-temperature relationship was determined by the National Bureau of Standards, Washington, D. C.

Apparatus for Cooling Experiments. Fig. 2 presents the flow diagram of the system employed in the cooling experiments. Suitable baffles were provided in the mixing chambers for thoroughly mixing the gas prior to measuring its temperature with calibrated shielded platinum versus platinum-10-per-cent-rhodium thermocouples. The test section was fabricated from type 347 stainless-steel pipe, precision ground to 0.535 in. OD and internally

Nomenclature

q_w = energy per unit time and area passing through the wall at location x, Btu/ft² sec
r = radial distance from the center line of the duct, ft
t = temperature at the point (x, y)
t_s = temperature of the gas at $x < 0$, constant with respect to y
t_δ = temperature at the location $y = \delta_h$
t^+ = nondimensional temperature, $(1 - t/t_w)/\beta$
u = velocity in the x direction at the point (x, y)
u^+ = nondimensional velocity, $u/\sqrt{\tau_w/\rho_w}$
x = co-ordinate parallel to the wall, ft ($x = 0$ at the entrance)
y = co-ordinate perpendicular to the duct wall, ft
y^+ = nondimensional distance from the wall, $y\sqrt{\tau_w/\rho_w}/(\mu_w/\rho_w)$
α = ratio ϵ_H/ϵ_M
β = heat-transfer parameter for wall temperature invariant with axial distance, $q_w\sqrt{\tau_w/\rho_w}/c_p g\tau_w t_w$
δ_h = thickness of the thermal boundary layer
ϵ_H, ϵ_M = eddy diffusivity for heat and momentum, respectively
ρ = mass per unit volume, lb sec²/ft⁴
μ = dynamic viscosity, lb sec/ft²
τ = shearing stress, lb/ft²

Subscripts

b = pertaining to or evaluated at the bulk temperature
i = pertaining to or evaluated at the initial temperature
w = pertaining to or evaluated at the wall temperature
δ = pertaining to the thermal boundary layer

Superscripts

$*$ = pertaining to a nominal value
$R\beta$ = corrected to a nominal value of Reynolds number and β
$-$ = a bar over the symbol denotes an average quantity over the length of the test section, L

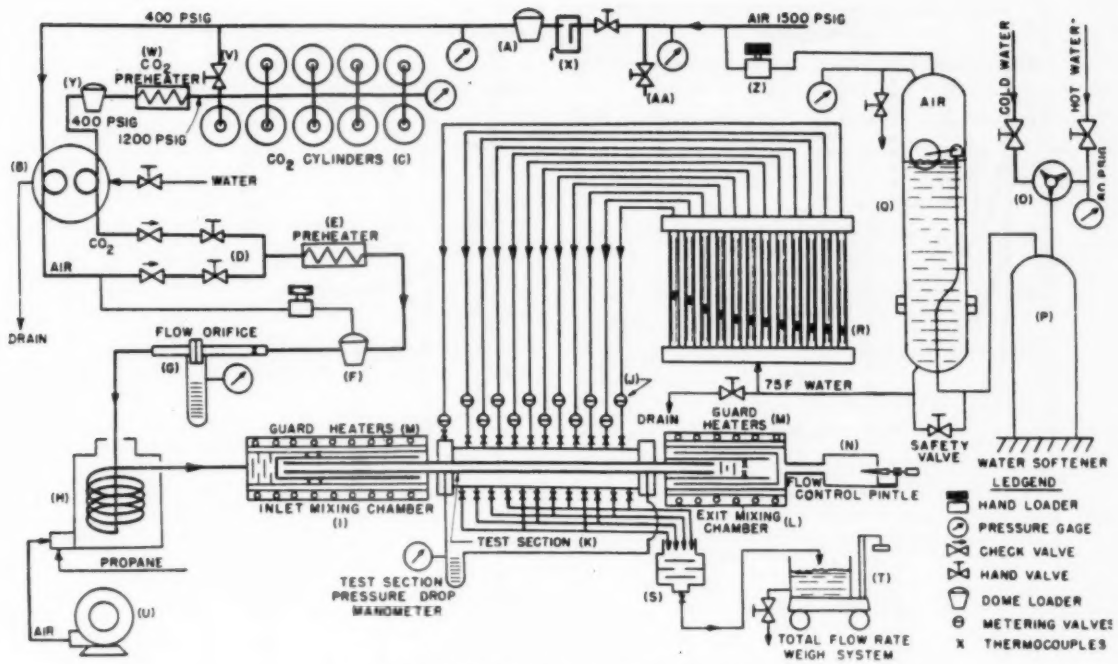

Fig. 2 Schematic flow diagram of cooling apparatus

precision bored and polished to 0.384 in. ID, and was fitted with a cooling jacket containing 12 separate cooling sections. Water was employed as the coolant in the experiments with low values of the wall temperature. The flow rates of the cooling water to the individual sections were measured with 12 calibrated rotameters. Fig. 2 also shows the system employed for supplying a uniform rate of cooling water at constant temperature to the test section cooling jacket. At values of the wall temperature greater than 710 R, the test section was cooled with air.

A detailed description of the components employed in the heating and cooling systems and of the various calibrations is given in reference [16].

Heat Balance. The heat balance e, stated in per cent, is defined by

$$e = [(Q_e - Q_{Ai})/Q_e]100 \quad (1)$$

For the electrically heated test sections, the quantity Q_{Ai} was computed as the difference between the energy Q_e generated by the current passing through the wall of the test section and the energy loss Q_L by conduction through the insulation surrounding it. For the cooling experiments, the quantity Q_{Ai} was assumed equal to the sensible energy increase Q_c of the coolant. The average of the *absolute* values of the heat balances obtained for the heating and cooling experiments with air and carbon dioxide are summarized in Table 1.

Table 1 Average absolute values of the heat balance

Heating experiments; air	3.05 per cent
Heating experiments; carbon dioxide	2.16 per cent
Cooling experiments; air	3.40 per cent
Cooling experiments; carbon dioxide	3.45 per cent

Experimental Results

Local Heat-Transfer Characteristics, Heating. Since the heating experiments were conducted in three different test sections, it was not possible in the experiments to maintain identical flow conditions in all three test sections. Also, the local values of the heat-transfer parameter β (the parameter β is a measure of the intensity of the heat transfer and may be considered approximately proportional to the wall-to-bulk temperature difference) were not constant along the length of a test section. Consequently, to correlate the results for the three test sections, the local Nusselt numbers were corrected to a nominal value for the bulk Reynolds number $N_{Re}{}^*$ and β^*. The method of making the afore-mentioned correction is presented in detail in reference [16]. The wall shear was evaluated from the experimentally measured friction pressure drop based upon the average bulk velocity of the gas (computed from $\bar{p}_b$ and $\bar{t}_b$) in the test section. Reference [16], p. 174, part II, gives a detailed derivation and discussion of the parameter β. The corrected values of the local Nusselt number $Nu_b{}^{R\beta}$ for air and carbon dioxide are presented in Fig. 3 as functions of the axial distance x/D, with $N_{Re}{}^*$ and β^* as parameters. It is seen from Fig. 3 that $Nu_b{}^{R\beta}$ decreases continuously along the length of the test section, due to the increase in the thermal conductivity of the gas with the bulk temperature. The latter figure demonstrates that as β^* is decreased from 0.04 to 0.03 the value of $Nu_b{}^{R\beta}$ decreases more rapidly at the higher values of $N_{Re}{}^*$. The aforementioned trend is in agreement with that predicted by theory [15, 16]. The Nusselt number $Nu_b{}^{R\beta}$ was computed by evaluating the physical properties of the gas at the local bulk temperature and correlated with the parameter β. Deissler [5] recommends the parameter $\phi = q_w/c_p\rho_i u_i t_i$ for correlating constant heat-flux data with the physical properties evaluated at the initial temperature t_i. The parameter ϕ is employed in the discussion of the thermal entrance length. The experimental values of the local heat-transfer coefficients for the heating experiments are presented in reference [16].

Local Heat-Transfer Characteristics, Cooling. Fig. 4(*a*) presents the local Nusselt number Nu_b for air [Fig. 4(*b*) for carbon dioxide] at constant wall temperature as a function of the dimensionless axial

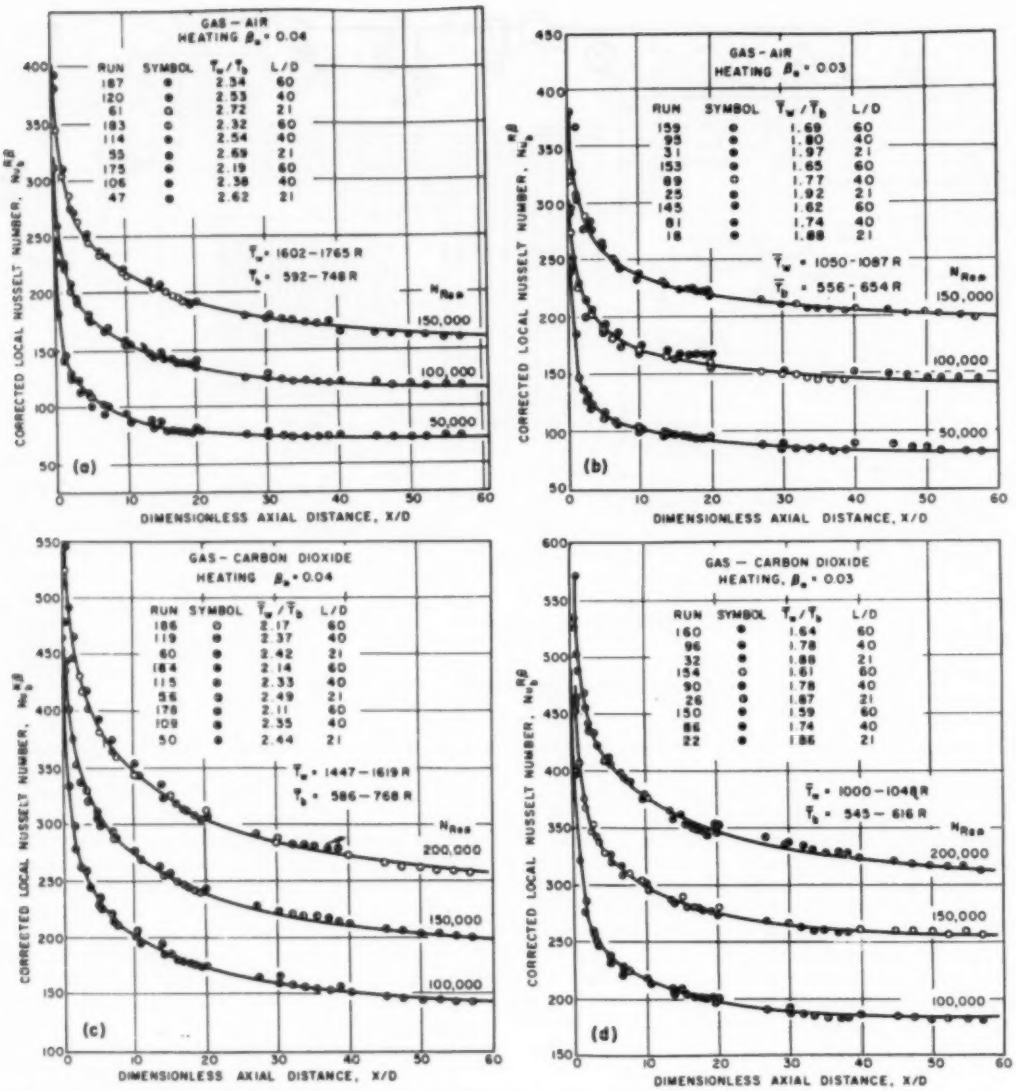

Fig. 3 Variation of corrected local Nusselt number with x/D for air and carbon dioxide; uniform initial temperature profile, fully developed initial velocity profile, constant heat flux

distance x/D with the Reynolds number as a parameter. The results presented in Figs. 4(*a* and *b*) demonstrate that, after the initial decrease in Nu_b caused by the developing temperature profile in the entrance region, the value of Nu_b continued to increase in the direction of flow. The increase in Nu_b is attributed to the decrease in the thermal conductivity of the gas with the local bulk temperature. The experiments conducted at low values of the average bulk temperature $\bar{t}_b$ = 750 R yielded a practically constant value for Nu_b with distance, as was expected. Fig. 4(*c*) presents the local Nusselt number Nu_b for air [Fig. 4(*d*) for carbon dioxide] as a function of the dimensionless axial distance x/D, with the wall temperature varying in the axial direction. Figs. 4(*c* and *d*) demonstrate that Nu_b did not vary appreciably with axial distance for either increasing or decreasing wall temperature gradient over the range of variables shown in the figures. The latter results may be attributed to the fact that for $\partial t_w/\partial x$ greater than zero, the local value of t_b does not decrease appreciably. Consequently, the thermal conductivity of the gas changes little along the length of the test section. For $\partial t_w/\partial x$ less than zero, the bulk temperature of the gas decreases rapidly with axial distance, and so does the thermal conductivity of the gas k_b. The experiments showed that the local heat-transfer coefficient h_x also decreased with axial distance. Apparently, the rates of decrease for h_x and k_b were such that the value for Nu_b remained constant.

The local heat-transfer coefficient h_x is defined by the following equation:

$$h_x = (q_w)/(t_w - t_b) \tag{2}$$

Expressing (q_w) by Fourier's law and substituting the result into equation (2) yields

$$h_x = k(\partial t/\partial y)_w/(t_w - t_b) \tag{3}$$

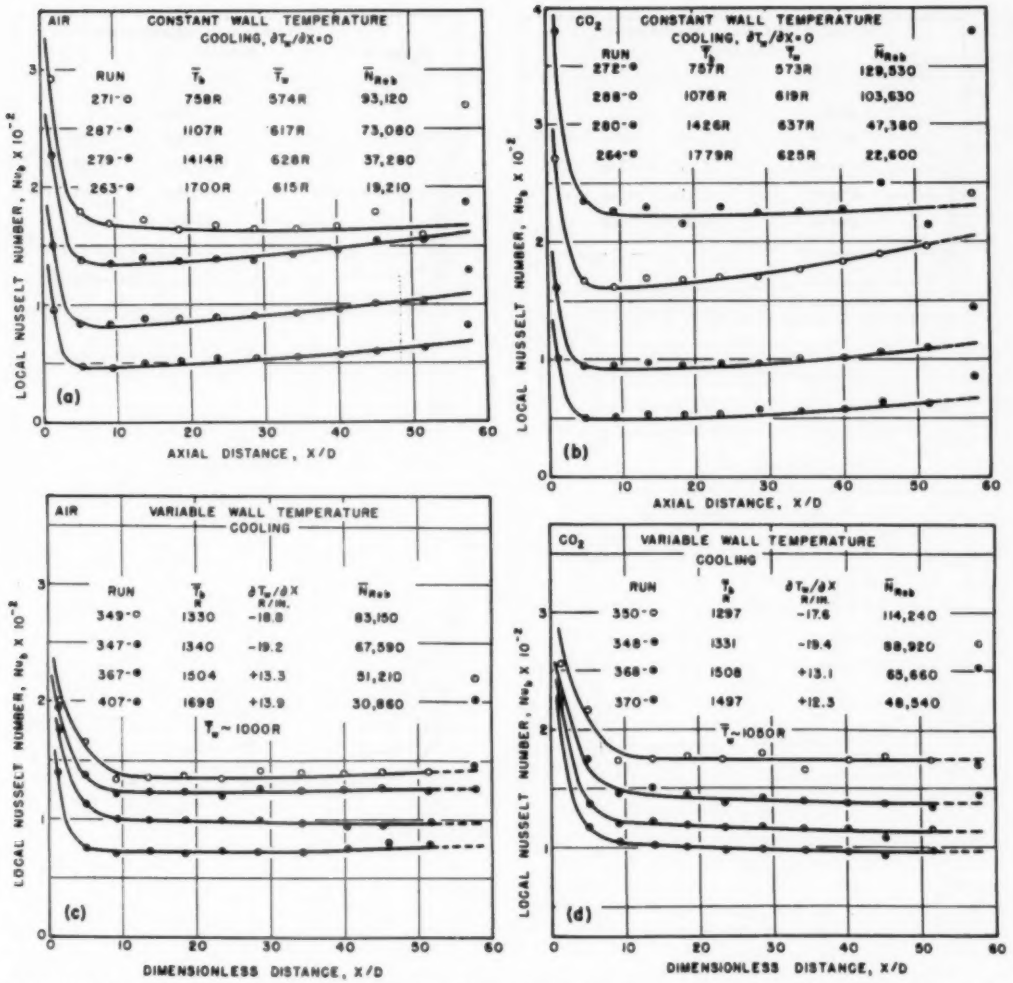

Fig. 4 Variation of local Nusselt number with x/D, Reynolds number, and wall temperature gradient for air and carbon dioxide; cooling

Analytic investigations of heat transfer in circular ducts have demonstrated that for laminar and turbulent flow [15, 17, 18] h_x decreases rapidly in the entrance region and then attains a substantially constant value. Reference to equation (3) shows that for h_x to remain constant outside the entrance region $(\partial t/\partial y)_w$ must vary in the same manner as $(t_w - t_b)$ for constant k. On the other hand, if the wall temperature is not constant with axial distance, then k in equation (3) varies with axial distance and so does $(t_w - t_b)$. Consequently, it cannot be expected that h_x will approach a constant value.

Fig. 5(*a*) presents the local heat-transfer coefficient h_x as a function of the axial distance x/D for air [Fig. 5(*b*) for carbon dioxide] for constant wall temperature. Figs. 5(*a* and *b*) demonstrate that after the first 12 to 26 diameters, depending on the Reynolds number, the value of the heat-transfer coefficient h_x is practically constant. Figs. 5(*c* and *d*) present h_x as a function of x/D for the cooling experiments conducted with air and carbon dioxide for positive and negative values of the wall temperature gradient. Figs. 5(*c* and *d*) demonstrate that for variable wall temperature h_x continues to decrease by a small amount for the entire length of the test section; h_x decreases more for carbon dioxide than for air.

Reference [16] presents tables of h_x, Nu_b, Nu_i, q_w, N_{Reb}, β, ϕ, t_b, and t_w as a function of x/D for the heating experiments and tables of h_x, Nu_b, q_w, N_{Reb}, β, t_w, and t_b as a function of x/D for the cooling experiments conducted with air and carbon dioxide.

Thermal Entrance Length. The thermal entrance length is defined as the distance from the entrance to the cross section where the temperature profile of the gas has no straight line portion perpendicular to the tube axis. A precise determination of the entrance length, as defined, requires a calculation or measurement of the thermal boundary layer. When that is not possible, the entrance length is determined as the distance required for either Nu or h_x to reach a value constant with axial distance. Figs. 3 through 5 and reference [19] demonstrate that, for fluids having physical properties that vary appreciably with temperature, the local Nusselt number is not a reliable criterion for establishing the value of the thermal entrance length. Accordingly, the thermal entrance lengths reported herein were inferred from the local heat-transfer coefficient h_x. Because it is difficult to determine precisely the point at which the local heat-transfer coefficient, when plotted as a function of x/D, reaches a value constant with x/D (denoted by h_a), it is convenient to define a "5 per cent" and a "1 per cent" entrance length L_{h5} and L_{h1}, respectively. The

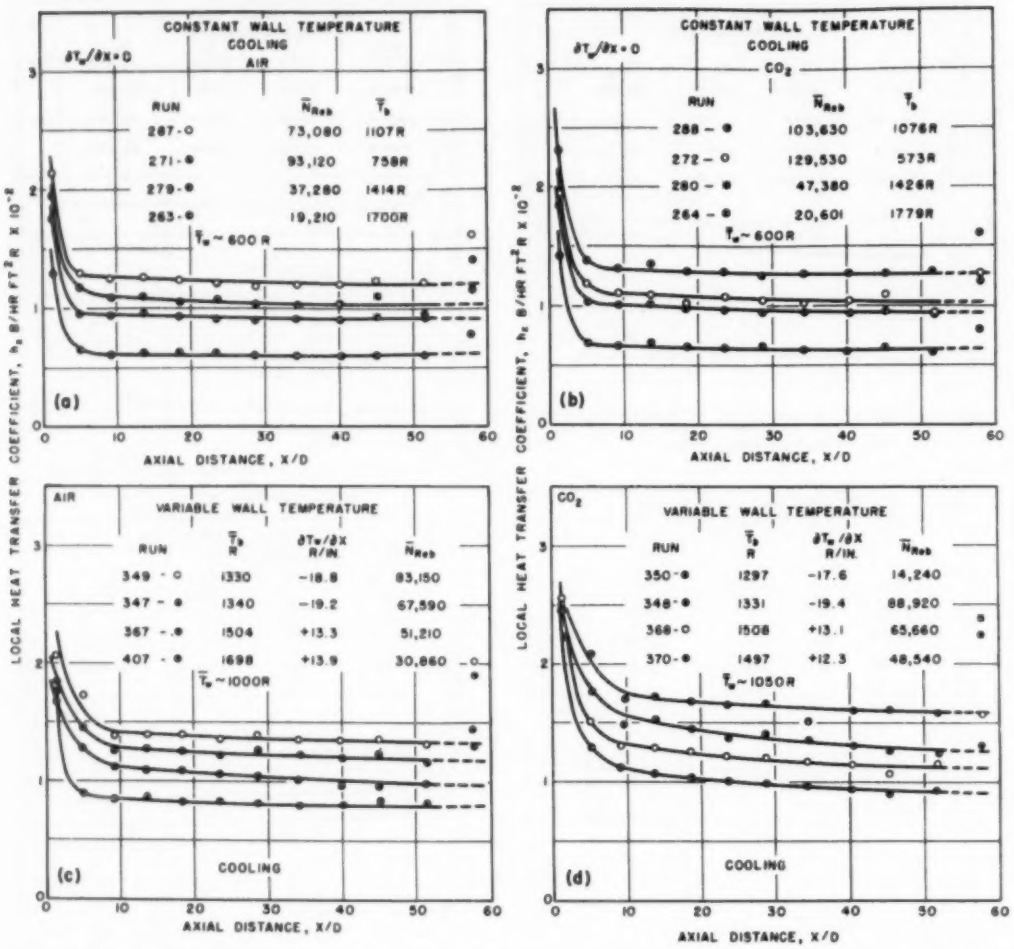

Fig. 5 Variation of local heat-transfer coefficient with axial distance, Reynolds number, and wall temperature gradient for air and carbon dioxide; cooling

quantity L_{h5} is the distance from the entrance to the cross section where $h_x = 1.05h_a$; similarly, L_{h1} is the distance from the entrance to the cross section where $h_x = 1.01h_a$.

Fig. 6 illustrates the variation of L_{h1} as a function of the initial Reynolds number N_{Re_i} with ϕ as a parameter for heating air and carbon dioxide. The results presented in Fig. 6 demonstrate that the values of L_{h1} for air are significantly larger than those for carbon dioxide at a given N_{Re_i}.

Fig. 7 presents the variation of L_{h1} as a function of the bulk Reynolds number with β as a parameter for cooling air and carbon dioxide with the wall temperature t_w constant with axial distance. The values of L_{h1} obtained for carbon dioxide are approximately 8 to 10 per cent smaller than those for air. The solid lines in Figs. 6 and 7 are the theoretically computed values for entrance length; the agreement between theory and experiment is conservative in all cases except that for heating carbon dioxide. Table 2 summarizes the range of values determined for L_{h1} and L_{h5} for the different experiments conducted by the writer.

Over the range of Reynolds numbers presented in Figs. 6 and 7, the values of L_{h1} can be represented, with an accuracy of ±10 per cent, by the following empirical equation:

$$L_{h1} = C\overline{N}_{Re}^{0.2} \tag{4}$$

Table 2 Range of experimental values for the thermal entrance length

Gas	L_{h5}	L_{h1}	N_{Re_i}	$\overline{N}_{Re_b}$
Air, heating CHF[a]	9–16	16–27	60,000 to 200,000	50,000 to 158,000
CO_2, heating CHF	6–9	11–19	100,000 to 300,000	96,000 to 246,000
Air, cooling CWT	7–12	16–25	...	25,000 to 152,000
Air, cooling VWT	8–43[b]	16–48[b]	...	20,000 to 94,000
CO_2, cooling CWT	5–14	12–26	...	23,000 to 218,000
CO_2, cooling VWT	12–28	20–38[b]	...	24,000 to 127,000

[a] CHF denotes constant heat flux.
CWT denotes wall temperature constant with axial distance.
VWT denotes variable wall temperature with axial distance.
[b] Estimated values.

Values of the constant C are given in Table 3 for heating and cooling air and carbon dioxide.

Table 4 summarizes and compares the results of other experimental determinations of entrance length with the results of the subject investigation. For fluids having Prandtl numbers

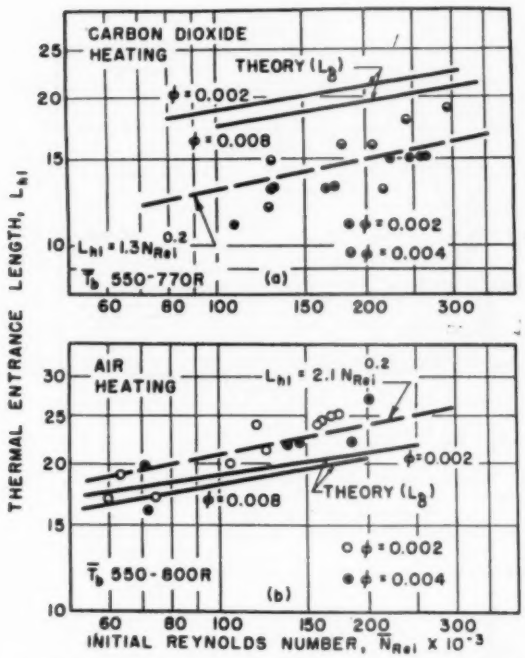

Fig. 6 Variation of thermal entrance length with initial Reynolds number and ϕ for air and carbon dioxide; heating, constant heat flux

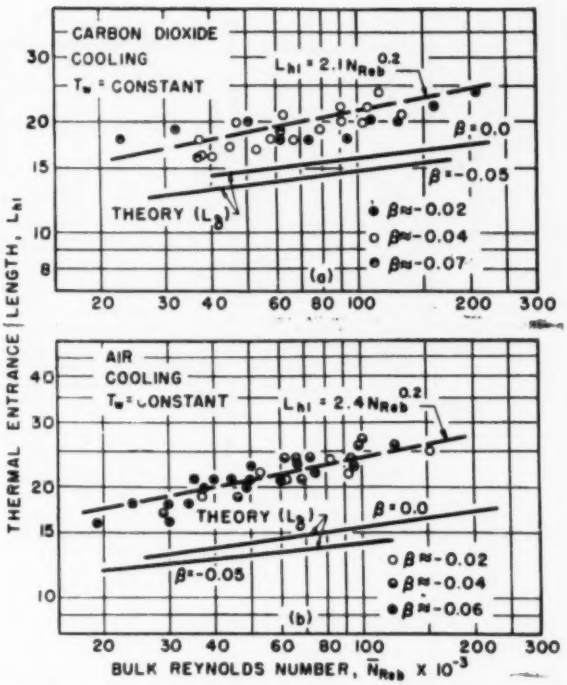

Fig. 7 Variation of thermal entrance length with bulk Reynolds number and β for air and carbon dioxide; cooling, constant wall temperature

Table 3 Values of the constant C in equation (4)

Gas	Heating or cooling	Temperature for evaluating the properties	C
Air	Heating	Initial	2.1
Air	Cooling	Bulk	2.4
CO_2	Heating	Initial	1.3
CO_2	Cooling	Bulk	2.1

between 0.7 and 8, Table 4 indicates entrance lengths from 8 to 35 diameters for Reynolds numbers ranging from 4000 to 250,000.

The physical properties employed in the correlation of the experimental data were those recommended by Nuttal, Benedict, Morey, and Masi in reference [21]. The afore-mentioned properties are substantially those recommended by Hilsenrath and Touloukian [22].

Theoretical Analysis

Of the heat-transfer analyses published in the open literature, only the work of Deissler and co-workers at NASA permits a readily obtainable solution for the case where the physical properties vary strongly with the temperature. The method presented by Deissler [9] assumed the specific heat and Prandtl number constant with temperature, identical variations of the viscosity and thermal conductivity with temperature for the constant heat-flux boundary condition only with properties variable.

Accordingly, the analysis by Deissler [9] was extended by employing an approximation for the variation of viscosity, thermal conductivity, and specific heat with temperature that closely agreed with the actual variation for air and carbon dioxide, and by investigating the constant wall-temperature boundary condition for the case of cooling the gases.

The assumptions employed in calculating the velocity and temperature profiles for fully developed turbulent flow employed in the analysis are given in references [15 and 16].

Boundary-Layer Equation. By making an energy balance on the boundary layer in the manner of Eckert [24], it is possible to relate the boundary-layer thickness δ_h to the axial distance from the point where either heating or cooling of the fluid is initiated. Thus

$$q_w r_w dx = \frac{d}{dx}\left[\int_0^{\delta_h} c_p g(t - t_b)\rho u(r_w - y)dy\right]dx \qquad (5)$$

Table 4 Summary of experimental determinations of entrance lengths in tubes; uniform initial temperature profile, fully developed initial velocity profile

Investigator	Boundary[a] condition	Prandtl number N_{Pr}	$\lvert t_w - t_b \rvert$, degrees R	Reynolds number N_{Reb}	Entrance length (one per cent)
Boelter [10]	CWT	0.7	140	27,000–53,000	10–17
Aladyev [11]	CWT	5–8	150	4000–60,000	35–20
Hartnett [12]	UHF	6–8	8–72	17,000–89,000	8–15
	UHF	61–350	48–390	5500–46,600	29–9
Chollette [13]	CWT	0.7	140	8000–12,500	10–15
Wolf	CWT	0.7	300–1200	23,000–218,000	12–26
(Purdue)	UHF	0.7	500–1000	50,000–246,000	11–27

[a] CWT denotes wall temperature constant with axial distance.
UHF denotes uniform heat flux.

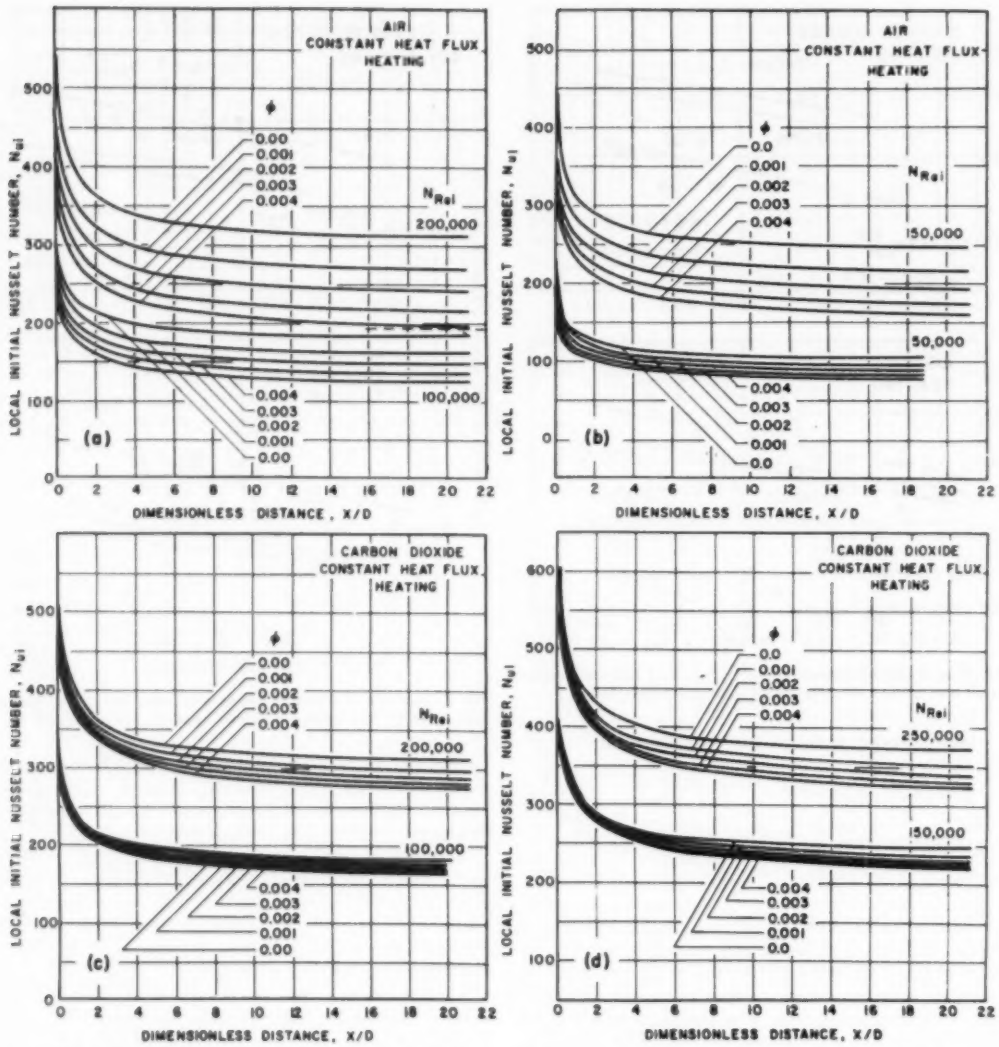

Fig. 8 Variation of local initial Nusselt number with axial distance, ϕ, and initial Reynolds number for air and carbon dioxide; constant heat flux (heating)

For the case where the wall temperature is constant with axial distance q_w is a function of x. Integration and nondimensionalization of equation (5) in terms of u^+ and y^+ yields

$$x/D] = \int_0^{f(\delta^+_h)} \frac{t_b^+}{2(r_w^+)^2} \frac{d}{dx} \left[\int_0^{\delta^+_h} \frac{(t_b^+ - t^+)(r_w^+ - y^+)u^+ dy^+}{t_b^+(1 - \beta t^+)^{1-a}} \right] dx \quad (6)$$

Constant Heat-Flux Solution. Equation (5) may be integrated directly for the constant heat-flux boundary condition; in that case q_w is not a function of x. Integrating equation (5), dividing both sides by $2r_w^2$, and nondimensionalizing the result gives

$$x/D = \frac{1}{2(r_w^+)^2} \int_0^{\delta^+_h} \frac{(t_b^+ - t^+)u^+(r_w^+ - y^+)}{(1 - \beta t^+)^{1-a}} dy^+ \quad (7)$$

To distinguish between the case where q_w is not a function of x, (i.e., constant heat flux) x/D is not enclosed by brackets.

Deissler [9] has proposed a parameter ϕ as a measure of the intensity of the heat transfer under the afore-mentioned condition. The parameter ϕ is defined as follows: Thus

$$\phi = \frac{q_w}{c_p g \rho_i u_i t_i} \quad (8)$$

The parameter ϕ may be related to the parameter β by noting that for a constant area duct $\rho_i u_i = \rho_b u_b$ and $t_i^+ = t_b^+$. The result is

$$\phi = \frac{(1 - \beta t_b^+)}{u_b^+(1 - \beta t_b^+)} \quad (9)$$

After solving equation (7) heat transfer and flow parameters were calculated for selected values of β as a function of x/D. The re-

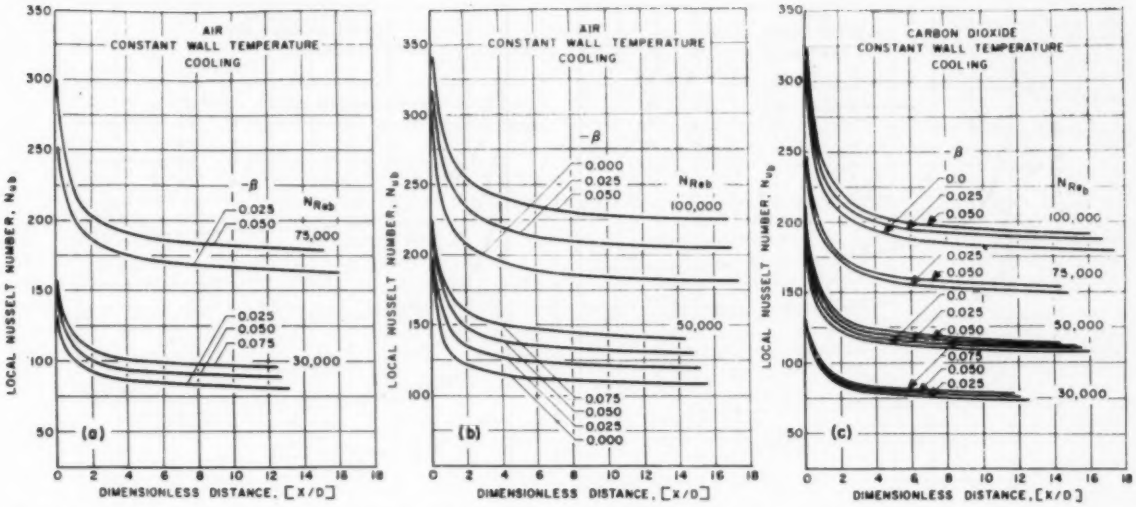

Fig. 9 Variation of local bulk Nusselt number with axial distance, β, and Reynolds number for air and carbon dioxide; constant wall temperature (cooling)

sults were then cross-plotted for constant values of ϕ. A detailed description of the procedure is presented by Wolf and Zucrow in reference [23].

The derivation and method of calculation of the bulk velocity, bulk temperature, Nusselt numbers, and Reynolds numbers, and a complete description of the numerical methods employed for the solution, and of the program for the computer is given in references [16] and [23].

Analytical Results

Values of the bulk Nusselt number Nu_b were computed as functions of axial distance x/D at nominal values of the bulk Reynolds number N_{Reb} for the constant wall temperature boundary condition; the calculations were performed for negative values of β (cooling the gas). For the constant heat-flux boundary condition, values of the initial Nusselt number Nu_i were computed as functions of x/D at nominal values of the initial Reynolds number N_{Rei}; the calculations performed for positive values of β (heating the gas) were cross-plotted to obtain Nu_i for constant ϕ.

Fig. 8 presents Nu_i, computed for air and carbon dioxide (with physical properties varying with temperature) as a function of x/D, with N_{Rei} and ϕ as parameters for the case of constant heat flux (heating). From the afore-mentioned figure it is seen that for air the values of Nu_i are influenced to a greater extent by a change in ϕ than are the corresponding values for carbon dioxide, the influence of ϕ increasing with the Reynolds number. It was shown in reference [16] that air and carbon dioxide have almost identical velocity profiles and boundary layer thicknesses; the calculated values of u_b^+, l_b^+, and t_b^+ cannot, therefore, be materially different for the two gases. Consequently, the computed value of the Nusselt number is primarily influenced by the variation of the thermal conductivity with temperature [the variation assumed was $(k/k_\infty) = (t/t_\infty)^b$; the values of b employed for air and carbon dioxide were 0.78 and 1.13, respectively.]

The effect of b on Nu_i for air and carbon dioxide in the case of heating is also evident in the case of cooling ($\beta < 0$) as can be seen in Fig. 9. As in the case of heating, increasing the intensity of cooling (increasing absolute values of β) causes a much larger change in the computed value of Nu_b for air than for carbon dioxide.

Comparison of Theory and Experimental Results

Fig. 10 compares the local experimental and analytical Nusselt numbers for air and carbon dioxide in turbulent flow as a function of axial distance and Reynolds number for different values of the parameters β and ϕ. The experimental results presented in Fig. 10 are those for which the average Reynolds number was in closest agreement with the nominal values employed in the analysis.

It is seen from Figs. 10(a and b) that for the given x/D and Reynolds number the predicted values[3] for Nu_i° are smaller than those obtained experimentally for the case of heating the gases, the deviation being larger for carbon dioxide. Figs. 10(c and d) demonstrate that when the gases were cooled the predicted values of Nu_b° were larger than those obtained experimentally, the difference being somewhat larger at larger values of $-\beta$. The shape of the predicted curves is quite similar to those obtained experimentally. It should be noted that the results of many investigations are presented in the form h_x/h_a or Nu/Nu_∞ as a function of axial distance rather than the relationship of the actual values with distance. For design purposes, however, it is more desirable to have the results presented in the form of local values as functions of axial distance, as is done here.

Discussion of Disagreement Between Theory and Experiment. The boundary conditions assumed in the theory were closely approximated by those obtaining in the experimental apparatus. The differences between the predicted and experimental results are attributed largely to the assumptions needed for computing the velocity and temperature profiles (from which Nu° and N_{Re}° were calculated).

The following assumptions are those most in question:

1 The value for α was assumed to be constant and equal to unity.

2 The value employed for the diffusivity in the region near the wall was assumed to be

$$\epsilon = n^2 uy(1 - e^{-n^2 uy/\nu}) \tag{10}$$

[3] For convenience in discussion, the analytically computed values of Nu and N_{Re} are designated with a superscript°.

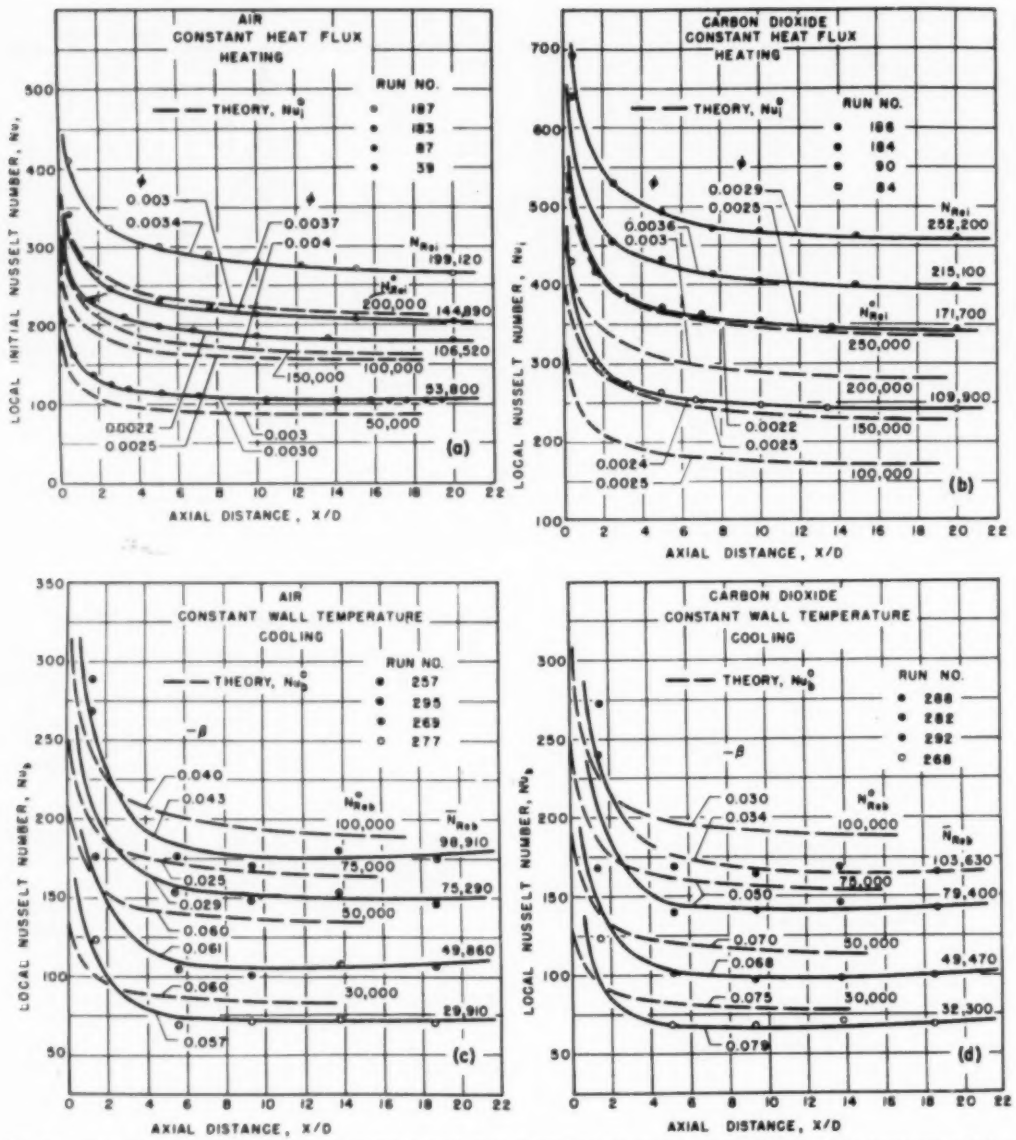

Fig. 10 Comparison of experimental and predicted local Nusselt numbers for air and carbon dioxide, fully developed initial velocity profile, uniform initial temperature profile, heating, and cooling

where the constant $n = 0.124$ was determined experimentally for adiabatic flow [19].

3 The value employed for the diffusivity in the region away from the wall was assumed to be that suggested by von Karman

$$\epsilon = \kappa^2(du/dy)^3/(d^2u/dy^2)^2 \qquad (11)$$

where κ was assumed equal to 0.38.

The constants n and κ were determined from experiments with adiabatic flow. When the flow field is strongly diabatic and the fluid properties vary markedly with temperature, it is recognized that the velocity field is dependent upon the temperature field. Consequently, it is doubtful that adiabatic flow information can be employed to calculate heat transfer in strongly diabatic flow. Information is lacking for determining the validity of assumptions 2 and 3.

It has been shown by several investigators[4] that the value for α depends upon distance from the wall (however, α is relatively constant once the turbulent core has been reached) and upon the flow conditions (Reynolds number) and Prandtl number. Values for α that range from approximately 0.2 to greater than 1.5 have been reported for Reynolds numbers from 20,000 to 300,000. Consequently, the assumption $\alpha = 1$ for all flow conditions does not agree with indicated experimental results.

Conclusions

The following conclusions were derived from the experimental and analytical investigations of the local heat-transfer character-

[4] A discussion of the results of the afore-mentioned investigations is presented on p. 55, Part II of reference [16].

istics for air and carbon dioxide ($N_{Pr} \approx 0.7$) flowing turbulently in smooth round tubes with a fully developed velocity profile and a uniform temperature distribution at the cross section where energy exchange was initiated.

1 For the case of heating, values of the one per cent thermal entrance length L_{h1} ranging from 11 to 27 diameters were determined for initial Reynolds numbers ranging from 59,580 to 296,000 for both air and carbon dioxide. For cooling with wall temperature invariant with axial distance, values of L_{h1} ranging from 12 to 26 diameters for air and carbon dioxide were determined for bulk Reynolds numbers ranging from 23,000 to 218,700.

2 The values of L_{h1} for heating and cooling air or carbon dioxide over the Reynolds number range investigated can be expressed, with an average deviation of ±2 diameters, by means of the empirical relationships given by equation (4) with the constants presented in Table 3.

3 The predicted values of entrance length L_δ compare favorably with the value of L_{h1} obtained experimentally.

4 The predicted values of local Nusselt numbers for air and for carbon dioxide are in moderate agreement with those obtained experimentally, except for the case of heating carbon dioxide. The predicted values of the local initial Nusselt number $Nu_i{}^\circ$ for heating carbon dioxide were approximately 40 per cent smaller than the corresponding experimental values for Nu_i.

Acknowledgment

The research reported herein was conducted at the Jet Propulsion Center, Purdue University, and was sponsored by Project SQUID which is supported by the Office of Naval Research under Contract N6 ori-105 T.O. III, ONR-098-038. Reproduction of this paper in full or in part is permitted for any use of the United States Government.

The author expresses his appreciation to Dr. M. J. Zucrow, Director, Jet Propulsion Center, Purdue University, and to Drs. C. F. Warner and B. A. Reese for their helpful guidance during the course of the research program, and to the staff of the Jet Propulsion Center for their assistance in constructing and maintaining the apparatus. Special thanks are due Mr. R. R. Kenyon of the Statistical Laboratory, Purdue University, for preparing computer routines employed in the analysis, and to Mr. J. H. Lehman for his help in operating the experimental apparatus and in reducing the experimental data.

References

1 H. Latzko, "Der Wärmeübergang an einem Turbulentem Flüssigkeits oder Gastrom," *Zeitschrift für Angewandte Mathmatik und Mechanik*, vol. 1, no. 4, August, 1921.

2 K. Elser, "Der Wärmeübergang in der Thermische Anlaufstrecke bei Hydrodynamisch Ausgebildeter Turbulenter Zuströmung im Rohr," *Schweizer Archiv*, Jahrgang 15, no. 12, 1949, p. 359.

3 H. F. Poppendiek and L. D. Palmer, "Forced Convection Heat Transfer in Thermal Entrance Regions—Part II," ONRL-914, Met. and Ceramics, Oak Ridge, Tenn., May, 1952.

4 C. A. Sleicher, Jr., and M. Tribus, "Heat Transfer in a Pipe With Turbulent Flow and Arbitrary Wall-Temperature Distribution," TRANS. ASME, vol. 79, 1957, p. 789.

5 R. G. Deissler, "Analysis of Turbulent Heat Transfer and Flow in the Entrance Regions of Smooth Passages," NACA TN 3016, October, 1953.

6 R. A. Seban and T. Shimazaki, "Calculations Relative to the Thermal Entrance Length for Fluids of Low Prandtl Number," University of California, Berkeley, Calif., January, 1950.

7 S. Levy, "Heat-Conduction Methods in Forced-Convection Flow," TRANS. ASME, vol. 78, 1956, p. 1627.

8 W. G. Schlinger, et al., "Prediction of Temperature Gradients in a Turbulent Stream," IME and ASME General Discussion of Heat Transfer, published by ASME, September, 1951, p. 150.

9 R. G. Deissler, "Turbulent Heat Transfer and Friction in the Entrance Regions of Smooth Passages," TRANS. ASME, vol. 77, 1955, p. 1221.

10 L. K. M. Boelter, D. Young, and H. W. Iverson, "An Investigation of Aircraft Heaters—XXVII," NACA TN 1451, July, 1948.

11 I. T. Aladyev, "Experimental Determination of Local and Mean Coefficients of Heat Transfer for Turbulent Flow in Pipes," NACA TM 1356, 1954.

12 J. P. Hartnett, "Experimental Determination of the Thermal-Entrance Length for the Flow of Water and of Oil in Circular Pipes," TRANS. ASME, vol. 77, 1955, p. 1211.

13 A. Chollette, "Heat Transfer—Local and Average Coefficients for Air Inside Tubes," *Chemical Engineering Progress*, vol. 44, 1948, p. 81.

14 H. E. Zellnick and S. W. Churchill, "Convective Heat Transfer From High Temperature Air Inside a Tube," AIChE Paper No. 57—HT-33, 1957.

15 J. M. Botje, "An Experimental and Analytical Determination of Heat Transfer by Forced Convection in Turbulent Flow for Air, Carbon Dioxide, and Helium," PhD thesis, Purdue University, January, 1956.

16 H. Wolf, "The Experimental and Analytical Determination of the Heat-Transfer Characteristics of Air and Carbon Dioxide in the Thermal Entrance Region of a Smooth Tube With Large Temperature Differences Between the Gas and the Tube Wall," PhD thesis (in two parts), Purdue University, March, 1958.

17 W. H. Geidt, Jr., "Effect of Turbulence Level of Incident Air Stream on Local Heat Transfer and Skin Friction of a Cylinder," *Journal of the Aeronautical Sciences*, vol. 18, 1951, p. 727.

18 M. Jakob, "Heat Transfer," John Wiley & Sons, Inc., New York, N. Y., vol. 1, 1950.

19 R. G. Deissler and C. S. Eian, "Analytical and Experimental Investigation of Fully Developed Turbulent Flow of Air in a Smooth Tube With Heat Transfer With Variable Fluid Properties," NACA TN 2629, February, 1952.

20 E. M. Sparrow, T. M. Hallman, and R. Siegel, "Turbulent Heat Transfer in the Thermal Entrance Region of a Pipe With Uniform Heat Flux," *Applied Science Research*, section A, vol. 7, 1957.

21 "NBS—NACA Tables of Thermal Properties of Gases," Table nos. 2.40, 2.39, 2.42, 13.24, 13.39, 13.42, United States Department of Commerce, 1949, 1950, 1951.

22 J. Hilsenrath and Y. S. Touloukian, "The Viscosity, Thermal Conductivity, and Prandtl Number for Air, O_2, N_2, NO, H_2, CO, CO_2, H_2O, He, and A," TRANS. ASME, vol. 76, 1954, p. 967.

23 Helmut Wolf and M. J. Zucrow, "The Analytical Determination of the Local Heat-Transfer Characteristics of Gases Flowing Turbulently in the Thermal Entrance Region of a Circular Duct With Large Temperature Differences Between the Gas and the Duct Wall," Report Number RM-57-2, Jet Propulsion Center, Purdue University, December, 1957.

24 E. R. G. Eckert, "Introduction to the Transfer of Heat and Mass," McGraw-Hill Book Co., Inc., New York, N. Y. 1950.

DISCUSSION

S. Levy[5]

The author's paper is a valuable addition to studies of the thermal entrance region. His contribution would be all the more useful if he sometimes would expand his discussion of results. Specific instances include:

1 Dr. Wolf does not show correlation of the data in terms of the standard parameters, Nusselt, Reynolds, and Prandtl numbers. Such correlations would help understand the effects of fluid property variations for fully established conditions. They would also make it possible to determine whether the large entry lengths shown in Fig. 3 are not due to changes in fluid viscosity, i.e., Reynolds number, in the flow direction. Without such correlations it is hard to see how the value of h_a was obtained since it varies along the heated length. Further, comparison of the nondimensional groupings with the data of Humble, et al.,[6] would permit evaluation of the present experimental data and accuracy.

2 The disagreement between the measured entry lengths for heating carbon dioxide and air is difficult to understand (see Fig. 6). The theory predicts the same value for the two gases. It is possible that the difference can be traced to the failure to account

[5] Specialist, Heat Transfer and Fluid Dynamics, General Electric Company, Schenectady, N. Y. Assoc. Mem. ASME.

[6] L. V. Humble, W. H. Lowdermilk, and L. G. Desmond, NACA Report 1020, 1951.

for variation of the coefficient h_a due to the change in *local* Reynolds number.

3 The deviation between theory and tests beyond x/D of 10 to 15 is hard to justify. Deissler's method is known to give good agreement for the case of constant properties and the discrepancy needs further amplification. If the analytical method cannot account for fluid property variation under fully developed conditions it must be critically examined before application to the thermal entrance region.

4 The variation of the 5 per cent entry length with Reynolds number is not mentioned. Is the exponent still the same and what happens if the thermal entry lengths are plotted versus exit or average Reynolds numbers?

5 The analysis postulates that the eddy diffusivities for heat and momentum are equal. This is hard to justify in the entrance region. Measurements of temperature distribution in the entry zone would be very helpful in determining the ratio α.

Author's Closure

Dr. Levy's comments raise some very interesting questions themselves. It was unfortunate that more discussion could not be included, especially regarding the correlation of the average heat-transfer results. However, since it was necessary to shorten the original manuscript considerably, that would not have been possible. The following discussion is numbered to correspond to Dr. Levy's specific comments.

1 The correlations obtained for the fully developed heat-transfer conditions are presented and discussed in detail in Reference [16]. Further discussion is presented here under paragraph 3. The values for entrance length for heating the gas were not determined from Fig. 3, they were determined from the variation of the experimental heat-transfer coefficient with x/D. The results presented in Fig. 3 are for a constant value of Reynolds number, the influence referred to by Dr. Levy is due to the variation of the thermal conductivity of the gas with temperature. In determining the entrance length from the experimental values of the heat transfer coefficient (h did achieve a constant value) the influence of the changing Reynolds number along the length of the tube was not accounted for. The results presented in Fig. 37 of Reference [16] demonstrated that h for air was a function of mass rate of flow per unit area and only slightly influenced by wall temperature· h for CO_2 was a function of mass flow per unit area only.

2 If the experimental results were corrected, by cross plotting the data, to a value of Reynolds number equal to the average Reynolds number in the tube it is doubtful that the value of h_a would change. It may be possible that the resulting entrance lengths may be slightly different from those reported herein.

3 With regard to fully developed heat transfer it must be pointed out that Deissler's method is based on a constant wall temperature with respect to axial distance. For the case of heating ($\beta > 0$) the theory predicts a decrease in Nu at a given N_{Re}. The experimental results for air employed by Deissler for comparison with his analytical results were obtained in an electrically heated tube having very nearly a uniform heat flux boundary condition and wall temperature variable with axial distance. For the case of heating the gas with the wall temperature increasing with axial distance (uniform heat flux) the experimental values of Nu decrease with increasing average wall temperature (increasing β) for air, and decrease to a smaller extent for CO_2. It is unfortunate that Deissler did not have extensive experimental results, either heating or cooling the gas, conducted with the wall temperature *constant with respect to axial distance*. Fig. 11 presents the results of the cooling experiments for air and CO_2 conducted by the author in the tube having an $L/D = 60$ with the wall temperature *constant with respect to axial distance*, the results are average values for fully developed flow hydrodynamically and thermally. For the experimental results of Fig. 11 the values of β extended from -0.002 to -0.10. The influence of β on the Nusselt number is small compared to that predicted by theory (the theory predicts approximately a 40 per cent increase in Nusselt number with a change in β from 0 to -0.1). The reason for this discrepancy is not immediately apparent. For the case of cooling the gases with positive and negative values of the wall temperature gradient in the axial direction, see Fig. 12, a negative gradient increased the Nusselt number, and a positive gradient decreased the value of the Nusselt number (at a given Reynolds number). The aforementioned results were harmonized by employing an extension of the theory due to Rubesin (NACA TN 2345) and summarized in a paper by the writer entitled "Heat Transfer

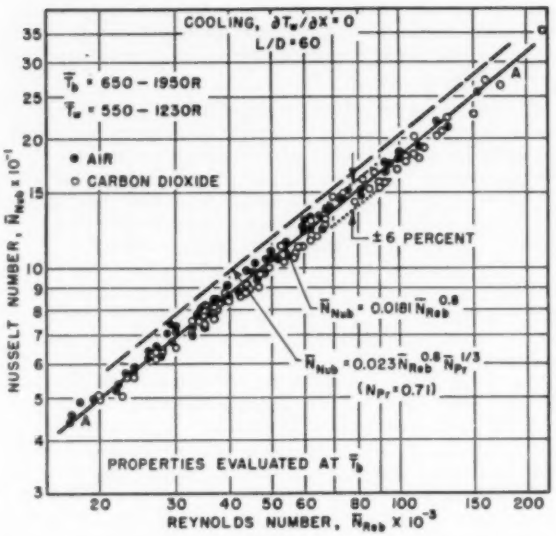

Fig. 11 Correlation of bulk Nusselt number with bulk Reynolds number for air and carbon dioxide; cooling, constant wall temperature

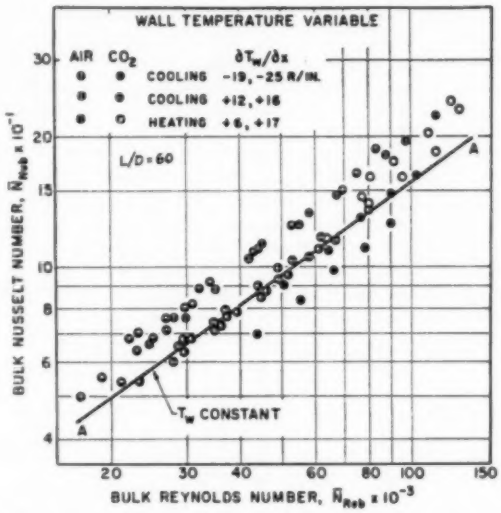

Fig. 12 The influence of wall temperature gradient upon the Nusselt number for air and carbon dioxide; heating and cooling

From Nonisothermal Surfaces" submitted to ASME, June, 1959, but subsequently not accepted for publication. The results presented in Figs. 11 and 12 are discussed in detail in Appendix D of Reference [16].

It is the writer's conviction that previous failure to correlate heating and cooling experiments satisfactorily with a single correlation equation employing dimensionless quantities, with the physical properties evaluated at one reference temperature, may be attributed for the most part to the different values of wall temperature gradients obtained in the experiments analyzed.

Specifically, the cooling data for air and CO_2 could not be correlated with the NACA modified Reynolds number method; the heating data was correlated with a maximum deviation of ± 5 per cent by employing the term $(T_w/T_b)^{0.55}$ and by evaluating the properties at the film temperature, a somewhat better correlation than that obtained with the modified Reynolds number. The experimental data for heating air are in full accord with that of NACA Report 1020.

4 The values of the 5 per cent entrance length are given in Table 2 for the range in Reynolds number obtaining in the experiments. The functional relationship of L_{A5} with N_{Re} was not determined.

R. SIEGEL

E. M. SPARROW

NASA, Lewis Research Center, Cleveland, Ohio. Assoc. Mem. ASME

Turbulent Flow in a Circular Tube With Arbitrary Internal Heat Sources and Wall Heat Transfer

An analysis has been carried out to determine the heat-transfer characteristics for turbulent flow of a heat generating fluid in a circular tube with wall heat transfer. The internal heat generation is uniform over the tube cross section, but may vary longitudinally in an arbitrary manner. The wall heat transfer may also vary in an arbitrary way in the longitudinal direction. The analysis applies along the entire length of the tube, that is, in thermal entrance as well as fully developed regions. The fluid is assumed to have a fully developed turbulent velocity profile throughout the length of the pipe. Numerical results are presented for fluids with Prandtl numbers ranging from 0.7 to 100 for Reynolds numbers from 50,000 to 500,000. The extension of the results to include radial heat source variations is indicated.

Introduction

FLOWING FLUIDS with internal heat generation are found in many sectors of modern technology. Such flows may occur, for example, in fluid-fueled nuclear reactors and chemical process equipment. The basic flow passage in many of these systems is the circular tube, and it is this configuration which is selected for analysis here.

Specifically, we are concerned with fully developed *turbulent* pipe flows in which the internal heat generation is uniform across the section, but which may vary in an *arbitrary* manner along the length. Furthermore, the heat transfer at the tube wall is also permitted to take on an arbitrary longitudinal variation. An example of a situation where such variations may occur is in a nuclear reactor core in which the neutron flux varies with position.

The findings of the analysis can be used to calculate the heat-transfer characteristics over the entire length of the passage, that is, in the thermal entrance as well as far downstream. Numerical results are provided over the Reynolds number range from 50,000 to 500,000 for Prandtl numbers varying from 0.7 to 100.

Previous analyses [1, 2, 3][1] of turbulent pipe flows with internal heat generation have been confined to the condition of fully developed heat transfer, and hence, the results pertain to the portion of pipe beyond the thermal entrance region. Also, these investigations were carried out under the restrictions that the internal heat generation and wall heat transfer are both longitudinally uniform. Laminar pipe flows have, however, lent themselves more readily to analysis. Results applicable over the entire pipe length have been given [4] for the general situation where the internal heat generation takes on arbitrary longitudinal and radial variations, while the wall heat transfer varies arbitrarily along the length. Of course, turbulent flows are of greater importance as they are almost always encountered in practice.

General Analytical Considerations

The system to be analyzed is pictured schematically on Fig. 1. Our attention is directed to the portion of the tube to the right of $x = 0$ where the fluid simultaneously experiences an internal heat generation $Q(x)$ and a wall heat transfer $q(x)$. The functions Q and q are permitted arbitrary variations with x. The fluid, moving from left to right, possesses a fully developed turbulent ve-

Contributed by the Heat Transfer Division and presented at the Semi-Annual Meeting, St. Louis, Mo., June 14–18, 1959, of THE AMERICAN SOCIETY OF MECHANICAL ENGINEERS.

NOTE: Statements and opinions advanced in papers are to be understood as individual expressions of their authors and not those of the Society. Manuscript received at ASME Headquarters, March 18, 1959. Paper No. 59—SA-19.

[1] Numbers in brackets designate References at end of paper.

Nomenclature

c_p = specific heat at constant pressure

D_n = coefficients in series expansion of temperature for case of internal heat sources; D_n', coefficients when heat source is a function of radial position

d = tube diameter, $2r_0$

E_n = coefficients in series expansion of *wall* temperature for case of internal heat sources, $D_n\phi_n(r_0^+)$

F_n = coefficients in series expansion of wall temperature for case of wall heat transfer

$G(r^+)$ = fully developed temperature distribution for case of uniform wall heat flux

$H(r^+)$ = fully developed temperature distribution for case of uniform internal heat generation

h = local heat-transfer coefficient

k = thermal conductivity

$M(r^+)$ = fully developed temperature distribution for case of heat sources dependent on r

Nu = local Nusselt number, hd/k

Pr = Prandtl number, ν/α

Q = rate of internal heat generation per unit volume

q = local heat-transfer rate per unit area at tube wall

r = radial co-ordinate measured from tube center line; r_0, tube radius

r^+ = dimensionless radial co-ordinate, $r\sqrt{\tau_0/\rho}/\nu$; r_0^+, dimensionless tube radius, $r_0\sqrt{\tau_0/\rho}/\nu$

Re = Reynolds number, $\bar{u}d/\nu$

(*Continued on next page*)

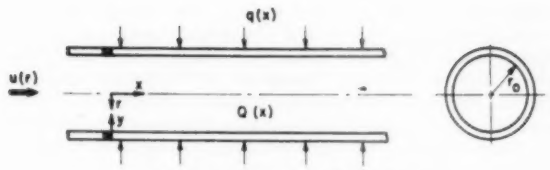

Fig. 1 Physical model and co-ordinates

locity profile which is unchanging with length. The temperature across the entrance section, $x = 0$, is taken to be uniform at the value t_0. It is desired to determine the heat-transfer characteristics of the fluid at all positions along the tube.

The starting point of our study is the equation expressing conservation of energy for axially symmetric turbulent flow in a pipe. For fully developed hydrodynamic conditions, this may be written as

$$u\frac{\partial t}{\partial x} = \frac{1}{r}\frac{\partial}{\partial r}\left[r(\alpha + \epsilon_h)\frac{\partial t}{\partial r}\right] + \frac{Q}{\rho c_p} \tag{1}$$

where α and ϵ_h represent, respectively, the molecular and eddy diffusivities for heat. To obtain the energy equation in this form, it has been assumed that the fluid properties are constant, and that viscous dissipation and axial heat diffusion are both negligible compared to heat diffusion in the radial direction.

Since equation (1) is linear in the temperature t, we are able to separate the general problem which includes both internal heat sources and wall heat transfer into two simpler situations in the following way: (*a*) A problem where there is an internal heat generation Q in an insulated tube ($q = 0$). For this case, the temperature is designated as t_Q. (*b*) A problem where there is a wall heat transfer q without internal heat generation ($Q = 0$). In this instance we denote the temperature by t_q. Then, from the linearity of the energy equation, the temperature in the combined problem is simply given by

$$t = t_Q + t_q \tag{2}$$

The governing equations and boundary conditions for t_Q and t_q may be written as follows:

$$u\frac{\partial t_Q}{\partial x} = \frac{1}{r}\frac{\partial}{\partial r}\left[r(\alpha + \epsilon_h)\frac{\partial t_Q}{\partial r}\right] + \frac{Q}{\rho c_p} \tag{3a}$$

$$\left.\begin{aligned} \partial t_Q/\partial r &= 0 \quad \text{at} \quad r = r_0 \quad \text{(insulated wall)} \\ \partial t_Q/\partial r &= 0 \quad \text{at} \quad r = 0 \text{ (symmetry)} \\ t_Q &= t_{Q,0} \quad \text{at} \quad x = 0 \text{ (entrance condition)} \end{aligned}\right\} \tag{3b}$$

and

$$u\frac{\partial t_q}{\partial x} = \frac{1}{r}\frac{\partial}{\partial r}\left[r(\alpha + \epsilon_h)\frac{\partial t_q}{\partial r}\right] \tag{4a}$$

$$\left.\begin{aligned} \partial t_q/\partial r &= q/k \quad \text{at} \quad r = r_0 \text{ (specified heat flux)} \\ \partial t_q/\partial r &= 0 \quad \text{at} \quad r = 0 \text{ (symmetry)} \\ t_q &= t_{q,0} \quad \text{at} \quad x = 0 \text{ (entrance condition)} \end{aligned}\right\} \tag{4b}$$

where $t_{Q,0}$ and $t_{q,0}$ are chosen so that

$$t_0 = t_{Q,0} + t_{q,0} \tag{2a}$$

The two problems as defined by equations (3) and (4) will be analyzed separately.

We begin by studying the problem of a flow with internal heat sources in an insulated tube, that is, t_Q. First, consideration is given to the situation of uniform heat sources, and a solution is obtained which applies both in the entrance and fully developed regions. Then, these results are generalized to the case where there are arbitrary variations of the heat sources along the length of the tube. Next, the results for the problem of uniform wall heat transfer with no heat sources, originally given in reference [5], are reviewed and generalized to apply for arbitrary longitudinal variations of heat flux. The linear combination of these solutions is then made to yield results for the general case of arbitrary longitudinal variations in both internal heat sources and wall heat flux. Extension of the analysis to the situation of radially nonuniform heat sources is made in the last section of the report.

The eddy diffusivity which appears in equations (3*a*) and (4*a*) bears a word of discussion. Current knowledge of the relationship between the eddy diffusivity for heat, ϵ_h, and the eddy diffusivity for momentum, ϵ_m, is still in a state of uncertainty. However, it appears that for the Prandtl numbers of this study, $0.7 \leq \mathrm{Pr} \leq 100$, the choice of $\epsilon_h = \epsilon_m$ is not unreasonable. Previous application of this assumption has led to excellent heat-transfer predictions over this Prandtl number range.

Uniform Internal Heat Sources in an Insulated Tube

For uniform heating conditions, it is well known that, as the flow proceeds farther and farther down the pipe, the heat-transfer characteristics approach more and more closely to a limiting condition. This limit is termed the fully developed heat-transfer situation and will be denoted by the subscript fd. Taking cognizance of the fully developed condition, we choose to write the temperature distribution t_Q as the following sum

$$t_Q = t_{Q,\mathrm{fd}} + t_Q^* \tag{5}$$

Nomenclature

T = absolute temperature; T_w, absolute wall temperature; T_b, absolute bulk fluid temperature

t = temperature; t_0, temperature of fluid entering tube (a constant); t^*, difference temperature defined in equation (5); t_b, bulk fluid temperature; t_w, tube wall temperature

u = fluid velocity in the x-direction; $\bar{u}$, mean fluid velocity

u^+ = dimensionless velocity in x-direction, $u/\sqrt{\tau_0/\rho}$

x = axial co-ordinate measuring distance from tube entrance

x^+ = dimensionless axial co-ordinate, x/d

$\bar{x}$ = dummy integration variable

y = radial co-ordinate measuring distance inward from tube wall, $r_0 - r$

y^+ = dimensionless co-ordinate, $y\sqrt{\tau_0/\rho}/\nu$

α = molecular diffusivity for heat, $k/\rho c_p$

β^2 = eigenvalues of equation (17*a*)

γ = dimensionless total thermal diffusivity, $(\alpha + \epsilon_h)/\nu$

ϵ_h, ϵ_m = eddy diffusivities for heat and momentum

ν = kinematic viscosity

ρ = fluid density

τ_0 = shear stress at tube wall

ϕ = eigenfunctions of equation (17*a*)

ψ = function of x given by equation (16)

Subscripts:

fd denotes fully developed heat-transfer condition

Q denotes situation where $Q \neq 0$ and $q = 0$

q denotes situation where $q \neq 0$ and $Q = 0$

t_Q^* is seen to be a difference temperature which plays an important role in the entrance region and approaches zero as x becomes large. We now proceed to solve separately for $t_{Q,fd}$ and t_Q^*.

The Fully Developed Solution. Since energy conservation must everywhere be obeyed, it is necessary that $t_{Q,fd}$ satisfy equation (3*a*), that is,

$$u\frac{\partial t_{Q,fd}}{\partial x} = \frac{1}{r}\frac{\partial}{\partial r}\left[r(\alpha + \epsilon_m)\frac{\partial t_{Q,fd}}{\partial r}\right] + \frac{Q}{\rho c_p} \tag{6}$$

where Q is now a constant and ϵ_h has been replaced by ϵ_m. A characteristic of the fully developed situation for uniform heat sources is that the temperature at all points in the cross section rises in a linear fashion along the pipe. Expressed in mathematical terms, the condition becomes

$$\frac{\partial t_{Q,fd}}{\partial x} = \text{constant} = \frac{Q}{\rho \bar{u} c_p} \tag{7a}$$

or alternately

$$\frac{t_{Q,fd} - t_{Q,0}}{Qr_0^2/k} = \frac{4}{\text{RePr}}\frac{x}{d} + H(r) \tag{7b}$$

The radial distribution $H(r)$ must, of course, satisfy the conservation of energy equation (6). Substituting (7*b*) into (6) and introducing dimensionless variables, the governing equation for H is found to be

$$\frac{2u^+}{\text{RePr}} = \frac{r_0^+}{r^+}\frac{d}{dr^+}\left[r^+\gamma\frac{dH}{dr^+}\right] + \frac{1}{(\text{Pr})r_0^+} \tag{8}$$

where u^+ and r^+ are the dimensionless counterparts of u and r as given in the Nomenclature and γ represents a dimensionless diffusivity defined as

$$\gamma = \frac{\alpha + \epsilon_m}{\nu} = \frac{1}{\text{Pr}} + \frac{\epsilon_m}{\nu}$$

The boundary conditions on H are found from equations (3*b*) to be

$$dH/dr^+ = 0 \quad \text{at} \quad r^+ = 0 \text{ and } r^+ = r_0^+ \tag{8a}$$

To obtain solutions of equation (8), it is necessary that the variation of u^+ and γ with r^+ be specified. The turbulent velocity distribution is given by the following equations (ref. [6]):

$$\frac{du^+}{dy^+} = \frac{1}{1 + (0.124)^2u^+y^+[1 - e^{-(0.124)^2u^+y^+}]}, \qquad 0 \le y^+ \le 26 \tag{9a}$$

$$u^+ = \frac{1}{0.36}\ln\left(\frac{y^+}{26}\right) + 12.8493, \quad 26 \le y^+ \tag{9b}$$[2]

where $y^+ = r_0^+ - r^+$, while γ is evaluated from (ref. [5])

$$\gamma = \frac{1}{\text{Pr}} + (0.124)^2u^+y^+[1 - e^{-(0.124)^2u^+y^+}], \quad 0 \le y^+ < 26 \tag{10a}$$

$$\gamma = \frac{1}{\text{Pr}} + 0.36y^+(1 - y^+/r_0^+) - 1, \quad y^+ > 26 \tag{10b}$$

The value of γ at $y^+ = 26$ is taken as the average of equations (10*a*) and (10*b*). The minus-one term appearing on the right side of equation (10*b*) is retained for $26 < y^+ < r_0^+/2$ and is deleted for larger values of y^+.

With these expressions for u^+ and γ, we can proceed with the integration of equation (8) in order to find H. An analytical solution was not possible and a numerical technique (Kutta-Runge method) had to be employed. Solutions were carried out on an IBM 653 electronic computer for Reynolds numbers of 50,000, 100,000, and 500,000 for Prandtl numbers of 0.7, 1, 10, and 100. The values of H thus obtained provide, in conjunction with equation (7*b*), the complete solution for the fully developed situation. Space considerations preclude tabulation of the solutions here, but they are available as IBM listings.

A result of practical engineering importance is the wall-to-bulk temperature difference for the fully developed situation. First, the bulk temperature is introduced by its definition

$$t_{Q,b} - t_{Q,0} = \frac{Q}{\rho\bar{u}c_p}x = \frac{Qr_0^2}{k}\frac{4(x/d)}{\text{RePr}} \tag{11}$$

Then, substituting into equation (7*b*) and evaluating H at the tube wall ($r^+ = r_0^+$) we find

$$\frac{(t_{Q,w} - t_{Q,b})_{fd}}{Qr_0^2/k} = H(r_0^+) \tag{12}$$

Using the numerical results for $H(r_0^+)$, the dimensionless wall-to-bulk temperature difference has been plotted on Fig. 2 as a function of the Reynolds and Prandtl numbers.

We will make further use of the fully developed solution in later sections.

The Thermal Entrance Region. According to equation (5), the temperature distribution in the thermal entrance region is found by adding the difference temperature t_Q^* to the fully developed temperature $t_{Q,fd}$. Having determined $t_{Q,fd}$, we now turn our attention to t_Q^*.

To find the governing equation for t_Q^*, we introduce equation (5) into the conservation-of-energy principle (3*a*). Then, taking account of the fact that $t_{Q,fd}$ satisfies (6), it follows that t_Q^* must obey

$$\frac{u^+}{2}\frac{\partial t_Q^*}{\partial x^+} = \frac{r_0^+}{r^+}\frac{\partial}{\partial r^+}\left[r^+\gamma\frac{\partial t_Q^*}{\partial r^+}\right] \tag{13}$$

where again dimensionless variables have been used. It is interesting to observe that the heat source term does not appear in equation (13).

The boundary conditions on t_Q^* may be derived from equations (3*b*), in conjunction with (5), giving

$$\partial t_Q^*/\partial r^+ = 0 \quad \text{at} \quad r^+ = 0 \quad \text{and} \quad r^+ = r_0^+ \tag{14a}$$

$$\left.\begin{aligned} &\text{and} && t_Q^* = t_{Q,0} - t_{Q,fd} \\ &\text{or} && \frac{t_Q^*}{Qr_0^2/k} = -H(r) \end{aligned}\right\} \quad \text{at} \quad x = 0 \tag{14b}$$

where we have also used equation (7*b*) in finding the last expression.

We seek a solution for t_Q^* in the form of a product

$$\frac{t_Q^*}{Qr_0^2/k} = D\phi(r^+)\psi(x^+) \tag{15}$$

where ψ and ϕ, respectively, depend on x^+ and r^+ alone. By substituting into the differential equation (13), we find that

$$\psi = e^{-4\beta^2x^+/\text{Re}} \tag{16}$$

$$\frac{d}{dr^+}\left(r^+\gamma\frac{d\phi}{dr^+}\right) + \left(\frac{2\beta^2}{\text{Re}}\frac{r^+}{r_0^+}u^+\right)\phi = 0 \tag{17a}$$

where $-2\beta^2/\text{Re}$ is the separation constant arising from the product solution. From (14*a*), the boundary conditions on equation (17*a*) are

[2] The constant 12.8493, evaluated to higher accuracy for the purpose of this investigation, differs slightly from that of reference [6].

$$d\phi/dr^+ = 0 \quad \text{at} \quad r^+ = 0 \quad \text{and} \quad r^+ = r_0^+ \tag{17b}$$

Equations (17*a*) and (17*b*) comprise an eigenvalue problem of the Sturm-Liouville type. Solutions are possible only for a discrete, though infinite, set of β values. Hence the solution for t_Q^* can be written as

$$\frac{t_Q^*}{Qr_0^2/k} = \sum_{n=0}^{\infty} D_n \phi_n(r^+) e^{-4\beta_n^2 x^+/\mathrm{Re}} \tag{15a}$$

where β_n are the eigenvalues and ϕ_n are the corresponding eigenfunctions of equations (17*a*) and (17*b*). Since the values of r_0^+ and γ in equation (17*a*) depend on the Reynolds and Prandtl numbers, there will be a different set of eigenvalues associated with each choice of these parameters. Utilizing numerical integration, the first six eigenvalues and eigenfunctions have been found for the same Reynolds and Prandtl numbers previously mentioned. The eigenvalues are listed in Table 1, while the corresponding eigenfunctions are available as IBM tabulations.

The coefficients D_n of equation (15*a*) are still to be determined. Applying the boundary condition at the tube entrance as given by equation (14*b*), we have

$$\sum_{n=0}^{\infty} D_n \phi_n = -H(r^+) \tag{18a}$$

From this, it follows immediately from the properties of the Sturm-Liouville system that

$$D_n = \frac{\int_0^{r_0^+} [-H(r^+)] r^+ u^+ \phi_n dr^+}{\int_0^{r_0^+} r^+ u^+ \phi_n^2 dr^+} \tag{18b}$$

It is seen that the computation of the D_n involves an integration of the fully developed temperature distribution. With the β_n, ϕ_n, and D_n determined, the difference temperature t_Q^* is known from equation (15*a*), and we may now proceed with the complete solution of the problem.

The Complete Temperature Solution. Combining the results of the preceeding sections in accordance with equation (5), we are able to write an expression for the temperature distribution which applies both in the entrance and fully developed regions, that is,

$$\frac{t_Q - t_{Q,0}}{Qr_0^2/k} = \frac{4}{\mathrm{RePr}} \frac{x}{d} + H(r^+) + \sum_{n=0}^{\infty} D_n \phi_n(r^+) e^{-\frac{4\beta_n^2}{\mathrm{Re}} \frac{x}{d}} \tag{19}$$

Of particular practical interest is the difference between the

Table 1 Listing of eigenvalues, β_n^2

(a) Re = 50,000.

Pr	β_0^2	β_1^2	β_2^2	β_3^2	β_4^2	β_5^2
0.7	0	1387	3730	7040	11,330	16,600
1.0	0	1380	3705	6981	11,220	16,410
10.0	0	1366	3651	6850	10,960	15,950
100.0	0	1364	3645	6835	10,930	15,880

(b) Re = 100,000.

Pr	β_0^2	β_1^2	β_2^2	β_3^2	β_4^2	β_5^2
0.7	0	2545	6822	12,850	20,630	30,190
1.0	0	2538	6796	12,790	20,520	30,000
10.0	0	2524	6742	12,660	20,270	29,560
100.0	0	2522	6737	12,640	20,240	29,510

(c) Re = 500,000.

Pr	β_0^2	β_1^2	β_2^2	β_3^2	β_4^2	β_5^2
0.7	0	10,680	28,520	53,560	85,810	125,300
1.0	0	10,670	28,490	53,490	85,690	125,100
10.0	0	10,660	28,440	53,360	85,440	124,700
100.0	0	10,660	28,430	53,350	85,410	124,600

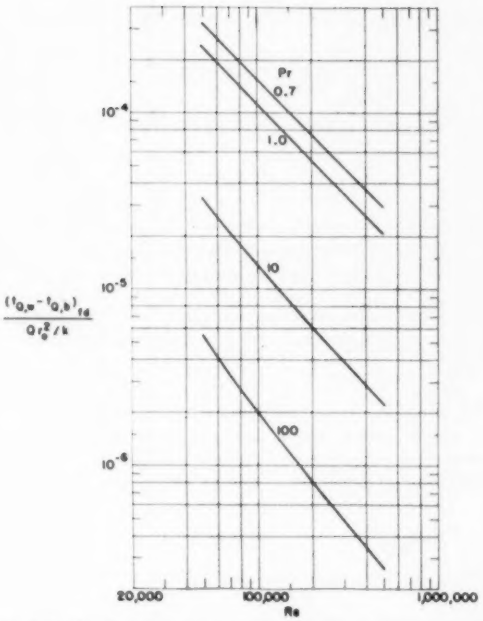

Fig. 2 Fully developed wall-to-bulk temperature difference for uniform internal heat source in an insulated tube

Table 2 Values of the coefficients, E_n

(a) Re = 50,000.

Pr	$-E_0$	$-E_1$	$-E_2$	$-E_3$	$-E_4$	$-E_5$
0.7	0	0.1755×10^{-3}	0.5039×10^{-4}	0.2405×10^{-4}	0.1422×10^{-4}	0.9719×10^{-5}
1.0	0	$.1242\times10^{-3}$	$.3616\times10^{-4}$	$.1752\times10^{-4}$	$.1055\times10^{-4}$	$.7362\times10^{-5}$
10.0	0	$.1293\times10^{-4}$	$.3973\times10^{-5}$	$.2071\times10^{-5}$	$.1379\times10^{-5}$	$.1093\times10^{-5}$
100.0	0	$.1328\times10^{-5}$	$.4263\times10^{-6}$	$.2377\times10^{-6}$	$.1734\times10^{-6}$	$.1576\times10^{-6}$

(b) Re = 100,000.

Pr	$-E_0$	$-E_1$	$-E_2$	$-E_3$	$-E_4$	$-E_5$
0.7	0	0.8775×10^{-4}	0.2454×10^{-4}	0.1128×10^{-4}	0.6421×10^{-5}	0.4180×10^{-5}
1.0	0	$.6186\times10^{-4}$	$.1742\times10^{-4}$	$.8076\times10^{-5}$	$.4640\times10^{-5}$	$.3056\times10^{-5}$
10.0	0	$.6325\times10^{-5}$	$.1851\times10^{-5}$	$.8799\times10^{-6}$	$.5304\times10^{-6}$	$.3708\times10^{-6}$
100.0	0	$.6388\times10^{-6}$	$.1892\times10^{-6}$	$.9353\times10^{-7}$	$.5879\times10^{-7}$	$.4341\times10^{-7}$

(c) Re = 500,000.

Pr	$-E_0$	$-E_1$	$-E_2$	$-E_3$	$-E_4$	$-E_5$
0.7	0	0.1781×10^{-4}	0.4789×10^{-5}	0.2114×10^{-5}	0.1158×10^{-5}	0.7194×10^{-6}
1.0	0	$.1249\times10^{-4}$	$.3366\times10^{-5}$	$.1489\times10^{-5}$	$.8174\times10^{-6}$	$.5094\times10^{-6}$
10.0	0	$.1256\times10^{-5}$	$.3405\times10^{-6}$	$.1519\times10^{-6}$	$.8421\times10^{-7}$	$.5310\times10^{-7}$
100.0	0	$.1259\times10^{-6}$	$.3428\times10^{-7}$	$.1537\times10^{-7}$	$.9581\times10^{-8}$	$.5459\times10^{-8}$

wall and *bulk* temperatures at all stations along the pipe. Evaluating equation (19) at the wall ($r^+ = r_0^+$) and substituting the bulk temperature from equation (11) yields

$$\frac{t_{Q,w} - t_{Q,b}}{Qr_0^2/k} = H(r_0^+) + \sum_{n=0}^{\infty} D_n \phi_n(r_0^+) e^{-\frac{4\beta_n^2}{\mathrm{Re}} \frac{x}{d}} \tag{20}$$

A convenient rephrasing of this result may be carried out by introducing the fully developed wall-to-bulk temperature difference from (12), giving

$$\frac{t_{Q,w} - t_{Q,b}}{(t_{Q,w} - t_{Q,b})_{fd}} = 1 + \frac{\sum_{n=0}^{\infty} E_n e^{-\frac{4\beta_n^2}{\mathrm{Re}} \frac{x}{d}}}{H(r_0^+)} \tag{20a}$$

where the product $D_n\phi_n(r_0^+)$ has been abbreviated by E_n. Numerical values of E_n have been listed in Table 2 as a function of the Reynolds and Prandtl numbers, while $H(r_0^+)$ may be read directly as the ordinate of Fig. 2. Using these numerical data,

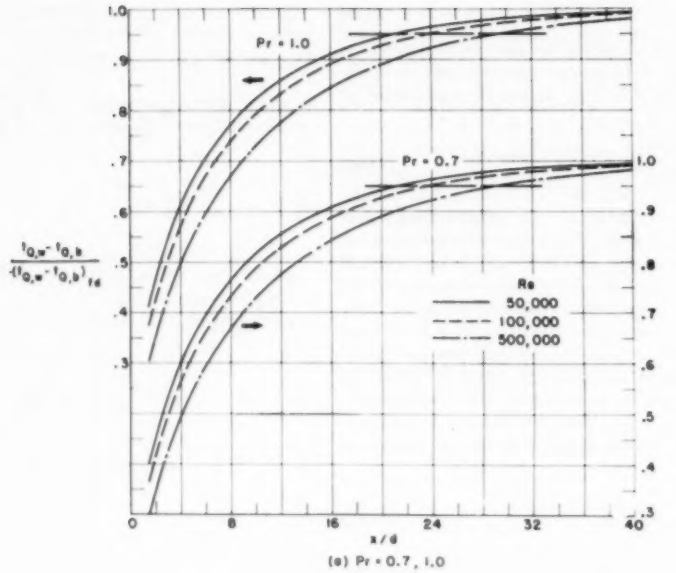

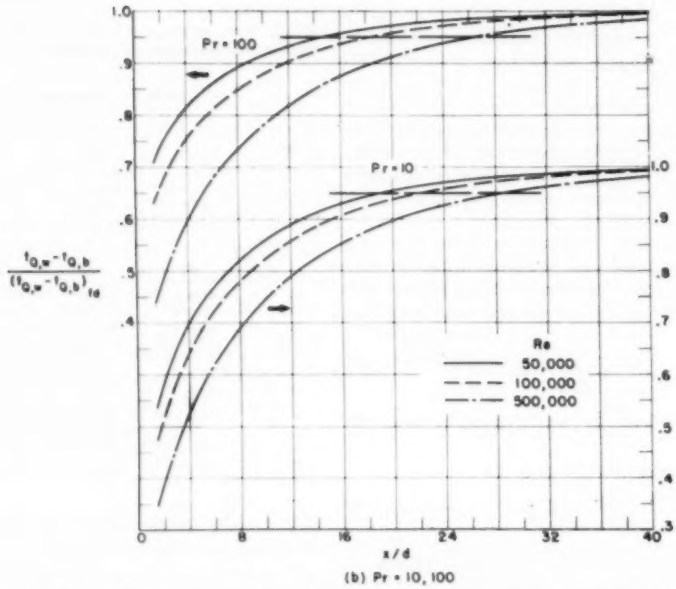

Fig. 3 Wall-to-bulk temperature variation for uniform internal heat source in an insulated tube

the ratio of temperature differences given by (20*a*) has been plotted on Figs. 3(*a* and *b*) as a function of distance along the tube for parametric values of the Reynolds and Prandtl numbers.[2] The information given on these plots, used in conjunction with Fig. 2, permits rapid evaluation of the wall-to-bulk temperature difference at various stations along the tube.

We can define a thermal entrance length as the heated length required for $(t_{Q,w} - t_{Q,b})$ to approach to within 5 per cent of the fully developed value. A dashed line has been drawn on Figs. 3(*a* and *b*) to facilitate finding the entrance length. So, for example, for Re = 50,000 and Pr = 100, the entrance length is 15 diameters; while for Re = 50,000 and Pr = 0.7, the entrance length is 21 diameters. A very significant finding is that, especially for high Prandtl numbers, these entrance lengths are substantially *greater* than those encountered in turbulent pipe flow with uniform wall heat transfer or uniform wall temperature. These differences in entrance length will be emphasized in a later section when the results for uniform wall heat flux are given.

[2] The curves do not extend all the way to $x = 0$ because the series has been truncated.

Arbitrary Longitudinal Heat-Source Variations in an Insulated Tube

We now proceed to generalize these results to apply for arbitrary variations of the internal heat generation along the tube. For

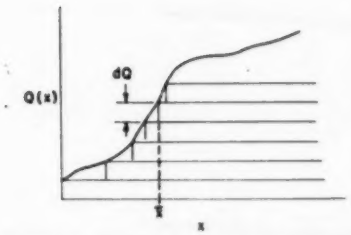

Fig. 4 Representation of an arbitrary longitudinal internal heat-source distribution

the purposes of analysis, suppose that $Q(x)$ can be represented as in Fig. 4. Envision for the moment an elementary heating process in which there is no internal heat generation up to a position $\bar{x}$; then, beyond $\bar{x}$, there occurs a uniform internal heating of magnitude dQ. The temperature response to such a process can be found by applying equation (19).

$$\frac{t_Q - t_{Q,0}}{r_0^2/k} = dQ\left[\frac{4}{\text{RePr}}\frac{(x-\bar{x})}{d} + H(r^+) + \sum_{n=0}^{\infty} D_n\phi_n e^{-\frac{4\beta_n^2}{\text{Re}}\frac{(x-\bar{x})}{d}}\right], \qquad x \geq \bar{x} \quad (21)$$

This elementary heating process can be considered as a differential step in the heat-source variation pictured in Fig. 4. By integrating the separate effects of these elementary steps, we are able to find the temperature distribution at any position corresponding to a prescribed upstream variation of $Q(x)$. The integral of the right side can be rephrased into a more convenient form by integrating by parts. The result of this operation is

$$\frac{t_Q - t_{Q,0}}{r_0/k} = \frac{2}{\text{RePr}}\int_0^x Q(\bar{x})d\bar{x} - \frac{2}{\text{Re}}\sum_{n=0}^{\infty} D_n\phi_n\beta_n^2\int_0^x Q(\bar{x})e^{-\frac{4\beta_n^2}{\text{Re}}\frac{(x-\bar{x})}{d}}d\bar{x} \quad (22)$$

Now, turning to the wall-to-bulk temperature difference, we evaluate equation (22) at $r^+ = r_0^+$ and introduce the bulk temperature by its definition

$$t_{Q,b} = t_{Q,0} + \frac{(d/k)}{\text{RePr}}\int_0^x Q(\bar{x})d\bar{x} \quad (23)$$

finally giving,

$$t_{Q,w} - t_{Q,b} = -\frac{2r_0/k}{\text{Re}}\sum_{n=0}^{\infty} E_n\beta_n^2\int_0^x Q(\bar{x})e^{-\frac{4\beta_n^2}{\text{Re}}\frac{(x-\bar{x})}{d}}dx \quad (24)$$

Numerical values of E_n and β_n^2 are given in Tables 1 and 2, so that the integration can be carried out (either analytically or numerically) for any prescribed variation of the internal heat generation $Q(\bar{x})$.

Wall Heat Transfer Without Internal Heat Generation

Uniform Wall Heat Flux. An analysis of turbulent pipe flow with uniform wall heat flux has been given in reference [5] and only the results need be reviewed here.

First, for the fully developed heat-transfer condition, the wall-to-bulk temperature difference corresponding to the uniform heating at the wall has been plotted on Fig. 5 for the same Reynolds and Prandtl number ranges as heretofore considered.[4] It may be noted that the ordinate is proportional to the reciprocal of the fully developed Nusselt number, which has its usual definition

$$\text{Nu}_{fd} = \frac{h_{fd}d}{k}, \quad h_{fd} = \frac{q}{(t_{q,w} - t_{q,b})_{fd}} \quad (25)$$

while the bulk temperature for uniform heat flux is given by

$$t_{q,b} - t_{q,0} = \frac{qr_0}{k}\frac{8(x/d)}{\text{RePr}} \quad (26)$$

Unpublished experimental air data of Presler and Loeffler [7] also appear in Fig. 5 and show excellent agreement with the theory. The fluid properties appearing in the experimental correlation were evaluated at the film temperature.

Results for the wall-to-bulk temperature difference which apply all along the tube are given in the form of the ratio

$$(t_{q,w} - t_{q,b})/(t_{q,w} - t_{q,b})_{fd}$$

which is plotted on Figs. 6(*a* and *b*) as a function of x/d for parametric values of the Reynolds and Prandtl numbers. The use of Fig. 6, in conjunction with Fig. 5, permits rapid computation of those temperature results of greatest practical interest. The ordinate of Fig. 6 can also be recognized as the ratio

$$\text{Nu}_{fd}/\text{Nu}$$

where Nu is the local Nusselt number defined by equation (25) with subscript fd deleted.

For this situation of uniform wall heat flux, a thermal entrance region can be defined as the length required for $(t_{q,w} - t_{q,b})$ to approach within 5 per cent of its fully developed value, or alternately, as the length required for the Nusselt number to approach within 5 per cent of its fully developed value. A dashed line has been drawn in Fig. 6 to aid in determining the thermal entrance lengths. Comparison of Fig. 6 with Fig. 3, especially for the high Prandtl numbers, verifies our previous statement about the considerably greater entrance lengths associated with the case of internal heat generation. Further, it is interesting to observe that the Reynolds number appears to play a much greater role in determining the entrance lengths for the heat-generation case.

While the important results of reference [5] have been graphed

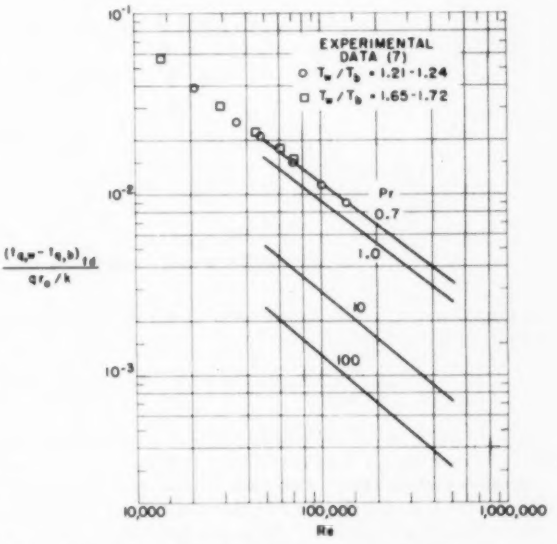

Fig. 5 Fully developed wall-to-bulk temperature difference for uniform wall heat flux and no internal heat source

[4] The results of reference [5] have been extended to cover the Pr = 1 case.

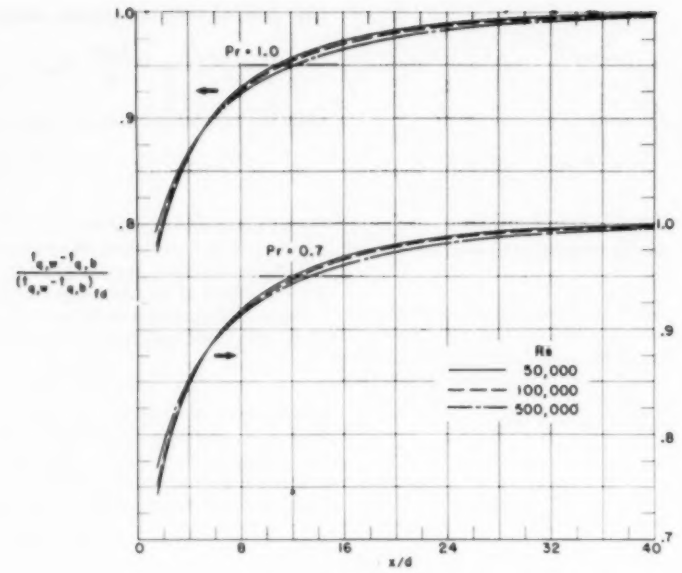

(a) Pr = 0.7, 1.0

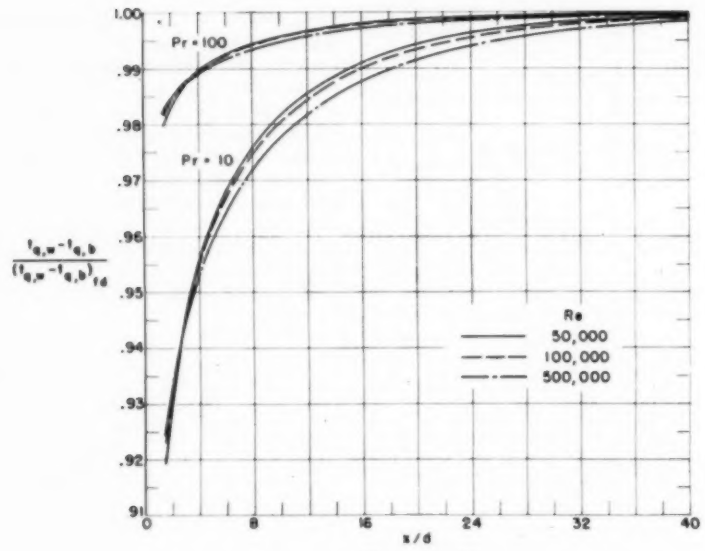

(b) Pr = 10, 100

Fig. 6 Wall-to-bulk temperature variation for uniform wall heat flux and no internal heat source

on Figs. 5 and 6, it will also be useful to give their analytical representation as follows

$$\frac{t_{q,w} - t_{q,0}}{qr_0/k} = \frac{8(x/d)}{\mathrm{RePr}} + G(r_0^+) + \sum_{n=0}^{\infty} F_n e^{-\frac{4\beta_n^2}{\mathrm{Re}}\frac{x}{d}} \quad (26)$$

where β_n^2 and F_n are listed in Tables 1[6] and 3, respectively, and $G(r_0^+)$ is read directly from the ordinate of Fig. 5.

Arbitrary Wall Heat Flux. Following a procedure identical to that outlined previously, the results for the uniform heat flux case as expressed by equation (26) may be generalized to apply to arbitrary longitudinal variations $q(x)$. First considering an elementary heating process and then integrating the effects of many such processes, we find that

$$t_{q,w} - t_{q,b} = -\frac{2}{k\mathrm{Re}} \sum_{n=0}^{\infty} F_n \beta_n^2 \int_0^x q(\bar{x}) e^{-\frac{4\beta_n^2}{\mathrm{Re}}\frac{(x-\bar{x})}{d}} d\bar{x} \quad (27)$$

where

$$t_{q,b} = t_{q,0} + \frac{4}{k\,\mathrm{RePr}} \int_0^x q(\bar{x}) d\bar{x} \quad (28)$$

Equation (27) gives the wall temperature at any position for a prescribed upstream variation in wall heat flux. Inasmuch as the constants β_n^2 and F_n are available in Tables 1 and 3, the in-

[6] The β_n^2 values listed here are slightly refined compared with those of ref. [5].

Table 3 Values of the coefficients, F_n

(a) Re = 50,000.

Pr	$-F_0$	$-F_1$	$-F_2$	$-F_3$	$-F_4$	$-F_5$
0.7	0	0.3507×10^{-2}	0.1848×10^{-2}	0.1278×10^{-2}	0.9842×10^{-3}	0.8209×10^{-3}
1.0	0	$.2505\times10^{-2}$	$.1342\times10^{-2}$	$.9486\times10^{-3}$	$.7480\times10^{-3}$	$.6409\times10^{-3}$
10.0	0	$.2653\times10^{-3}$	$.1546\times10^{-3}$	$.1213\times10^{-3}$	$.1106\times10^{-3}$	$.1109\times10^{-3}$
100.0	0	$.2748\times10^{-4}$	$.1742\times10^{-4}$	$.1513\times10^{-4}$	$.1614\times10^{-4}$	$.1962\times10^{-4}$

(b) Re = 100,000.

Pr	$-F_0$	$-F_1$	$-F_2$	$-F_3$	$-F_4$	$-F_5$
0.7	0	0.1947×10^{-2}	0.1034×10^{-2}	0.7110×10^{-3}	0.5407×10^{-3}	0.4400×10^{-3}
1.0	0	$.1375\times10^{-2}$	$.7375\times10^{-3}$	$.5136\times10^{-3}$	$.3963\times10^{-3}$	$.3277\times10^{-3}$
10.0	0	$.1426\times10^{-3}$	$.7971\times10^{-4}$	$.5887\times10^{-4}$	$.4881\times10^{-4}$	$.4403\times10^{-4}$
100.0	0	$.1455\times10^{-4}$	$.8475\times10^{-5}$	$.6375\times10^{-5}$	$.6809\times10^{-5}$	$.5836\times10^{-5}$

(c) Re = 500,000.

Pr	$-F_0$	$-F_1$	$-F_2$	$-F_3$	$-F_4$	$-F_5$
0.7	0	0.4786×10^{-3}	0.2590×10^{-3}	0.1796×10^{-3}	0.1376×10^{-3}	0.1114×10^{-3}
1.0	0	$.3348\times10^{-3}$	$.1818\times10^{-3}$	$.1265\times10^{-3}$	$.9715\times10^{-4}$	$.7693\times10^{-4}$
10.0	0	$.3389\times10^{-4}$	$.1860\times10^{-4}$	$.1312\times10^{-4}$	$.1026\times10^{-4}$	$.8479\times10^{-5}$
100.0	0	$.3401\times10^{-5}$	$.1877\times10^{-5}$	$.1333\times10^{-5}$	$.1048\times10^{-5}$	$.8783\times10^{-6}$

tegration can be carried out as soon as the variation of q is given.

Combined Internal Sources and Wall Heat Transfer

We can now proceed to write the solution for the situation where internal heat generation and wall heat transfer occur simultaneously. According to equation (2), results for this combined problem are found by adding the contributions due to each of the separate problems.

The most important result of practical interest is the wall temperature variation corresponding to given heating conditions. To compute this, we apply equation (2) to the wall and bulk temperatures

$$t_w = t_{Q,w} + t_{q,w} \qquad t_b = t_{Q,b} + t_{q,b} \tag{29}$$

Then, subtracting the second of these from the first gives

$$t_w - t_b = (t_{Q,w} - t_{Q,b}) + (t_{q,w} - t_{q,b}) \tag{30a}$$

Consideration is first given to the situation where both the internal heating and the wall heat flux are uniform along the length. For these circumstances, equation (30a) can be recast into a form more convenient for rapid calculations as follows:

$$t_w - t_b = \left[\frac{t_{Q,w} - t_{Q,b}}{(t_{Q,w} - t_{Q,b})_{fd}}\right](t_{Q,w} - t_{Q,b})_{fd} + \left[\frac{t_{q,w} - t_{q,b}}{(t_{q,w} - t_{q,b})_{fd}}\right](t_{q,w} - t_{q,b})_{fd} \tag{30b}$$

where the subscript fd denotes the fully developed situation. Numerical values of the first square bracket may be read directly from Figs. 3(a and b); while the second square bracket is read directly from Figs. 6(a and b). The fully developed temperature differences $(t_{Q,w} - t_{Q,b})_{fd}$ and $(t_{q,w} - t_{q,b})_{fd}$ are found from Figs. 2 and 5, respectively. The bulk temperature for the situation of combined uniform heat generation and wall heating is computed from

$$t_b = t_0 + \frac{4(x/d)}{\mathrm{RePr}}\left[\frac{Qr_0^2}{k} + \frac{2qr_0}{k}\right] \tag{31}$$

So, with this information, equation (30b) may be easily evaluated to give the wall temperature at various stations along the tube.

Now, we turn to the situation where the internal heating and wall heat transfer vary in an arbitrary way along the length. Equation (30a) is then applied, and the temperature differences $(t_{Q,w} - t_{Q,b})$ and $(t_{q,w} - t_{q,b})$ are, respectively, evaluated from equations (24) and (27). The numerical values of β_n^2, E_n, and F_n needed in the computations are listed in Tables 1, 2, and 3, while the bulk temperature corresponding to the longitudinally nonuniform heating is given by

$$t_b = t_0 + \frac{1}{k\,\mathrm{RePr}}\left[4\int_0^x q(\bar{x})d\bar{x} + d\int_0^x Q(\bar{x})d\bar{x}\right] \tag{32}$$

Once the longitudinal variations are prescribed, equation (30a) may then be used to compute the wall temperature at various positions.

Radial Variations of the Internal Heat Generation

In this paper numerical results have been provided for the case of internal heat sources which are uniform across the tube cross section. However, the results can be extended to heat sources which vary in the radial direction. In this instance, the fully developed temperature distribution is given by

$$\frac{t_{Q,fd} - t_{Q,0}}{\dfrac{2}{k}\displaystyle\int_0^{r_0} Q(r)r\,dr} = \frac{4}{\mathrm{RePr}}\frac{x}{d} + M(r) \tag{33}$$

which is of a form similar to equation (7b). The function $M(r^+)$ must be found by integrating the equation

$$\frac{2u^+}{\mathrm{RePr}} = \frac{r_0^+}{r^+}\frac{d}{dr^+}\left[r^+\gamma\frac{dM}{dr^+}\right] + \frac{r_0^+}{2\mathrm{Pr}}\frac{Q(r^+)}{\displaystyle\int_0^{r_0^+} Q(r^+)r^+dr^+} \tag{34}$$

With $Q(r^+)$ specified, this can be solved numerically in the same manner and with the same boundary conditions as equation (8).

The eigenvalues and eigenfunctions arising in the solution of the difference temperature t_Q^* remain unchanged, but the D_n in equation (18b) now have to be evaluated using $-M(r^+)$ in place of $-H(r^+)$. Hence, for the difference temperature t_Q^*, we can write

$$\frac{t_Q^*}{\dfrac{2}{k}\displaystyle\int_0^{r_0} Qr dr} = \sum_{n=0}^{\infty} D_n'\phi_n(r^+)e^{-\frac{4\beta_n^2 x^+}{\mathrm{Re}}} \tag{35}$$

where

$$D_n' = \frac{\displaystyle\int_0^{r_0^+}[-M(r^+)]r^+u^+\phi_n dr^+}{\displaystyle\int_0^{r_0^+} r^+u^+\phi_n^2 dr^+} \tag{36}$$

These expressions can be evaluated for any prescribed radial heat-source variation, and the extension to longitudinal variations proceeds in the same manner as described previously for uniform heat sources.

References

1 H. F. Poppendiek and L. D. Palmer, "Forced-Convection Heat Transfer in Pipes With Volume Heat Sources Within the Fluids," ORNL-1395, 1952.

2 H. F. Poppendiek, "Forced-Convection Heat Transfer in Pipes With Volume-Heat Sources Within the Fluids," Chem. Eng. Progress Symposium Series No. 50, 1954, Nuclear Engineering, Part I, pp. 93–104.

3 H. F. Poppendiek and L. D. Palmer, "Application of Temperature Solutions for Forced Convection Systems With Volume Heat Sources to General Convection Problems," ORNL-1933, 1955.

4 E. M. Sparrow and R. Siegel, "Laminar Tube Flow With Arbitrary Internal Heat Sources and Wall Heat Transfer," *Nuclear Science and Engineering*, vol. 4, no. 2, 1958, pp. 239–254.

5 E. M. Sparrow, T. M. Hallman, and R. Siegel, "Turbulent Heat Transfer in the Thermal Entrance Region of a Pipe With Uniform Heat Flux," *Applied Scientific Research*, vol. 7, Section A, 1957, pp. 37–52.

6 Robert G. Deissler, "Analysis of Turbulent Heat Transfer, Mass Transfer, and Friction in Smooth Tubes at High Prandtl and Schmidt Numbers," NACA Rep. 1210, 1955. (Supersedes NACA TN 3145.)

7 Personal communication with A. E. Presler and A. L. Loeffler, Jr., NASA Lewis Research Center.

DISCUSSION

Stuart W. Churchill[6]

At what L/D as one approaches the inlet of the tube do the five eigenvalues and coefficients which you tabulate become inadequate for computation of the temperature distribution and/or heat-transfer rate?

How do your solutions for heat transfer without internal generation compare with those of Sleicher and Tribus?[7]

L. S. Dzung[8]

The present paper is a much welcomed supplement to the authors' previous works on less general subjects. The published data of eigenvalues and coefficients are certainly very valuable, although cases may arise in which higher-order functions than the fifth are necessary and it would be more preferable to have a method to estimate higher-order terms.

Such methods are indeed available. In another connection, the writer has solved the problem of prescribed wall heat transfer without internal heat sources [8],[9] using Fourier series instead of authors' convolution integral. It was shown that the eigenvalues and the coefficients of eigenfunction expansion can be readily obtained analytically if the two radial distribution functions of velocity and eddy diffusivity, namely, authors' u^+ and γ, writer's $f = u/\bar{u}$, $g = \gamma \mathrm{Pr}$, are known or can be assumed. Then the eigenfunctions depend only upon two quantities, the slope of f at tube wall and an integral

$$I = \int_0^1 (2f/g)^{1/2} d(r/r_0) \tag{37}$$

The analytical expressions are most suitable for high-order eigenfunctions, but low-order terms can also be calculated accurately with a simple correction.

Eigenvalues for the present problem are, except that of the zeroth order, given by

$$\sqrt{\lambda_m'}\, I = \pi\left(m + \frac{1}{3}\right) - \delta' \tag{38}$$

where λ_m' is authors' $\beta_m^2 \mathrm{Pr}$, I is the integral given in equation (37), m the order number, and δ' a correction term negligible for high o rders.

Two qualitative features can be inferred from equation (38) if δ' is neglected. Firstly, $\sqrt{\lambda_m'}$ increases linearly with the order m. Secondly, $\sqrt{\lambda_m'}\, I$ is independent upon the type of flow, namely, the number Pr or Re. Now the square of the integrand of equation (37) can be written as, using authors' notations,

$$2 \cdot \frac{u}{\bar{u}} \cdot \frac{\nu}{\nu + Pr \cdot \epsilon_m}$$

If Re and Pr are sufficiently high, ν in the denominator of this expression is negligible compared with $\mathrm{Pr}\epsilon_m$ except near the wall. The integral I is therefore roughly inversely proportional to the square root of Pr and hence λ_m'/Pr is almost independent of Pr.

Both these features are borne out by the authors' calculations. From Table 1, the independence of $\lambda_m'/\mathrm{Pr} = \beta_m^2$ of Pr is at once evident. The linear relation is also clear if β_m is plotted against the order number.

This fact seems to indicate that the choice of β_m as eigenvalues instead of λ_m' is more fortunate. This may be the case in purely turbulent flow, but in a general treatment λ_m' is certainly more appropriate since the laminar case is included without modification.

Authors' $-F_m$, which is Z_m/λ_m' in writer's notations, has been expressed analytically in a simple equation (71) of reference [8] as

$$-F_m = \frac{Z_m}{\lambda_m'} = K_z \frac{N}{I} p^{-1/3} \lambda_m'^{-1/3} \tag{39}$$

where N is a numerical constant, p is the slope of the function f at wall, K_z is a correction factor approaching unity for high-order eigenvalues.

In case of laminar flow, equation (39) gives results which agree perfectly with another publication [9] of the authors.

Equation (39) suggests that F_m decreases approximately with the $-1/3$ power of λ_m'. Plotting authors' values of E_m and F_m against β_m^2 logarithmically, this decrease is indeed observed in the case of E_m, although analytic expression of E_m is more difficult to work out. The decrease of F_m is less rapid. In fact, in some cases F_m even increases with β_m^2 (Pr = 100). Since the series $-\Sigma F_m$ must converge toward $G(r_0^+)$ as explained in reference [8], equation (93), this increase is rather doubtful.

If the dependence of I and λ_m' upon Pr as explained in the foregoing is taken into account, equation (39) indicates that F_m is approximately inversely proportional to the cubic root of Pr. This is not borne out by the authors' data. However, since other influences have not been considered, this kind of argument may not be pushed too far.

Additional References

8 L. S. Dzung, "Heat Transfer in a Round Duct With Sinusoidal Heat Flux Distribution," Second International Conference on Atomic Energy, Geneva, Switzerland, 1958, Paper P 253.

9 R. Siegel, E. M. Sparrow, and T. M. Hallman, "Steady Laminar Heat Transfer in a Circular Tube With Prescribed Wall Heat Flux," *Applied Scientific Research*, vol. 7, series A, 1958, pp. 386–392.

S. Levy[10]

The authors have done an excellent job of extending the forced convection analyses to the case of internal heat generation. The proposed series solutions will undoubtedly yield useful theoretical predictions. However, the solutions are only as accurate as the assumptions used in their derivations and it may be worth-while to dwell upon one of the important approximations made by the authors. Siegel and Sparrow assumed that the eddy diffusivity for momentum and heat are equal. It is an accepted assumption for fully developed flow and thermal conditions, but it remains to be justified when the heat generation or temperature vary in the flow direction. If von Karman's similarity theory is used to express the two eddy diffusivities, one obtains

$$\epsilon_h = \epsilon_m = l^2 \left(\frac{d\bar{u}}{dy}\right)$$

where l is the similarity scale length and is equal to

$$l = \frac{d^2\bar{u}}{dy^2} \Big/ \frac{d\bar{u}}{dy} = \frac{d^2t}{dy^2} \Big/ \frac{dt}{dy}$$

According to these equations, the temperature profile should be proportional to the velocity distribution. If the two eddy

[6] Professor, Chemical Engineering, Department of Chemical and Metallurgical Engineering, University of Michigan, Ann Arbor, Mich. Mem. ASME.

[7] C. A. Sleicher, Jr., and M. Tribus, "Heat Transfer in a Pipe With Turbulent Flow and Arbitrary Wall-Temperature Distribution," TRANS. ASME, vol. 79, 1957, pp. 789–797.

[8] Brown Boveri & Company, Ltd., Baden, Switzerland.

[9] Numbers 8 and 9 in brackets designate additional References at end of this discussion.

[10] Specialist, Heat Transfer and Fluid Dynamics, General Electric Company, Schenectady, N. Y. Assoc. Mem. ASME.

diffusivities are equal such proportionality is not obtained with internal heat generation or in the entrance zone. Reference to the work of Lin and Shen[11] also points out that the foregoing expressions for the scale length are based upon fully developed profiles (note the total derivative used in the equation) and are not necessarily valid when the temperature and velocity distributions vary in the flow direction. The momentum and heat diffusivities are probably not equal at the beginning of the entrance region and their difference may even vary with heat generation in the flow direction.

A. B. Metzner[12]

The authors are to be commended for a well-written and erudite analysis of a number of rather difficult heat-transfer problems. The following comments, while critical, are not intended to detract appreciably from the conclusion that the paper is a very worth-while contribution to the heat-transfer literature from an over-all viewpoint. Specific adverse comments are as follows:

1 The introduction mentions a number of previous analyses that are partially related, but a rather large amount of high-quality work which has been carried out by people interested in viscous heat generation in the plastics industry goes unmentioned. In particular the publications of Toor,[13] Gee and Lyon,[14] and Colwell,[15] appear to be very worth-while contributions whose solutions are perhaps more complex than the one laminar flow solution (reference [4]) singled out for mention in this paper.

2 The choice of Deissler's eddy diffusivity variations represents what is perhaps the best available choice but nevertheless one which is without experimental confirmation in the region near the wall. Furthermore, a more recent paper[16] indicates that the eddy diffusivity variations chosen by Deissler predict coefficients which are perhaps somewhat low by approximately 15 to 20 per cent at Prandtl numbers of 100, due to the fact that undue weight was placed by Deissler on mass-transfer data which have been shown to be subject to some experimental error in the aforementioned paper. As a result of these uncertainties the results predicted in the present analysis must necessarily be used with considerable caution until experimental confirmation is obtained. The experimental confirmation shown in Fig. 5 is entirely noncritical as far as the choice of a set of equations for eddy diffusivity is concerned in view of the fact that at a Prandtl number of 0.7 the variation in the region close to the wall is entirely insignificant.

The present reviewer is puzzled by a statement which appears on page 282 of the paper to the effect that "a result of practical engineering importance is the wall-to-bulk temperature difference." The present reviewer does not understand why anyone would be interested in this quantity in the case of strictly adiabatic flow. Instead it would appear that the entire temperature distribution is the interesting result and tabulation of the results obtained for the temperature distribution rather than the abbreviated results shown in Fig. 2 might have been the more useful data to show.

In summary, this reviewer concludes that while there might be some rather specific limitations to the results developed in the current paper the authors are nevertheless to be strongly commended for clearly showing the method of analysis of a difficult problem and for developing several specific sets of results in sufficient detail that experimental verification can be undertaken to determine whether any of these criticisms are serious shortcomings or of much lesser importance.

Ralph P. Stein[17]

This paper is a very welcome addition to the collection of analytical solutions of various convection heat-transfer problems presently available in the literature. The combined clarity and conciseness of the authors' presentation is to be commended, with one possible exception. This has to do with their explanation of how they derive an expression for temperature distribution with arbitrary heat-source variation from the uniform heat-source case.

Apparently, the authors wish to avoid direct use of a formal mathematical technique (Duhamel's theorem), with which Equation (22) can be written immediately from Equation (19) but with which many of their readers might not be too familiar. Instead, they attempt an explanation with more physical significance, an approach which is always welcome, if done properly. I am not sure that their method of explanation will be easily understood by those readers not already familiar with the more formal mathematical technique. Perhaps clear indication that the integration referred to is for the purpose of calculating the temperature distribution at any position x, and that the integration is performed with respect to the variable ξ, which accounts for the heating of the fluid as it flows from $\xi = 0$ to $\xi = x$, would help. Incidentally, isn't dQ or ξ misplaced in Fig. 4?

Authors' Closure

The authors extend their sincere thanks to the discussers for their interesting remarks and contributions to the paper.

Turning first to Professor Churchill's question relating to the range of x/d over which the solutions are applicable, we observe that in Figs. 3 and 6 the curves have not been drawn all the way back to $x = 0$. Rather, all curves have been cut off at some small value of x/d as was explained in footnote 3 of the paper. This cut-off value represents the smallest x/d for which five terms were sufficient to compute the wall temperature results. Professor Churchill also makes mention of the analysis of Sleicher and Tribus. This work was principally directed to the uniform wall temperature case. The generalization of their results to apply to other wall temperature variations cannot be carried out to good numerical accuracy because too few eigenvalues are given. Hence, no comparison of their work with the uniform wall heat flux case may be made here.

The remarks submitted by Dr. Dzung represent an important adjunct to the paper. It would appear that an immediate utility of his findings would be in extrapolating the results of the present paper to higher eigenvalues. From Dr. Dzung's discussion, it appears that this extrapolation is quite promising for the eigenvalues β_n^2 and the coefficients E_n, but not for the coefficients F_n. This situation with regard to the F_n is not easy to understand. We agree that the trend of F_n increasing with n as exhibited for the higher eigenvalues for high Prandtl numbers and low Reynolds number is open to suspicion. But, we rechecked the numerical integration by rerunning a few cases with a smaller step size, and this did not alter the trend of the coefficients. In any event, this behavior is not too important since the higher eigenvalues play essentially no role for the high Prandtl number results. For the low Prandtl number-high Reynolds number cases, where the step size is not as critical we see no reason why Dr. Dzung's theory, if correct, should not

[11] C. C. Lin and S. F. Shen, "Studies of von Karman's Similarity Theory and Its Extension to Compressible Flows," NACA TN 2541 and 2542, November, 1951.

[12] University of Delaware, Newark, Del.

[13] H. L. Toor, "Energy Equation for Viscous Flow," *Industrial and Engineering Chemistry*, vol. 48, 1956, pp. 922–926; also, *Trans. Society of Rheology*, vol. 1, 1957, p. 177.

[14] R. E. Gee and J. B. Lyon, "Nonisothermal Flow of Viscous Non-Newtonian Fluids," *Industrial and Engineering Chemistry*, vol. 49, 1957, pp. 956.

[15] Colwell, Christmas Symposium, 1958, American Chemical Society.

[16] W. L. Friend and A. B. Metzner, *AIChE Journal*, vol. 4 1958, p. 393.

[17] Columbia University, New York, N. Y.

agree with the results of Table 3. It may also be of interest to mention an approximate procedure developed by R. D. Cess[18] for finding the higher eigenvalues and eigenfunctions for turbulent heat transfer. He applied the method to Latzko's analysis for the case of flow in a circular tube with uniform wall temperature, but presumably other applications are possible.

The remarks of Dr. Levy and Professor Metzner about the need for experimental verification are, of course, quite in order. In this connection, there are some entrance region heat-transfer data shown in reference [5] which agree fairly well with predictions based on the current eddy diffusivity expressions. Additional data have recently been taken at the University of Minnesota[19] which also are in fair agreement with the theory. The authors feel that Deissler's eddy diffusivitiy expressions are the best that are currently available.

[18] R. D. Cess, "Approximation of the Eigenvalues for Heat Transfer in Turbulent Tube Flow," *Journal Aero/Space Sciences*, vol. 26, 1958, pp. 723-724.

[19] Redfield W. Allen, PhD thesis, University of Minnesota, Department of Mechanical Engineering, 1959.

Now, turning to Professor Metzner's comments on the wall-to-bulk temperature difference, we first note that the flow is not strictly adiabatic. Rather, there is a heat source within the fluid and hence the bulk temperature varies along the length. Since the wall temperature is frequently the quantity which one wishes to know and since the bulk temperature is usually known, the authors felt that $T_w - T_b$ was a convenient way of presenting the results. We agree that, for the maximum utility, the entire temperature distribution should have been presented. However, such a presentation would have required considerably more space in the Journal. As noted in the paper more detailed information is available as IBM tabulations.

We thank Dr. Stein for making mention of Duhamel's theorem. This should make the derivation clearer to those who are familiar with this mathematical technique. As to Fig. 4, we feel that both $\bar{x}$ and dQ are properly placed (see for example Figure 4.1, page 403 of Karman and Biot[20]).

[20] T. von Karman and M. A. Biot, "Mathematical Methods in Engineering," McGraw Hill Book Company, Inc., New York, N. Y., 1940.

E. M. SPARROW
J. L. GREGG
NASA, Lewis Research Center, Cleveland, Ohio. Assoc. Mem. ASME

Laminar Condensation Heat Transfer on a Horizontal Cylinder

A boundary-layer analysis is made for laminar film condensation on a horizontal cylinder. The formulation includes both the inertia forces and energy convection terms, which are neglected in Nusselt's simple theory. A similarity transformation, valid over most of the cylinder, is found which reduces the partial differential equations of the problem (the conservation laws) to ordinary differential equations. Numerical solutions of the resulting ordinary differential equations are available for the Prandtl number range from 0.003 to 100. Heat-transfer results are presented and discussed.

Introduction

A THEORY OF LAMINAR FILM CONDENSATION was first given by Nusselt in 1916 [1].[1] Postulating a simple model of the physical phenomenon, he successively analyzed the condensation problem for a variety of geometrical configurations. Attention is directed here to the horizontal cylinder. Our aim is to provide a modern and more complete analysis of the condensation problem, bringing it within the framework of *boundary-layer theory*.

The physical model used by Nusselt is as follows: The hydrodynamics of the problem were expressed as a simple balance between the gravity and the shear forces, inertia effects being disregarded. With regard to the heat transfer, only heat conduction was assumed to operate, energy convection not being considered. In the boundary-layer formulation, both the inertia forces and energy convection are fully accounted for.

The starting point of our study is the boundary layer equations appropriate to the horizontal cylinder. It will be shown that these partial differential equations can be transformed to ordinary differential equations which are valid over a major portion of the surface of the cylinder. The transformation can be carried out in such a manner that the resulting ordinary differential equations coincide with those for condensation on a vertical flat plate. Utilizing numerical solutions of the transformed equations, heat-transfer results are presented for the horizontal cylinder over the Prandtl number range from 0.003 to 100.

[1] Numbers in brackets designate References at end of paper.

Contributed by the Heat Transfer Division and presented at the Semi-Annual Meeting, St. Louis, Mo., June 14–18, 1959, of THE AMERICAN SOCIETY OF MECHANICAL ENGINEERS.

NOTE: Statements and opinions advanced in papers are to be understood as individual expressions of their authors and not those of the Society. Manuscript received at ASME Headquarters, March 6, 1959. Paper No. 59—SA-13.

Analysis

The Conservation Equations. The system under consideration is shown in schematic view in Fig. 1. The x-co-ordinate measures the distance along the circumference of the cylinder, while y measures the distance normal to the surface. It will be supposed that the cylinder is situated in a large body of quiescent, pure vapor which is at its saturation temperature T_{sat}. The surface temperature of the cylinder T_w is uniform and $T_w < T_{sat}$. A continuous film of condensate runs downward over the cylinder.

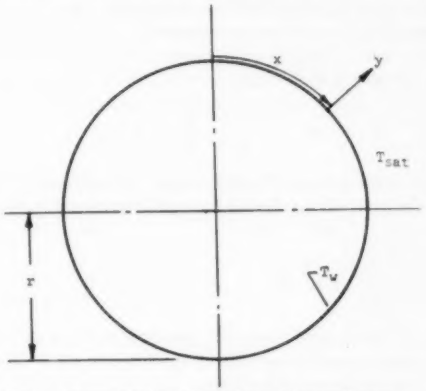

Fig. 1 Geometrical configuration and co-ordinates

Nomenclature

c_p = specific heat at constant pressure
d = cylinder diameter
F = dimensionless velocity function
g = acceleration of gravity
h_{fg} = latent heat of condensation
h = average heat-transfer coefficient, $Q/\text{area}\cdot\Delta T$
k = thermal conductivity
L = height of vertical plate
Nu = over-all Nusselt number; $\text{Nu}_d = \bar{h}d/k$; $\text{Nu}_L = \bar{h}L/k$
Pr = Prandtl number, $c_p\mu/k$
p = static pressure
Q = over-all heat-transfer rate (per unit width)
q = local heat-transfer rate per unit area
r = cylinder radius
T = temperature; T_w, wall temperature; T_{sat}, saturation temperature of vapor; $\Delta T = T_{sat} - T_w$
u = velocity component in x direction
v = velocity component in y direction
X = dimensionless co-ordinate, x/r
x = co-ordinate measuring distance along circumference from upper stagnation point
y = co-ordinate measuring radial distance outward from cylinder surface
δ = thickness of condensate film
γ = function of X appearing in definition of η
η = similarity variable, $(y/r)\{gr^3/\nu^2\}^{1/4}\gamma$
θ = dimensionless temperature, $(T - T_{sat})/(T_w - T_{sat})$
μ = absolute viscosity
ν = kinematic viscosity
ρ = density
τ = shear stress
ϕ = function of X appearing in definition of F
ψ = stream function

The condensation problem is governed by the basic conservation principles: mass, momentum, and energy. The boundary-layer form of these laws for constant property, nondissipative, gravity flow over a horizontal cylinder is

$$\frac{\partial u}{\partial x} + \frac{\partial v}{\partial y} = 0 \tag{1}$$

$$\rho\left(u\frac{\partial u}{\partial x} + v\frac{\partial u}{\partial y}\right) = \rho g \sin\frac{x}{r} + \mu\frac{\partial^2 u}{\partial y^2} \tag{2}$$

$$\rho c_p\left(u\frac{\partial T}{\partial x} + v\frac{\partial T}{\partial y}\right) = k\frac{\partial^2 T}{\partial y^2} \tag{3}$$

The static pressure gradient $\partial p/\partial x$ has been neglected in equation (2) relative to the gravity force $\rho g \sin x/r$.

The conservation of mass equation (1) is immediately satisfied by defining the stream function ψ in the usual way, i.e.,

$$u = \partial\psi/\partial y, \qquad v = -\partial\psi/\partial x \tag{4}$$

Then, the velocity components u and v appearing in equations (2) and (3) are replaced in favor of ψ, giving

$$\frac{\partial\psi}{\partial y}\frac{\partial^2\psi}{\partial x\partial y} - \frac{\partial\psi}{\partial x}\frac{\partial^2\psi}{\partial y^2} = g\sin(x/r) + \nu\frac{\partial^3\psi}{\partial y^3} \tag{2a}$$

$$\frac{\partial\psi}{\partial y}\frac{\partial T}{\partial x} - \frac{\partial\psi}{\partial x}\frac{\partial T}{\partial y} = \frac{k}{\rho c_p}\frac{\partial^2 T}{\partial y^2} \tag{3a}$$

Faced with this formidable pair of partial differential equations, we are motivated to seek some means for reducing them to ordinary differential equations, which are easier to solve.

Reduction to Ordinary Differential Equations. Guided by previous experience with boundary layer theory, we propose a new independent variable η as follows:

$$\eta = \frac{y}{r}\left[\frac{gr^3}{\nu^2}\right]^{1/4}\gamma(X) \tag{5a}$$

where γ is a function of X which is not yet determined. In addition, new dependent variables are constructed in the following way:

$$F(\eta) = \psi\Big/\nu\left[\frac{gr^3}{\nu^2}\right]^{1/4}\phi(X), \qquad \theta(\eta) = \frac{T - T_{sat}}{T_w - T_{sat}} \tag{5b}$$

where $\phi(X)$ is also undetermined. The variable θ is seen to be a dimensionless temperature, while F is related to the velocities of the problem by the equations

$$u = \frac{\nu}{r}\left[\frac{gr^3}{\nu^2}\right]^{1/2}\gamma\phi F' \tag{5c}$$

$$v = -\frac{\nu}{r}\left[\frac{gr^3}{\nu^2}\right]^{1/4}\left[\frac{d\phi}{dX}F + \frac{\phi(d\gamma/dX)}{\gamma}\eta F'\right] \tag{5d}$$

The primes denote differentiation with respect to η. Inspection of equations (5a) through (5d) reveals that the structures of the variables η, F, and θ are those normally found in similar-type boundary-layer formulations.

Using these new variables, a formal transformation of equations (2a) and (3a) may be carried out. The end result of this operation is

$$F'''(\phi\gamma^3) + FF''\left(\phi\frac{d\phi}{dX}\gamma^2\right) - (F')^2\left[\phi\frac{d\phi}{dX}\gamma^2 + \phi^2\gamma\frac{d\gamma}{dX}\right] = -\sin X \tag{6}$$

$$\theta'' + \Pr F\theta'\left(\frac{1}{\gamma}\frac{d\phi}{dX}\right) = 0 \tag{7}$$

In order that equations (6) and (7) be ordinary differential equations, it is required that factors which depend on X be eliminated. Specifically, it is necessary that

$$\phi\gamma^3 = a\sin X \tag{8a}$$

$$\phi\frac{d\phi}{dX}\gamma^2 = b\sin X \tag{8b}$$

$$\phi^2\gamma\frac{d\gamma}{dX} = c\sin X \tag{8c}$$

$$\frac{d\phi}{dX} = e\gamma \tag{8d}$$

where a, b, c, and e are constants. Thus there is seen to be a set of *four* equations for determining the *two* functions γ and ϕ. In order that two functions be determined by four equations, it is required that the equations are not independent of each other; but rather, that two of the equations follow from the other two. Provided that a unique solution can be found, then equations (6) and (7) will truly be ordinary differential equations and the transformation defined by equations (5a) and (5b) will have achieved its end.

The problem of finding ϕ and γ from equations (8a) through (8d) is precisely the same one faced by Hermann in analyzing free convection about a horizontal cylinder [2]. He found that a unique solution could be achieved except for small values of X. However, the boundary layer assumptions are already invalid for small X for other reasons. In view of this, it has been generally accepted that the failure to find a unique solution for ϕ and γ in this region will not introduce errors in the *over-all* heat transfer significantly different from those already present in the boundary layer analysis.

The functions ϕ and γ as given by Hermann are listed in Table 1.[2]

Table 1 ϕ and γ functions

X	0°	30°	60°	90°	120°	150°	165°	180°
ϕ	0	1.181	2.337	3.430	4.41	5.24	5.55	5.84
γ	0.760	0.752	0.718	0.664	0.581	0.458	0.360	0

The level of these functions has been adjusted so that the constants a, b, c, and e of equations (8a) through (8d) are simple integers which will lead to a particularly desirable form when inserted in equations (6) and (7). The γ function and the product $\gamma\phi$, originally presented as figure 17 of reference [2], have been reproduced in Fig. 2.

[2] In reference [2], the ϕ function is denoted as f, while the γ function is denoted as g.

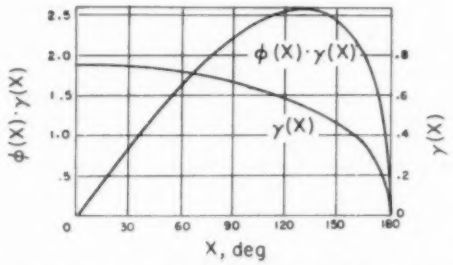

Fig. 2 The functions γ and $\phi\gamma$ (reproduced from Fig. 17, reference [2])

Returning now to equations (6) and (7) and utilizing the ϕ and γ functions, there results

$$F''' + 3FF'' - 2(F')^2 + 1 = 0 \tag{9a}$$

$$\theta'' + 3(\mathrm{Pr})F\theta' = 0 \tag{9b}$$

It is of first importance to observe that these equations coincide precisely with the governing equations for film condensation on a vertical plate [3]. (This correspondence was assured by adjustment of the levels of ϕ and γ.) The boundary conditions on F and θ, to be discussed, are also the same as for the vertical plate problem. As a consequence, the available mathematical solutions for the F, θ of the vertical plate are immediately at our disposal as solutions for the F, θ of the horizontal cylinder. However, since different transformations were used, the physical variables (such as heat transfer, velocity, and temperature) do not follow the same laws in the two problems.

The Boundary Conditions. To complete the statement of the problem, the boundary conditions must be specified. At the surface of the cylinder, both velocity components must vanish as a consequence of the no-slip condition of viscous flow and of the impermeability of the wall. Also, the condensate immediately adjacent to the wall must take on the temperature T_w. At the interface between the liquid and vapor ($y = \delta$), the condition is imposed that the vapor offers negligible shearing resistance to the condensate flow. This assumption is standard in condensation theory. In addition, it will be required that the condensate take on the temperature T_{sat} at the liquid-vapor interface. The formal statement of these conditions is

$$\left.\begin{aligned} u &= 0 \\ v &= 0 \\ T &= T_w \end{aligned}\right\} \; y = 0 \qquad \left.\begin{aligned} \tau &= \mu \partial u/\partial y = 0 \\ T &= T_{sat} \end{aligned}\right\} \; y = \delta \tag{10}$$

The thickness of the condensate layer δ, which will vary with position around the cylinder, must be determined from the analysis. In terms of the new variables of equations (5a) through (5d), these boundary conditions become

$$\left.\begin{aligned} F &= 0 \\ F' &= 0 \\ \theta &= 1 \end{aligned}\right\} \; \eta = 0 \qquad \left.\begin{aligned} F'' &= 0 \\ \theta &= 0 \end{aligned}\right\} \; \eta = \eta_\delta \tag{10a}$$

where η_δ corresponds to the value of η at $y = \delta$.

As a consequence of the transformation (5), our problem has been reduced to the task of solving equations (9) subject to the boundary conditions (10a). Evidently, these solutions will depend on the choice of two parameters: Pr and η_δ. From the mathematical standpoint, this is a completely satisfactory situation. But, practically speaking, the problem is incomplete, since the dimensionless condensate layer thickness η_δ would not be known a priori. So, there remains the need to relate η_δ to another parameter which contains physical quantities which are all known.

To relate η_δ (and hence δ) to known physical quantities, we invoke an over-all energy balance as follows

$$h_{fg} \int_0^\delta \rho u \, dy + \int_0^\delta \rho u c_p (T_{sat} - T) \, dy = \int_0^x k \left(\frac{\partial T}{\partial y} \right)_{y=0} dx \tag{11}$$

The first term on the left is the energy released as latent heat, while the second term is the energy liberated by subcooling of the condensate. The right-hand side represents the heat transferred from the condensate to the cylinder over a span of circumference from $x = 0$ to $x = x$. In writing equation (11), the standard assumption of negligible heat conduction across the liquid-vapor interface has been invoked. In terms of the transformed variables as given by equation (5), the over-all energy balance becomes

$$\frac{c_p \Delta T}{h_{fg}} = -3\mathrm{Pr} \, \frac{F(\eta_\delta)}{\theta'(\eta_\delta)} \tag{11a}$$

where $F(\eta_\delta)$ and $\theta'(\eta_\delta)$, respectively, denote the values of F and $d\theta/d\eta$ at $\eta = \eta_\delta$.

From a solution of equations (9) corresponding to specified values of the parameters Pr and η_δ, the values of $F(\eta_\delta)$ and $\theta'(\eta_\delta)$ are available, and the right side of equation (11a) may be evaluated. So, $c_p \Delta T/h_{fg}$ is determined. For a fixed Prandtl number, equations (9) may be solved for a sequence of values of η_δ, and a corresponding set of values of $c_p \Delta T/h_{fg}$ may then be computed from equation (11a). In other words, for a fixed Prandtl number, there is a unique relation between η_δ and $c_p \Delta T/h_{fg}$. So, we may regard the solutions as depending on the parameters Pr and $c_p \Delta T/h_{fg}$, rather than on Pr and η_δ.

Solutions. It has already been remarked that equations (9) and the boundary conditions (10a) coincide with those for condensation on a vertical flat plate. Further, the relationship between $c_p \Delta T/h_{fg}$ and η_δ for a fixed Prandtl number, as given by equation (11a), is the same as that for the plate. So, immediate application of the mathematical solutions for the plate can be made to the horizontal cylinder.

For the vertical plate, solutions of equations (9) subject to the boundary conditions (10a) have been carried out numerically in reference [3] for Prandtl numbers of 0.003, 0.008, 0.03, 1.0, 10, and 100. The first three of these Prandtl numbers correspond to liquid metals, while the last three correspond to ordinary liquids. Utilizing these numerical solutions, heat-transfer results for the horizontal cylinder will be reported here for values of the parameter $c_p \Delta T/h_{fg}$ ranging from essentially 0 to 1.

Results

Heat Transfer. The quantity of greatest practical interest is the heat transferred from the condensate to the cylinder. The local heat flux is computed from Fourier's Law, i.e.,

$$q = k \left(\frac{\partial T}{\partial y} \right)_{y=0} \tag{12}$$

In terms of the transformed variables of equation (5), the expression for q becomes

$$q = \frac{k}{r} (T_{sat} - T_w) [-\theta'(0)] \left(\frac{gr^3}{\nu^2} \right)^{1/4} \gamma(X) \tag{12a}$$

where $\theta'(0)$ is an abbreviation for $(d\theta/d\eta)_{\eta=0}$. The variation of q around the circumference is seen to be proportional to the variation of the γ function. Using Fig. 2, it may be observed that q has its maximum value at $X = 0$ (upper stagnation point) and decreases monotonically with increasing X.

The over-all heat transfer to the entire cylinder may be found by integrating the local values according to the relation

$$Q = 2 \int_0^{\pi r} q \, dx = 2r \int_0^\pi q \, dX \tag{13}$$

Introducing q from equation (12a) and integrating, there is obtained

$$Q = 2k(T_{sat} - T_w)[-\theta'(0)] \left(\frac{gr^3}{\nu^2} \right)^{1/4} \int_0^\pi \gamma \, dx \tag{13a}$$

The value of the integral is given by Hermann as

$$\int_0^x \gamma \, dX = 0.616\pi$$

It is customary to phrase the heat-transfer results in terms of an over-all heat-transfer coefficient and an over-all Nusselt number defined as follows:

$$\bar{h} = \frac{Q}{2\pi r(T_{sat} - T_w)}, \quad \mathrm{Nu}_d = \frac{\bar{h}d}{k} \tag{14}$$

With this, the over-all heat-transfer result of equation (13*a*) becomes

$$\mathrm{Nu}_d \Big/ \left(\frac{gd^3}{\nu^2}\right)^{1/4} = 0.733[-\theta'(0)] \tag{15}$$

Since $\theta'(0)$ depends upon both Pr and $c_p\Delta T/h_{fg}$, so then does the dimensionless heat-transfer representation of equation (15). Previous experience with condensation heat-transfer theory suggests that the dependence on Pr and $c_p\Delta T/h_{fg}$ can be substantially reduced by rephrasing the dimensionless heat transfer in the form

$$\mathrm{Nu}_d \Big/ \left[\frac{g\rho h_{fg}d^3}{k\nu(T_{sat} - T_w)}\right]^{1/4} = 0.733\,[-\theta'(0)] \left[\frac{c_p\Delta T/h_{fg}}{\mathrm{Pr}}\right]^{1/4} \tag{16}$$

Utilizing the numerical solutions of equations (9), the right-hand sides of equations (16) and (11*a*) can be evaluated. The results thus obtained have been plotted on Fig. 3.[3] This graph contains the complete theoretical prediction of the heat transfer as given by boundary-layer theory.

By inspection of the figure, it is immediately seen that for small values of $c_p\Delta T/h_{fg}$, the heat-transfer results for fluids of any Prandtl number are given by

$$\mathrm{Nu}_d = 0.733 \left[\frac{g\rho h_{fg}d^3}{k\nu(T_{sat} - T_w)}\right]^{1/4} \tag{17}$$

[3] The curves for liquid metals have been extended only to $c_p\Delta T/h_{fg} = 0.1$ in consideration of the relatively small magnitudes of c_p/h_{fg} possessed by these fluids.

Now, it has been shown in reference [3] that the thickness of the condensate film varies monotonically with $c_p\Delta T/h_{fg}$. So, small values of $c_p\Delta T/h_{fg}$ correspond to thin films. In very thin condensate films, the effects of both energy convection and inertia forces are very small. So, equation (17) describes the heat-transfer process in the limiting situation where the energy convection and inertia play a negligible role. It is interesting to observe that Nusselt's analysis, which deals only with this limiting situation, leads to a result identical to equation (17), except that his constant is 1 per cent lower.

Relative to the prediction of equation (17), the role of energy convection would be to *increase* the heat transfer, while the role of the inertia forces would be to *decrease* the heat transfer. So, these two effects are in conflict. With this, we can provide perspective for the trends displayed on Fig. 3. For the high Prandtl number fluids, where the inertia forces are completely overriden by the viscous forces, the effects of energy convection win out and the curves rise with increasing film thickness (increasing $c_p\Delta T/h_{fg}$). For the low Prandtl number fluids, where the heat conductivity overrides the energy convection, the effects of the inertia forces win out and the curves fall with increasing film thickness.

Heat-Transfer Results for Small Cylinders. For a given temperature condition and a given fluid (i.e., given $c_p\Delta T/h_{fg}$ and Pr), our theory predicts that

$$\eta_\delta = \frac{\delta}{r}\left[\frac{gr^3}{\nu^2}\right]^{1/4}\gamma(X) = \text{constant} \tag{18}$$

or

$$\frac{\delta}{r} \sim \frac{1}{r^{3/4}\gamma(X)} \tag{18a}$$

At any circumferential position X, it is seen that the ratio δ/r will increase as the cylinder radius decreases. Since the boundary layer equations for the horizontal cylinder are based on the assumption that δ/r is small, it follows that boundary-layer theory fails for cylinders of very small radius.

The boundary-layer heat-transfer results may be corrected for the effects of small radius in a manner identical to that used by Eckert (ref. [4], p. 165) for the free convection problem. Translating his findings into the context of the condensation problem, there is obtained

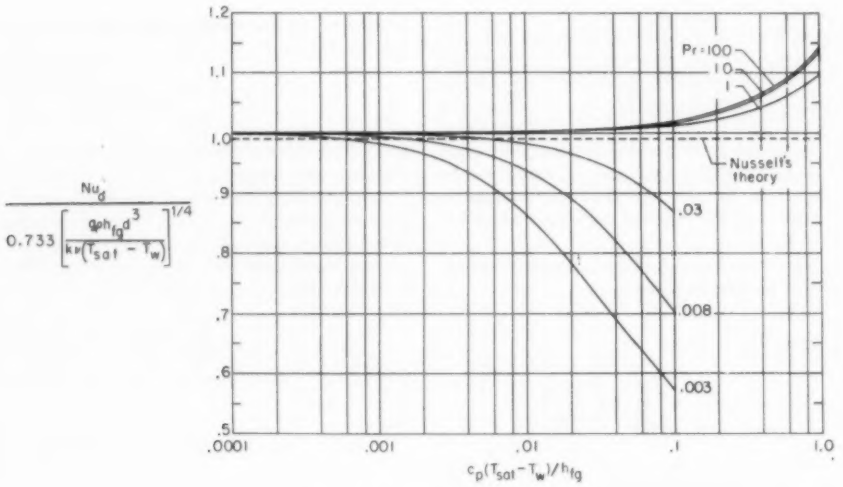

Fig. 3 Heat-transfer results

$$\mathrm{Nu}_d' = \frac{2}{\ln\left(1 + \frac{2}{\mathrm{Nu}_d}\right)} \tag{19}$$

where Nu_d' is the corrected Nusselt number and Nu_d is the prediction for full-sized cylinders (e.g., Fig. 3). For normal applications, $2/\mathrm{Nu}_d \ll 1$, so

$$\ln\left(1 + \frac{2}{\mathrm{Nu}_d}\right) \approx \frac{2}{\mathrm{Nu}_d}, \quad \mathrm{Nu}_d' \approx \mathrm{Nu}_d$$

Comparison With Vertical Plate Heat Transfer. For film condensation on a vertical plane of height L, the dimensionless heat-transfer prediction of boundary-layer theory takes the form

$$\mathrm{Nu}_L \Big/ \left[\frac{g\rho h_{fg} L^3}{k\nu(T_{sat} - T_w)}\right]^{1/4} = 0.943[-\theta'(0)]\left[\frac{c_p \Delta T / h_{fg}}{\mathrm{Pr}}\right]^{1/4} \tag{20}$$

where $\theta'(0)$ is the same function of Pr and $c_p\Delta T/h_{fg}$ as appears in equation (16) and

$$\mathrm{Nu}_L = \frac{\bar{h}L}{k}, \quad \bar{h} = \frac{Q}{L(T_{sat} - T_w)}$$

So, for a given Pr and $c_p\Delta T/h_{fg}$, it follows that

$$\mathrm{Nu}_L \Big/ 0.943\left[\frac{g\rho h_{fg} L^3}{k\nu(T_{sat} - T_w)}\right]^{1/4} = \mathrm{Nu}_d \Big/ 0.733\left[\frac{g\rho h_{fg} d^3}{k\nu(T_{sat} - T_w)}\right]^{1/4} \tag{21}$$

As a consequence of this correspondence, Fig. 3 can be used equally well for the flat plate as for the horizontal cylinder.

It is interesting to inquire about the relationship between plate height and cylinder diameter required to produce equal *heat-transfer coefficients* for plate and cylinder. Equating heat-transfer coefficients, temperature differences, and fluid properties in equation (21), it is found that[4]

$$L = 2.78\, d \tag{22}$$

Using this equivalence, correlations of the heat-transfer coefficient for cylinders may also be used for vertical plates and vice versa.

Circumferential Variation of Film Thickness. For a particular physical situation (i.e., given fluid, ΔT and r), the circumferential variation of the film thickness δ is found from equation (18) to be

$$\delta \sim \frac{1}{\gamma(X)} \tag{23}$$

The function $\gamma(X)$ is graphed on Fig. 2, and its reciprocal provides us with the variation of δ. Utilizing Fig. 2, it is seen that the condensate layer thickness, starting from a *finite value* at $X = 0$, grows rather slowly over the upper portion of the cylinder and then increases quite rapidly over the lower part of the cylinder. At the lower stagnation point ($X = \pi$), the theoretical prediction of an infinite film thickness can be interpreted as signifying the dropping away of the condensate from the cylinder surface.

Comparison With Experimental Heat Transfer. Experiments on film condensation over a horizontal cylinder have been carried out primarily for fluids with Prandtl numbers lying above unity. Data for these high Prandtl number experiments are summarized by McAdams (ref. [5], p. 340). In general, the conditions of the tests corresponded to small values of $c_p\Delta T/h_{fg}$. Since the analytical predictions of Nusselt closely correspond to those of the boundary-layer formulation for low $c_p\Delta T/h_{fg}$, the comparison of McAdams (table 13-4) between experimental data and Nusselt's theory also applies here.

For the low Prandtl number range, experiments on sodium and mercury have been carried out by Misra and Bonilla for values of $c_p\Delta T/h_{fg}$ up to 0.03. Their heat-transfer results were only 5 to 15 per cent of equation (17). While boundary-layer theory predicts a lowering of the Nusselt number for these low Prandtl number fluids (see Fig. 3), the predicted reduction is much smaller than that found by experiment. So, it would appear that the effect of the inertia forces is by no means sufficient to explain the experimental findings. There still remains the need for further experiments to clearly define the departures between the test conditions and the analytical model.

[4] According to Nusselt's simple theory, as quoted by McAdams (ref. [5], p. 341) the equality of coefficients is achieved when $L = 2.87\ d$; a result which is very close to equation (22).

References

1 W. Nusselt, "Die Oberflächen Kondensation des Wasserdampfes," *Zeitschrift des Vereines Deutscher Ingenieure*, vol. 60, 1916, pp. 541 and 569.

2 R. Hermann, "Heat Transfer by Free Convection From Horizontal Cylinders in Diatomic Gases," NACA TM 1366, 1954.

3 E. M. Sparrow and J. L. Gregg, "A Boundary-Layer Treatment of Laminar-Film Condensation," Trans. ASME, series C, Journal of Heat Transfer, vol. 81, 1959, pp. 13–18.

4 E. R. G. Eckert, "Introduction to the Transfer of Heat and Mass," first edition, McGraw-Hill Book Company, Inc., New York, N. Y., 1950.

5 William H. McAdams, "Heat Transmission," third edition, McGraw-Hill Book Company, Inc., New York, N. Y., 1954.

6 B. Misra and C. F. Bonilla, "Heat Transfer in the Condensation of Metal Vapors," *Chemical Engineering*, Progress Symposium Series no. 18, vol. 52, pp. 7–21.

DISCUSSION

L. A. Bromley[5]

The authors are to be commended for bringing laminar-film condensation on a horizontal cylinder "within the framework of boundary-layer theory." I believe it would be of interest to compare the result reported here with an approximate one I derived[6] and corrected after discussions with Rohsenow[7] for high Prandtl number fluids.

In the authors' nomenclature, it may be written:

$$\mathrm{Nu}_d = 0.7280\left\{\frac{\left(1 + \frac{3}{8}\frac{c_p\Delta T}{h_{fg}}\right)}{\left(1 + \frac{11}{40}\frac{c_p\Delta T}{h_{fg}}\right)^{8/4}}\right\}\left[\frac{g\rho h_{fg} d^3}{k\nu(T_{sat} - T_w)}\right]^{1/4}$$

the term in braces has the following values as a function of $c_p\Delta T/h_{fg}$

$\frac{c_p\Delta T}{h_{fg}}$	0.01	0.1	0.5	1.0	2.0
{ }	1.0017	1.017	1.078	1.146	1.260

From Fig. 3 in the text, it appears that the agreement is good for high Prandtl numbers.

The results for Prandtl number near unity should apply to film boiling (within the limits imposed on the derivation) with the

[5] Associate Professor of Chemical Engineering, University of California, Berkeley, Calif.

[6] L. A. Bromley, *Industrial and Engineering Chemistry*, vol. 44, 1952, pp. 2966–2969.

[7] W. M. Rohsenow, "Heat Transfer and Temperature Distribution in Laminar-Film Condensation," Trans. ASME, vol. 78, 1956, pp. 1645–1648.

physical properties of liquid and vapor interchanged. Of course, the assumption of no drag at the liquid-vapor interface would be poor.

Although I am sure the author is aware of other limitations of the derivation as applied to "laminar-film" condenser calculations, I think it is well to point out some of them to the reader.

1 Surface tension produces droplets covering appreciable areas on the underside of a horizontal tube.

2 Resistance at the vapor-liquid interface may be present either due to "accommodation or evaporation coefficient" effects or to presence of impurities at the interface.

3 Ripples may be present.

4 Vapor drag is seldom negligible.

Authors' Closure

The authors extend their thanks to Professor Bromley for his interesting discussion. From these comments, it will be possible to gain further physical insights into the problem.

First of all, it is found that, when the values tabulated by Professor Bromley are plotted on Fig. 3, good agreement is obtained with the Pr = 100 curve. Now, the Bromley-Rohsenow formulation was carried out under the assumption that the inertia forces (fluid accelerations) are negligible. This situation does occur either for very viscous liquids or for very thin condensate films. The viscous liquids are characterized by high Prandtl numbers; and so it is reasonable that the Bromley predictions should agree with the high Prandtl number results of the present analysis, where the effects of inertia forces are included. Thin films are characterized by small values of $c_p\Delta T/h_{fg}$; and according to Fig. 3, the results for all Prandtl numbers approach the Nusselt asymptote, which neglects the inertia terms.

The restricting assumptions mentioned at the end of Professor Bromley's discussion are, unfortunately, common to almost all condensation analyses. In terms at our present analytical skills these problems would be intractable were these simplifications not made.

E. L. LUSTENADER
Engineer, General Engineering Laboratory. Mem. ASME

R. RICHTER
Engineer, Knolls Atomic Power Laboratory

F. J. NEUGEBAUER
Consulting Engineer, General Engineering Laboratory. Mem. ASME

General Electric Company, Schenectady, N. Y.

The Use of Thin Films for Increasing Evaporation and Condensation Rates in Process Equipment

This paper describes an experimental investigation of an evaporating and condensing test apparatus in which over-all heat-transfer coefficients as high as 8000 Btu/(hr) (sq ft) (deg F) were obtained with water by utilizing thin films both in evaporation and condensation. The films were obtained by wiping on the evaporating surface and utilizing surface tension effects on the condensing surface. The phenomena on both the evaporating and the condensing surfaces are amenable to theory.

Introduction

THE PROBLEM OF DESIGN in heat-transfer equipment is generally an economic one influenced by three factors—cost of energy consumption, initial cost of equipment, and cost of maintenance. Since both low operating cost and low initial investment contribute to an economic optimum, a reduction in over-all resistance to heat transfer is a desirable achievement since it allows either a decrease in the required heat-transfer surface area or a reduction in the energy demand by lowering the over-all temperature difference across the surface.

The program undertaken by the authors was aimed at evaluating a new concept in heat transfer in which the over-all resistance to heat flow is decreased through the combined use of thin films both for evaporation and condensation. The thin films for evaporation were achieved by spreading the fluid on the surface by means of a slowly rotating wiper. Thin films for condensation resulted from the utilization of surface tension. The experimental program was undertaken during the period from 1955 to 1958. A vapor compression-type evaporator, using water as a heat-transfer fluid, was used to investigate the parameters involved. Over-all heat-transfer coefficients as high as 8000 Btu/(hr) (sq ft) (deg F) were reached with the experimental apparatus.

Description of the Heat-Transfer System

The apparatus used to study the evaporation of thin wiped films is shown in Fig. 1. It is composed of a heat-transfer surface, a vapor compressor, and a rotating wiper. The heat-transfer surface, upon which water is evaporated and condensed, is a copper tube 24 in. long and 3 in. in diameter with a wall thickness of 0.035 in. The 3-in. copper tube is surrounded by a concentric 6-in. pyrex glass tube which is wrapped with nichrome ribbon and electrically heated to prevent the formation of condensation on the inner glass surface. A glass tube was selected to allow observation of the condensing surface.

Inside the center tube is a wiper which rotates about the vertical axis of the cylinder. Secured to the top of the wiper shaft is a water distributor to which raw water is supplied. The distributor discharges the water to the inner wall just in advance of the wiper so that the liquid flows down the surface in advance of the wiper and is spread by the wiper into a thin film over the inner surface of the cylinder. As the thin film evaporates, the vapor formed is drawn off and transported to the outer annular chamber by means of a compressor. The compressed vapor, which is superheated, is condensed on the outer surface of the center tube releasing its heat of vaporization which passes through the tube wall and evaporates more water.

Thin Film Evaporation

As the wiper rotates inside of the center tube, it distributes a thin film of water for evaporation. Because of the low temperature difference across the film, evaporation will occur without bubble formation. The agreement of test and theory indicates that the heat of vaporization passes through the film by conduction alone. The pressure and temperature of the vapor adjacent to the evaporating liquid film are slightly lower than the values corresponding to saturation at the liquid-vapor interface. For evaporation to continue, the vapor leaving the liquid surface must be removed from the immediate vicinity.

The rate of evaporation depends on three factors:

Contributed by the Heat Transfer Division and presented at the Semi-Annual Meeting, St. Louis, Mo., June 14–18, 1959, of THE AMERICAN SOCIETY OF MECHANICAL ENGINEERS.

Statements and opinions advanced in papers are to be understood as individual expressions of their authors and not those of the Society. Manuscript received at ASME Headquarters, March 2, 1959. Paper No. 59—SA-30.

Nomenclature

k = thermal conductivity, Btu/(hr) (sq ft) (deg F per ft)
h = heat-transfer coefficient, Btu/(hr) (sq ft) (deg F)
h_{fg} = latent heat or vaporization, Btu/lb
U = over-all coefficient of heat transfer, Btu/(hr) (sq ft) (deg F)
τ = time, hr
v = wiper-blade velocity, ft/hr
t = saturation temperature, deg F
ρ = density, lb/cu ft
L = length of wiper, ft
ϑ_o, ϑ_i, ϑ = film thickness defined in Fig. 2, ft
δ = wall thickness, ft
V = volume, cu ft
Q = quantity of heat, Btu
W = quantity of matter, lb
x_o, x_f, x = linear distances defined in Fig. 2, ft
w = flow rate, lb/hr
A = area, sq ft
D = diameter, ft
n = speed of rotation, rev/hr
M = number of wiper blades
G = mass velocity, lb/(hr) (sq ft)
c = specific heat, Btu/(lb) (deg F)

Subscripts

e = evaporation
c = condensation
w = wall
f = liquid

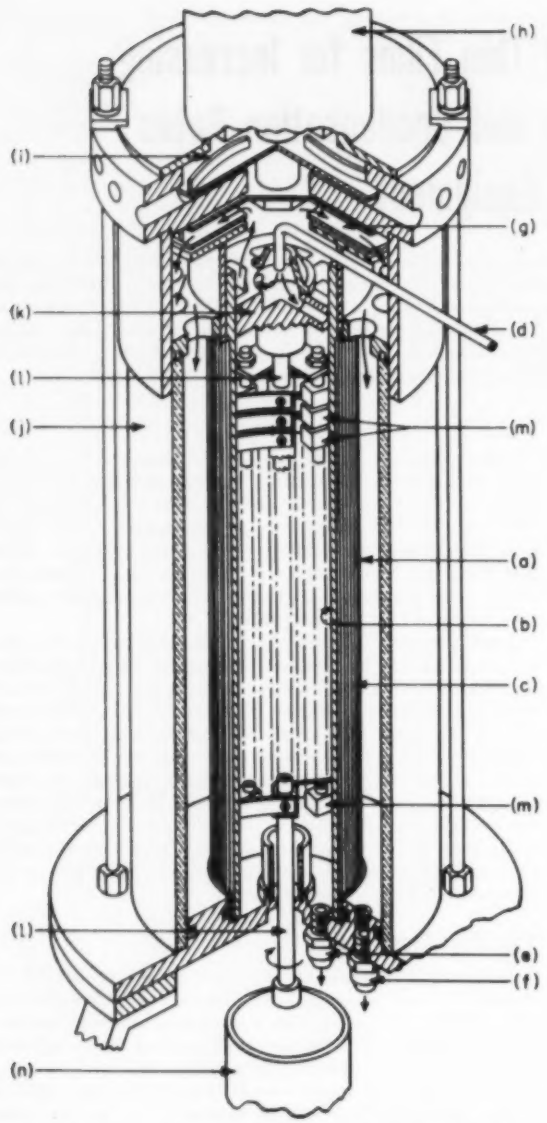

Fig. 1 Cutaway view of experimental heat-transfer apparatus
(a) Heat-transfer tube, (b) surface for thin film evaporation, (c) surface for thin film condensation, (d) raw water inlet, (e) concentrate outlet, (f) condensate outlet, (g) vapor compressor, (h) vapor compressor drive motor, (i) drive motor cooling fan, (j) pyrex glass jacket, (k) raw water distributor, (l) wiper, (m) spring-loaded carbon brushes, (n) wiper drive motor

(1) The initial thickness of the liquid film spread by the wiper on the inner wall. This thickness is controlled by the wiper design, wiper speed, and wiper load.

(2) The temperature drop across the evaporating liquid film.

(3) The rate at which the film is renewed on the inner wall.

The simplified analysis of the wiped film which will be presented is for a vapor compression-type evaporator similar to that shown in Fig. 1. The evaporation system is one in which the heat of vaporization is supplied by a vapor condensing on the rear side of the evaporating surface. The analysis is based on the following assumptions:

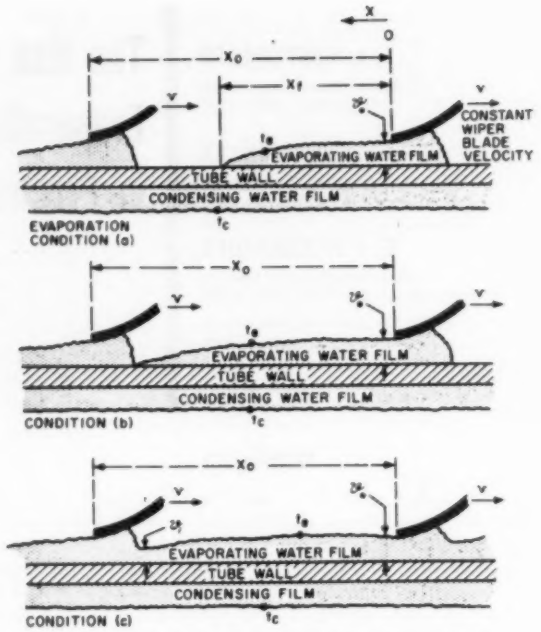

Fig. 2 Three conditions of wiped thin film evaporation

1 The heat-transfer surface is sufficiently thin and the wiper speed sufficiently low so that effects of heat storage in the tube wall can be neglected.

2 The increase in sensible heat in the evaporating liquid film is small compared with the latent heat of vaporization and can therefore be neglected.

3 The heat-transfer coefficient on the condensing surface remains constant regardless of surface loading and, therefore, for a constant over-all temperature difference between the evaporating and the condensing surfaces, the heat flow through the evaporating liquid film becomes a function only of film thickness.

4 The wiper is adjusted in such a manner that the initial thickness of the liquid film spread on the inner wall is not a function of wiper rpm.

5 The circumferential flow of heat in the tube wall is small compared with the radial flow and can be neglected.

6 The mineral concentration in the water is small so that the boiling point elevation can be neglected.

With these assumptions, it can be envisioned that three conditions of evaporation will occur as shown in Fig. 2. Condition (a) will take place when the wiper velocity is low so that, at a given over-all temperature difference, the wall becomes partially dry before the next wiper blade renews the evaporated liquid film. Under this condition, only a portion of the available heat-transfer surface is utilized. Condition (b) occurs when the wiper velocity is increased, while keeping the same over-all temperature difference, to the point where the entire heat-transfer surface just becomes wet between wiper blades. Condition (c) occurs when the wiper velocity is further increased so that the result is an increase in the average liquid film thickness between the wiper blades. The extreme for condition (c) is reached when wiper velocity becomes infinite. The liquid film thickness between wiper blades would then become constant and equal to the initial thickness of the film spread on the wall.

Considering first condition (a) in which case the wall is partially dry between wiper blades, the time required for the water film thickness to decrease from its initial thickness ϑ_0 to zero is

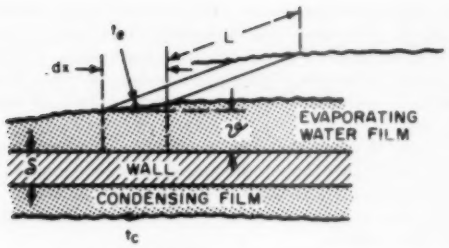

Fig. 3 Cross section of heat-transfer surface

equal to the time it takes for the wiper blade to travel a distance x_f.

For constant wiper blade velocity

$$v = \frac{x_f}{\tau_d} \tag{1}$$

where τ_d is the time required for a water film to evaporate from a thickness ϑ_0 to zero. The evaporation time can be found as follows.

Referring to Fig. 3, the over-all heat-transfer resistance for a flat surface is

$$\frac{1}{U} = \frac{1}{h_c} + \frac{\delta}{k_w} + \frac{\vartheta}{k_f} \tag{2}$$

The heat transferred through the wall in a time increment $d\tau$ is

$$dQ = UdxL(t_c - t_e)d\tau \tag{3}$$

The change in volume of this evaporating water film is

$$dV = -\frac{1}{\rho}\frac{dQ}{h_{fg}} = Ldxd\vartheta \tag{4}$$

Combining equations (2), (3), and (4)

$$\left(\frac{1}{h_c} + \frac{\delta}{k_w} + \frac{\vartheta}{k_f}\right)d\vartheta = \frac{(t_c - t_e)}{\rho h_{fg}}\,d\tau \tag{5}$$

Integrating equation (5) and inserting the limits $\tau = 0$ at $\vartheta = \vartheta_0$ gives

$$\left(\frac{1}{h_c} + \frac{\delta}{k_w}\right)(\vartheta_0 - \vartheta) + \frac{(\vartheta_0^2 - \vartheta^2)}{2k_f} = \frac{(t_c - t_e)}{\rho h_{fg}}\,\tau \tag{6}$$

Equation (6) describes the evaporating water film thickness as a function of time, provided the over-all temperature difference and the condensing heat-transfer coefficient remain constant.

The time required for the water film to completely evaporate is

$$\tau_d = \frac{\rho h_{fg}}{(t_c - t_e)}\left[\left(\frac{1}{h_c} + \frac{\delta}{k_w}\right)\vartheta_0 + \frac{\vartheta_0^2}{2k_f}\right] \tag{7}$$

The wiper velocity can be determined from equations (7) and (1)

$$v = \frac{x_f(t_c - t_e)}{\rho h_{fg}\left[\left(\frac{1}{h_c} + \frac{\delta}{k_w}\right)\vartheta_0 + \frac{\vartheta_0^2}{2k_f}\right]} \tag{8}$$

where x_f represents the wetted distance between wiper blades.

The weight of water spread by one wiper blade is

$$w = \rho L\vartheta_0 v \tag{9}$$

Combining equations (8) and (9)

$$w = \frac{Lx_f(t_c - t_e)}{h_{fg}\left(\frac{1}{h_c} + \frac{\delta}{k_w} + \frac{\vartheta_0}{2k_f}\right)} \tag{10}$$

Equation (10) describes the evaporation rate per wiper blade as the wetted distance x_f varies between 0 and x_0. When x_f is equal to x_0, the evaporation rate reaches a maximum value and the film condition corresponds to that shown in Fig. 2(*b*).

As the wiper velocity further increases, the average film thickness increases as shown in Fig. 2(*c*). For condition (c), the wiper velocity can be expressed as

$$v = \frac{x_0}{\tau_1} \tag{11}$$

where τ_1 represents the time required for the film to evaporate from ϑ_0 to ϑ_1.

Combining equations (6) and (11) and solving for τ_1

$$\tau_1 = \frac{\rho h_{fg}}{(t_c - t_e)}\left[\left(\frac{1}{h_c} + \frac{\delta}{k_w}\right)(\vartheta_0 - \vartheta_1) + \frac{\vartheta_0^2 - \vartheta_1^2}{2k_f}\right] \tag{12}$$

The time rate of water spread by a single wiper blade is

$$w = \rho L(\vartheta_0 - \vartheta_1)v \tag{13}$$

Combining equations (11), (12), and (13)

$$w = \frac{Lx_0(t_c - t_e)}{h_{fg}\left[\frac{1}{h_c} + \frac{\delta}{k_w} + \frac{(\vartheta_0 + \vartheta_1)}{2k_f}\right]} \tag{14}$$

Equation (14) gives the rate of evaporation per wiper blade for the condition of evaporation shown in Fig. 2(*c*).

The average over-all heat-transfer coefficient can be expressed as

$$U = \frac{wh_{fg}M}{A(t_c - t_e)} \tag{15}$$

The relationship between wiper velocity and rpm for the test still is

$$v = \pi Dn \tag{16}$$

In order to evaluate the theory, it was required to have an estimate of the initial thickness of the evaporating water film and the condensing heat-transfer coefficient. These estimates were obtained by simultaneously solving the equations describing the wiped film process using test data where wiper rpm was the only variable. The calculations showed that the condensing coefficient was about 10,000 Btu/(hr) (sq ft) (deg F) and the initial water film thickness ϑ_0 was in the order of 0.0005 in. Assuming that these values would remain constant regardless of surface loading, equation (6) was used to obtain a set of curves showing water film thickness as a function of evaporation time. Equations (6), (8), and (16) were then used to find the fraction of the tube wall in the test apparatus which remained wet as a function of wiper speed, over-all temperature difference, and initial water film thickness. Predicted evaporation rates and average over-all heat-transfer coefficient as a function of wiper rpm were determined from equations (6), (9), (10), (11), (13), (14), (15), and (16).

The curves which result are shown in Figs. 4, 5, 6, and 7 Fig. 4 shows evaporation or distillation rates for the test apparatus plotted against wiper rpm for constant temperature difference and water film thickness. Note that at constant temperature difference the evaporation rate increases linearly with rpm until a maximum point is reached. This maximum corresponds to con-

dition (b) where the entire tube wall just remains wet. At the maximum point the water film resistance to heat flow is a minimum, the average film thickness being $\delta_0/2$. The wall will become partially dry if wiper rpm is decreased. As the wiper rpm is increased, the average water film thickness and the resistance to heat flow increase. As the wiper rpm approaches infinity, water film thickness approaches a constant value equal to the initial thickness of the film spread.

Fig. 5 shows the evaporation rate plotted against the temperature difference for constant wiper rpm and water film thickness. The evaporation rate increases nonlinearly with increasing temperature difference until a maximum is reached. The maximum occurs when the entire tube wall just remains wet and the water is evaporating from the wall as fast as it is being spread. At this point, the only way in which the evaporation rate can be increased is to either increase wiper rpm or increase water film thickness, both combined with an increase in temperature difference.

Figs. 6 and 7 show the corresponding over-all heat-transfer coefficients plotted against wiper rpm and temperature difference. The area for heat transfer was taken as the wiped area. Note that, in the curves in which wiper rpm is plotted against temperature difference, the zero temperature difference point corresponds to the condition of maximum water film thickness. For example in Fig. 7, as the over-all heat-transfer coefficient increases, the average water film thickness on the wall is decreasing. When the maximum coefficient point is reached, the wall is just starting to dry. A further increase in temperature difference has the effect of having a greater fraction of the wall dry. As the temperature difference approaches infinity, although the distillation rate has reached a maximum value, the average over-all heat-transfer coefficient approaches zero at the point where the wall is completely dry. As thinner water film thicknesses are desired which correspond to higher over-all heat-transfer coefficients, either lower temperature differences, higher wiper speeds, or a greater number of wiper blades are required to prevent the wall from becoming dry.

It should be noted that the temperature difference and the wiper rpm have no effect on the magnitude of the minimum and maximum over-all heat-transfer coefficient. The initial water film thickness and the condensing heat-transfer coefficient determine these values.

The Influence of Heat Storage in the Heat-Transfer Surface

The measurements taken on the experimental evaporator were found to agree reasonably well with the theory presented, provided that:

(1) The entire wall remains wetted by the evaporating film.

(2) Part of the wall is dry but the product of wiper rpm times the number of wiper blades is low.

For the condition of a partially dry wall and a high product of wiper rpm times number of wiper blades, the effect of heat storage in the tube wall was evident.

Fig. 8 describes the storage phenomenon. The wall is assumed to have a resistance considerably lower than the condensing film resistance so that temperature differences within the wall can be neglected. Also neglected is heat conduction in the axial and the circumferential direction and the heat storage capacity of the condensing film.

The lower slanted line shows the temperature gradient after

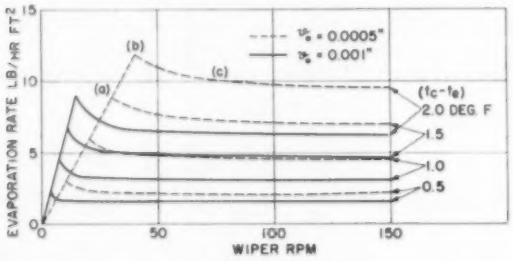

Fig. 4 Predicted evaporation rates versus wiper rpm for constant temperature difference and film thickness

Curves calculated for t_s = 212 deg F, 2 wiper blades each 18 in. long, 3-in. diameter copper tube, δ = 0.035 in., h_c = 10,000 Btu/(hr) (sq ft) (deg F). Refer to Fig. 2 for conditions (a), (b), and (c).

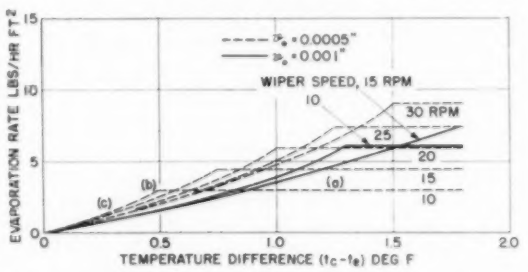

Fig. 5 Predicted evaporation rates versus temperature difference for constant wiper rpm and film thickness

Conditions same as in Fig. 4

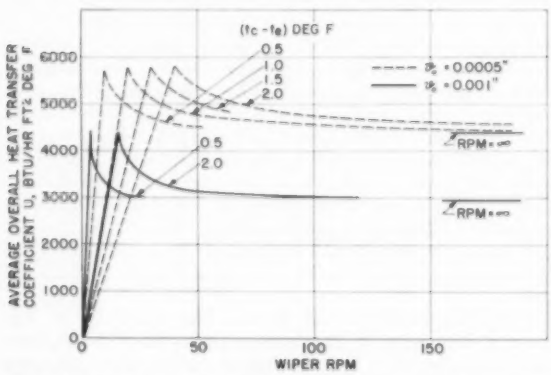

Fig. 6 Predicted over-all heat-transfer coefficients versus wiper rpm for constant temperature difference and film thickness

Conditions same as in Fig. 4

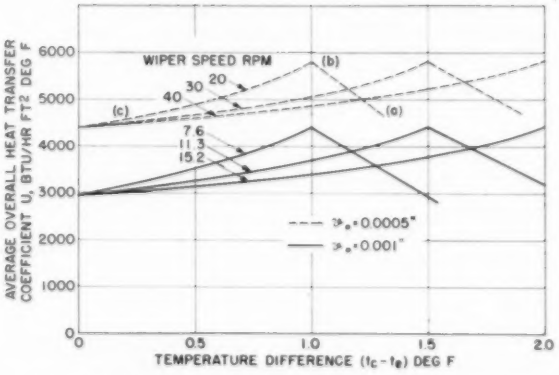

Fig. 7 Predicted over-all heat-transfer coefficients versus temperature difference for constant wiper rpm and film thickness

Conditions same as in Fig. 4

the evaporating film has just dried. The upper slanted line shows the gradient after the time interval τ.

The heat transferred to the wall during the time differential $d\tau$ is

$$dQ = \left(\frac{x_0 - x_f}{x_0}\right) A h_s (t_c - t_w) d\tau \tag{17}$$

This is equal to the heat stored in the wall

$$dQ = \left(\frac{x_0 - x_f}{x_0}\right) A \delta c_w \rho_w dt_w \tag{18}$$

The combination of equations (17) and (18) results in

$$\frac{h_c}{\rho_w c_w \delta} d\tau = \frac{dt_w}{(t_c - t_w)} \tag{19}$$

For the condition $\tau = 0$ at $t_w = t_{w_0}$ the integration yields

$$t_w = t_c - (t_c - t_{w_0}) e^{-\frac{\tau h_c}{\delta c_w \rho_w}} \tag{20}$$

Since the water film resistance is extremely low at the point where the film dries, it can be assumed that

$$t_{w_0} = t_e \tag{21}$$

The heat stored in the wall is therefore

$$Q = \left(\frac{x_0 - x_f}{x_0}\right) A c_w \rho_w \delta (t_c - t_e) \left(1 - e^{-\frac{\tau h_c}{\delta c_w \rho_w}}\right) Mn \tag{22}$$

The time τ and the dry wall fraction $\left(\frac{x_0 - x_f}{x_0}\right)$ can be eliminated from equation (22) by combining with equations (1), (7), (16) and (22).

The stored heat Q is picked up by the surplus water wave which proceeds each wiper and is used for additional evaporation. This consideration, which is given in detail in Reference [18],[1] leads to satisfactory agreement between test and theory.

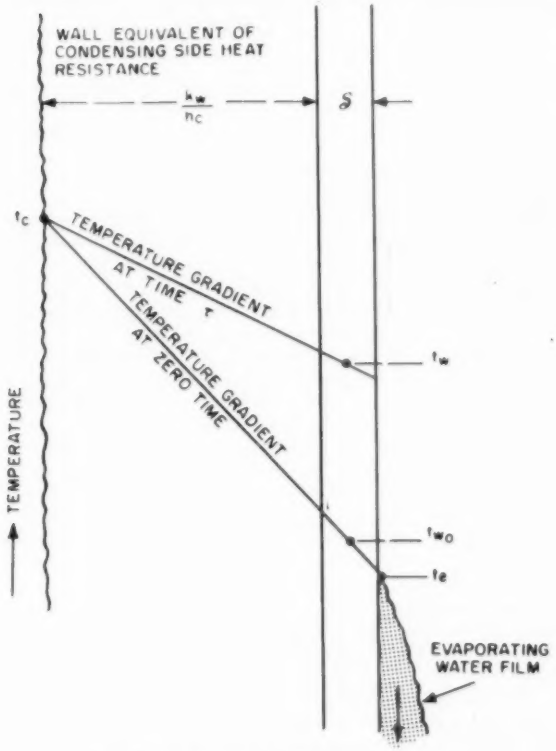

Fig. 8 Heat storage in the heat-transfer surface

Condensation and Its Effects on Evaporator Performance

Tests on the heat-transfer apparatus indicated that extremely thin water films could be spread by the wiper on the evaporating surface. These films offered such a small resistance to heat flow that the maximum over-all heat-transfer coefficient was controlled essentially by the maximum condensing coefficient. For this reason, a program was undertaken to study the factors influencing the rate of condensation. It is known that two types of condensation could occur—filmwise and dropwise.

Filmwise Condensation on Smooth Surfaces. The vapor which leaves the compressor as shown in Fig. 1 is in a condition of superheat as it surrounds the center tube for condensation. The shape of the condensate film which is formed on the smooth surface of the vertical tube and the condition of the vapors are shown in Fig. 9. To determine the average rate of heat transfer under these conditions, the analyses of Nusselt [4], Jakob [5], and Rohsenow [8] are valid. Rohsenow's recent work includes the effect of vapor velocity on condensing film thickness.

In the analysis presented in this report for thin film evaporation, the condensing coefficient was assumed constant and equal to the average value over the entire length of the tube. Actually the average coefficient for condensation on a smooth surface decreases as tube length increases. The average theoretical values of the condensing coefficient as calculated by the Nusselt method are in reasonable close agreement with test. Fig. 10 shows the magnitude of the average condensing coefficients that can be expected for filmwise condensation on a 3-in. diameter tube 2 ft long.

The initial tests on the compression-type evaporator were made with a clean, smooth, copper condensing surface. Since

[1] Numbers in brackets designate References at end of paper.

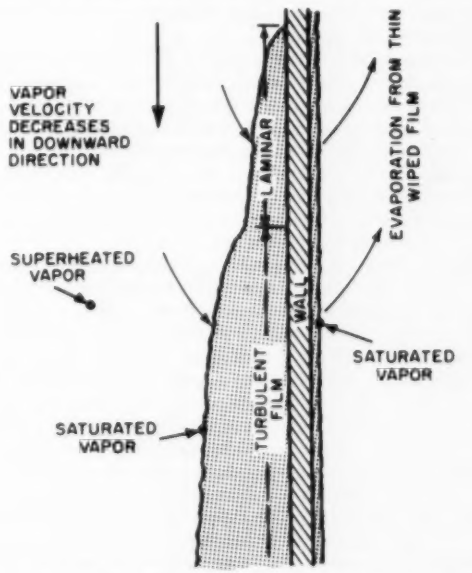

Fig. 9 Cross section of the condensate film formed on a smooth surface in the experimental evaporator

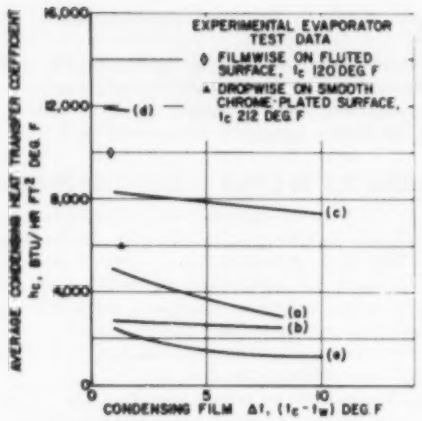

Fig. 10 Average condensing coefficient versus temperature difference for various types of condensation

Curves (a) dropwise on Teflon, 1/2-in. diameter tube 3 ft long, t_c = 212 deg F, reference [2]; (b) filmwise on smooth brass, 1/2-in. diameter tube, 3 ft long, t_c = 212 deg F, reference [19]; (c) filmwise on fluted surface, 2 ft long, t_c = 212 deg F, reference [13]; (d) filmwise on fluted surface, 2 ft long, t_c = 86 F, reference [13]; (e) calculated from Nusselt theory, laminar film condensation on smooth surface, 2 ft long, reference [5]

the thin films spread for evaporation on the inner tube surface offered little resistance to heat flow, the maximum over-all heat-transfer coefficient approached the value of the condensing coefficient.

Dropwise Condensation on a Smooth Surface. It is well known that of the two types of condensation available, dropwise and filmwise, the heat transfer under normal operating conditions can be many times higher with dropwise. With this in mind the outer surface of the center tube in the test evaporator was highly polished and flash chrome plated in order to promote dropwise condensation. The test series that followed indicated an increase in over-all heat-transfer coefficient with maximum values approaching 5000 Btu/(hr) (sq ft) (deg F). This level of dropwise coefficients is in general agreement with the values measured by other investigators as shown in Fig. 10.

After about 200 hours of testing on the smooth chrome plated tube, the dropwise condensation turned to a mixed condensation as shown in Fig. 11, in which part became filmwise. Test data reported by other investigators indicated that the potential available with dropwise condensation had still not been reached in the evaporator setup. Therefore a test program was initiated in order to study the effect of dropwise condensation promoters. The results obtained with various dropwise condensation promotors are summarized in Table 1.

The results of the dropwise condensation studies were disappointing. The reason is probably the low pressure level at which the evaporator was operated in these particular tests. A certain amount of uncertainty exists as to the actual effect of the pressure level on dropwise condensation. Most of the tests reported in the literature have been made at atmospheric pressure. The excellent low pressure tests reported by Gnam [14] are unfortunately clouded by the vapor velocity effects which occurred when the vapor pressure was decreased in the test apparatus. Kinetic gas theory, however, indicates that with decreasing pressure level the coefficient of condensation should decrease.

The conclusion is that our knowledge of the process of dropwise condensation is still rather limited. A further extensive theoretical and experimental study will be required in order to achieve the same understanding as in film condensation.

Film Condensation on a Fluted Tube. If the condensing surface of a tube is grooved as shown in Fig. 12(*a*), a condensing heat-transfer coefficient many times higher than the coefficient for a smooth tube can be achieved. The phenomenon was first analyzed and reported by Gregorig [13] before the Swiss Physical Society in 1952. The effect is due to the pressure gradient produced by surface tension in the plane at right angles to the axis of the tube. Fig. 12(*b*) shows the profile of the condensing surface as suggested by Gregorig. The convexity of the surface at point 1 produces an overpressure in the film of the condensate as compared to the vapor pressure. The pressure in the condensate is determined by the surface tension and the radius of curvature of the condensate film. At point 2, owing to the change in sign of the surface curvature, a low pressure is formed in the liquid condensate. This produces a pressure gradient in the condensate film in the direction from the crest to the base of the groove. The surface of the condensate film is therefore sucked into the base of the groove. It should be noted that the high rates of condensation are confined only to the zone about the crests. The base of the groove is filled with condensate resulting in a relatively lower heat-transfer coefficient in this area. The heat-transfer coefficient averaged over the total tube surface is smaller than the crest coefficient but is still considerably greater than that for a smooth tube.

The variation of coefficient with tube length is practically constant for a given condition of steam and condensate film temperature drop. As the temperature difference increases, the condensate in the groove takes on a different profile. Each profile

Table 1 Principal results of dropwise promoter tests

Surface conditions	Experimental results
(1) Wax on polished chrome	Appearance of dropwise condensation excellent; performance extremely low, less than filmwise condensation
(2) Oleic acid on copper	Dropwise condensation returned to filmwise after five hours
(3) Stearic acid on polished chrome	Dropwise condensation returned to mixed condensation after five hours
(4) Oleic acid mixed with light machine oil on polished chrome	Dropwise condensation returned to mixed condensation after 30 minutes
(5) Benzene mercaptan on copper	Promoter applied by submerging tube in a solution of mercaptan and benzene for a period of two hours. Excellent dropwise condensation returned to filmwise after 30 minutes.
(6) Mercaptan dissolved in 1-1-1 trichlorethane on copper	Excellent dropwise condensation; lasted thirty hours
(7) Mercaptan applied directly to heated copper	Excellent dropwise condensation; returned to filmwise after 30 minutes
(8) Dodecanethiol dissolved in benzene on copper	Promoter applied by submerging tube for 12 hours. Excellent dropwise condensation for three hours.
(9) Dodecanethiol dissolved in chlorethan on copper	The condensate produced was cloudy immediately after injection. After five minutes of operation cloudiness disappeared. Odor present in the condensate. Excellent dropwise condensation; long life.
(10) Mercaptan injected into vapor	The condensate produced was cloudy immediately after injection. After five minutes of operation cloudiness disappeared. Odor present in the condensate. Excellent dropwise condensation; long life.

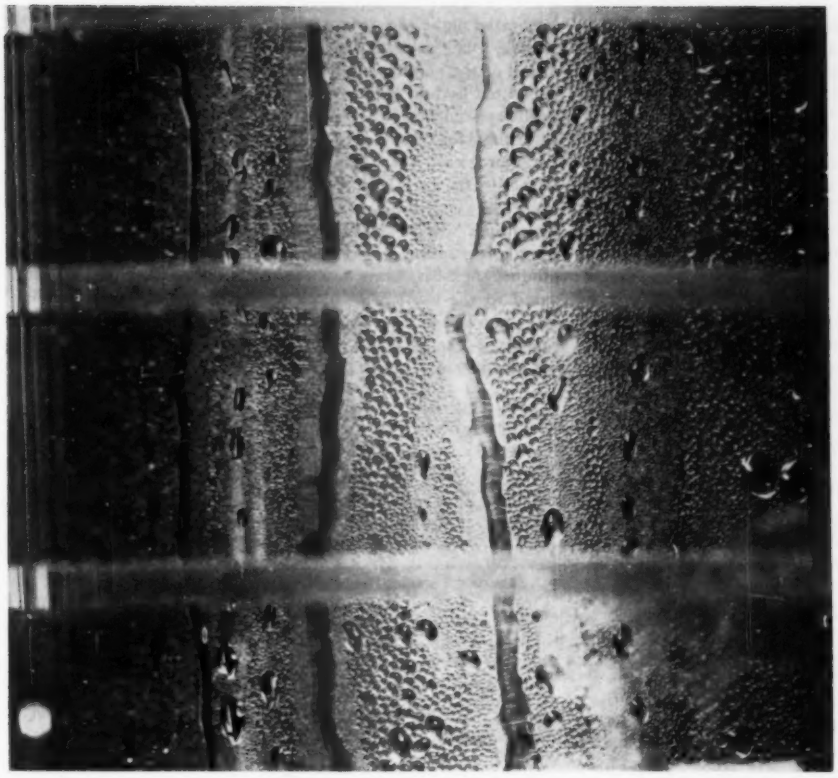

Fig. 11 Condensing side of experimental apparatus showing mixed condensation on an untreated chrome plated surface

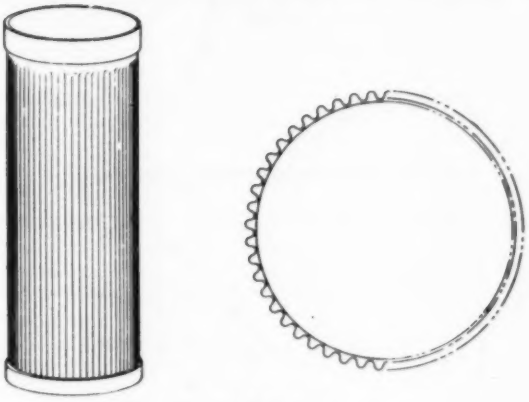

Fig. 12(a) Fluted tube

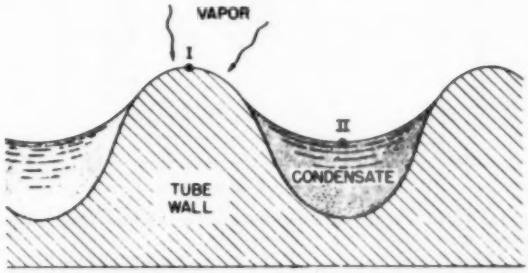

Fig. 12(b) Profile of the condensing surface used by Gregorig

	ANGLE β	RADIUS r
0	31°	0.018"
1	13°	0.019"
2	12-1/2°	0.020"
3	11°	0.023"
4	10°	0.028"
5	7°	0.037"
6	4-1/2°	0.060"
7	1°	0.208"

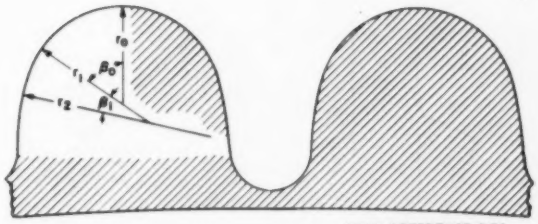

FROM REFERENCE (18)

Fig. 13 Optimized profile dimensions of the fluted surface

corresponds to a certain condensation rate which is a function of tube length. If the temperature difference is increased well beyond the fluted surface design point, a sudden sharp drop in condensing heat-transfer coefficient occurs at the base of the tube as the grooves become filled with condensate and the pressure gradient is eliminated. When the grooves are not filled, the condensing side heat-transfer coefficient is essentially independent of tube length.

Based on the concept of using surface tension to maintain a thin film, an improved fluted profile was designed. A sketch of the fluted surface is shown in Fig. 13. The tube was manufactured by milling the surface with a profile cutter ground to the contour shown.

Evaluation of the fluted surface in the thin film evaporator, Fig. 1, produced a maximum over-all heat-transfer coefficient of 8300 Btu/(hr) (sq ft) (deg F). This was the highest coefficient achieved on the test apparatus. The tests indicated that the fluted condensing surface had an average condensing coefficient of approximately 10,000 Btu/(hr) (sq ft) (deg F) at an over-all temperature difference of 1.5 deg F. This coefficient was approximately four times larger than was achieved with plain filmwise condensation on a smooth surface of the same over-all dimensions.

It is of interest to note that, during test operations with the fluted tube, a dropwise promoter was injected and a marked drop in over-all heat-transfer coefficient occurred. As the promotor washed from the fluted condensing surface with time the high performance was restored.

Wiper Design and Its Effect on Evaporator Performance

The function of the wiper is to spread a thin film of water on the evaporating surface. This film should be distributed uniformly along the entire length of the tube. Shearing losses should be kept to a minimum so as to maintain high mechanical efficiency. The wiper should be constantly supported on a fluid film so as to minimize friction and wear.

During the development program, wiper blades of various designs were evaluated in the test apparatus. Table 2 presents a summary of the designs tested. It was determined early in the program that water wettability was the most important wiper design criteria. Although the design of the wiper is intended to provide some hydrodynamic or hydrostatic effect, a certain amount of contact can exist between the wiper blade and the heat-transfer surface which will result in material transfer. If the wiper material is not wettable, a hydrophobic film will gradually be formed on the heat-transfer surface which in time will prevent the formation of a thin wiped film for evaporation.

An analysis of a hydrodynamic slipper bearing type wiper similar to the one shown in Fig. 14 indicated that the pressure generated under the wiper blade depends to a large extent on the leading edge boundary conditions. The surplus fluid flowing ahead of the blade must also be considered in the analysis. The generated hydrodynamic force under the wiper is equal and opposite to a normal force, which can be provided by a spring or by centrifugal force or by the combination of both. While the centrifugal force varies as the square of the wiper rpm, for all practical purposes, the spring force can be considered constant. Calculation of the centrifugal force at low wiper rpm indicated that its magnitude was inadequate for the control of film thickness. Therefore a spring arrangement as shown in Fig. 15 was used to produce the desired pressure. With the spring force large as compared to the centrifugal force, the thickness of the water film spread on the wall is proportional to the square root of the wiper velocity. Therefore, as wiper rpm increases, the film thickness will also increase as shown in Fig. 16. The film thickness can be

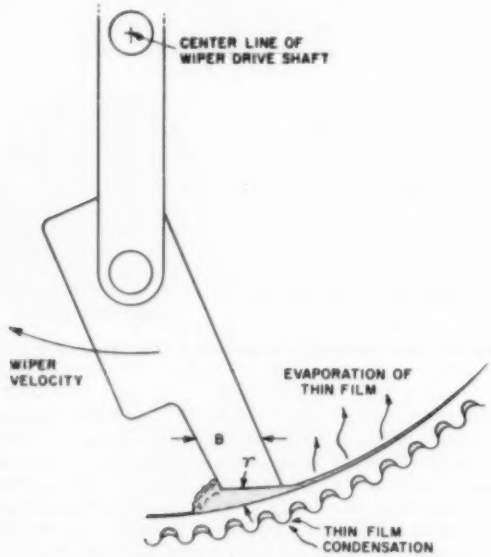

Fig. 14 Hydrodynamic type wiper in fluted tube

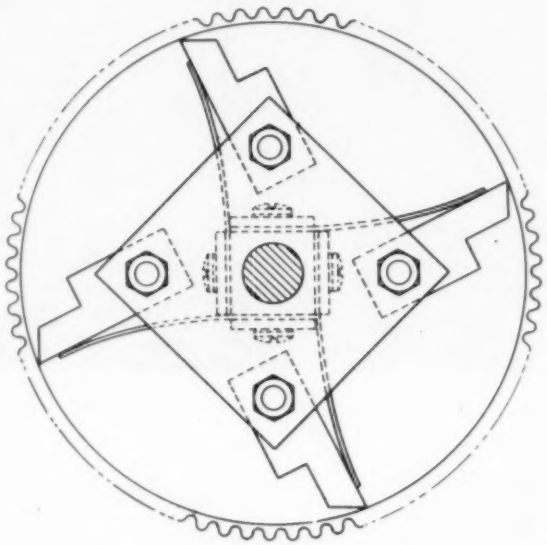

Fig. 15 Sketch of a spring-loaded carbon wiper

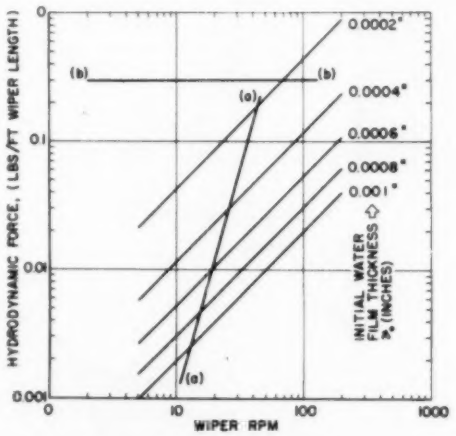

Fig. 16 Curve of a hydrodynamic force versus wiper rpm for a hydrodynamic type wiper

Film thickness curves for water, t_s = 120 deg F, B = 0.250 in., carbon brush; curve (a)-(a), wipers actuated by centrifugal force; curve (b)-(b), wipers actuated by a strong spring force

Table 2 Principal results of wiper evaluation tests

Wiper material	Experimental results
(a) 1/16 in. neoprene sheet	Wiper material rubbed on evaporating surface making surface nonwetting
(b) 1/16 in. neoprene sheet covered by cotton cloth	Neoprene material took permanent set in saturated steam at 212 F
(c) 1/16 in. neoprene sheet covered by cotton cloth and spring loaded with 0.005 inch thick phosphor bronze	Short wear life
(d) 0.020 in. thick sheet Kel-F covered by cotton cloth	Wipers produced thin films providing excellent heat transfer. The wiper life was twenty hours.
(e) 0.002 in. brass shim stock	Produced extremely thin films. High wiper speeds required to keep wall wet.
(f) 0.020 in. thick sheet Kel-F covered by two layers of cotton cloth and one layer coarse weave glass cloth.	Wear characteristics good. Wiper produced a heavy film.
(g) 0.001 in. thick stainless-steel shim stock spring-loaded	Produced extremely thin films. High wiper speeds required to keep wall wet.
(h) Carbon brushes alone	Excellent wear characteristics; high wiper speed required to produce a thin film
(i) Carbon brushes plus weights to increase centrifugal force	High wiper speed required to produce a thin film
(j) Carbon brushes spring-loaded with rubber spring	Spring force not adequate to produce a thin film at low wiper rpm; rubber took permanent set
(k) Carbon brushes with bronze screening as backup spring	Thin films produced at low wiper speeds; long life

additionally controlled by varying the angle between the wiper and the heat-transfer surface. Theoretically, with the centrifugal force and the correct spring load in combination, it is possible to design a wiper to provide constant film thickness with varying rpm.

Experimental Program

The experimental evaporator pictured in Fig. 1 was operated for a total of approximately 500 hours. During this time about 50 combinations of wiper design and condensing surface conditions were evaluated. The tests were made at pressure levels corresponding to saturation temperatures ranging between 120 and 212 F. Fig. 17 shows several typical sets of test performances for various wiper-condensing surface combinations. Included are performance data for the following:

1 Glass cloth wiper, two blades, smooth chrome plated condensing surface, dropwise condensation, 212 F evaporation.

2 Glass cloth wiper, two blades, smooth copper tube treated for dropwise condensation, 120 F evaporation.

3 Glass cloth wiper, four blades, fluted tube with film condensation, 120 F evaporation.

4 Carbon wiper, four blades, fluted tube with film condensation, 120 F evaporation.

The curves in Fig. 17 show the measured rate of condensation per square foot of heat-transfer area plotted against over-all temperature difference for constant wiper rpm. The over-all temperature difference is the difference between the evaporating and condensing saturation temperatures. The curves show that the condensation rate increases with increasing temperature difference until a maximum over-all heat-transfer condition is reached. This point corresponds to the evaporation condition (b) shown in Fig. 2.

Fig. 18 shows a plot of the over-all heat-transfer coefficient versus wiper rpm for constant over-all temperature difference. At zero wiper rpm some evaporation develops from the liquid

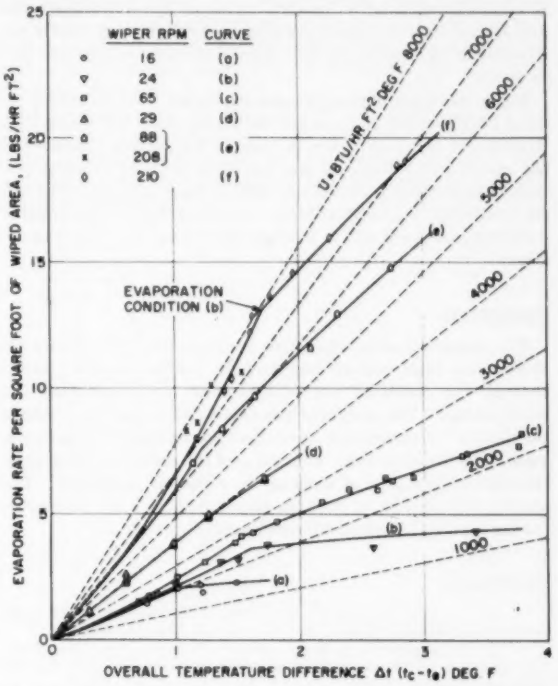

Fig. 17 Plot of measured evaporation rate per square foot of wiped area versus over-all temperature difference for constant wiper rpm

Curves (a), (b), and (c) experimental data for cloth wiper, two blades, smooth copper condensing surface promoted to give dropwise condensation with 1-dodecanethiol and chlorethan, t_c = 120 deg F; curve (d) for cloth wiper, two blades, smooth chrome plated condensing surface, t_c = 212 deg F; curve (e) for carbon wiper, four blades, film condensation on fluted surface, t_c = 120 deg F; curve (f) for cloth wiper, four blades, film condensation on fluted surface, t_c = 120 deg F

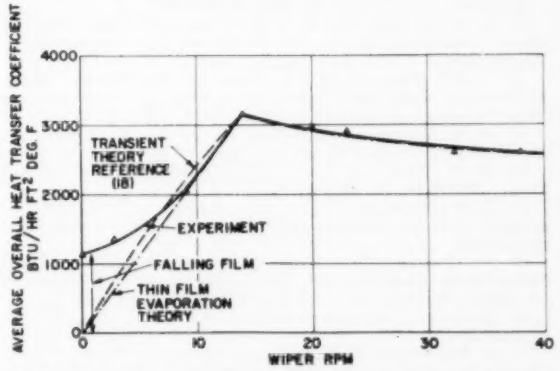

Fig. 18 Measured over-all heat-transfer coefficients versus wiper rpm for constant over-all temperature difference

Experimental data for cloth wiper, two blades, 3-in. diameter copper tube chrome plated on condensing surface, δ = 0.35 in., t_c = 212 deg F, $(t_c - t_e)$ = 1.7 deg F. Evaporation occurs at zero wiper rpm as a result of the liquid distributed to the wall in front of each wiper blade. With wiper at standstill, the liquid spreads as a falling film.

which flows down in front of the wiper's edges. As the wiper is slowly rotated the fluid is spread as a thin film. Part of the film evaporates completely depending on the over-all temperature difference and the wiped surface can become partially dry. As wiper rpm increases more of the wall remains wet and the average over-all heat-transfer coefficient increases until a maximum value is reached. A further increase in wiper speed increases the average thickness of the evaporating water film which results in a decrease of the distillation rate and the over-all heat-transfer performance.

Scaling Resistance of Wiped Evaporating Surface. In the search for other possible advantages of surface wiping, tests were made with natural sea water in order to observe the scaling resistance of the evaporator surface. A test was made at 212 F at which sea-water evaporators are usually subject to heavy scaling. The test run was extended over 50 hours. No decrease in heat-transfer coefficient occurred and a freedom from scale deposits was observed.

Conclusions

The experimental investigation conducted by the authors has shown that high over-all heat-transfer coefficients are possible through the combined use of thin films for evaporation and condensation. The results of this investigation are applicable to the design of compact and economically operating process equipment. Sea-water tests have shown that the slowly rotating wiper retards the formation of scale on the evaporating surface. The absence of bubbling in the thin film minimizes brine carry-over and as a result a high purity condensate is produced.

References

1 F. L. Shea, Jr., and N. W. Krase, "Dropwise and Film Condensation of Steam," *Trans. AIChE*, vol. 36, 1940,pp. 463–490.

2 J. P. Fitzpatrick, S. Baum, and W. H. McAdams, "Dropwise Condensation of Steam on Vertical Tubes," *Trans. AIChE*, vol. 35, 1939, pp. 97–107.

3 H. Hampson, "Dropwise Condensation on a Metal Surface," *Engineering*, vol. 179, 1955, pp. 464–469.

4 E. R. G. Eckert, "Introduction to the Transfer of Heat and Mass," McGraw-Hill Book Company, Inc., New York, N. Y., 1950.

5 Max Jakob, "Heat Transfer," John Wiley & Sons, Inc., New York, N. Y., vol. 1, 1955.

6 A. P. Colburn, "Calculation of Condensation With a Portion of Condensate Layer in Turbulent Motion," *Industrial and Engineering Chemistry*, vol. 26, 1934, pp. 432–434.

7 R. A. Seban, "Remarks on Film Condensation With Turbulent Flow," TRANS. ASME, vol. 76, 1954, pp. 299–303.

8 W. M. Rohsenow, J. H. Webber, and A. T. Ling, "Effect of Vapor Velocity on Laminar and Turbulent Film Condensation," TRANS. ASME, vol. 78, 1956, pp. 1637–1643.

9 L. C. F. Blackman, M. J. S. Dewar, and H. Hampson, "An Investigation of Compounds Promoting the Dropwise Condensation of Steam," *Journal of Applied Chemistry*, vol. 7, 1957, pp. 160–171.

10 H. W. Emmons, "Mechanism of Dropwise Condensation," *Trans. AIChE*, vol. 35, 1939, pp. 109–125.

11 W. M. Nagle and T. B. Drew, "Dropwise Condensation," *Trans. AIChE*, vol. 30, 1933–1934, pp. 217–255.

12 H. Humpson and N. Ozisik, "An Investigation Into the Condensation of Steam," *Proceedings, I. Mech. E.*, vol. 1, series B, 1952, pp. 282–294.

13 R. Gregorig, "Hautkondensation an feingewellten Oberflächen bei Berücksichtigung der Oberflächenspannungen," *Zeitschrift für angewandte Mathematik und Physik*, vol. V, 1954, pp. 36–49.

14 E. Gnam, "Tropfenkondensation von Wasserdampf," Forschungsheft 382, 1937.

15 E. Kirschbaum, G. Winckelsesser, and A. K. Wetjen, "Neues über den Wärmeaustausch," *Chemie-Ingenieur Technik*, vol. 23, 1951, pp. 361–367.

16 E. L. Lustenader, Rensselaer Polytechnic Institute master thesis, M. E. Department, 1957.

17 N. Fatica and D. L. Katz, "Dropwise Condensation," *Chemical Engineering Progress*, vol. 45, 1949, pp. 661–674.

18 R. Richter, Rensselaer Polytechnic Institute master thesis, M. E. Department, 1958.

19 J. A. Eibling and D. L. Hyatt, "Methods of Improving Heat Transfer in Evaporators of Small Thermocompression Sea-Water Stills," Preprint 28, AIChE-ASME Heat Transfer Conference, Chicago, Ill., August 18–20, 1958.

DISCUSSION

Lloyd MacGregor Trefethen[2]

The authors' findings about the effectiveness of their fluted condensation surfaces suggest that such surfaces will be widely used in the future. The ability continuously to achieve condensation coefficients comparable to those of drop condensation is a breakthrough of significance to one of the world's most important problems, that of getting enough fresh water.

I find myself most delighted, however, with the simplicity and elegance of the solution, with the "Why didn't I think of that?" aspect of those fluted surfaces. Once the principle is pointed out, it is clear that fluted surfaces are likely to work very well indeed. In fact, one wonders why they were not developed a decade or two ago. It may well be that the attention given in the past to film condensation in two dimensions has impeded our thinking; it is obvious, in retrospect, that, by utilizing three dimensions, and removing the condensate sidewise, much higher coefficients can be obtained, a conclusion that might have been suggested years ago by the high coefficients of drop condensation. If there is a moral in the authors' condensation achievements, it is probably that huge and unexpected gains can come from deliberate exploitation of all the dimensions that exist in real heat-transfer situations as compared to the limited dimensionality of the stereotype cases that apparently dominate our thinking.

The authors do not mention a possibly important aspect of the fluted condensing surfaces. The pressure gradient that is introduced by the imposed gradient in surface curvature causes the free surface as well as the bulk of the film to move sidewise to the hollows. Noncondensed gases therefore cannot rest on the condensing ridges, but instead will be moved toward the hollows. A noncondensing gas may therefore be less of a poison to condensation on fluted surfaces than it is to film condensation on flat surfaces.

I should like to question the authors on only one point. Their statement about drop condensation, "Kinetic gas theory indicates that with decreasing pressure level the coefficient of condensation should decrease," would seem to presuppose a model for drop condensation. There appears to be no generally accepted model for drop condensation and indeed the subject seems at the present time to be characterized primarily by lack of understanding. If there is any validity to a drop-circulation model, which I have developed, one would be led to the same conclusion as the authors, namely, that the coefficient goes down with decreased vapor pressure, but for an entirely different reason; the viscosity of the condensed liquid increases. Perhaps the authors could elaborate on this point to indicate what properties of the vapor they consider significant to drop condensation.

[2] Professor of Mechanical Engineering, Tufts University, Medford, Mass.

Authors' Closure

The authors wish to thank Professor Trefethan for his interest and comments on this paper.

Professor Trefethan has pointed out a very interesting aspect of the fluted condensing surface: That of its ability to operate in the presence of a noncondensable gas. In our continued tests, we hope that we will be able to show that this is the case.

In answer to the question regarding pressure level effect on condensation, we can only state that we agree that there appears to be no generally accepted model for drop-wise condensation and that there exists considerable confusion in this field. We do not have a definite model which will describe the mechanism of dropwise condensation. Our statement relating to the kinetic gas theory was made with the assumption that the bulk of condensation takes place on the surface between the droplets. We, of course, have no proof that this is a correct premise. The kinetic theory was used merely to indicate significant trends. We do not have available test data to verify this theory.

The variables which we considered to have influence on dropwise condensation were: The pressure level at which condensation occurs, the corresponding saturation temperature, the specific volume of liquid and vapor, heat of vaporization, and the ratio of the fraction of the surface which is free of droplets to the total condensing surface area.

At the present time we do not intend to delve further into the theory of dropwise condensation, since we find that we can achieve better results using film condensation on the fluted surface. This can be done with less complication than that associated with the injection of promoters.

Some General Considerations of the Heating of Satellites

ALFRED J. EGGERS, JR.
Chief, 10-by-14 Inch Supersonic Wind Tunnel Branch

THOMAS J. WONG

ROBERT E. SLYE
Aeronautical Research Scientists

NASA, Ames Research Center, Moffett Field, Calif.

Heating of satellites is treated in connection with flight in planetary atmospheres and in interplanetary space. Heating during entry into the earth's atmosphere is generally more severe than that encountered during launch or exit, although it can be substantially reduced by employing blunt shapes and small entry angles. Decelerations and heating rates during entry can be further reduced by employing lifting satellites. These techniques in combination with known radiation, heat-sink, and ablation cooling techniques appear adequate to handle the entry problem at speeds up to escape speed. Return flights from distant planets like Saturn and beyond may be characterized by much higher entry speeds, and more advanced techniques for coping with the heating problem may be required. Heating during entry into the atmospheres of planets neighboring Earth tends to be more or less severe than that in the earth's atmosphere depending on whether the planets are larger or smaller than Earth.

Heating in interplanetary space due to solar radiation becomes severe only if a satellite approaches to within a small fraction of an astronomical unit of the sun, or if the vehicle has an inefficient radiation shield. A cooling problem is encountered in the outer portion of our solar system, and an auxiliary power source may be required to supplement the reduced amount of heat from the sun. The sputtering or erosion of material from the surface of a satellite, caused by impact at hypervelocities with small particles in space, may also pose direct or indirect heating problems. Further research is required to assess the magnitude of these problems.

Introductory Remarks

In order to explore the heating of satellite vehicles, it is essential to understand the environment in which they operate. If we think of satellites in the broad sense as being bodies captured in the sun's gravitational field, either directly by the sun itself, or indirectly by a planet, then this environment is our solar system [1][1] which is shown schematically in Fig. 1. We see that the extent of this system is large indeed, the planet Earth being 1 astronomical unit or almost 100 million miles from the sun, while the outermost planet Pluto is about 40 astronomical units or 4 billion miles from the sun. Now satellites, as we view them, include everything from artificial satellites of Earth and the other planets to interplanetary spacecraft. In our general considerations of heating, therefore, we must contend with an environment that includes planetary atmospheres which may be relatively dense with material, as well as interplanetary space which is relatively void of material but may be relatively dense with radiation.

The heating of satellites is largely determined by their motion. We shall first treat the heating associated with launch or exit of a satellite from the earth's atmosphere and then we shall attend to heating as it arises during entry. Thereafter we shall compare this entry heating problem with the corresponding ones likely to be encountered during entry into other planetary atmospheres. Attention will then be turned to heating of satellites by solar radiation in interplanetary space, and finally, brief consideration will be given to sputtering of surface material from satellites colliding with particles in space.

[1] Numbers in brackets designate References at end of paper.

Contributed by the Heat Transfer Division and presented at the Aviation Conference, Los Angeles, Calif., of The American Society of Mechanical Engineers, March 8–12, 1959.

Note: Statements and opinions advanced in papers are to be understood as individual expressions of their authors and not those of the Society. Manuscript received at ASME Headquarters, June 3, 1959. This paper was not preprinted.

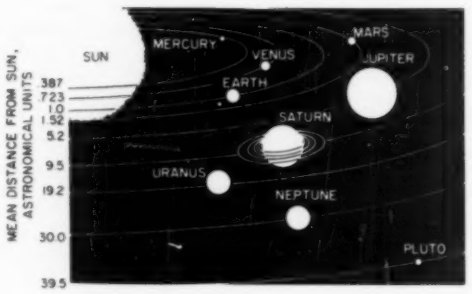

Fig. 1 Solar system

Heating in Planetary Atmospheres

Flight of a satellite in a planetary atmosphere tends to be at very high velocities because of booster thrust during exit and because of gravitational pull prior to and during entry. These velocities may measure in the tens of thousands of feet per second, thereby causing intense shearing action between the surface of a satellite and the atmosphere. The result is that heat is generated at rates and in quantities which may be ample to vaporize the entire vehicle unless careful attention is given to its design. In order to get a better feeling for this problem and how it can be minimized, we have shown atmosphere exit and entry trajectories schematically in Fig. 2 along with basic heating equations [2]. Considering first convective heating,[2] we note that the heat rate dH/dt can be reduced by reducing the product of equivalent friction coefficient C_F', which is proportional to Stanton number, and atmosphere density ρ at a given flight velocity V. This product is most readily reduced by employing trajectories that

[2] The convective heating equations given are applicable for the case of a cool wall, that is, when the wall temperature is small compared to the recovery temperature.

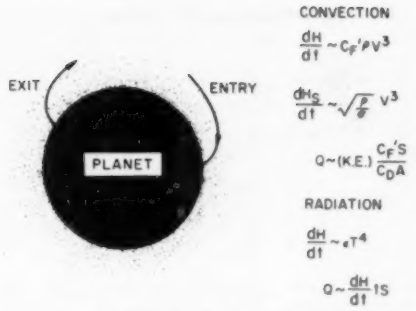

Fig. 2 Trajectories and heating equations

restrict high flight speeds to high altitudes where there is the least amount of air. Thus it is usual to accomplish the exit maneuver with a locally vertical launch followed by a turn and acceleration to satellite speed well out in the atmosphere. The entry maneuver, on the other hand, is characterized by reduced heating rates if it is initiated at a shallow angle to the local horizontal thereby permitting deceleration at high altitudes, followed by a lower speed descent through the denser atmosphere at low altitudes. Now heating rates in the stagnation region of the nose of a satellite vehicle tend to be high at best because shearing action tends to be most severe in this region. Accordingly, we are urged to be especially aware of fundamental factors influencing heating rate at the nose, and we see from the second equation that the radius of curvature of the surface, σ, comes into play through its effect on friction coefficient. Specifically, it is indicated that increasing the radius of curvature will markedly reduce stagnation region heating rate dH_s/dt, so we anticipate that satellite vehicles will tend to have blunt noses.

We have anticipated the need for reducing heating rates in order to alleviate the problem of finding a kind of surface material or structure, or both, suitable for a satellite vehicle. In like manner we anticipate a need for reducing total heat transfer in order to reduce the quantity of material required. This need may become particularly acute in connection with atmosphere entry and so we turn attention to the equation for total heating Q which holds for this maneuver. It states that total heating is proportional to the loss in kinetic energy of the vehicle, and to the ratio of friction force to total drag force $C_F'S/C_DA$, where S is the surface area over which C_F' acts and A is the reference area for C_D. Since essentially all the kinetic energy is lost in completing the entry maneuver, the principal factor of interest to us is the ratio of friction force to total drag force. One of the most effective ways of reducing this ratio and hence total heating is to increase total drag by employing satellites which have highly inclined forward faces in addition to blunt noses. In this manner relatively strong shock waves are generated to heat the atmosphere, while relatively weak surface shearing is developed to heat the body.

In addition to convective heat transfer, we will be concerned with radiant heat transfer during flight in a planetary atmosphere. Radiation to the surface of a satellite from the hot gas surrounding it may contribute to heating the vehicle, and radiation from the surface may contribute to cooling the vehicle. In either case we are reminded by the radiation equations that the rate and amount of such heat transfer are proportional to the emissivity and the fourth power of the temperature of the radiating medium. To minimize radiation heating rates, therefore, it is again attractive to restrict high flight speeds to high altitudes where there is less dense atmosphere and hence reduced emission of the hot gas surrounding a satellite. Reducing heating rates increases the practicality of radiation cooling, of course, because it reduces the surface temperatures required to counterbalance these rates by radiation.

We have, then, a qualitative picture of the heating problem of satellites during flight in a planetary atmosphere and some techniques which may be employed to alleviate this problem. Now these techniques did not, in fact, evolve from studies of satellite heating, but rather from earlier studies of ballistic missiles [3] and other types of hypervelocity vehicles [4] in the earth's atmosphere. Quantitative studies of the heating of satellites entering the earth's atmosphere are of more recent vintage and they include those of Kemp and Riddell [5] and Ferri [6], while Gazley [7] and Chapman [8] have attended to the heating of satellites in other planetary atmospheres as well. The present authors have studied these problems [2] with simplified analytic techniques suitable for many engineering applications, and it is the results of this study which will be reviewed and added to herein. Because of the relative importance of heating during entry, it will receive the bulk of our attention.

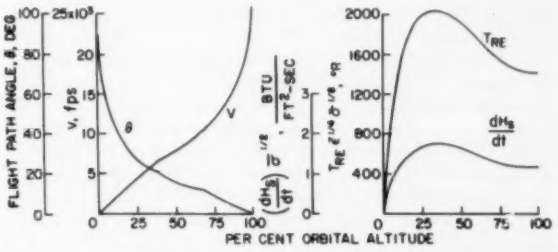

Fig. 3 Motion and heating in a launch to circular orbit about earth

Exit From Earth's Atmosphere. Considering first the exit maneuver, we have shown in Fig. 3 some calculated motion and heating results for an idealized three-stage launch to a near-earth satellite orbit. The variations with altitude of velocity and flight path angle θ relative to the local horizontal are about as we would expect with angle decreasing to zero and velocity increasing to satellite value at orbital altitude. Launch accelerations are restricted to 8 g's or less in this maneuver and orbital altitude is somewhat less than 100 miles. Heating rates and hence equilibrium surface temperatures for complete radiation cooling of the stagnation region of the nose are a maximum at relatively low altitudes and at velocities of about 5000 ft per sec. These rates for a nose of 1 ft radius[3] are less than 2 Btu per sq ft per sec, however, so that surface temperatures do not exceed about 2000 deg R which is well within the range of useful strengths of molybdenum alloys and other high temperature structural materials [9]. In general, then, heating during the exit maneuver should be maintainable at levels tolerable to more or less conventional types of materials and structures.

Entry Into Earth's Atmosphere. We are concerned with heating during atmosphere entry following an abortive launch and following normal flight of a satellite through space.

Entry From Abortive Launch. In the event of an abortive launch due to failure of the rocket booster in flight, the vehicle may fall back to Earth along an elliptical trajectory reaching relatively high velocities and steep flight path angles at entry into the atmosphere. For launches of the type we have just considered, failure at about 18,000 ft per sec tends to yield the most critical entry conditions. The conditions in terms of heat-

[3] Bars over σ in Fig. 3 and all subsequent symbols or groupings thereof shown in this paper indicate that the dimensions of these quantities have been omitted; σ and $C_DA\sigma/m$ have the dimensions of feet and cubic feet per slug, respectively. In the discussion of these and subsequent heating results, a typical value of unity is assumed for the barred quantities.

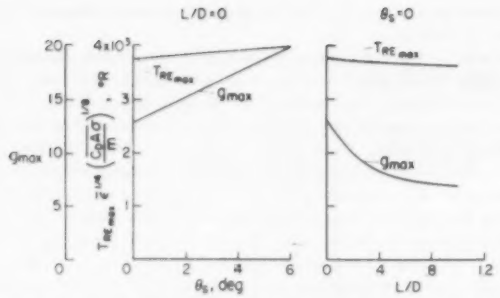

Fig. 4 Maximum decelerations and temperatures during entry following abortive launch

ing and decelerations are shown in Fig. 4. On the left of the figure maximum decelerations and temperatures for ballistic vehicles (i.e., $L/D = 0$) are presented as a function of θ_s, the flight path angle that would have occurred at satellite speed if the launch had been successful. The case $\theta_s = 0$ would be a launch to a circular satellite orbit, while the larger angles might be used for launch to a parabolic or hyperbolic orbit into space. The maximum deceleration following an abortive launch is about 13 g's for $\theta_s = 0$ and increases quite rapidly to about 20 g's for $\theta_s = 6$ deg. The temperature rise with θ_s is small; however, the level of temperature is close to 4000 deg Rankine which is approximately twice that encountered during a successful launch. Accordingly, successful recovery following an abortive launch may require the use of ceramics like zirconia for at least the nose of a satellite if it is to be radiation cooled, although certainly heat-sink and ablation cooling techniques should be considered for this region. On the right of the figure we have the variation of maximum deceleration and temperature with lift-drag ratio for a final launch angle of 0 deg. The temperature decreases only a small amount with increasing L/D; however, there is a marked reduction in maximum deceleration with increasing L/D (about 40 per cent for $L/D = 1/2$). It is apparent then that the hazards of an abortive launch for a manned vehicle may be greatly reduced if a vehicle having a lift-drag ratio of at least 1/2 can be utilized. Assuming that we have a vehicle successfully launched, we may consider next the motion and heating during atmosphere entry from satellite flight.

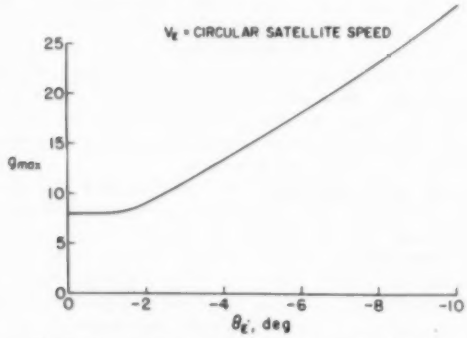

Fig. 5 Effect of entry angle on maximum deceleration

Entry From Satellite Flight. The maximum deceleration of ballistic vehicles entering at various angles from near-earth satellite orbits is shown in Fig. 5. It is indicated that near zero entry angle this deceleration is about 8 g's. Note too that the deceleration is only weakly dependent on entry angle for angles up to a degree or so; however, for larger angles, the deceleration increases rapidly.

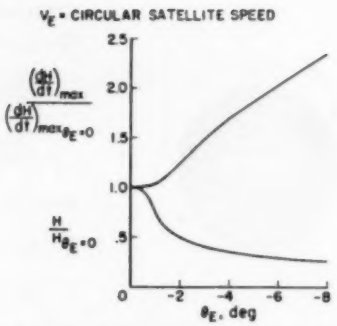

Fig. 6 Effect of entry angle on heating

For manned vehicles it would appear desirable to use the low entry angles in order to minimize the decelerations.

The effect of entry angle on the heating of ballistic vehicles is shown in Fig. 6, assuming laminar flow since flight Reynolds numbers are generally less than one million [2]. Ratios of heating to the heating at zero entrance angle are presented. It is seen that increasing the entry angle substantially reduces net heat transfer, while the maximum heating rates and hence equilibrium temperatures are substantially increased. Thus with a heat-sink or ablation-cooled design, higher entry angles may be advantageous; whereas with a radiation-cooled design it appears desirable to keep the entry angles as low as possible. At zero entry angle, maximum heating rate is about the same as in the abortive launch case for $\theta_s = 0$, whereas total heating of the stagnation region is about twice as great and is equal to 33,000 Btu per sq ft for a unit value of the parameter, $m/C_D A\sigma$. Average heating rates and average heat transfer per unit area for a complete vehicle are much less [2, 10]. Thus for example, a vehicle having a cone semiapex angle of 45 deg, a nose radius of 1 ft, and a base area of 25 sq ft, has an average heating rate and total heat transfer equal to about $^1/_4$ the stagnation values for entry at circular satellite speed.

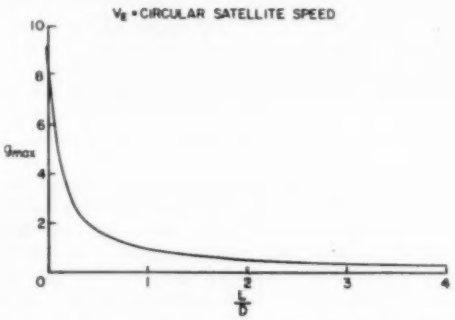

Fig. 7 Effect of lift-drag ratio on maximum deceleration during entry

We will consider now the effect of lift on entry from circular orbit. The effect of lift-drag ratio on maximum deceleration is shown in Fig. 7. It is seen that just as in the abortive launch case even very small lift-drag ratios, for example of the order of 1/2, markedly reduce maximum deceleration below that experienced by a ballistic vehicle. With increasing L/D above 1, decelerations rapidly approach those of conventional flight.

The calculated effect of lift-drag ratio on stagnation region heating is shown in Fig. 8. Ratios of heat rates and total heat to the respective quantities for $L/D = 0$ are presented as a function of lift-drag ratio. We see that increasing lift-drag ratio reduces the

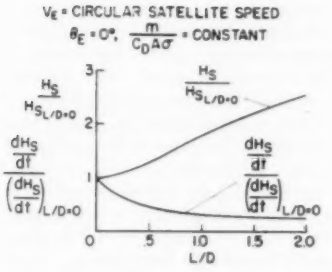

Fig. 8 Effect of lift-drag ratio on heating during entry

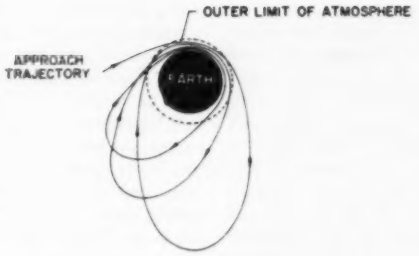

Fig. 9 Decay of an approach trajectory to a near-earth satellite orbit

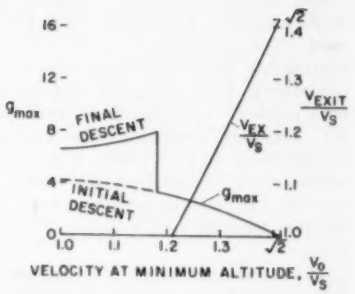

Fig. 10 Maximum deceleration during a graze

heat rates.[4] However, increasing L/D also increases the time of flight so that the net effect is to increase the total heat flux. It is apparent then that for higher lift-drag ratios, in order to minimize weight of heat sink or coolant, as much as possible of the total heat should be handled by radiation from the satellite.

We have discussed some factors which influence heating and its relation to motion during atmosphere entry at near-earth circular satellite speed of about 26,000 ft per sec. Let us consider next the problems of atmosphere entry when the entrance velocity is escape speed of about 36,000 ft per sec, which may be characteristic of return flights from some of our neighboring planets, such as Venus or Mars, and also our Moon. We will again confine our attention to the trajectories characterized by small entrance angles and we shall term these grazing trajectories. As in the case of entry from near-earth circular orbits, these trajectories lead to deceleration in the low density air at relatively high altitudes, with the result that radiation heat transfer to the vehicle is probably of relatively minor significance [11]. Grazing trajectories can, with accurate guidance, be used to decay a parabolic orbit into an elliptical orbit without subjecting a space vehicle to excessive decelerations or heating.[5] The decay process is shown schematically in Fig. 9. It is noted that with each graze the major axis of the orbit is reduced and is caused to precess. Several grazes at most are required in order to decay a parabolic orbit into a low-altitude elliptical orbit from which the final descent can be made with relative ease. Let us examine, in some detail, the motion and heating for this type of entry.

The maximum decelerations during a graze for a nonlifting vehicle are presented in Fig. 10. In addition, we show exit velocity as a function of velocity at minimum altitude. For weak grazes, the vehicle leaves the atmosphere with little loss in velocity and several grazes are required before the final descent can be made. For stronger grazes, that is deeper in the atmosphere, the maximum deceleration is larger and if the graze is sufficiently strong, the vehicle does not leave the atmosphere but merely rises somewhat from the minimum altitude point and then falls back in a final descent. For a strong graze, the deceleration reaches a peak twice—once in the initial descent, and a maximum value in the final descent. It is interesting to note that the maximum deceleration during the final descent from a strong graze may be less than 8 g's which is the maximum encountered following entry at near-earth satellite speed. Stagnation region heating in a graze of a ballistic vehicle is presented in Fig. 11. As would be expected, equilibrium surface temperature and total heat transfer increase as the graze becomes stronger.[6] The maximum temperature for a strong graze is about 30 per cent higher than for entry at circular satellite speed and the total heat transfer is about 50 per cent higher. In order to reduce this temperature to about the same magnitude as for entry at circular satellite speed, the parameter $(C_D A\sigma/m)$ must be increased by a factor of about 8.

It would appear from these considerations that the use of a strong graze for atmosphere entry of ballistic satellites at escape speed need not impose prohibitive heating problems nor would the decelerations necessarily be greater than those encountered during entry at circular satellite speed. In addition, the time duration of the entry for the strong graze is much less than that for the several revolutions required in weak grazes. In studying the effect of lift on grazing entry, therefore, we will consider only the strong graze, and in particular we will consider only the use of negative lift. As the vehicle enters the atmosphere the

[4] For a given class of configurations, stagnation region heating rates tend to be a minimum when $m/C_L A\sigma$ is a minimum and, for constant σ, this tends to occur in the range of L/D from 1/2 to about 1 [2, 8].

[5] Impacting trajectories characterized by larger entry angles may be useful for recovering some instrumented packages which can withstand very high decelerations provided they are well protected (perhaps with an ablation heat shield) from severe entry heating environment [2].

[6] The heat transfer in a strong graze ($V_0/V_s \leq$ about 1.18) includes all the heat transferred from entrance to impact.

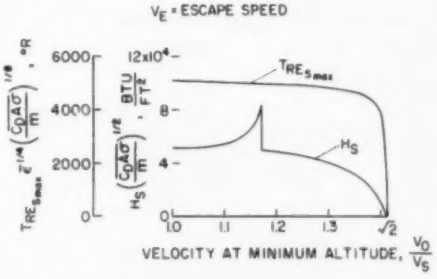

Fig. 11 Stagnation region heating in a graze

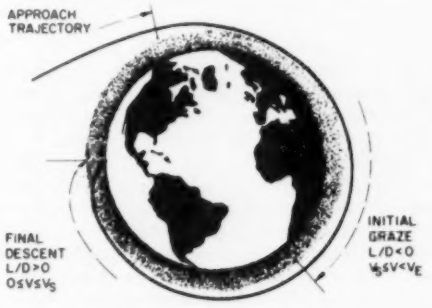

Fig. 12 Strong graze with lift

negative lift is used to balance the excess centrifugal force. Consequently, the velocity in the graze can be decayed to circular satellite speed at much higher altitudes than if positive lift were used. This, of course, results in much lower decelerations and heating rates than for a strong graze with positive lift. The entry procedure is shown in Fig. 12. The vehicle approaches the planet on a parabolic orbit and enters the atmosphere using negative lift. Maximum decelerations and heating occur in the vicinity of the minimum altitude point. From here, the vehicle rises and approaches a maximum altitude where the velocity has decayed to about local circular satellite speed. From this point, positive lift is used and the vehicle makes a final descent on a glide trajectory.

The calculated effect of lift-drag ratio on maximum decelerations during a strong graze is presented in Fig. 13. There is a marked reduction in maximum decelerations with increasingly negative L/D and they are about 50 to 60 per cent lower than those encountered in the final descent. The effect of lift-drag ratio on heating in a strong graze is presented in Fig. 14. The total stagnation region heating for all lift-drag ratios is approximately twice that for entry at circular satellite speed and at being of the types we have just discussed. In this event the maximum decelerations in the initial graze would be about four to five times those for a strong graze at escape speed. For lifting vehicles these decelerations may not be excessive. For example, with an L/D of $-1/2$, the maximum deceleration is about 5 g's and for larger negative L/D it is substantially less. Let us now examine stagnation-region heating in entry at superescape speeds, and this is presented in Fig. 15. We see that both the temperatures and the total heat are substantially higher than for the second graze, temperatures by about 50 per cent and total heat by about 75 per cent. The problems of entry at superescape speeds are indeed severe, and it is probable that more advanced cooling techniques will be required to cope with these problems.

Entry Into Other Planetary Atmospheres. In closing our discussion of atmosphere entry it is appropriate to consider satellites entering the atmospheres of planets other than Earth. Estimates of relative decelerations and heating encountered during entry into atmospheres of various planets are summarized in Fig. 16. These results agree with those of Gazley [7], and the more recent and extensive studies of Chapman [8]. It is indicated that the problem of landing on Venus is, from the standpoint of decelera-

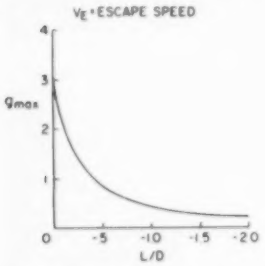

Fig. 13 Effect of lift-drag ratio on deceleration during a strong graze

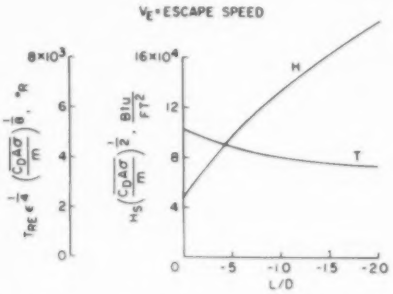

Fig. 14 Effect of lift-drag ratio on heating during a strong graze

	BALLISTIC $\theta_E = 0°$			BALLISTIC θ_E LARGE			LIFTING, CONSTANT L/D		
	$\frac{dV}{dt}$	$\frac{dH}{dt}$	H	$\frac{dV}{dt}$	$\frac{dH}{dt}$	H	$\frac{dV}{dt}$	$\frac{dH}{dt}$	H
EARTH	1.0	1.0	1.0	1.0	1.0	1.0	1.0	1.0	1.0
VENUS	1.0	.9	.9	1.0	1.0	.8	.9	.8	.9
MARS	.2	.1	.3	.1	.3	.4	.4	.1	.2
JUPITER	70	80	60	20	130	40	26	50	100

Fig. 16 Relative deceleration and heating

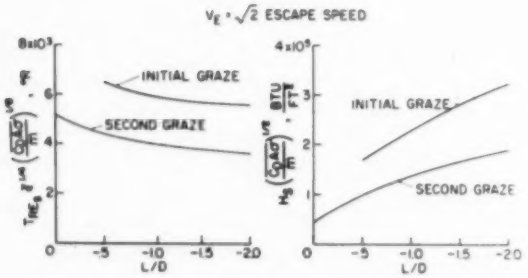

Fig. 15 Effect of lift-drag ratio on heating during entry from hyperbolic orbit

$L/D = -1/2$, it is about twice that for $L/D = 0$. The corresponding equilibrium surface temperatures are about 25 per cent higher than for a descent at circular satellite speed, indicating that heating rates may be sufficiently high to require the use of an ablating material in the stagnation region. Equilibrium surface temperatures over the afterportion of a vehicle may be sufficiently low that most of the heat may be handled by a radiation shield with possibly a ceramic coating for the surface.

On a return flight from the vicinity of Saturn and planets even further removed from Earth, the entrance velocities may be of the order of 1.4 times the escape velocity from earth. In the first graze the velocity should at least be reduced to a value slightly less than escape speed, with the second graze and final descent tions, comparable to that for landing on Earth, while that of landing on Mars is, in this respect, substantially less severe. Entry into Jupiter's atmosphere, however, is much more severe and perhaps should not be attempted with other than instrumented vehicles. More or less the same situation is predicted for heating. However, precise estimates of the heating associated with entering the atmosphere of any planet other than Earth must await the accurate determination of the properties of these atmospheres. It is useful to note, nevertheless, that the problem of entering the earth's atmosphere appears, from the motion and heating point of view, to be equally if not more severe than that of entering the atmosphere of Venus or Mars. Accordingly, designs suitable for entering our atmosphere may also be adequate for entering these other atmospheres. A qualification of this statement should be made in the case of entering the atmosphere of Venus which may be largely carbon dioxide [12]. In this event radiation heat transfer to a satellite may be far more severe than in the earth's atmosphere, depending on the emissivity of CO_2, under entry conditions.

Heating in Interplanetary Space

Heating by Solar Radiation. While radiant heating is frequently, if not commonly of secondary importance during atmosphere entry, it is of primary importance during space flight. The principal source of radiant energy in this case is, of course, the sun. For most of our purposes the sun may be considered a point source of radiant energy with the heating rate inversely proportional to the square of the distance from the sun. The heating of unit area of

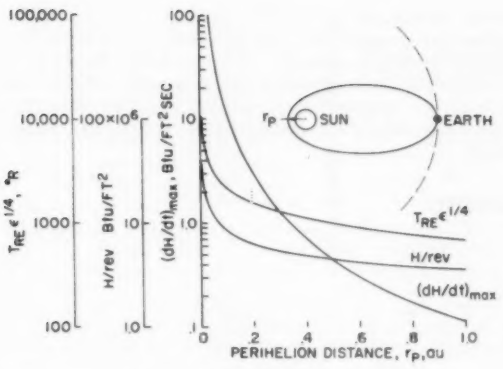

Fig. 17 Radiant heating by sun

a satellite which is always considered to be facing the sun has been calculated[7] for one revolution around the sun. The results of these calculations for vehicles launched from Earth are shown in Fig. 17 which includes radiation equilibrium temperature, total heat transferred, and the radiation heat rate as a function of perihelion distance from the sun. The total heat increases quite rapidly as the perihelion distance is decreased and the amount is generally so large that structural designs based on the heat-sink principle with no radiation cooling do not appear feasible. For approaches as close as $^1/_{25}$ astronomical unit the heat rates and hence the equilibrium surface temperatures do not exceed those encountered by vehicles entering the earth's atmosphere at circular satellite speed. It is indicated, therefore, that with radiation shields of ceramic design a satellite could "weather" exceedingly close approaches to the sun and, if properly instrumented, such a sun probe might provide highly valuable data. For satellite flights to regions far more removed from the sun than Earth, our "so-called" heating problem will in fact become a cooling problem. For example, in the vinicity of Jupiter, the solar heating rate is only 0.0042 Btu/ft²-sec which is approximately 3 per cent of the value at the earth and the radiation equilibrium temperature ($T_{RE}\epsilon^{1/4}$) is −160 deg F. The reduced amount of heat from the sun may have to be supplemented with energy from an auxiliary power source.

Sputtering by Hypervelocity Particles. Another source of heating of satellites in space may be due to hypervelocity collisions with particles like micrometeorites or gas molecules. Surface erosion due to hypervelocity impact with gas molecules has been termed "sputtering." In general, the rate at which material is sputtered or eroded from the surface and the heating due to impact with these particles are small. However, sputtering may limit the useful lifetime of satellites, and could conceivably roughen the surface so as to induce turbulent flow during the critical heating period of atmosphere entry, thereby making entry heating even more severe.

Experiments to determine the nature of sputtering of various materials are being conducted at the Ames Research Center. The equipment used is the Ion Beam Apparatus shown in Fig. 18. The apparatus consists of an ion source, accelerator, analyzer, and focusing system. The source yields molecular and atomic oxygen and nitrogen ions with intensities in the milliampere regime. The accelerating system provides a continuously variable range of energies from a few electron-volts to 9 k electron-volts, corresponding to speeds of about 30,000 to 800,000 ft per sec for nitrogen molecules. The flat faced aluminum model shown at the right was about 1 centimeter in diameter and was exposed to an ionized nitrogen stream for 3 hr at an energy level of 3.0 kev corresponding to a stream velocity of about 460,000 ft per sec. A total charge of about 1 coulomb was used. About 150 micrograms of material were removed and evidence of surface roughness is shown in the view on the lower right. The velocity of the experiment corresponds to that of a vehicle at a perihelion distance of about 0.09 astronomical unit or about 8 million miles from the sun. Calculations indicate that sputtering, even at these velocities, would be small provided the surface temperature is moderately

[7] The heating equations are as follows:

Radiation rate, $q = 0.119/r^2$, Btu/ft² sec
Temperature, $T_{RE}\epsilon^{1/4} = 706/\sqrt{r}$, deg R
Total heat, $H/\text{rev} = 3.88 \times 10^6/(h/h_\oplus)$, Btu/ft²

where

r = distance from sun in astronomical units
$h/h_\oplus$ = ratio angular momentum to angular momentum in Earth's orbit

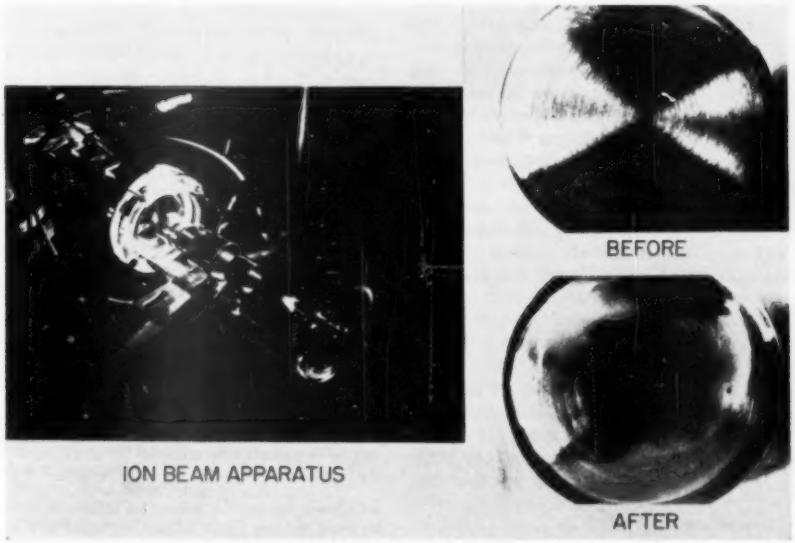

Fig. 18 Sputtering at hypervelocities

low. Surface temperatures at this distance from the sun may, however, reach about 2500 deg R. At elevated temperatures materials lose their strength and probably their resistance to sputtering, so the effects of sputtering may become more severe near the sun.

Concluding Remarks

Recapitulating our general considerations of satellite heating, we observe that they can logically be divided into two parts, one dealing with flight in planetary atmospheres and the other dealing with flight in interplanetary space. Convective heating during launch or exit from the earth's atmosphere appears to be relatively modest provided high flight speeds are restricted to high altitudes where air density is low. Reduced entry angles substantially reduce heating rates during atmosphere entry, although the rates remain severe at best by comparison to those encountered during exit. Lifting satellites experience much lower heating rates and decelerations, which may make them especially attractive for manned applications. Heating during atmosphere entry from abortive launches, near-earth circular orbits, and near-planetary orbits appears tractable if blunt shapes and known radiation, heat-sink, or ablation cooling techniques are used. However, more advanced cooling techniques may be required to cope with the heating during entry following a space trip from the outer planets. Entry into the atmosphere of Venus appears to be comparable, from the heating and deceleration point of view, to entry into the earth's atmosphere, while entry into the atmosphere of a smaller planet like Mars appears to be much less severe, and entry into the atmosphere of a larger planet like Jupiter appears to be much more severe.

Heating by solar radiation of a satellite in interplanetary space becomes severe only if the vehicle approaches to within a small fraction of an astronomical unit of the sun, or if it is equipped with an inefficient radiation shield. Interplanetary flight to the outer portions of our solar system will pose a cooling rather than a heating problem, and an auxiliary power source will probably be required to supplement the reduced amount of heat received from the sun. Sputtering or erosion of material from the surface of a satellite impacting at hypervelocities with small particles in space may also pose problems in the form of reduced lifetimes of the vehicles or increased entry heating because of surface roughness effects.

References

1 Cecilia Payne-Gaposchkin, "Introduction to Astronomy," Prentice-Hall, Inc., New York, N. Y., May, 1955.

2 A. J. Eggers, Jr., "The Possibility of a Safe Landing," Space Technology, ch. 13, John Wiley & Sons, Inc., New York, N. Y.

3 H. Julian Allen and A. J. Eggers, Jr., "A Study of the Motion and Aerodynamic Heating of Missiles Entering the Earth's Atmosphere at High Supersonic Speeds," NACA TN 4047, 1957.

4 A. J. Eggers, Jr., H. Julian Allen, and Stanford E. Neice, "A Comparative Analysis of the Performance of Long-Range Hypervelocity Vehicles," NACA TN 4046, 1957.

5 N. H. Kemp and F. R. Riddell, "Heat Transfer to Satellite Vehicles Re-Entering the Atmosphere," *Jet Propulsion*, vol. 27, no. 2, 1957, pp. 132–137.

6 Antonio Ferri, Lewis Feldman, and Walter Daskin, "The Use of Lift for Re-Entry From Satellite Trajectories," *Jet Propulsion*, vol. 27, no. 11, 1957.

7 Carl Gazley, Jr., "Deceleration and Heating of a Body Entering a Planetary Atmosphere From Space," RAND Rep. P-955, 1957.

8 Dean R. Chapman, "An Approximate Analytical Method for Studying Entry Into Planetary Atmospheres," NACA TN 4276, 1958.

9 Samuel B. Batdorf, "Structural Problems in Hypersonic Flight," *Jet Propulsion*, vol. 27, no. 11, 1957, pp. 1157–1161.

10 Lester Lees, "Laminar Heat Transfer Over Blunt-Nosed Bodies at Hypersonic Flight Speeds," *Jet Propulsion* vol. 26, no. 4, 1956, pp. 259–269.

11 F. R. Riddell, "Real Gas Effects in the Re-Entry Problem," "Vistas in Astronautics," Pergamon Press, London, England, 1958, pp. 50–54.

12 S. H. Dole, "The Atmosphere of Venus," RAND Rep. P-978, October, 1956.

The Penetration of Planetary Atmospheres

CARL GAZLEY, JR.
Aeronautics Department, The RAND Corporation, Santa Monica, Calif. Mem. ASME

The problems of penetrating a planetary atmosphere are reviewed and techniques for penetration are discussed. These techniques are resolved into two general classes: (1) Gradual entry into the atmosphere with relatively low deceleration loads and heating rates low enough so that the heat may be rejected by thermal radiation from the surface; and (2) direct entry with higher deceleration loads and higher heating rates with the heat being absorbed by the body surface.

Introduction

THE PROBLEM OF atmospheric penetration arises for any vehicle which approaches a planetary atmosphere and for which physical recovery or survival is desired at the planetary surface. This includes a gamut of possibilities from simple sounding rockets to manned vehicles returning from interplanetary trips. Several types of atmospheric entry are illustrated in Fig. 1.

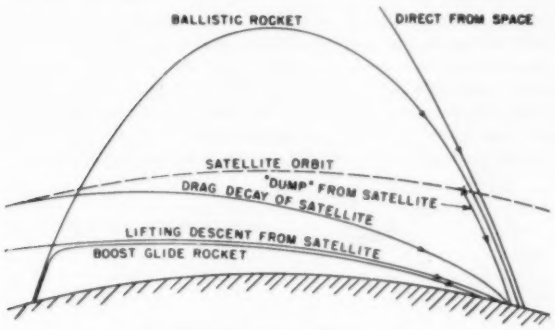

Fig. 1 Various types of atmospheric entry

The approach to a planet from space is presumed to involve the classical technique of first getting the vehicle into the planet's solar orbit and then "falling" into the planet. The approach velocity is, then, essentially the escape velocity of the planet—corresponding to a parabolic orbit. (In the vicinity of the earth, the escape velocity is about 37,000 ft/sec; a highly eccentric elliptical orbit, such as a circumlunar orbit, involves a velocity almost as high—about 35,000 ft/sec.) It is expected that rather precise control of velocity and direction would be required to obtain a hit or a near-miss. A direct hit would involve an entry path similar to the ballistic rocket—but with a higher initial velocity. A more gradual descent can be accomplished by either a tangential shallow entry or by first maneuvering into a satellite orbit and then descending.

Although the heating and deceleration accompanying atmospheric entry bring about severe design problems, the presence of a planetary atmosphere is advantageous in that it acts as a cushion to reduce a space vehicle's velocity to a safe landing speed. Otherwise, one would be forced to the costly expedient of rocket braking. Landing on the moon, which has effectively no atmosphere, requires an appreciable portion of the vehicle's weight to be allocated to a braking rocket. Landing on a planet with an atmosphere requires a clever approach shot, a surface-cooling scheme, and/or a clever aerodynamic design.

Contributed by the Heat Transfer Division and presented at the Aviation Conference, Los Angeles, Calif., March 8–12, 1959, of THE AMERICAN SOCIETY OF MECHANICAL ENGINEERS.

NOTE: Statements and opinions advanced in papers are to be understood as individual expressions of their authors and not those of the Society. Manuscript received at ASME Headquarters, January 26, 1959. Paper No. 59—Av-27.

Characteristics of Atmospheric Penetration

A body approaching a planetary atmosphere possesses a large amount of energy—potential energy because of its position above the planet's surface and kinetic energy because of its velocity. In most cases, the kinetic form predominates. A satellite in a circular orbit at 200 mi altitude possesses a kinetic energy of about 13,000 Btu/lb. An interplanetary vehicle approaching the earth possesses a kinetic energy of about 26,000 Btu/lb. That these energies are not negligible is illustrated by comparison with the energy required to vaporize water, 1000 Btu/lb, and to vaporize carbon, 25,000 Btu/lb. The latter is among the highest heats of vaporization of known materials.

One of the problems of atmospheric penetration is to convert this energy into a form that will not prove disastrous to the vehicle, either during penetration or on landing. If all of the body's potential and kinetic energy were converted into thermal energy within the body itself, it would be more than sufficient to vaporize the entire body, unless the body were entirely constructed of some material such as carbon. The survival of meteorites, however, is an obvious indication that not all of the energy goes into the body.

Actually, the body's initial energy is transformed, through the mechanism of gasdynamic drag, into thermal energy in the air around the body, and only part of this energy is transferred to the body as heat. The fraction of the original energy that appears as heat in the body depends upon the characteristics of the flow around the body.

Gasdynamic Effects During Penetration. Before entry into a planetary atmosphere, a body's motion is governed only by the principles of celestial mechanics; i.e., its motion is governed only by its own inertia and by gravitational forces. However, such motion is modified when the vehicle enters the outer fringes of a planetary atmosphere. In the rarefied upper atmosphere where the molecular mean free path is large compared with the body size, the flow is of the so-called free-molecular type and a gasdynamic drag force begins to act in a direction opposite to the vehicle's motion. In the free-molecule flow region, appreciable lift forces (i.e., forces normal to the direction of motion) are not attained (at velocities of the orbital or escape magnitude). In the denser lower atmosphere, where the flow is of the continuum type, both lift and drag forces affect the vehicle's motion.

The effects accompanying atmospheric entry that are manifested in the vehicle are a reduction in velocity accompanied by appreciable deceleration loads and by appreciable heating rates. The deceleration, and consequent velocity reduction, is due to aerodynamic drag, which varies with air density (ρ) and the square of the vehicle velocity (u^2):

$$\text{Deceleration} \sim \rho u^2$$

Now, as the vehicle approaches the planet it first encounters an

atmosphere of very low density. As it penetrates further, the density increases rapidly; and, due to drag, the velocity begins to decrease. Thus the deceleration is the product of two quantities, one increasing and the other decreasing. Initially, the deceleration increases; however, at some point, the velocity begins to decrease more rapidly than the density increases, resulting in a maximum deceleration with subsequent decreasing deceleration in most cases. This is illustrated in Fig. 2. For entry from space, these decelerations may be very appreciable; for example, entry at right angles into the earth's atmosphere at escape velocity involves a maximum deceleration of over 300 g.

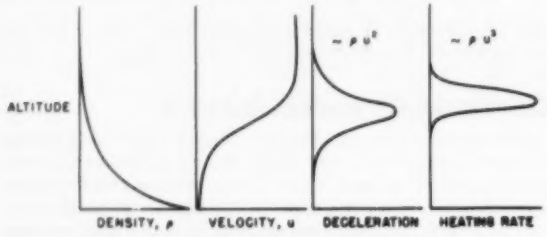

Fig. 2 Changes during atmospheric entry

Gasdynamic heating of the vehicle surface during entry varies in a somewhat similar fashion. The heating rate varies approximately with the atmospheric density and the cube of the vehicle velocity:

$$\text{Heating rate} \sim \rho u^3$$

Here, also, the increasing density and decreasing velocity during entry interact to produce a maximum heating rate. This is also illustrated in Fig. 2.

These expressions indicate that both deceleration and heating are most severe when there is a combination of high atmospheric density and high vehicle velocity, i.e., when high velocities are allowed to persist to low altitudes.

Factors Affecting Penetration Characteristics. The way in which velocity changes with altitude during entry, the deceleration forces, and the surface heating rates depend upon several factors:

- o Atmospheric approach (Fig. 3)
  - Velocity of approach, u_i
  - Angle of approach, θ
- o Vehicle characteristics (Fig. 4)
  - Mass-drag ratio, $\dfrac{W}{C_D A_c}$ (W = mass, C_D = drag coefficient, A_c = frontal area)
- o Atmospheric characteristics (Fig. 5)
  - Surface density, ρ_{SL}
  - Density variation with altitude, $\rho = f(h)$

The velocity and angle of atmospheric approach, illustrated in Fig. 3, are primary factors in determining the severity of the entry deceleration and heating. As indicated previously, combinations of high velocity and low altitude produce the most severe entry conditions. These are most apt to occur when the initial velocity is high or when the entry is perpendicular (θ = 90 deg). On the other hand, a lower initial velocity or a shallow entry angle tends to restrict higher velocities to higher altitudes. The initial entry velocity is determined by the planet's gravitational characteristics and by the type of entry, i.e., from satellite orbit, directly from space, etc. Since usually one is not able to choose the initial entry velocity (except by rocket braking), adjustment of the angle is one means of reducing the severity of entry. Effectively, high velocities can be restricted to the upper atmosphere either by a lowered initial velocity or by a shallow entry-angle so that deceleration takes place high in the atmosphere.

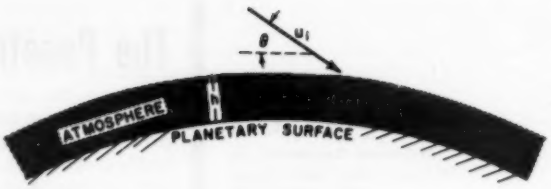

u_i = INITIAL ENTRY VELOCITY
θ = PATH ANGLE (WITH LOCAL HORIZONTAL)
h = ALTITUDE

Fig. 3 Entry into a planetary atmosphere

Similarly, deceleration high in the atmosphere can be affected by the use of a body having a small mass-drag ratio and/or some aerodynamic lift. A reduced mass per unit drag allows deceleration in the less dense region of the atmosphere, while aerodynamic lift decreases the rate of descent and, thus, allows time for deceleration high in the atmosphere. For example, the slender body shown in Fig. 4(a) has a high mass-drag ratio and would penetrate (at high velocity) further into the atmosphere than the blunt body with a low mass-drag ratio illustrated in Fig. 4(b). If the latter body is oriented in the position shown in Fig. 4(c), a lift force would be developed which would force it into a more shallow path and hence restrict deceleration to a high altitude.

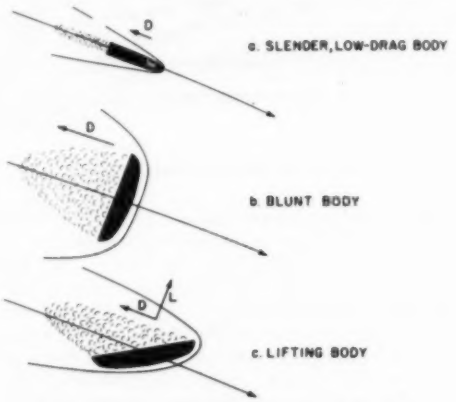

Fig. 4 Aerodynamic forces on various bodies

The physical and chemical characteristics of the planetary atmosphere also determine the entry characteristics. For a first approximation to the gasdynamic forces and heating, a knowledge of the density variation in the atmosphere is sufficient. For hydrostatic equilibrium in an isothermal atmosphere, it can be shown that the atmospheric density at altitude, in ratio to the sea-level density, is given by

$$\sigma = \frac{\rho}{\rho_{SL}} = e^{-\alpha h}$$

where e is the base of natural logarithms, h is altitude, and α is a coefficient dependent upon the temperature and composition of the atmosphere. This equation indicates that the density decreases exponentially as the altitude increases. While the planetary atmospheres are far from isothermal, an expression of this type represents the earth's atmosphere reasonably well. The approximate density variation in the earth's atmosphere and

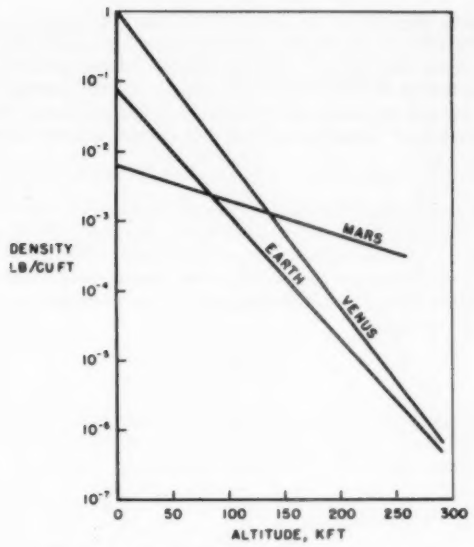

Fig. 5 Density variation in planetary atmospheres

the estimated density variation in the atmospheres of Venus and Mars are shown in Fig. 5 [1].[1] The atmosphere of Venus, estimated to consist of about 10 per cent nitrogen and 90 per cent carbon dioxide, is somewhat more dense than the earth's atmosphere but varies in a similar way with altitude. The atmosphere of Mars, estimated as about 95 per cent nitrogen and 5 per cent carbon dioxide, is appreciably less dense at sea level but varies much more gradually with altitude and is actually more dense at high altitudes. The more gradual density variation in the Martian atmosphere effectively makes it "softer" and consequently reduces the severity of entry.

Dynamics of Atmospheric Penetration

As illustrated in Fig. 1, there are three general types of atmospheric penetration:

1 Relatively steep descent path, characteristic of direct entry from space, "dump" from a satellite orbit, and re-entry of a ballistic rocket.

2 More gradual descent path, characteristic of a satellite orbit decay.

3 Very gradual descent, characteristic of a boost-glide rocket or a lifting descent from a satellite orbit.

While the equations of motion for atmospheric penetration require a numerical or machine computation for exact solution, approximate analytic solutions are possible for the three cases listed above and have been described elsewhere [1].

Direct Entry. For the case of a relatively steep ($\theta > 5$ deg) direct entry on a linear path, a simple approximate solution may be obtained for a nonlifting vehicle. If the gravitational force is neglected in comparison to the decelerating aerodynamic force, if the atmosphere is assumed isothermal, and if the drag coefficient is assumed constant, the velocity variation is given by [2, 3, 4, 5]

$$\frac{u}{u_i} = e^{-\frac{C_D A_e}{W \sin\theta} \frac{\rho_{SL}}{2\alpha}}$$

Comparison of this approximate equation with the results of exact machine computations indicates good agreement for cases where the entry angle is greater than about 5 deg and in the velocity range where deceleration loads and gasdynamic heating are important considerations. (For small entry angles, Cases 2 and 3 above, other approximations apply.) After the major deceleration has occurred, the vehicle's path bends over into a vertical descent; and the velocity is essentially a local terminal-fall velocity.

Fig. 6 illustrates the velocity variation with altitude for direct penetration of the earth's atmosphere ($\alpha = 4.15 \times 10^{-5}$ per ft) for several values of the drag-mass-angle parameter, $\frac{C_D A_e}{W \sin\theta}$.

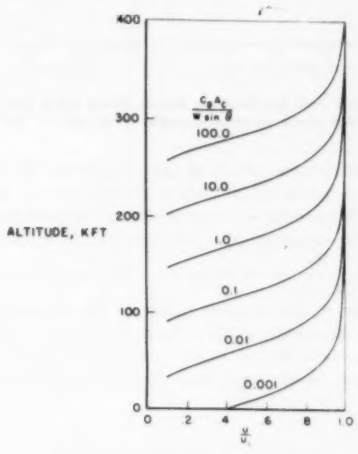

Fig. 6 Velocity variation during direct penetration of the earth's atmosphere

One interesting facet of these results is that the major deceleration of the body takes place in a stratum of the atmosphere of constant thickness. The level of this stratum in the atmosphere is, however, dependent upon the value of the drag-mass-angle parameter. Large values of this parameter cause deceleration high in the atmosphere, while smaller values delay deceleration until the lower atmosphere is reached. Thus the use of a high-drag, light body at a small entry angle enables deceleration at high altitudes. Since severe deceleration loads and gasdynamic heating rates occur when high velocities persist down to low altitudes, the use of a light, high-drag body at a shallow entry appears advantageous.

The deceleration during a relatively direct atmospheric penetration is found to rise to a maximum value and then decrease during descent (see Fig. 2). The maximum value of the deceleration occurs when the velocity has been reduced to about 61 per cent of its initial value.

$$\frac{u}{u_i} = \frac{1}{e} = 0.607$$

The maximum deceleration is

$$\left(-\frac{du}{dt}\right)_{max} = \frac{\alpha u_i^2 \sin\theta}{2e}$$

It is interesting to note that the maximum deceleration during direct entry is independent of the drag-mass characteristics of the body. It is dependent only upon the path angle, the initial velocity, and the atmospheric characteristics. For a given entry velocity, entry angle, and atmosphere, the maximum deceleration is independent of the body characteristics; however, the altitude of maximum deceleration is dependent upon the mass-drag characteristics of the body.

[1] Numbers in brackets designate References at end of paper.

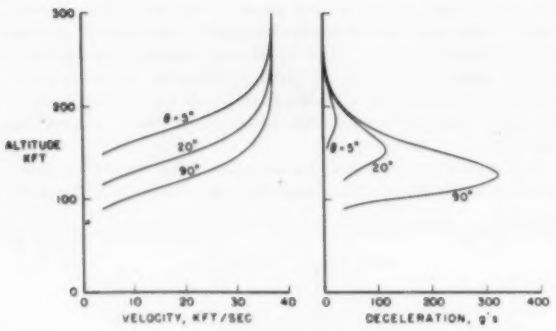

Fig. 7 Velocity and deceleration during direct entry into the earth's atmosphere from space at various angles $W/(C_DA_e) = 10$ lb/sq ft

Fig. 7 illustrates the effect of entry angle on the variation of velocity and deceleration during penetration of the earth's atmosphere from space by a body having the mass-drag characteristics of the Vanguard scientific satellite ($W = 21.5$ lb, diameter = 20 in., $\frac{W}{C_DA_e} \simeq 10$ lb/sq ft). The smaller entry angle is seen to result in deceleration higher in the atmosphere and a smaller peak deceleration. If a lighter body were used at these entry angles, these curves would be shifted to higher altitudes. A heavier body would result in a shift to lower altitudes.

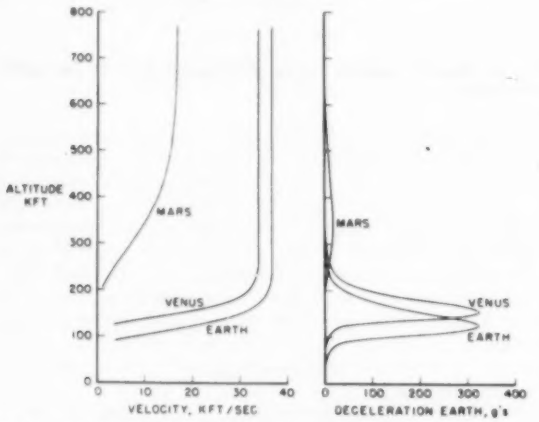

Fig. 8 Velocity and deceleration during direct entry from space at $\theta = 90$ into three planetary atmospheres $X/(C_DA_e) = 10$ lb/sq ft

The variation of velocity and deceleration of the same body is shown in Fig. 8 for vertical penetration of the atmospheres of Venus, Earth, and Mars [1]. The different gravitational attraction accounts for the different initial velocities. The effect of atmospheric density variation is apparent in the shape and position of the curves. The more dense atmosphere of Venus results in deceleration at a higher altitude; however, the velocity variation with altitude and the maximum deceleration is about the same as for Earth because of the similar density variation (see Fig. 5). However, the more gradual variation of density in the Martian atmosphere results in a more gradual variation of velocity with altitude and a lower peak deceleration.

Orbit Decay. In the case of the more gradual descent path characteristic of the decay of a satellite orbit (see Fig. 1), the assumptions used in the previous section are no longer applicable. The path is far from linear, and the path angle changes during descent. In the region of appreciable deceleration and heating, the path angle is of the order of 3–4 deg. An approximate analytic solution for this case [1] yields results somewhat similar to those for direct entry in that the altitude of deceleration in the atmosphere is dependent upon the mass-drag characteristics of the body and the maximum deceleration is independent of these characteristics. Velocity variation with altitude is shown in Fig. 9, with $\frac{W}{C_DA_e}$ as parameter. (The path angle does not appear in this parameter since it cannot be specified and since it varies during descent—it is an output from rather than an input to the problem.) The deceleration varies in a somewhat similar manner to that in the previous case, rising to a maximum and then falling off. Here the maximum deceleration occurs when the velocity has been reduced to

$$\frac{u}{u_i} \simeq 0.53$$

and has a relatively low value because of the low path angle. For example, the decay from a circular satellite orbit into the earth's atmosphere involves a maximum deceleration of about $9g$.

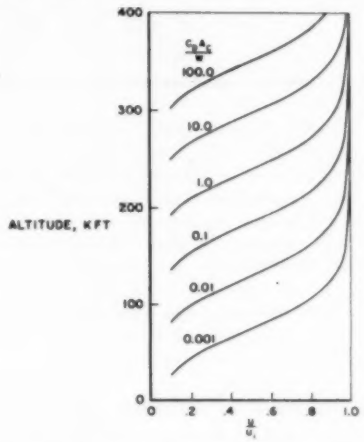

Fig. 9 Velocity variation during penetration of the earth's atmosphere by orbital decay

It should, perhaps, be emphasized that the orbital decay described here refers to the last stage of decay where heating and deceleration are appreciable—about the last 2000 miles and last few minutes of the satellite lifetime. This phase is preceded by a much longer period, many revolutions, in which the satellite orbit gradually decays. This initial phase of decay consists of an extremely gradual spiral during which the orbit becomes more circular. The rate of energy loss by the vehicle due to aerodynamic drag is small enough so that the vehicle's kinetic energy and potential energy adjust themselves to a momentary "equilibrium" orbit. In this process, the potential energy decreases and the kinetic energy increases—with a net decrease in total energy. Thus the satellite's velocity actually increases in the initial phases of orbital decay.

Lifting Descent. A lifting descent involves a still more gradual atmospheric penetration (see Fig. 1). Here again, the path angle adjusts itself to the forces acting on the vehicle and turns out to be quite small—of the order of a few tenths of a degree. The velocity variation with altitude, as indicated by an approximate analytic solution [1], is shown in Fig. 10 as a function of a lift-mass parameter, $\frac{C_LA_e}{W} = \frac{L}{D}\frac{C_DA_e}{W}$, which is related to the drag-mass parameter by the lift-drag ratio, L/D. It is seen that

here again the level of deceleration in the atmosphere is determined only by the mass and aerodynamic-force characteristics of the body. In this case, however, the deceleration does not go through a maximum value, but asymptotically approaches a value

$$\left(-\frac{du}{dt}\right)_{max} = \frac{g}{L/D}$$

Since aerodynamic shapes with lift-drag ratios as high as five appear feasible, it is clear that relatively small decelerations can be obtained in a lifting descent.

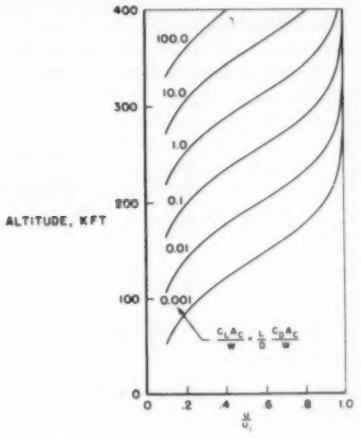

Fig. 10 Velocity variation during penetration of the earth's atmosphere by a lifting vehicle

Comparisons. In comparing the three types of atmospheric penetration just discussed, it is necessary to keep in mind the fact that the more gradual descents involve longer times and greater ranges than a steeper descent (see Fig. 1). For example, descent through the "Corridor of Continuous Flight" [6] can be accomplished by the three types of penetration described with essentially the same velocity-altitude variation, as shown in Fig. 11. However, the direct descent would involve a distance of only up to a few hundred miles and about one half minute. The orbital decay might involve a range of about 2000 miles and 5 or 10 minutes. The lifting descent would extend over 5000 to 10,000 miles and about two hours. A gradual descent involves velocity reduction and consequent energy dissipation over a long period of time. Thus deceleration loads and aerodynamic heating rates are reduced by lengthening the time of deceleration. The maximum deceleration loads experienced during penetration of the earth's atmosphere, with initial entry at satellite velocity, is shown in Fig. 12 for direct descents at various entry angles, for orbital decay, and for descent with various degrees of aerodynamic lift. The maximum deceleration loads for direct entry from space at escape velocity would be twice as high as those shown for direct entries at satellite velocity. It is clear that a steep direct

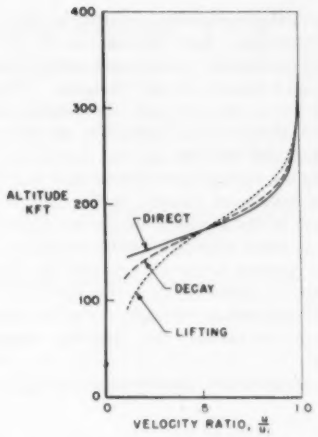

Fig. 11 Velocity variation with altitude for three types of atmospheric penetration

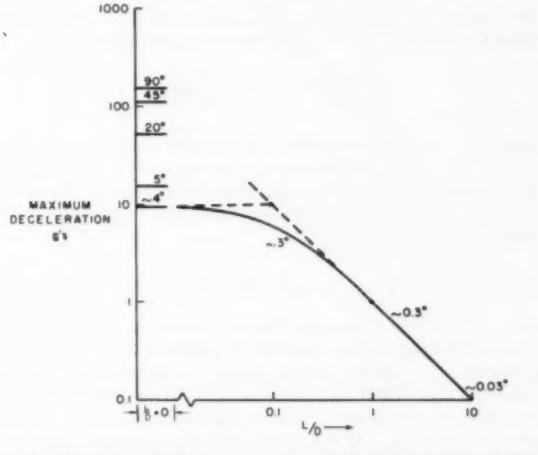

Fig. 12 Maximum deceleration into the earth's atmosphere at orbital velocity

entry at either velocity would probably not be humanly tolerable and that the atmospheric penetration by a manned vehicle would require a relatively shallow descent path. The descent paths for vehicles with aerodynamic lift involve quite tolerable deceleration loads—less than one g. The maximum deceleration for various types of entry into the atmospheres of Venus, Earth, and Mars are given in Table 1.

Heating During Atmospheric Penetration

As described earlier, the reduction of the vehicle's kinetic and potential energy during descent is accompanied by an increase in

Table 1 Maximum deceleration experienced during various types of atmospheric penetration (Values given in Earth g's)

Planet	Direct entry at escape velocity			Direct entry at orbital velocity			Entry by decay from satellite orbit	Entry of lifting vehicle at orbital velocity		
	$\theta = 5$	20	90	$\theta = 5$	20	90		$\frac{L}{D} = 1$	2	5
Venus	28.6	112	326	14.3	56	163	8.9	0.88	0.44	0.18
Earth	28.3	111	324	14.2	55.5	162	9.5	1.0	0.5	0.2
Mars	1.6	6.3	18.3	0.8	3.2	9.2	1.4	0.38	0.2	0.076

thermal energy in the surrounding air, some of which is transferred to the vehicle's surface. Now the fraction of the vehicle's lost kinetic and potential energy which reaches the vehicle surface as heat is of primary concern to the designer. This fraction, or conversion efficiency, depends upon the vehicle's shape and on its velocity and altitude—and ultimately on the mechanism of heat transfer between the hot gas and the vehicle surface. At very high altitudes, in the free-molecule flow regime, where the heat energy is developed directly at the vehicle's surface, as much as one half of the vehicle's lost energy can appear as heat in the body. At lower altitudes, in the continuum flow regime, thermal energy appears in the air between the shock wave and the body. Heat is transferred from this hot air to the body by conduction and convection through a viscous boundary layer; radiation from the hot gas may also contribute appreciably to the surface heating.

The rate of change of the vehicle's kinetic energy per unit mass is

$$-\frac{d\left(\frac{u^2}{2}\right)}{dt} = \frac{C_D A_c}{W}\,\frac{1}{2}\,\rho u^3$$

The portion of this reaching the body as heat, i.e., the heating rate per unit mass, can be expressed as, approximately,

$$\frac{q}{W} \simeq C_{H_c} A_c \eta_R\,\frac{1}{2}\,\rho u^3$$

where C_{H_c} is a dimensionless heat-transfer coefficient (Stanton number) based on frontal area A_c, and η_R is the recovery factor. Ratioing these two equations gives the instantaneous "efficiency" of converting the vehicle's kinetic energy to heat energy in the body

$$f = \frac{C_{H_c}\eta_R}{C_D}$$

The value of this conversion fraction f depends upon the heat-transfer mechanism, the velocity, the altitude, and the vehicle's geometry. A typical variation of f for a relatively blunt body at a velocity of 35,000 ft/sec at various altitudes is shown in Fig. 13. It is seen to vary from $^1/_2$ at very high altitudes down to about 0.01 at 100,000 ft. At still lower altitudes it increases again due to a turbulent boundary-layer condition and to appreciable radiation from the hot gas. At a lower velocity, e.g., satellite velocity, the radiation contribution becomes small and can usually be neglected.

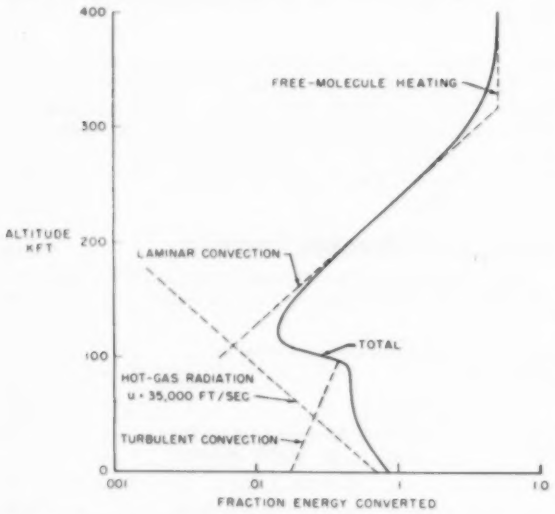

Fig. 13 Conversion efficiency (kinetic to thermal energy) as a function of altitude

The maximum heating rate, for the several types of penetration described in the previous section, occurs when the velocity has been reduced to about 85 per cent of the initial velocity. The peak heating rate, therefore, occurs before the point of maximum deceleration load.

The surface heating rate is dependent both upon the rate of reduction of the vehicle's kinetic energy and upon the conversion efficiency. At high altitudes where, although f is high, the rate of energy reduction is low, the heating rates will be low. Similarly, at moderate altitudes, where f is low, the rate of energy reduction is high and high surface heating rates will occur. This is illustrated in Fig. 14.

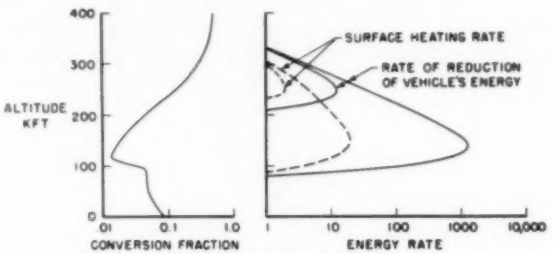

Fig. 14 Variation of rate of reduction of vehicle's kinetic energy and surface heating rate

The total heat input to the body during atmospheric penetration is obtained by integrating the heating rate over the time of descent. If the conversion factor f were constant, the total heat load would be independent of the type of entry, since a given fraction of the body's initial energy would be converted into heat in the body. However, the actual variation of f (Fig. 13) allows one to minimize the total heating by positioning the maximum rate of energy reduction at the minimum value of f. In the case of the examples illustrated in Fig. 14, the total heat load for the vehicle decelerating in the upper atmosphere would be greater than that for the vehicle decelerating at a lower altitude. The former would involve lower heating rates over a longer period of time, but with a greater accumulated heat load.

If the heating rate is sufficiently low, it can be rejected by radiation from the heated surface. This type of cooling is, of course, limited by the temperature limitations of the surface material. When all of the incoming aerodynamic heating is rejected by thermal radiation from the surface, we may write a simple heat balance

$$\frac{q}{A_S} \sim \epsilon T_w^4$$

which says that the incoming heat from hot air surrounding the body is proportional to the surface emissivity and the fourth power of the surface temperature. This temperature is the so-called radiation equilibrium temperature, and serves as a convenient parameter for the expression of heating rates. In Table 2 the maximum heating rate, in terms of this radiation equilibrium temperature, is given for several types of penetration into the atmospheres of Venus, Earth, and Mars for a body with a heated surface area twice its frontal area. In some cases, it is apparent that the temperatures are within the range of current materials. In other cases, the heating rates correspond to temperatures above the range of current materials.

Whether it is desired to minimize the peak heating rate or to minimize the total heat load depends upon the penetration

Table 2 Maximum heating rate experienced during various types of atmospheric penetration for $\frac{W}{C_D A_c} = 10 \frac{\text{lb}}{\text{sq ft}}$ [a]

(Values expressed as equivalent radiation equilibrium temperature, deg R)

Planet	Direct entry at escape velocity			Direct entry at orbital velocity			Entry by decay from satellite orbit	Entry of lifting vehicle at orbital velocity		
	$\theta = 5°$	20°	90°	$\theta = 5°$	20°	90°		$\frac{L}{D} = 1$	2	5
Venus	4700	5500	6300	3600	4200	4900	3400	2300	2100	1900
Earth	5000	5900	6800	3900	4600	5200	3600	2500	2300	2000
Mars	2400	2800	3200	1900	2200	2500	1900	1500	1350	1200

[a] Note that the maximum heating rate, unlike the maximum deceleration, is dependent on the mass-drag parameter.

technique chosen. If one chooses to reject heat by thermal radiation, it is desirable to minimize heating rates and hence surface temperatures. On the other hand, if heat is being absorbed by a vaporizing surface, it is desirable to minimize the total heat load. These considerations are discussed more completely in the next section.

Penetration Techniques

While a great variety of techniques for successful atmospheric penetration have been suggested, a synthesis of the principles outlined in the preceding sections suggests two general classes:

1 The first involves the use of a vehicle having a relatively small mass-drag or mass-lift parameter, or a shallow entry path, so as to effect deceleration high in the atmosphere. In this case, the aerodynamic heating rates are low enough so that the heat may be rejected by thermal radiation from the vehicle surface. This corresponds to a descent through the Corridor of Continuous Flight [6], since the descent is slow enough so that steady-state conditions apply. Examples of this type of descent are the descent of a glide rocket, the orbital decay of a Vanguard satellite [7], or the direct entry from space of a relatively light, high-drag body. These three examples involve successively greater deceleration loads—thus a manned descent would probably require either a lifting vehicle or a very shallow descent.

2 The second general class involves the use of a vehicle whose mass-drag characteristics and entry path are adjusted so as to place the point of maximum energy reduction at the point where the efficiency of conversion of vehicle energy to surface heat is a minimum, i.e., so the total heat load is minimized. In this case, the heat is absorbed by the body surface. An example is the direct descent of an unmanned vehicle from space [8]. The technique of heat absorption may consist of a solid heat sink, internal cooling, or a vaporizing surface. This type of atmospheric penetration generally involves higher deceleration loads and is most applicable to unmanned vehicles.

While it does not appear possible to specify the most desirable system of atmospheric penetration for a given mission without a detailed design study, one can indicate general areas of feasibility. For example, Fig. 15 indicates a schematic estimate of the penetration systems applicable to various situations. Here are plotted the entry angle and the mass-drag ratio. Small values of these variables yield relatively low heating rates and radiation cooling is feasible. Large entry angles and large mass-drag ratios mean high heating rates (but lower total heat loads), and heat absorption schemes are applicable. Thus the regions of radiation cooling and heat absorption are indicated. Deceleration loads are primarily dependent upon entry angle (for a given entry velocity). Manned descent is therefore restricted to the smaller angles. It will be noted that both radiation and heat absorption techniques are applicable to both manned and unmanned atmospheric penetration.

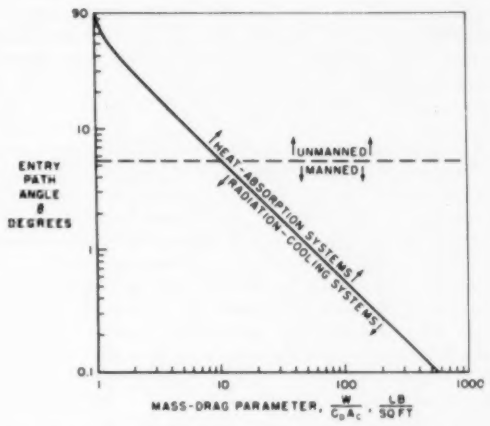

Fig. 15 Approximate regions for various types of entry from space

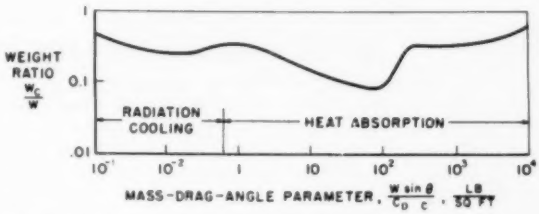

Fig. 16 Cooling-system weight requirements for direct entry from space at escape velocity

One method of deciding which type of cooling scheme to use is the examination of the weight which must be charged to the solution of the heating problem. This weight may be either that of a heat absorbing surface or the weight of drag brakes or lifting surfaces used to bring about the reduced heating rates characteristic of high-altitude deceleration. Such cooling system weight, in ratio to total weight, is shown in Fig. 16 as a function of the mass-drag parameter. At low values of the mass-drag parameter (large, light bodies) weight is required for drag brakes or lifting surfaces and surface heating is handled by radiation. At large values of the mass-drag parameter (small, heavy bodies) weight is required for heat absorption. The shape of the curve is seen to be somewhat similar to the conversion efficiency (Fig. 13)—although here two minimums appear. One minimum weight corresponds to the point where f is a minimum, i.e., where the sum of the convective and radiative heating is a minimum. The other minimum corresponds to the point where the mass-drag parameter is just small enough so that radiative cooling is possible

and yet not large enough to require a large weight in drag brakes or lifting surfaces.

References

1 Carl Gazley, Jr., "Deceleration and Heating of a Body Entering a Planetary Atmosphere From Space," section in "Vistas in Astronautics," Pergamon Press, London, England, 1958.

2 C. Wagner, "Skin Temperatures of Missiles Entering the Atmosphere at Hypersonic Speed," TR 60, Ordnance Research and Development Division, Suboffice (Rocket), Fort Bliss, Texas, September, 1949.

3 H. J. Allen and A. J. Eggers, Jr., "A Study of the Motion and Aerodynamic Heating of Missiles Entering the Earth's Atmosphere at High Supersonic Speeds," NACA RM A53D28, August 25, 1953.

4 Carl Gazley, Jr., "Aerodynamic Heating of Bodies During Re-Entry Into the Earth's Atmosphere," The RAND Corporation Research Memorandum, RM-1150, October, 1953.

5 Carl Gazley, Jr., "Heat-Transfer Aspects of the Atmospheric Re-Entry of Long-Range Ballistic Missiles," The RAND Corporation Report, R-273, August 1, 1954.

6 David J. Masson and Carl Gazley, Jr., "Surface-Protection and Cooling Systems for High-Speed Flight," *Aeronautical Engineering Review*, vol. 15, November, 1956, pp. 46–55.

7 Carl Gazley, Jr., and David J. Masson, "A Recoverable Scientific Satellite," The RAND Corporation, Paper P-958, February 27, 1957.

8 Carl Gazley, Jr., and David J. Masson, "The Recovery of a Circum-Lunar Instrument Carrier," Proceedings of the Eighth International Astronautical Congress, Barcelona, 1957, Springer-Verlag, Vienna, Austria, 1958.

D. B. MANN
Mechanical Engineer,
Cryogenic Engineering Laboratory,
National Bureau of Standards,
Boulder, Colo.

R. B. STEWART
Associate Professor
of Mechanical Engineering,
University of Colorado,
Boulder, Colo. Mem. ASME

Thermodynamic Properties of Helium at Low Temperatures and High Pressures[1]

The thermodynamic properties of helium have been compiled and correlated for a temperature range from 3.0 to 20° K for pressures to 100 atmospheres and for specific volumes from 5 to 800 liters per kilogram. The properties are presented on both the temperature-entropy and the enthalpy-entropy co-ordinate systems and include pressure, temperature, volume, entropy, and enthalpy.

Introduction

RECENT INTEREST in compressed liquid helium has resulted in considerable new experimental data of the thermodynamic properties of helium. Investigations of liquefaction or refrigeration cycles and the design of heat exchange equipment indicate the need for a correlation of the thermodynamic properties and their presentation in an accurate and convenient manner.

The most comprehensive investigations of the thermodynamic properties of normal helium I and II were published over a period of the last thirty years by W. H. Keesom, and a culmination of most of this work was published by Keesom [1][2] in 1942. Since this time, numerous investigators have determined considerable additional data, particularly values for compressed liquid in the temperature range below 20 K, an area not covered extensively by Keesom. These recent investigations in this low temperature range have been published as separate and sometimes isolated articles of very narrow interest and in some cases the results are not in readily usable form. The authors have made a compilation and a critical correlation of the present data on the thermodynamic properties of helium below 20 K and have presented them in the form of two convenient charts. The resulting diagrams include the properties of pressure, volume, temperature, enthalpy, and entropy for pressures up to 100 atmospheres, for specific volumes from 5 to 800 liters per kilogram, and for temperatures between 3.0 and 20 K. The first of these charts uses temperature-entropy co-ordinates which will be generally useful in analysis of thermodynamic systems and processes. The second chart presents the data with enthalpy-entropy co-ordinates. This second chart was found necessary since the slopes of the volume, pressure, and enthalpy lines approach a common value in the compressed liquid region on the temperature-entropy plot, making interpolation difficult and inaccurate. This graph is not extended to low pressures and high temperatures as the temperature-entropy diagram published by J. Zelmanov [2] is adequate for these regions.

Data

The greatest quantity of information prior to 1944 on the thermodynamic properties of helium in the region being considered comes from two sources. The first of these is a compilation by W. H. Keesom [1] of the theoretical and experimental investigations performed at the University of Leiden, Holland. This work is quite extensive and covers the temperature range from 0 to 400 K and pressures from 0.001 to 200 atmospheres. Secondly, an investigation of the Joule-Thomson effect in helium by J. Zelmanov [2, 3] adds considerable data at low temperatures. This work was undertaken because of discrepancies found in Keesom's values at temperatures below 20 K, and at pressures between 0.5 to 60 atmospheres.

More recent data have been presented by R. W. Hill [4, 5] in the region from the critical pressure of 2.2 atmospheres to 100 atmospheres and for temperatures from 2.5 to 20 K. The data given are values of temperature, specific volume, and entropy. Data from O. V. Lounasmaa [6], which only recently have become available, list experimental values of pressure for the data presented earlier by Hill. Several articles on the temperature scale add to the data on vapor pressures of helium of which some use has been made. A summation and extension of the experimental data of the solid for a pressure range of 25 to 225 atmospheres and for temperatures from 0 to 6 K, have been published by C. Domb and J. S. Dugdale [7]. In addition, Berman and Mate [8] and Van Dijk and Durieux [9] have presented extensive data on temperature, vapor pressure, saturation densities, and heats of vaporization.

CONSTRUCTING THE CHART

Reference Values for Entropy and Enthalpy

It was first necessary to establish a fixed point for values of entropy and then to refer the data of the several investigators to this fixed point In addition, the temperature scales used by the earlier investigators were corrected to agree with a presently acceptable temperature scale designed as T_{58E}, proposed by Clement, Logan, and Gaffney [10]. The normal boiling point of liquid helium was selected as the fixed reference point, that is, 4.21 K and one atmosphere pressure. The value of entropy at this reference point was calculated by the relation,

$$S_{4.21°K} - S_{0°K} = \int_{T=0° K}^{T=4.21° K} \frac{C_{sat}}{T}\, dT,$$

where $S = 0$ cal/gm deg K at $T = 0$ K. Then, according to the Nernst-Simon statement of the Third Law of Thermodynamics [1, 11], the entropy of the solid at 0 K and 25 atmospheres pressure and the saturated liquid for vaporization at 0 K and zero pressure are identical and equal to zero. Thus the values of entropy for the saturated solid from Domb and Dugdale [7], which were reported with 0 K and 25 atmospheres at zero entropy as the reference point, could be compared with the values of entropy from the other references. The values of C_{sat} from the data of Kramers, Wasscher, and Gorter [12] were used to calculate the entropy differences below 1.9 K, while the values of C_{sat} between 1.8 K and 5.05 K are from data of Hill and Lounasmaa. The entropy difference between saturated liquid in equilibrium with its vapor at 0 K and at 4.21 K was determined as 0.830 cal/gm K, which is in agreement with the value reported by Lounasmaa.

[1] Results of a study made under contract with the Bureau of Aeronautics, Department of the Navy at the National Bureau of Standards, Boulder Laboratories.

[2] Numbers in brackets designate References at end of paper.

Contributed by the Heat Transfer Division of THE AMERICAN SOCIETY OF MECHANICAL ENGINEERS and presented at the ASME-AIChE Heat Transfer Conference, Storrs, Conn., August 9–12, 1959.

NOTE: Statements and opinions advanced in papers are to be understood as individual expressions of their authors and not those of the Society. Manuscript received at ASME Headquarters, May 20, 1959. Paper No. 59—HT-19.

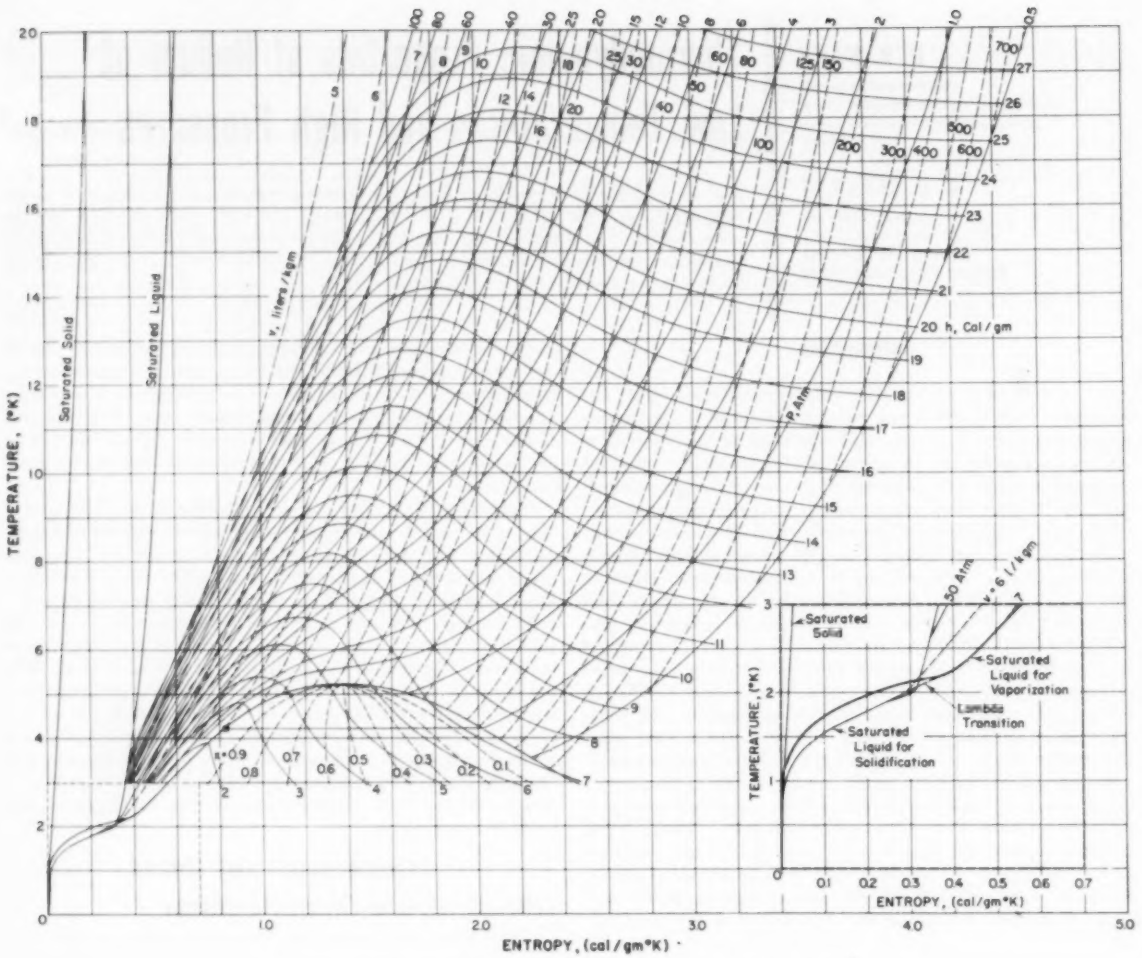

Temperature-entropy diagram. Thermodynamic properties of helium.

The fixed point for enthalpy was also selected at the normal boiling point of liquid helium. This value of 2.39 cal/gm was determined by the relation, $h - h_0 = \int_{T_0} T c_{sat} dT + \int_{P_0}^{P} V dP$, using C_{sat} values as discussed in determination of the saturation entropies. Values of vapor pressure were from Clement, Logan, and Gaffney, and values of specific volume at saturation from Berman.

Construction of Isobars

Lines of constant pressure were calculated for the charts from Hill's data using the Maxwell relation, $(\partial S/\partial V)_T = (\partial P/\partial T)_V$. Only the pressure differences along the isometrics of 5, 5.5, 6, 7, and 8 liters per kilogram were used for this purpose as the Zelmanov data were found to adequately describe the isometrics for larger values up to 800 liters per kilogram. These calculated values for pressure were also compared with values from Lounasmaa when they became available. Differences between these calculated values and Lounasmaa's experimental values were less than 5 per cent, confirming the compatibility of these data. Since the calculation of slopes is inherently inaccurate, the calculated values of pressure of the authors are considered in error when in conflict with the experimental pressure data from Lounasmaa. In addition to the Lounasmaa data, values for pressures from 0.5 to 2 atmospheres are from Zelmanov.

Construction of Isenthalpic Lines

Values of enthalpy at saturation were determined as discussed above. Starting from these saturation values, the values of enthalpy in the compressed liquid region were then found using the relation, $dh = T\,ds + v\,dP$, first along an isentropic path from the normal boiling point, using small increments of pressure and average values of specific volume. Having established enthalpy values along this isentropic line at pressures to 100 atm the other values of enthalpy were determined along the constant pressure paths. When the Lounasmaa data became available, these calculations were again checked using the new values for pressure. Below 2 atmospheres pressure, the data of Zelmanov were used in addition to the Lounasmaa data.

Values for the Isomeric Lines

Specific volumes from 5 to 70 liters per kilogram were from Lounasmaa and Hill and from 70 to 800 liters per kilogram from

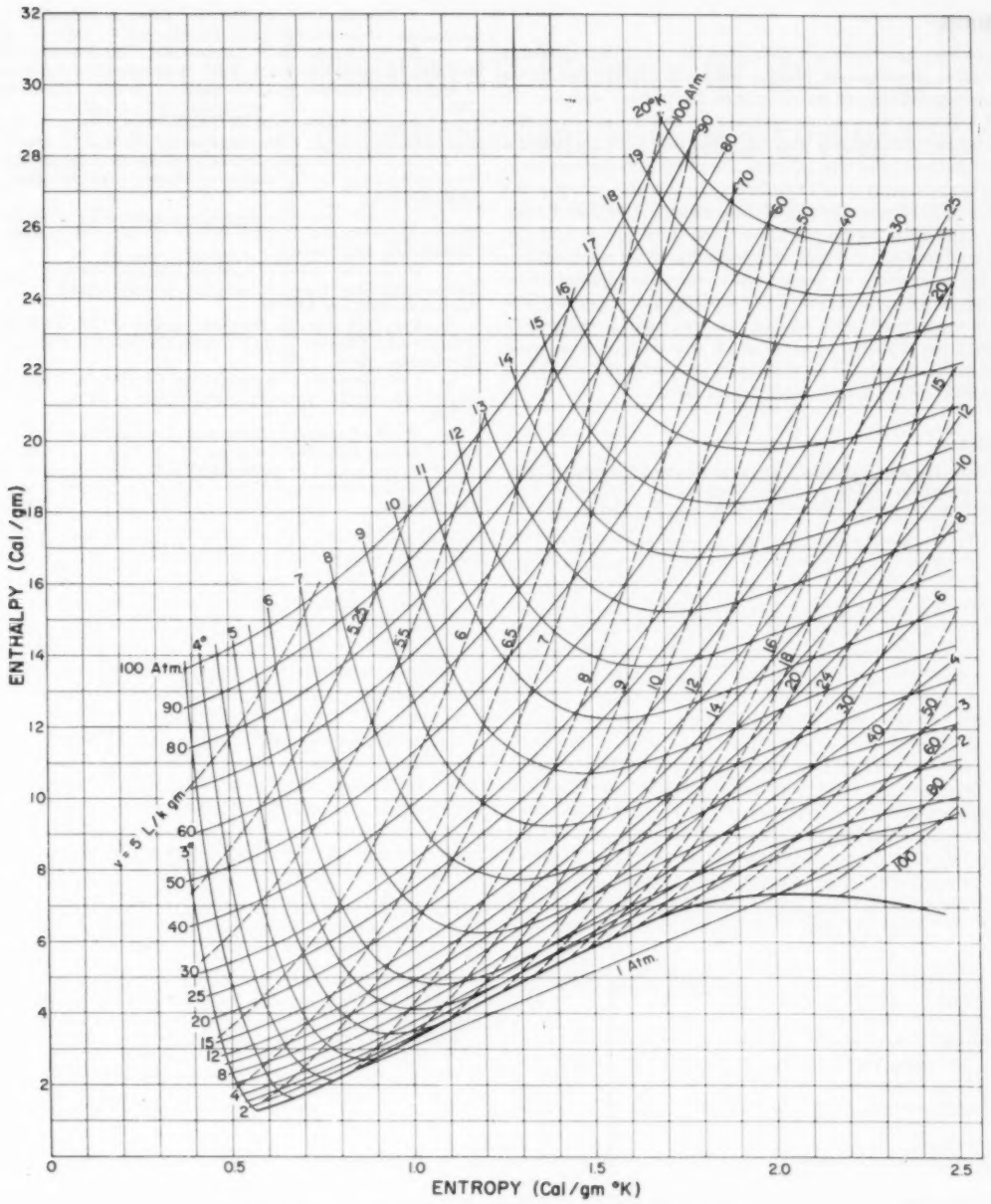

Enthalpy-entropy diagram. Thermodynamic properties of helium.

Zelmanov. The values for specific volume, 7 to 70 liters per kilogram from Zelmanov, are also in excellent agreement with those from Lounasmaa and Hill. However, where differences existed the data from Lounasmaa and Hill were used.

Properties of the Saturated Vapor

The heats of vaporization from Berman were used to determine the entropy differences of saturated vapor and saturated liquid. By using the Clausius-Clapeyron equation, $\frac{dP}{dT} = \frac{h_{fg}}{T(v_g - v_f)}$, data from Berman were also used to determine the densities of the gases at saturation.

Properties at Solid-Liquid Equilibria

The Domb and Dugdale data were used for these boundaries.

Lambda Transition

Properties along this boundary were taken from Keesom.

Conclusions

The authors have carefully compared all of the data available in the region investigated, making extensive calculations to insure the compatibility of the data from the various sources. In all but a limited area concurrent values determined from the various sources differed less than one per cent This limited area of larger discrepancies was between 2 and 60 atmospheres pressure for temperatures from 12 to 20 K. In this area many of the values from Zelmanov [3, 4] and Lounasmaa [6] differed more than one per cent, ranging to as much as three per cent at the higher temperatures. These discrepancies were resolved primarily by comparison of these data to values in adjacent areas. As a result of a careful review of the experimental apparatus and the techniques used, and making use of each investigator's estimate of the probable accuracy of his own data, it is believed that the values presented on the charts are accurate to within 5 per cent and in most cases to within 3 per cent.

References

1 W. H. Keesom, "Helium," Ilsevier, Amsterdam, 1942, p. 494.

2 J. Zelmanov, "The Entropy Diagram for Helium at Low Temperatures," *Journal of Physics* (*USSR*), vol. 8, 1944, pp. 135–41.

3 J. Zelmanov, "Joule-Thomson Effect in Helium at Low Temperatures," *Journal of Physics* (*USSR*), vol. 8, 1940, pp. 43–52.

4 R. W. Hill and O. V. Lounasmaa, "The Entropy Diagram of Helium," paper presented at Fifth International Conference on Low Temperature Physics and Chemistry, Madison, Wis., August 26, 1957.

5 Personal Letter to R. B. Scott, Chief, Cryogenic Engineering Laboratory, Boulder, Colorado, from R. W. Hill, October 7, 1957.

6 O. V. Lounasmaa, "Specific Heats at Low Temperatures," thesis submitted for the degree of Doctor of Philosophy, Univ. of Oxford, 1958.

7 C. Domb and J. S. Dugdale, chapter XI, "Progress in Low Temperature Physics," vol. II, North Holland Publishing Company, Amsterdam, 1957, 480 pp.

8 R. Berman and C. F. Mate, "Some Thermal Properties of Helium and Their Relation to the Temperature Scale," *Philosophical Magazine*, 1958, pp. 461–69.

9 Van Dijk and M. Durieux, chapter XIV, "Progress in Low Temperature Physics," vol. II, North Holland Publishing Company, Amsterdam, 1957.

10 J. R. Clement, J. K. Logan, and J. Gaffney, "Liquid Helium Vapor Pressure-Temperature Scale," *Physical Review*, vol. 100, 1955 p. 743.

11 M. W. Zemansky, "Heat and Thermodynamics," fourth edition, McGraw-Hill Book Company, New York, N. Y., 1957, p. 397.

12 H. Kramers, J. Wasscher, and C. Gorter, "The Specific Heat of Liquid Helium Between 0.25° K and 1.9° K," *Physica*, vol. 18, 1952, pp. 329–339.

R. L. CHAMBERS
Analytical Department,
Westinghouse Electric Corporation,
East Pittsburgh, Pa. Assoc. Mem. ASME

E. V. SOMERS
Research Laboratories
Westinghouse Electric
Corporation, Pittsburgh, Pa.

Radiation Fin Efficiency for One-Dimensional Heat Flow in a Circular Fin[1]

The one-dimensional steady-state solution for radiation from one side of an annular fin has been computed for values of the two design parameters $0 \leqslant \sqrt{\frac{\epsilon\sigma\theta_i^3}{K}}(r_o - r_i) \leqslant 2.0$ *and* $1.001 \leqslant \rho = \frac{r_o}{r_i} \leqslant 15.0$. *The solution supplies design information needed for satellite thermal-power dissipating surfaces.*

Introduction

IT HAS LONG BEEN KNOWN that the rate of heat transfer from a hot body to a cooler fluid may be increased by extending the body surface. Furthermore, the addition of fins extending into the fluid will cause an increased heat flow not directly proportional to the increase in body surface, since the temperature near the tip of the fin approaches the fluid temperature and causes a heat rate less than that which might be anticipated.

All of the previously published literature considering heat transfer from an extended surface has considered only the convective type of heat transfer. Convection from straight fins was considered by Parsons and Harper [1],[2] Harper and Brown [2], Avrami and Little [3], and Carrier and Anderson [4]. Convection from annular fins was the subject of papers by Harper and Brown [2], Carrier and Anderson [4], Murray [5], Gardner [6], and Keller and Somers [7].

Only recently, radiation heat transfer from fins has become of practical engineering importance; especially in the field of auxiliary power units for satellite vehicles or high altitude missiles. At high altitudes such vehicles dissipate heat only by radiation, since atmospheric convection is impossible. In the design of such power units, the principle design factor of weight per unit power is controlled by the heat dissipation rate at the heat-rejection surface of the engine, i.e., by the temperature distribution of the surface, since the heat rejection rate is controlled by the fourth power of the absolute temperature [8], i.e., the Stefan-Boltzmann law. Weight reductions are accomplished by finning techniques, and thus the dissipation of heat by radiation from fins has become important. To date, estimates of the fin efficiency for these applications have been made by linearizing the radiation rate, i.e., by replacing the fourth-power law by an equivalent convection constant multiplied by the first power of the absolute temperature, and then using the available data already cited [6]. That this procedure will introduce significant errors in the computed heat rate, as great as 60 per cent, will be shown by a comparison of the results of such a procedure with the results of this paper. The work reported here discusses the solution of a typical fin geometry applicable to certain auxiliary power units and cooled only by radiation from the fin surface to space.

Statement of the Problem

The problem is to obtain the steady-state, one-dimensional temperature distribution and fin efficiency for a flat mushroom annular fin with variable size and material properties. The fin geometry is shown in Fig. 1. The heat enters by conduction through the peg and leaves by radiation from the exposed surface

[1] This paper is based on an MS thesis submitted by R. L. Chambers to the Mechanical Engineering Department of the University of Pittsburgh on the Westinghouse Advanced Mechanics Fellowship Program.

[2] Numbers in brackets designate References at end of paper.

Contributed by the Heat Transfer Division of THE AMERICAN SOCIETY OF MECHANICAL ENGINEERS and presented at the ASME-AIChE Heat Transfer Conference, Storrs, Conn., August 9–12, 1959.

NOTE: Statements and opinions advanced in papers are to be understood as individual expressions of their authors and not those of the Society. Manuscript received at ASME Headquarters, May 4, 1959. Paper No. 59—HT-8.

Nomenclature

h = two-side heat-transfer coefficient for convection, Btu/hr ft² deg F

h' = one-side heat-transfer coefficient for convection, Btu/hr ft² deg F

k = thermal conductivity of fin material, Btu/hr ft deg F

m = total number of concentric elements that subdivide the fin

$m = \sqrt{\frac{2h}{k\delta}} = \sqrt{\frac{h'}{k\delta}}$, ft

n = an integer

Q = heat flow rate, Btu/hr

Q_{max} = heat flow rate of a fin at the constant temperature of the base, Btu/hr

r = radius at any point in the fin, ft

r_i = inside radius of the fin, ft

r_o = outside radius of the fin, ft

Δr = width of a concentric fin element, ft

r' = dimensionless ratio of radii = $\frac{r - r_i}{r_o - r_i}$

ϵ = emissivity, dimensionless

σ = Stefan-Boltzmann constant = 0.1714×10^{-8} Btu/hr ft² deg R⁴

δ = fin thickness, ft

η = fin efficiency, dimensionless

ρ = dimensionless ratio of r_o/r_i

θ = temperature at some point in the fin, deg R

θ_i = temperature at the fin base or r_i, deg R

θ' = dimensionless ratio of $\frac{\theta}{\theta_i}$, $\theta' = \theta'(r')$

γ = dimensionless parameter, $\frac{(r_o - r_i)^2\epsilon\sigma\theta_i^3}{k\delta}$

ψ = dimensionless ratio of $\frac{r_i}{\Delta r}$

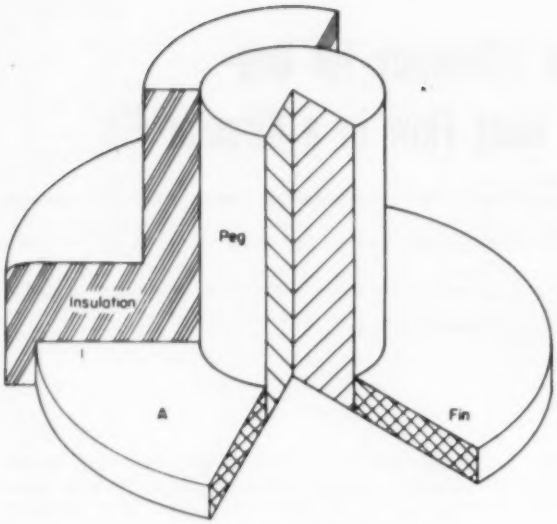

Fig. 1 Circular fin for radiant heat transfer

of the fin.[3] The purpose of this paper is to solve the equations governing the temperature distribution and fin efficiencies for a nonlinear heat transfer, i.e., fourth-power law of absolute temperatures, and to present curves relating the fin efficiency to the dimensionless independent variables. In addition, a comparison of the fin efficiencies for convective linear heat-transfer data [6] as shown by Kays and London [9] to those calculated for nonlinear radiation heat transfer is given.

Treatment of the Problem

The diffusion of heat in an annular fin of constant thickness reduces to the problem of obtaining the steady-state temperature distribution in a finite hollow circular cylinder representing the annular fin. Several restrictions and assumptions are inherent in solving this fin problem.

1 The heat flow and temperature distribution throughout the fin are independent of time, i.e., the heat flow is steady state.
2 There is no heat source in the fin.
3 The temperature at the base of the fin is uniform.
4 The fin thickness is so small compared with its radius that the temperature gradient across the width may be neglected, i.e., heat flow occurs in the radial direction only.
5 The fin radiates to a vacuum space which is at a constant arbitrary temperature of absolute zero.
6 The fin material is isotropic.

These restrictions combine with the physical laws of heat transfer to establish a second order nonlinear differential equation which describes the heat flow within the fin and a set of two boundary conditions, one each at the radial extremities of the fin. The equations in dimensionless form are

$$\frac{d^2\theta'}{dr'^2} + \frac{1}{r' + \dfrac{1}{\rho - 1}}\frac{d\theta'}{dr'} - \gamma\theta'^4 = 0 \qquad (1)$$

$$\theta'(0) = 1 \qquad \frac{d\theta'(1)}{dr} = 0$$

[3] The peg is considered to be of infinite thermal conductivity; radiation from the exposed end of the peg is not considered in the solution presented, but must be calculated separately.

By definition the fin efficiency η equals Q/Q_{max}; therefore fin efficiency due to radiation, based on the solution for temperature from equations (1), is[4]

$$\eta = \frac{2\int_0^1 \theta'^4[r'(\rho - 1) + 1]dr'}{\rho + 1} \qquad (2)$$

The solution to equations (1) is not known to be tabulated, and a numerical computation of it for different parametric values of ρ and γ was necessary. The solution was accomplished with the use of an IBM 704 digital computer, and the adiabatic boundary condition at $r' = 1$, equations (1), was checked zero to within five significant figures.

After θ' as a function r' is known, there are several methods of numerical integration that may be applied to find the fin efficiency. One method of calculating the fin efficiency was derived explicitly by breaking the fin into a series of concentric annuli of annular distance Δr, and specifying a fin temperature θ_n' at $r_n' = \dfrac{n\Delta r}{r_o - r_i}$. By definition the fin efficiency is thus given by

$$\left.\begin{aligned} \eta &= \frac{Q}{Q_{max}} \\ Q_{max} &= \pi\epsilon\sigma\theta_i^4(r_o^2 - r_i^2) \\ Q \simeq \pi\epsilon\sigma\theta_i^4\Delta r^2 &\left\{\left(\psi + \frac{1}{4}\right) + \left(\rho\psi - \frac{1}{4}\right)\theta_m'^4 \right. \\ &\left. + 2\sum_{n=1}^{m-1}(n + \psi)\theta_n'^4\right\} \end{aligned}\right\} \qquad (3)$$

In reduced form, equations (3) become

$$\eta \simeq \frac{\psi + \dfrac{1}{4} + \left(\rho\psi - \dfrac{1}{4}\right)\theta_m'^4 + 2\sum_{n=1}^{m-1}(n + \psi)\theta_n'^4}{\psi^2(\rho^2 - 1)} \qquad (4)$$

In the limit as m approaches infinity, the dependence of the right-hand side of equation (4) on ψ disappears, and the right-hand side, now equalling η, is a function of ρ and γ only, recalling that θ' is a function of ρ and γ. Thus equation (4), shows that, within the degree of approximation associated with the selection of the value of m,

$$\left.\begin{aligned} \eta &\simeq f_1(\psi, \rho, \gamma) \\ \eta &= f_2(\rho, \gamma) \\ f_2(\psi, \rho, \gamma) &= \simeq f_3(\rho, \gamma) \end{aligned}\right\} \qquad (5)$$

Another quadrature method of approximating η was employed, that of Lowan, Davids, and Levenson [10]. This method uses the Gauss mechanical quadrature method with Legendre polynominal representation of the integrand. The two methods of numerical integration agreed to within 1 per cent, and this tends to confirm the approximation in equations (5). While the Gaussian method is probably the more accurate, the summation method was used because of the simplicity of programming for the digital computer.

Discussion

Fig. 2 shows the fin efficiency as a function of two independent parameters, ρ and γ. Thus if the two independent conditions of geometry and operating material constants are known, the fin efficiency can be determined from these curves. An interesting

[4] Since $r' = \dfrac{r - r_i}{r_o - r_i}$, the fin efficiency applies only to the fin and not to the exposed end of the peg.

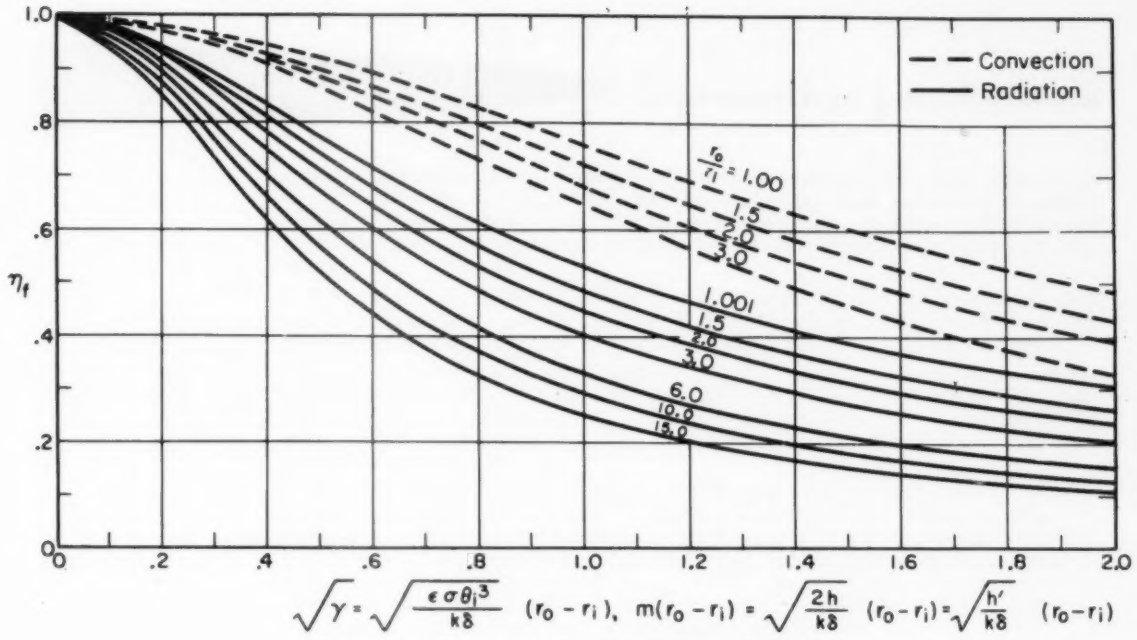

Fig. 2 Comparison of convection and radiation fin efficiencies

comparison of the work reported here with estimates of the fin efficiency based on linearizing the radiation rate, i.e., by replacing the fourth-power law by an equivalent convection constant, $h' = \epsilon\sigma\theta_i^3$, multiplied by the first power of the absolute temperature and then using the available data cited [6, 9], is shown in Fig. 2. From the curves it can be seen that an estimate based upon linearizing the radiation rate will lead to a significant error unless $\sqrt{\gamma}$ is less than 0.2. An attempt to adjust the estimate by using a mean or average temperature of the fin surface will lead to an even greater error since an average temperature will lead to a smaller γ and thus to a higher efficiency instead of the correct one. It therefore appears that there is no accurate way to determine the correct radiation rate except to consider the fourth-power law of the absolute temperature.

Because of recoding complexities in the IBM program, the work presented in this paper did not consider the case of a straight fin, $\rho = 1.000$. However, values were computed for $\rho = 1.001$ and $\rho = 1.1$ and the difference in fin efficiency was found to be negligible. It is therefore reasonable to consider that a straight fin may be approximated by $\rho = 1.001$.

Conclusions

The one-dimensional steady-state solution for radiation from one side of an annular fin supplies needed design information for satellite thermal-power dissipating surfaces. It is presented here in graphical form with the fin efficiency plotted versus the design parameters $\sqrt{\frac{\epsilon\sigma\theta_i^3}{k}}\ (r_o - r_i)$ and ρ. The previous method of linearizing the radiation rate and using the convective analysis [6] introduces a significant error which can approach a maximum of 60 per cent. The results presented here permit correct computation of the heat-transfer rates for radiation-controlled heat-dissipating fins of circular geometry.

References

1 S. R. Parsons and D. R. Harper, "Radiation for Aircraft Engines," U. S. Bureau of Standards, Technical Paper No. 211, 1922, pp. 327–330.

2 D. R. Harper and W. B. Brown, "Mathematical Equations for Heat Conduction in the Fins of Air-Cooled Engines," NACA, Report No. 158, 1922.

3 M. Avrami and J. B. Little, "Diffusion of Heat Through a Rectangular Bar and the Cooling and Insulating Effect of Fins, I. The Steady State," *Journal of Applied Physics*, vol. 13, 1942, pp. 255–264.

4 W. H. Carrier and S. W. Anderson, "The Resistance of Heat Flow Through Finned Tubing," *Heating, Piping and Air-Conditioning*, vol. 10, 1944, pp. 304–320.

5 W. M. Murray, "Heat Dissipation Through an Annular Disk or Fin of Uniform Thickness," *Journal of Applied Mechanics*, vol. 5, Trans. ASME, vol. 60, 1938, p. A-78.

6 Karl A. Gardner, "Efficiency of Extended Surface," Trans. ASME, vol. 67, 1945, pp. 621–631.

7 H. H. Keller and E. V. Somers, "Heat Transfer From an Annular Fin of Constant Thickness," Trans. ASME, series C, Journal of Heat Transfer, vol. 81, 1959, pp. 151–156.

8 S. J. Angello and E. V. Somers, "Practical Power Generation—Consideration of Power, Weight, and Fuel Cost," Conference Paper A.I.E.E. Winter General Meeting, February 7, 1958, New York.

9 W. M. Kays and A. L. London, "Compact Heat Exchangers," The National Press, Palo Alto, Calif., p. 31, 1955.

10 Arnold N. Lowan, Norman Davids, and Arthur Levenson, "Table of the Zeros of the Legendre Polynomials of Order 1–16 and the Weight Coefficients for Gauss's Mechanical Quadrature Formula," *Bulletin of the American Mathematical Society*, vol. 48, October, 1942, pp. 739–743.

Journal of HEAT TRANSFER

Information for Authors

• Manuscripts should be submitted in final form to the Editor. Each manuscript must be accompanied by a statement that it has not been published elsewhere nor has it been submitted for publication elsewhere. A paper which would occupy more than 8 pages of the Journal may be returned to the author for abridgment.

• The author should state his business connection, the title of his position, and his mailing address. A short abstract (50 to 100 words) should be included on the first page immediately preceding the introductory paragraph of the paper.

Three copies of the manuscript are required. One of these must be a carefully prepared printer's copy, typed in double spacing, on one side of the page only, with wide margins, on $8^1/_2$ by 11-in. opaque white paper. Mimeographed manuscripts, if prepared with exceptional care, can be accepted provided they are completely edited.

• As far as possible, all mathematical expressions should be typewritten. Greek letters and other symbols not available on the typewriter should be carefully inserted in ink. Care should be taken to distinguish between capital and lowercase letter, between zero (0) and the letter (*O*), between the numeral (1) and the letter (*l*), etc. A letter representing a vector cannot be printed with an arrow above or below it. The letter should be underscored with a single wavy line, wherever it appears in the text, to designate boldface type.

• A list of symbols carefully marked for the use of the editor (thus: κ, Greek l.c. kappa), if it has not been included in the body of the paper, should accompany the manuscript on a separate page.

• Before preparing a manuscript the author should study printed articles in the Journal, with special attention to the form and style of mathematical expressions, tables, footnotes, references, and abstract. Numbers that identify mathematical expressions should be enclosed in parentheses. Numbers that identify references at the end of the paper should be enclosed in brackets. Care should be taken to arrange all tables and mathematical expressions in such a way that they will fit into a single column when set in type. Equations that might extend beyond the width of one column (fractions that should not be broken or long expressions enclosed in parentheses) should be rephrased to go on two or more lines within column width. Fractional powers are preferred to root signs and should always be used in more elaborate formulas. The solidus should be used instead of the horizontal line for fractions wherever possible.

• A normal paper should not exceed 8 pages in the Journal. It is about 8000 words or 20 double-spaced typewritten pages exclusive of drawings. A Technical Brief should not exceed 750 words or about one page in the Journal inclusive of drawings.

• Originals and two copies of figures must accompany the manuscript. Line drawings should not be larger than $8^1/_2 \times 11$ in. and should be planned for reduction to column width. Lettering should be large enough to be clearly legible when the illustration is reduced. The originals of line drawings must be in India ink on white or pale blue tracing paper or tracing cloth. Photographs of equipment or test specimens must be glossy prints and should be used sparingly. Captions for figures should be typed double-spaced and included as the last page of the manuscript. The figure number and author's name should be written in the margin or on the back of each illustration.

• Titles of papers should be brief.

• Authors can obtain copies of the ASME Manual MS-4, "An ASME Paper," from the Editor and are urged to do so before drafting their papers in final form.

• Papers published in Journals of the Transactions of the ASME must be presented at a Meeting, either in person or by title.

• An author is entitled to 25 preprints free of charge (in the case of two authors, 15 each; three or more authors, 10 each). Larger quantities of preprints or reprints can be ordered from Editorial Department, The American Society of Mechanical Engineers, 29 West 39th Street, New York 18, N. Y. Quotations will be sent on request.

Please address all communications to:

Editor, ASME,

29 West 39th Street,

New York 18, N. Y.

ASME Publications Committee